Geophysical Studies of the Northeastern Indian Ocean with special emphasis to the evolution of the Ninetyeast Ridge

Thesis submitted to Goa University

for the award of the Degree of

DOCTOR OF PHILOSOPHY

in

Marine Sciences

by

Honey Abraham

Goa University
Taleigao, Goa
2016

Geophysical Studies of the Northeastern Indian Ocean with special emphasis to the evolution of the Ninetyeast Ridge

Thesis submitted to Goa University

for the award of the Degree of

DOCTOR OF PHILOSOPHY

in

Marine Sciences

by

Honey Abraham

CSIR - National Institute of Oceanography
Dona Paula, Goa-403004, India

&

Oil and Natural Gas Corporation Limited (ONGC)
Chennai, Tamil Nadu – 600 001

Goa University
Taleigao, Goa
2016

to my family

Statement

As required under the University ordinance 0.19.8.(vi), I state that the present thesis entitled "**Geophysical Studies of the northeastern Indian Ocean with special emphasis to the evolution of the Ninetyeast Ridge"** is my original research work carried out at CSIR - National Institute of Oceanography, Goa and Oil and Natural Gas Corporation Limited, Centre of Delivery- HPHT, Chennai, and it has not been submitted for any other degree or diploma in any university or institution. The literature related to the problem investigated has been cited. Due acknowledgements have been made wherever facilities and suggestions have been availed of.

Honey Abraham

Oil and Natural Gas Corporation Limited
Centre of Delivery -HPHT
Chennai Tamil Nadu - 600001

Certificate

This is to certify that the thesis entitled **"Geophysical Studies of the northeastern Indian Ocean with special emphasis to the evolution of the Ninetyeast Ridge"** submitted by Honey Abraham for the award of the degree of Doctor of Philosophy in the Department of Marine Sciences, Goa University is based on her original studies carried out under my supervision. The thesis or any part thereof has not been previously submitted for any other degree or diploma in any university or institution.

Ph.D. thesis Guide:

Dr. K.S. Krishna, FNA, FASc, FNASc, FAPAS
JC Bose National Fellow
Chief Scientist
CSIR - National Institute of Oceanography
Dona Paula
Goa- 403 004

Additional Designations:
Professor & Dean, Academy of Scientific and Innovative Research

Acknowledgements

This Ph.D. research work was a great experience and I am grateful to each and every person who has been helped me in different stages for completion of this adventure.

First and foremost, I would like to express my heartfelt gratitude to my research supervisor, Dr. K.S. Krishna, Chief Scientist, NIO, Goa for introducing me to the research topic and also for his valuable guidance and involvement in the discussions during all phases of the research work. I am gratefully indebted to him for his mentorship, patience, encouragement throughout the years and for encouraging me to continue research work even after leaving NIO for the employment. His constant support and encouragement was instrumental in giving me strength and confidence to complete this work. Throughout my thesis-writing period, he had provided encouragement, sound advice and good teaching. It would not have been possible to complete this work without his constant motivation and support.

I would like to thank my thesis co-supervisor, Prof. G.N. Nayak, Department of Marine Sciences, Goa University for his encouragement and support during the course of the Ph.D. work. I thank Vice-Chancellor's nominee, Dr. A.K. Chaubey, NIO, Goa for duly assessing progress of my work and giving invaluable suggestions and support throughout my research work. I am grateful to J.P Dobriyal, ONGC, Chennai, for helping me with basics of structural geology to carry out a part of this research work. I further thank Dr. K Srinivas, NIO, Visakhapatnam and Prof. H.B. Menon, Department of Marine Sciences, Goa University for their encouragement and support to carry out this research work. I wish to express my deep sense of gratitude to Dr. Satish R. Shetye, Vice-Chancellor, Goa University and other Faculty Members of research council for sanctioning an additional three months time to submit my thesis.

I thank University Grant Commission (UGC) for awarding NET-JRF for carrying out research work at NIO.

I thankfully acknowledge Dr. S.W.A Naqvi, Director NIO for providing me the opportunity and necessary facilities to carry out my research work. I am thankful to C. Natarajan, Head, COD-HPHT and P. Raja former Head, COD-HPHT, ONGC for kindly permitting me to continue my Ph.D work while working in ONGC. I am grateful to A.S. Reddy, Deputy General Manager, COD-HPHT, ONGC for permitting me to take leave for thesis writing. I also thank my other colleagues in ONGC for their support and motivation to complete the research work.

I express my sincere thanks to Dr. Yatheesh for support and help extended especially at the final stage of thesis report formatting. I am extremely thankful to all my friends in NIO for their sincere help and encouragements. I owe to mention the names of Saritha, Suresh, Prachi, Tresa, Ashwini, Shynu and Harris for helping me a lot while editing the thesis report and completing the university formalities. I specially thank Dr. Laju Michael, Dr. K.M. Sreejith and Mohammad Ismael, who also happened to be students of my supervisor for sharing their knowledge and experience in scientific research. I am thankful to nuns of the convent of Fransiscan Missionaries of Mary in Dona Paula, Goa for providing me accommodation during thesis writing period.

I get overwhelmed and short of words while I express my note of thanks to my family. My parents, in-laws and all family members have supported me with love and prayers during my long journey of this research work. My husband has always stood with me extending lot of support and immense motivation for completion of the work.

Finally I wish to thank all who have consciously and sub-consciously helped; friends, acquaintances and colleagues, for the support, confidence and love given to me over the years.

Honey Abraham

Preface

The Indian Ocean is the third largest of the world's oceanic domains covering approximately 20% of water on the Earth's surface. It is youngest as well smallest among the three major global oceans and encompasses an area of 74.11×10^6 square km from 25°N to 70°S latitudes and from 30°E to 130° E longitudes. The Indian Ocean, besides having mid-ocean ridge system, includes several prominent linear aseismic ridges running for thousands of kilometers from north to south. Two of them, Ninetyeast, Chagos-Laccadive ridges, are known for preserving the signals of several major tectonic processes including the early plate motions, continental collisions, lithospheric plate reorganizations and interactions between spreading centers and mantle plumes. The evolutionary history of the northeastern Indian Ocean from early Cretaceous to middle Eocene was dominantly associated with the formation of the Ninetyeast Ridge by the Kerguelen mantle plume. The Ninetyeast Ridge - longest, linear, age-progressive seamount chains on the Earth - extends ~5600 km in the N–S direction from the Bay of Bengal to almost near the Southeast Indian Ridge. The Kerguelen hotspot during its second phase of volcanism approximately between 80 Ma and 40 Ma accreted the Ninetyeast Ridge along the 90°E meridian between 17°N and 29°S latitudes. Detailed geophysical studies of the Ninetyeast Ridge are important from the point of better understanding of the Indian Ocean, particularly gaining new insights on dynamics associated with interactions between the Wharton spreading centers and the Kerguelen hotspot and evolution of the diffuse plate boundary of the Indian Ocean.

In the present study, magnetic data collated from different sources are aimed to detail various possible tectonic settings between the Wharton spreading centers and the Kerguelen hotspot and role of series of southward ridge jumps during the accretion of the Ninetyeast Ridge. The magnetic data compilation on either side of the Ninetyeast Ridge bounded by latitudes from 20°N to 30°S and longitudes from 82°E to 96°E, includes existing and new data acquired during the KNOX06RR cruise in 2007. The main results are discussed in Chapters 4 and 5.

Multichannel seismic reflection data acquired at six grid locations of the Ninetyeast Ridge under the same KNOX06RR cruise programme, are aimed to detail the basement topography, sediment structure and fault pattern of the ridge. While formation of the Ninetyeast Ridge near the Wharton spreading ridge, the prevalent extensional regime led to form E - W oriented horst-graben type structures as well as series of normal faults from north to south along the ridge. High magnitude seismicity generally attributed to the conventional plate boundaries was found associating with most part of the northern Ninetyeast Ridge, whereas the southern part of the ridge is not much associated with the seismicity. During the Miocene time, the Indo-Australian plate

broke into three sub plates - Indian, Australian and Capricorn – with encircling of diffuse plate boundaries and with different direction of relative movements. Since most part of the Ninetyeast Ridge lies within the diffuse plate boundary, the relative movements of sub-plates have reactivated the existing normal faults of the ridge in different style and in different ages from north to south. Further an attempt has been made to determine the active stress directions in terms of net fault strike directions delineated by correlation of active faults between the seismic data and multibeam bathymetry data. The results are discussed further in Chapter 6.

The thesis is divided into the seven chapters. Brief discussion of each chapter is given below.

CHAPTER 1 starts with a general introduction to the Indian Ocean, Plate Tectonics, Mantle Convection, Mantle Plumes and Hotspot trails on the Earth. The importance of mantle plumes in understanding the evolution of ocean is emphasized. The chapter then details the major physical features and geological history of the Indian Ocean elaborating details on its plate tectonics, particularly the seafloor spreading phases and major plate reorganizations. The Bengal Fan deposition and regional onlap unconformities documented are discussed in association with the geological history of the northeastern Indian Ocean. The focus of present research and list of objectives are also included in the chapter.

CHAPTER 2 is dealt elaborately on structure and tectonics of the Ninetyeast Ridge. Geological and geophysical studies carried out so far on the ridge and adjacent oceanic basinal regions and numerous hypotheses proposed on origin of the ridge are described in detail. Updated chronological data obtained from the DSDP Legs 22 and 26 and ODP leg 121 sites from the Ninetyeast Ridge are discussed and compared with the rates of accretion of oceanic crust in adjacent Central Indian and Wharton basins for describing the plate motions. Variable values of elastic plate thickness along the Ninetyeast Ridge and its isostatic compensations are also summarized and discussed.

CHAPTER 3 presents details of geophysical data utilized for investigations, source of database and methods of data analysis. Utility of satellite gravity and bathymetry are emphasized for outlining the precise locations of the oceanic fracture zones. The details of KNOX06RR seismic reflection and multibeam bathymetry data are also briefed. Methods followed for interpretation of magnetic profile data and 2D seismic reflection data are explained. The algorithms and softwares used for forward modeling of seafloor spreading type magnetic anomaly sequences and fault pattern analysis are enlisted with detailed descriptions.

CHAPTER 4 is focused on discussing the details required for the preparation of the synthetic magnetic anomaly profile for comparison to the observed magnetic profile and for identification of seafloor spreading anomalies. The chapter further describes the theory of geomagnetic field reversals and magnetic polarity timescale used in the present work. Considering the split-ups between the anomalies of magnetic profiles of the Central Indian and Wharton basins and estimated spreading rates, synthetic magnetic models are prepared and these models are improved by refining the half spreading rates to match with the observed magnetic profiles. Magnetic pattern of both the Central Indian and Wharton Basins have provided locations of magnetic lineations from 19 through 34 and fossil ridge segments which ceased spreading at 65 and 42 Ma. The Ninetyeast Ridge trends N10°E and obliquely crosses N5°E oriented fracture zones. Thus in the south, the 89°E FZ borders the Ninetyeast Ridge on the east side, whereas in the north the same fracture zone borders the ridge on the west side. In the central part between 11°S and 18°S, the fracture zone obliquely crosses the ridge.

CHAPTER 5 examines the newly improved magnetic isochron map of the region adjacent to the Ninetyeast Ridge and available new chronological data of the ridge for obtaining new insights on understanding of the tectonics of the Ninetyeast Ridge. Three magnetic patterns are observed in the study area: the Central Indian Basin west of 86°E Fracture zone (FZ), the Wharton Basin east of the 90°E FZ and between the 86°E FZ and the 90°E FZ including the Ninetyeast Ridge and found that age of oceanic crust to the west of the 86°E FZ (Central Indian Basin) increases toward the north from early Cenozoic to late Cretaceous, while the crust to the east of the 90°E FZ (Wharton Basin) increases its age in both the north and south directions about 42 Ma fossil Wharton Ridge segments. Contrasting to these patterns, the crust between the FZs near the ridge shows a complex age succession together with fossil ridge segments of different ages (65 and 42 Ma). A comparison between the ages of oceanic crust (2000 km) and newly determined radiometric ages (DSDP Sites 216, 214, 254 and ODP Sites 756–758) of the Ninetyeast Ridge (3980 km) is remarkable and requires a geodynamical explanation. During the formation of the ridge, the distance between the Kerguelen hotspot and spreading ridge segments changed because of the northward migration of the Wharton spreading ridge, southward ridge jumps, and possibly southward motion of the hotspot. Spreading ridge migration probably resulted in the Kerguelen hotspot underlying the Antarctic plate during the early Cenozoic, and led to formation of volcanic edifices on the Antarctic plate by ridge-flank volcanism and by lateral transport of hotspot melt along the ridge axis. The southward ridge jumps transferred parts of the ridge originally formed on the Antarctic plate to the Indian plate and were the major contribution to the extra lengthening of the NER

(The results discussed in Chapters 4 and 5 are published in Journal of Geophysical Research – Solid Earth, 117, B04101, 2012, doi:10.1029/2011JB008805)

CHAPTER 6 introduces the on-going intraplate deformation of the central Indian Ocean and describes the utility of 2D seismic reflection and multibeam bathymetry data over the Ninetyeast Ridge for understanding the tectonics of the diffuse plate boundary. Seismic boundaries interpreted at each grid location are correlated with lithological/ acoustic markers identified in DSDP/ ODP drilled wells are presented. The faults observed with compressional/ extensional/ strike-slip components at each grid location are described and a detailed analysis of active faults with the help of multibeam bathymetry map for delineating ambient stress at each grid location is provided. The fault analysis further revealed that present stress activity is varying from north to south along the ridge and also timings of onset of the deformation. Sub lithospheric plates on either side of the Ninetyeast Ridge and their net direction of movement with respect to the ridge are described.

CHAPTER 7 summarizes the work carried out in the present study. The new understandings on tectonics of the Ninetyeast Ridge, interactions of hotspot with Wharton spreading ridge segments and mid-ocean ridge northward migration with respect to the Antarctic plate, fault pattern of the ridge along its track in response to the on-going plate boundary activities and probable ages of fault reactivations from north to south of the ridge are enlisted. Suggestions and scope of future work in this region are also included.

Contents

Chapter 3 – Geophysical data and Methodology

Chapter 4- Generation of synthetic magnetic model Profiles and correlation to observed magnetic profile data

Chapter 5 - Tectonics of the Ninetyeast Ridge derived from spreading records of adjacent ocean basins and age constraints of the Ridge

Chapter 6 - Seismic Structure and fault activity along the Ninetyeast Ridge

List of Tables

List of Figures

Chapter 1

1 Introduction

1.1 General introduction of the Indian Ocean

Many processes of the dynamic Earth are still enigmatic to the geoscientists of the world. Major advances were actually made to the branch of Earth Science, when the global oceans were explored quite reasonably in 1960s, which eventually lead to the formulation of new theory called PLATE TECTONICS. Around this time magnetic reversals of the Earth also came to be known to marine geoscientists, and these lead to preparation of magnetic anomaly maps of ocean floor for plate reconstruction studies. Seafloor spreading process was proposed as a consequence of continental drift (Dietz, 1961; Hess, 1962), it is a major hypothesis in the field of Earth Science connecting magnetic reversals with seafloor magnetic records (Vine and Mathews, 1963).

The Indian Ocean is the third largest of the world's oceans covering approximately 20% of water on the Earth's surface. It is the youngest and smallest among the three major global oceans and encompasses an area of 74.11×10^6 square km from 25°N to 70°S latitudes and from 30°E to 130° E longitudes (Figure 1.1). Geographically the ocean is bordered in the north by the Asian continent, in the south by Antarctica, in the west by Africa and Madagascar and in the east by Java-Sumatra subduction zone and Australian continent (Figure 1.1). The Indian Ocean's average water depth is 3960 m and its deepest point lies at a depth of 7450 m in the Sunda deep of the Java Trench. Towards north the ocean is closed by the continental land mass and Himalayan mountain range, which has profound impact on ocean circulation and Asian climate. As a consequence northern part of the ocean receives high rate of sediment discharge from deltaic systems of the subcontinent, leading to the development of geosynclines and fans in the Bay of Bengal as well as in the Arabian Basin (Figure 1.1). The seafloor topography of the Indian Ocean is highly complex. Further details are discussed in detail in section 1.4 – major structural features of the Indian Ocean.

1.2 Plate tectonics and seafloor spreading

Planet Earth has remained dynamic both by endogenic and exogenic mechanisms throughout its geologic history. Geologists were aware of this fact since 17th century and

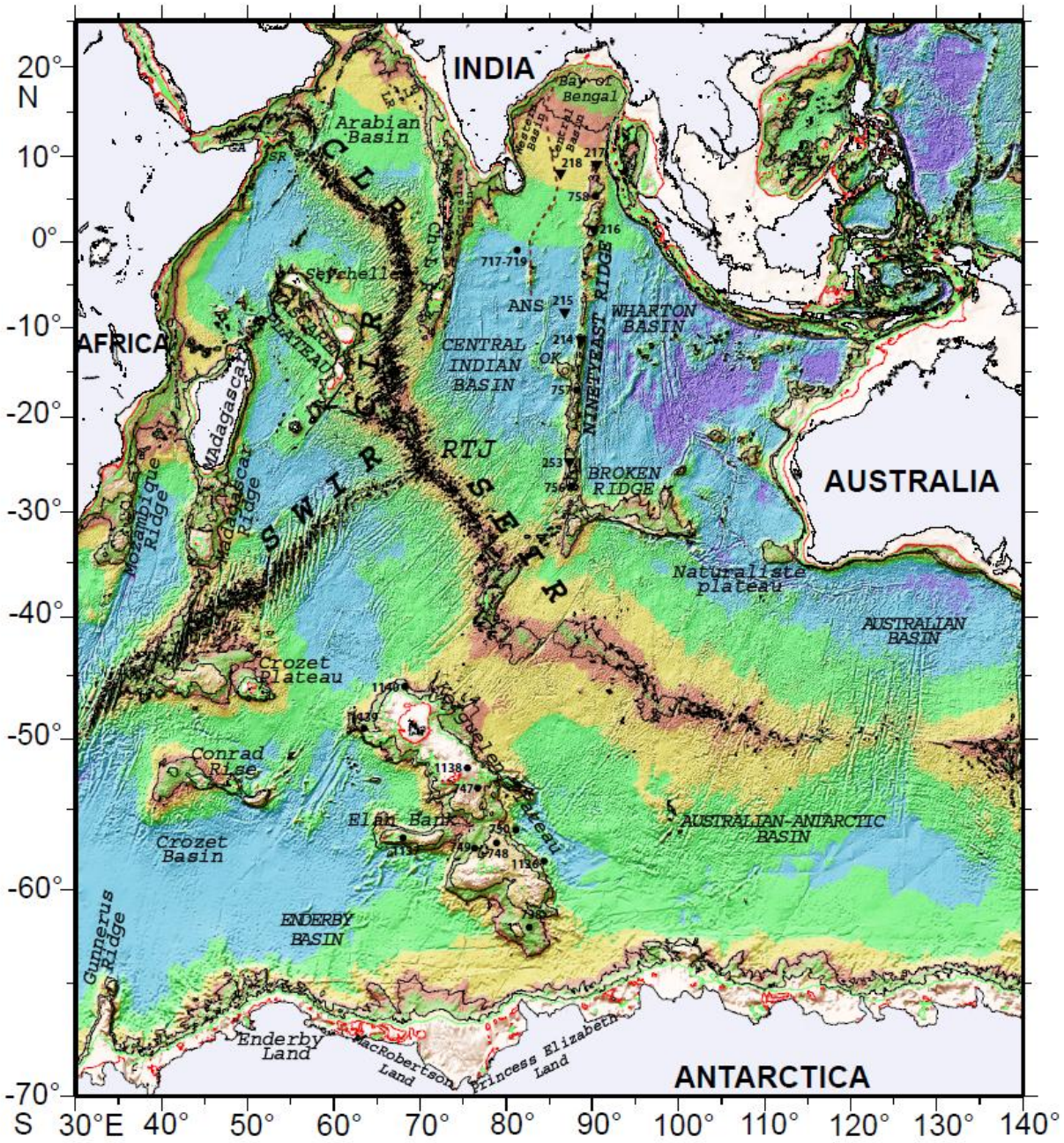

Figure 1.1: Bathymetric map of the Indian Ocean showing Major structural features with annotation. CLR -Carlsberg Ridge, CIR- Central Indian Ridge, SWIR- South West Indian Ridge, SEIR- South East Indian Ridge. Dashed curved line - 85°E Ridge. Black solid circles - ODP drill sites, Black solid triangles - DSDP drill sites.

many theories were attempted to explain why mountains, earthquakes and volcanoes occur on the surface. The congruity of opposing coasts were noticed and several hypothesis were put forth to explain the mechanism with the evolution of geoscience. Late 19th Century saw emergence of two main theories of tectonic evolution.

The congruity of opposing coasts were noticed and several hypothesis were put forth to explain the mechanism with the evolution of geoscience. Late 19th Century saw emergence of two main theories of tectonic evolution. One theory was based on the contraction of earth due to cooling, wherein contracting Earth would result in formation of fold/thrust mountains. The theory could explain the compression features, but failed to give explanation for extensional features. The second theory was based on the expansion of the Earth due to heating. This theory could bring out why continents broke-up hence explaining the extensional features, but could not explain formation of compression features.

Alfred Wegner, a German Scientist put together the evidences of ancient glaciations and fossil distribution in the year 1912 and formulated a theory that the continents have moved on the surface of the Earth over the geological period. He proposed that prior to 200 Ma (million years ago before present) all continents were together as one large mass called Pangea, which had subsequently moved apart by large scale horizontal movements of crustal blocks of continental dimensions. The theory - continental drift - was not readily accepted by geoscientists, but for lack of explanations for proper driving mechanisms in spite of his reasoning of slow horizontal movements of large lithospheric plates which proved correct later on and well-reasoned geologic evidences. The secret key to unveil the plate driving mechanism was submerged under the oceans at that time. It was only in1950s and 1960s, especially at the time of World War II, the ocean floors were explored extensively and the mid-ocean ridges and magnetic anomaly sequences of the ocean floor were revealed providing essential clues to geoscientists to formulate the theory of plate motion (Figures 1.2 - 1.4).

The concept of seafloor spreading was proposed by Dietz (1961) and Harry Hess (1962) and suggested the movement of continents apart in response to the push of new oceanic

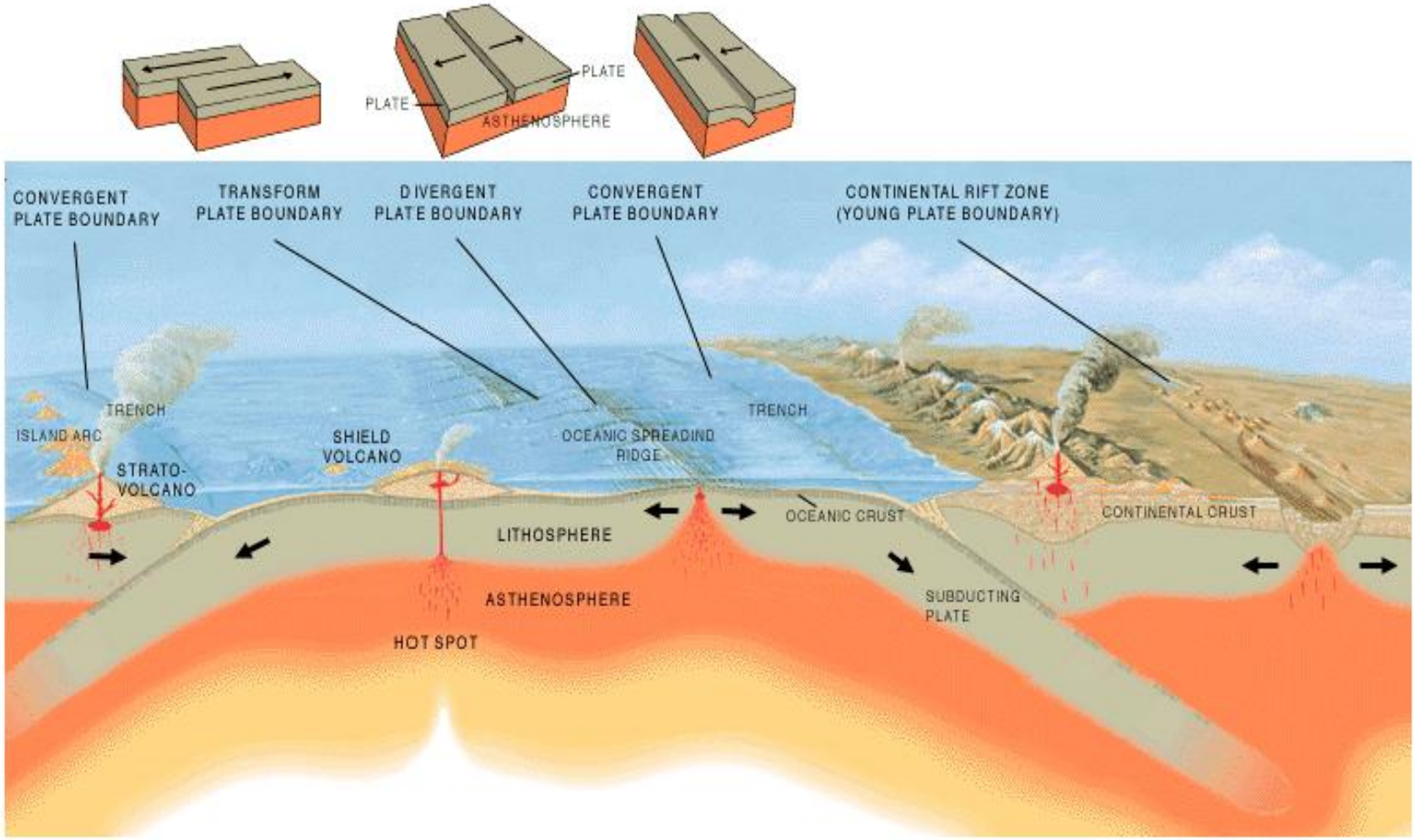

Figure 1.2: Schematic figure on major elements of plate tectonics (after Kious and Tilling, 2008)

crust created on either side of mid-oceanic ridge. Seafloor spreading was confirmed by the proposal that synchronised the magnetic lineations of ocean floor with geomagnetic reversals and seafloor spreading rates (Vine and Mathews, 1963), in which the ocean floor is aptly modelled as a conveyor belt that records the Earth's ancient magnetic field variations (Figure 1.4) .

Thus plate tectonics (Morgan, 1968) was constructed as a unifying theory of all concepts related to continental drift, like hypotheses of seafloor spreading and magnetic reversals. According to the theory of plate tectonics the lithosphere of the Earth is divided into a number of large but thin and rigid blocks called plates, which are bounded by three types of plate margins (Figure 1.4).

The mid-ocean ridges are classified as constructive or accretive plate margins. These are also termed as divergent plate margins as the plates get diverged away from the ridge crest in order to form a new lithosphere out of mantle upwelling. The plate movement is generally perpendicular in direction to the strike of ridge system.

The trenches, where old oceanic crust of the plate gets thrust under the other plate are defined as destructive plate margins. As two lithospheric plates get converged along this boundary, they are even called convergent margins. This is a complementary process to construction of plate at other plate boundary, by which the surface area of the Earth is balanced without much expansion. Volcanism is associated with landward side of subduction zone leading to formation of island arcs of regularly spaced volcanoes, which closely parallel the trench geometry in most cases. The convergent boundary also includes the uplifted parts of continental plates or orogens resulting from collision of two continental plates which is the later stage of subduction.

The transform faults with tangential motion of plates are categorised as conservative margins with neither construction nor destruction of plate, but only relative movement occur generally parallel to the transform fault. Though elements of plate tectonics were identified and qualitative geological evidences were established by late 1960s the questions of plate rigidity and adequate driving mechanism remained. These are explained by the hypothesis of thin shell-like cold rigid plate sliding over hot fluid-like asthenosphere and the process is controlled by thermal convection cells in the upper mantle. Though elements of plate tectonics were identified and qualitative geological evidences were established by late 1960s the questions of plate rigidity and adequate driving mechanism remained. These are

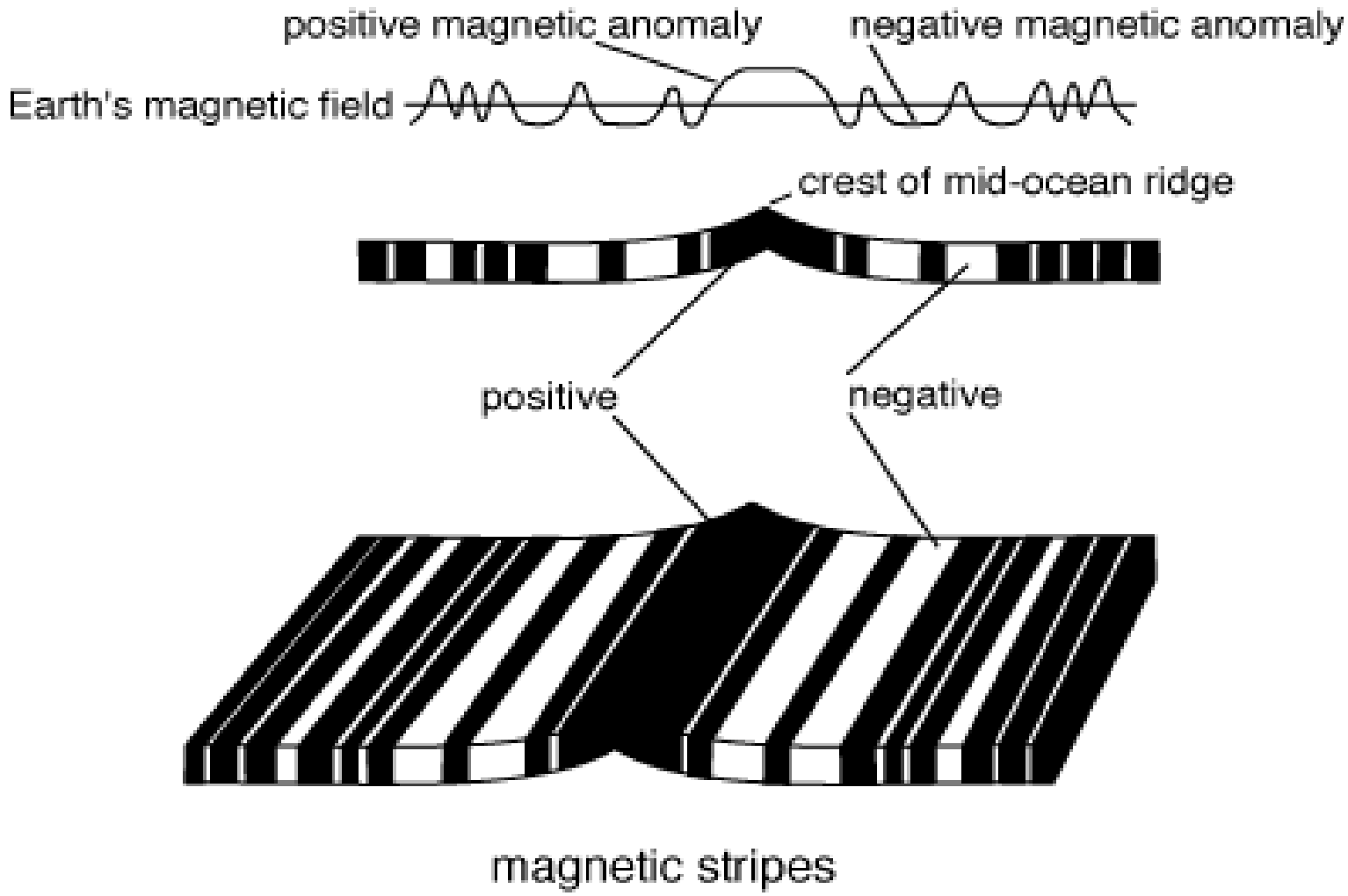

Figure 1.3: Schematic figure on Magnetic isochrons from the ocean floor based on Vine and Mathews (1963) simple oceanic crustal blocks of magnetization

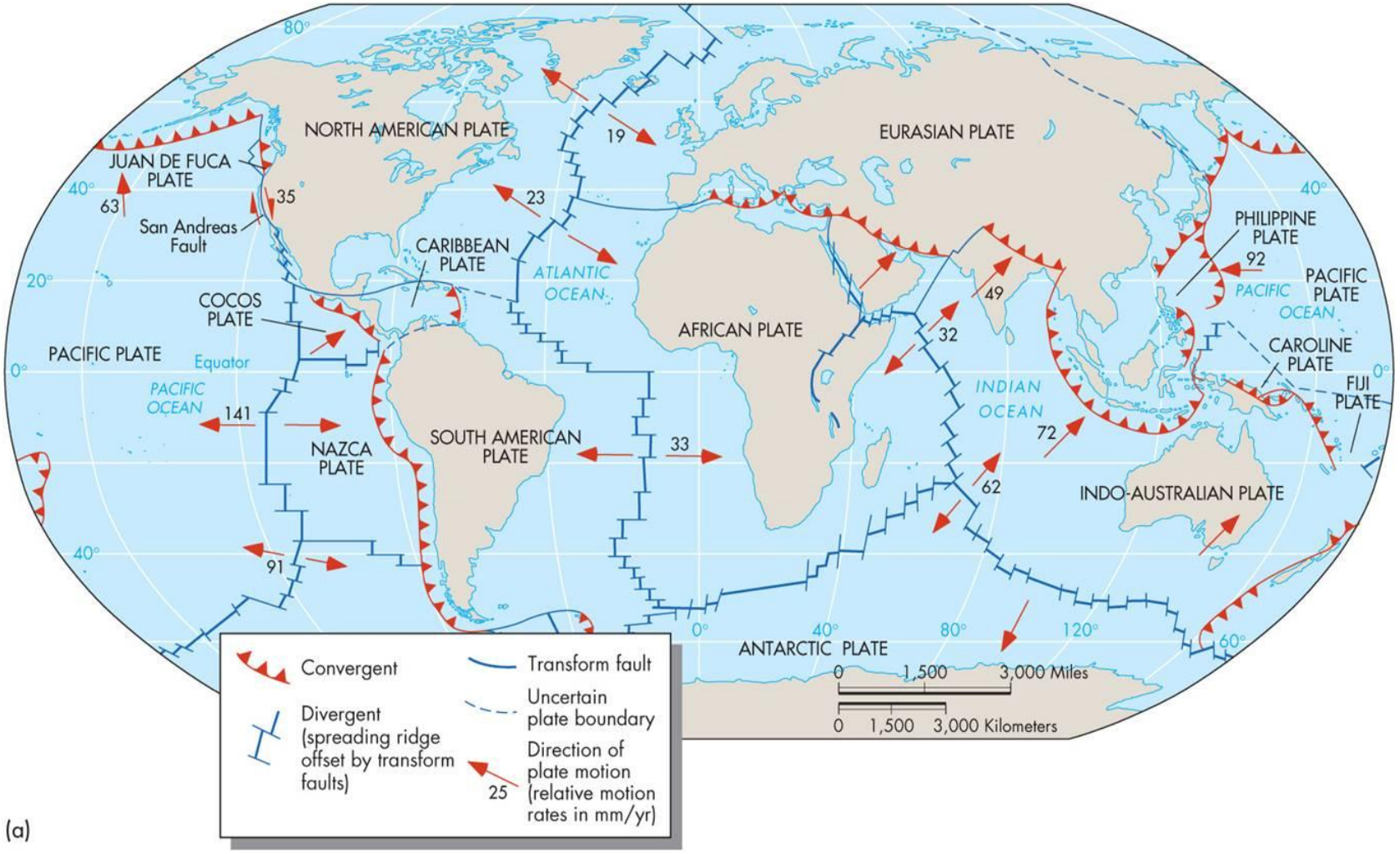

Figure 1.4: Distribution of major plates and location of different plate boundaries (after Keller, 2008).

explained by the hypothesis of thin shell-like cold rigid plate sliding over hot fluid-like asthenosphere and the process is controlled by thermal convection cells in the upper mantle.

1.3 Mantle convection

Mantle convection is defined as thermal convection in the rocky mantle, a layer lying between the crust and core, in which hot material rises, cold material sinks and induced flow governs plate tectonics and volcanic activity. This thermal convection governs chemical segregations and cooling of the entire planet (Bercovici, 2010). The theory was originally developed in 1930 to explain the thermal history of Earth and as a mechanism that drives the continental drift (Schubert et al., 2001; Bercovici, 2007). When the theory of plate tectonics was established by late 1960s, the concept of mantle convection revived its strength, which could successfully explain all elements of plate driving mechanisms like plate velocities, seafloor subsidence, volcanism, gravity anomalies of plate boundaries, etc.

In mantle convection theory the upper mantle is assumed as a viscous fluid with positive temperature gradient, this leads to development of convection cells and initiating upwelling of hot light mantle and the cold heavy fluid sinking under gravitational field at the other boundary of the cell.

Convection in fluids is driven by buoyancy that originates in thermal boundary layers. Earth's mantle has two boundary layers. The upper boundary layer is the lithosphere, which cools through its upper crustal surface and eventually becomes denser than the underlying mantle. The lower boundary layer is the contact between the Earth's molten iron–nickel outer core and the lower mantle. Experimental studies of the melting point of iron–nickel alloys at high-pressure show that the core is several hundred degrees hotter than the overlying mantle. A temperature difference of this magnitude is expected to produce an unstable boundary layer above the core which, in turn, should produce plumes of hot, solid material that rise through the mantle, driven by their thermal buoyancy (Figure 1.5). Therefore, from theoretical considerations, mantle plumes are the inevitable consequence of a hot core (Campbell, 2005).

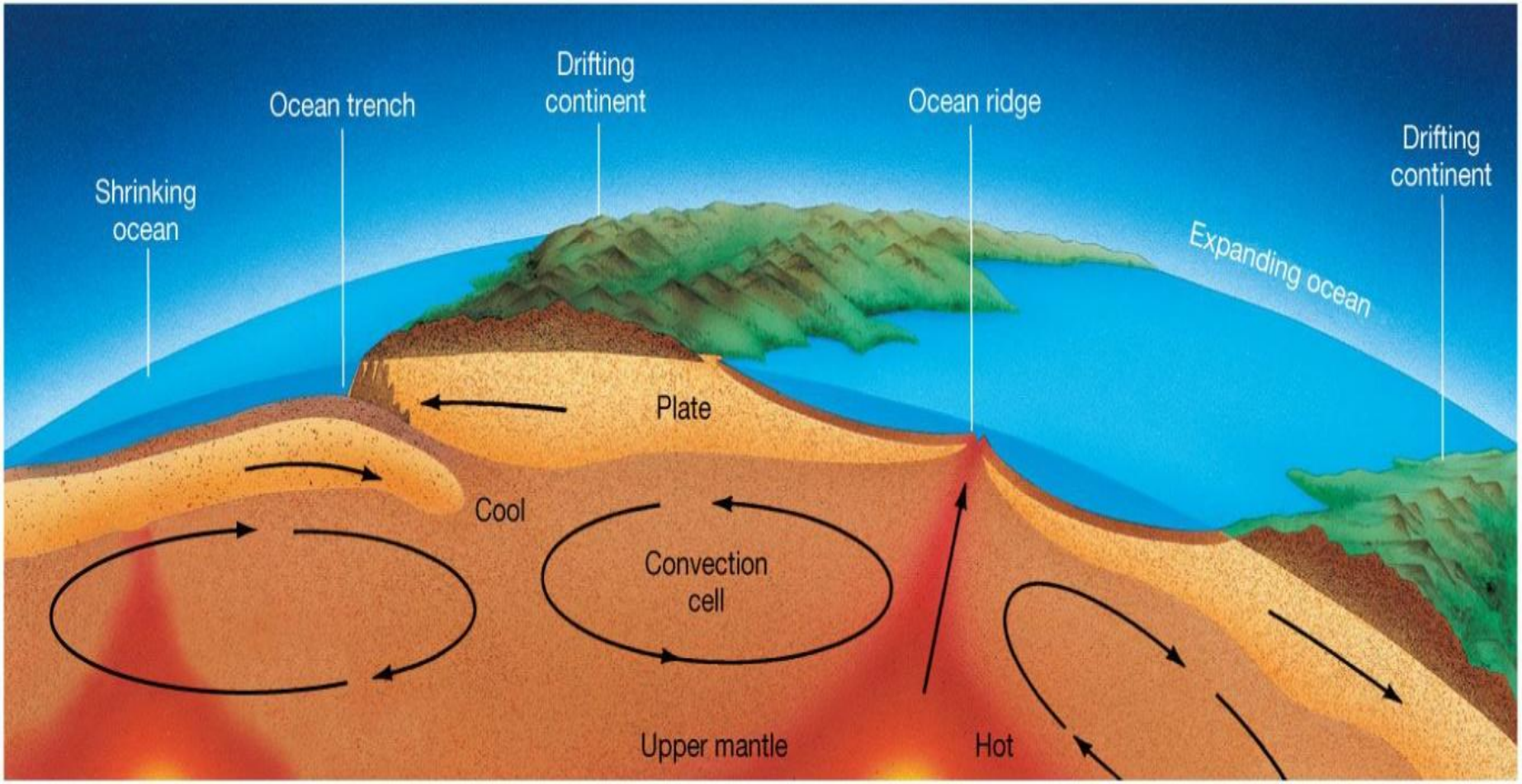

Figure 1.5: Schematic model of Mantle convection
(Source: http://pages.uoregon.edu/jimbrau/BrauImNew/Chap07/7th/AT_7e_Figure_07_16.jpg)

1.3.1 Mantle plumes on the Earth

Mantle plumes are quasi-cylindrical pipe-like structures and up-wells concentrated hot mantle material representing a basic form of mantle convection (Figure 1.6). Deep hot narrow upwelling plumes are inferred to explain anomalous intraplate volcanisms as well as the fixity of volcanic hotspots relative to each other. Hotspots are anomalous areas of surface volcanism that cannot directly be explained with plate tectonic processes (Morgan, 1971, 1972). They are caused by upwelling of mantle rocks from a deep thermal boundary layer below the upper mantle; they are driven by thermal buoyancy rather responding to plate tectonics and subduction. The classical hotspot model proposed by Wilson (1963) and Morgan (1971, 1972) requires magma source deep in the mantle and thus the rising magma are chemically distinct from those of mid-oceanic ridges. Further, their nearly stationary mantle plumes on the base of moving lithospheric plate could explain the age progression of volcanic chains. Numerical simulations and laboratory experiments show that the plumes initiate with a leading plume head followed by a narrow conduit or plume tail connecting the plume head to the source region (Turcotte and Schubert, 2002). Supporting this result, observational evidences suggest that flood basalt eruptions mark the initiation of hotspots. For example, the Reunion hotspot track follows after emplacement of the Deccan flood basalt province on western Indian Shield (White and McKenzie, 1989). However, recent studies shows that very few hotspots are associated with upper or lower mantle tomography anomalies and majority of them lack prominent swells or surface volcanism. The Ninetyeast Ridge, the focus of the study, is an expression of hotspot activity during the northward migration of Indian plate. Among the prominent swell hotspots many are lacking geochemical evidences for its deeper origin. Most significant and geochemically distinct hotspots like Hawaii, Iceland and Reunion are not underlined by lower mantle P-wave seismic anomalies. These studies have lead to an alternate hypothesis that the anomalous volcanism is attributed to plate tectonic processes at the Earth's top thermal boundary layer. Below the tectonic plates the mantle is at near melting point temperature, and it is inhomogeneous by the recycling of crustal rocks, these two conditions can cause volcanism and this is controlled by the stress conditions of the plate. The most significant processes that cause stress to vary in the lithosphere are differential cooling and variable plate boundary types. Thus, according to this model, anomalous volcanism occurs, where the stress field is

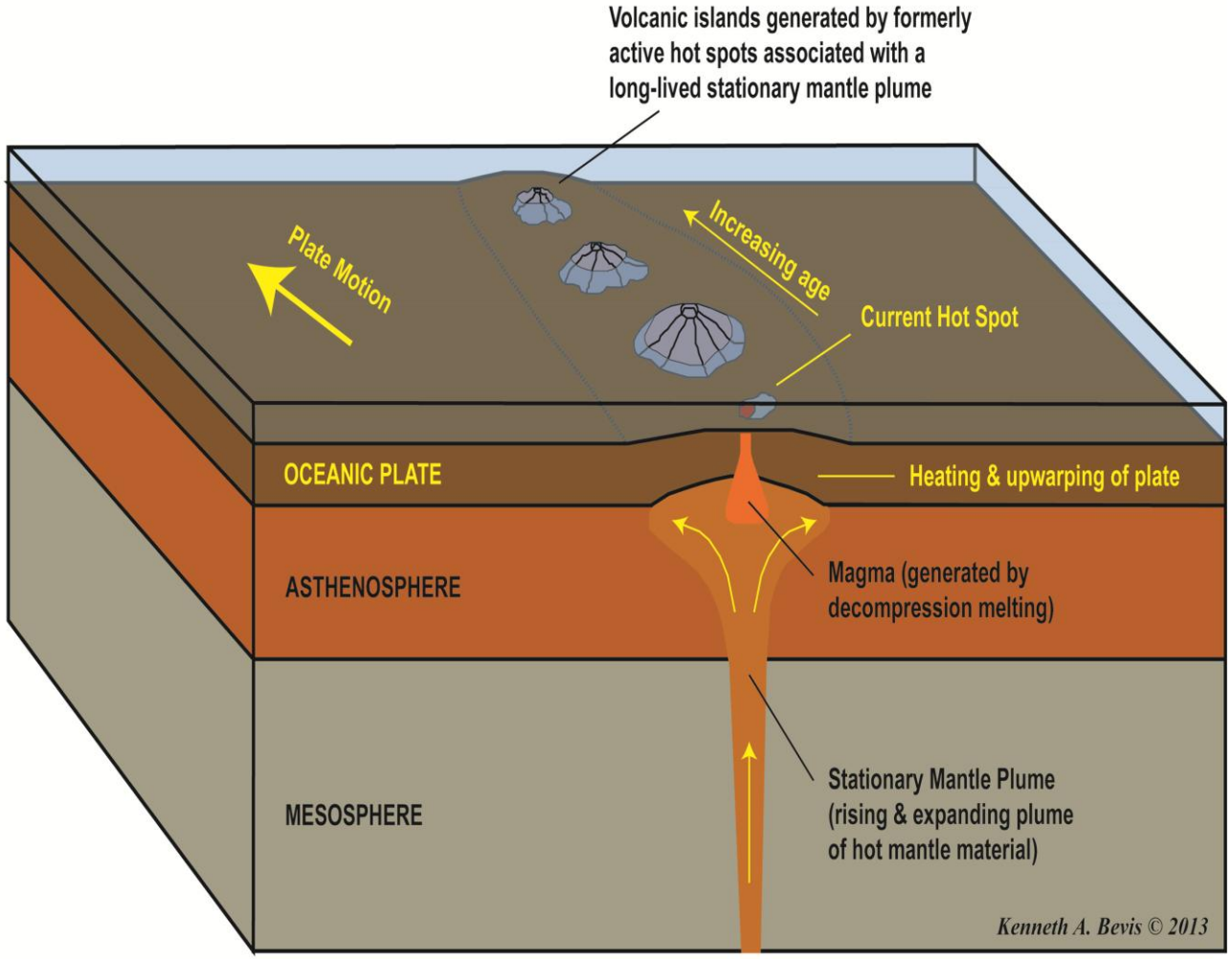

Figure 1.6: Schematic Drawing on Hotspot emplacement sequence on moving plate (after Kenneth, 2013)

extensional and mantle is unusually fusible, therefore this model does not requires temperature anomalies deep in the mantle.

There are about 43 hotspots existing globally and occupying an area of 11-42% of the total Earth's surface. Generally the plume volcanism at its initial stage of eruption is much more voluminous than normal ocean ridge volcanism; resulting in the emplacement of Large Igneous Provinces (LIP) such as Deccan traps and thick crustal Iceland, which has elevation above sea level. In many cases hotspots lie at the end of well-defined lines of volcanic edifices or volcanic ridges, known as hotspot tracks. The hotspot track associated with the Hawaiian hotspot is the Hawaiian–Emperor island–seamount chain that extends across the Pacific plate to the Aleutian Islands, and another prominent one in the Indian Ocean associated with the Deccan flood basalts and Chagos-Laccadive Ridge presently lies beneath the Reunion Island. The Ninetyeast Ridge of present study is hotspot trail of Kerguelen mantle plume presently underneath the northwest part of the Kerguelen Plateau.

1.3 Importance of plumes in understanding the evolution of oceans

The entire mantle of the Earth has been proved to behave as convecting and overturning along small portions of melting near the surface delineated by volcanism and thus flows extremely slowly. As down-welling mantle material travel from near surface to the base of the mantle, its density and temperature increases due to compression called adiabatic compression and heating, while hot upwelling mantle material approaches the surface it actually travels along a gradually cooling adiabatic temperature profile and eventually melt when it gets near the surface. Such "pressure release" melting is vital for chemical segregation of the mantle and development of oceanic and continental crust. Upwelling mantle reaching the Earth's surface undergoes melting and is manifested in two types of volcanic settings; along mid oceanic ridges where the tectonic plates spread apart and draw mantle to fill up the opening gap creating new oceanic crust or sometimes ocean-islands and second manifestation are the hotspots, which are anomalous localized volcanic activity that are not necessarily associated with the tectonic activity. The melts coming from the mantle along the mid ocean ridges are relatively silica poor and hence produce Mid-Ocean Ridge Basalts (MORB).

As the mantle plume sources lay deep into the mantle, the signatures corresponding to dynamics of the lithospheric plates are well documented in ridge emplacement process. The plates generally undergo relative and/ or absolute motions: the relative plate motion is

described by keeping one plate fixed and moving the other one, whereas absolute plate motion is described with respect to a stationary point deep inside the Earth. The volcanic emplacements are also used to determine the response of the lithosphere to the overlying loads in terms of isostasy, in other words how the emplacement loads were compensated in terms of Airy or flexural models. Further the hotspot traces are used to understand the mobility of the plumes and behaviour of the mid-ocean ridge segments.

1.3.3 Mantle plumes in the Indian Ocean

The Indian Ocean consists of traces of 6 hotspots such as Kerguelen, Reunion, Crozet, Comores, Marion and Afar emplaced during the last approximately 150 Ma. Three hotspots are apparently responsible for major six features (Morgan, 1981) in the Indian Ocean (Figure 1.7). The Kerguelen hotspot resulted in manifestation of the Kerguelen Plateau, Broken Ridge and Ninetyeast Ridge. The Reunion hotspot resulted in formation of Chagos-Laccadive Ridge and the Mascarene plateau and Crozet hotspot emplaced the Crozet Plateau. The complex tectonic evolution of the Indian Ocean is responsible for hotspots creating multiple Large Igneous Provinces (LIP).

The Deccan Traps, typical flood basalt forming a LIP are found to be connected to 200-300 km wide Chagos-Laccadive aseismic ridge, across the Carlsberg-Central Indian Ridge spreading centers and the Mascarene plateau. This ridge is attributed to active melting volcanic plume tail presently located at Reunion. The Rajmahal Traps being typical flood basalt forming a LIP can be attributed to the Kerguelen hotspot.

1.4 Major structural features of the Indian Ocean

Although the Indian Ocean is the youngest among the global oceans, it is physically most complex of the world's three major oceans and is home to many interesting tectonic and geomorphologic features. The major feature of the ocean is the Mid-Oceanic Ridge (MOR) system of inverted Y shape with triple junction around 25°S in the vicinity of the Rodriguez Island, constituting Southwest Indian Ridge (SWIR) as its western limb trending NE-SW, Southeast Indian Ridge (SEIR) trending in NW-SE as its eastern limb and Central Indian Ridge (CIR) and Carlsberg Ridge (CLR) in near N-S and NW-SE trend respectively, as the northern limb. The Java Sumatra subduction zone is one of its typical kinds marking oblique thrust of Indo-Australian oceanic plate under Eurasian continent. Abundant distribution of

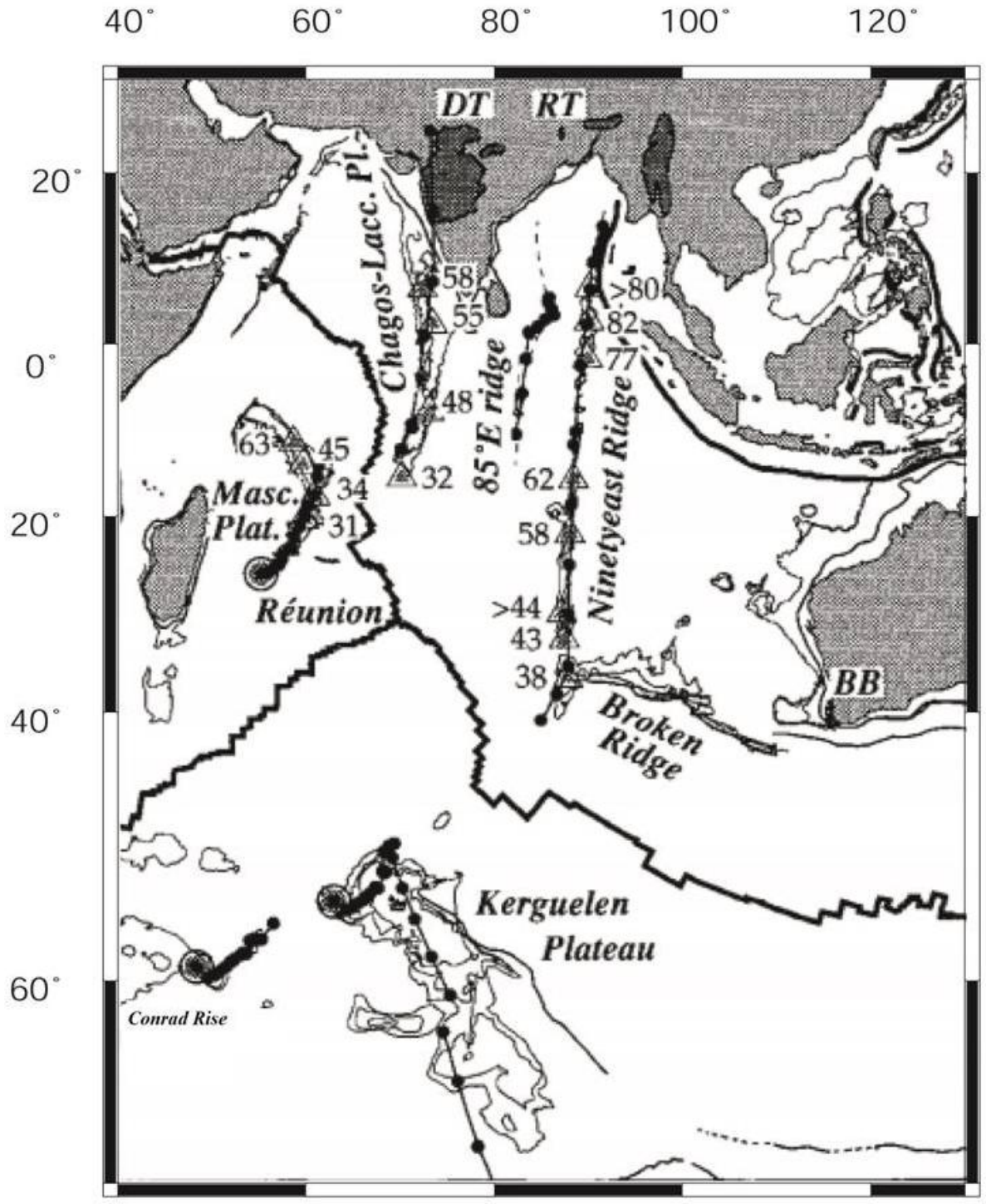

Figure 1.7: Mantle plumes and hotspot emplacement of Indian Ocean (after Muller et al., 1993)

submarine plateaus and aseismic ridges are the next striking features in bathymetric map of the Indian Ocean (Figure 1.1). The most prominent of these are the Ninetyeast Ridge in the eastern Indian Ocean, Chagos-Laccadive Ridge, Seychelles Bank, Mascarene plateau, Madagascar and Mozambique ridges in the western Indian Ocean, Agulhas plateau, Crozet plateau and Kerguelen-Heard plateau in Southern Indian Ocean. Broken ridge at the southern tip of Ninetyeast Ridge and Naturalist plateau are two other important features in eastern Indian Ocean. The major ocean basins are divided further into sub-basins by these ridges and plateaus. Thus, there are Central Indian Basin, Wharton Basin on west and east of Ninetyeast Ridge, Arabian Basin, Mascarene Basin, Mozambique Basin, Crozet Basin and Enderby Basin. Besides, these there are number of minor features of smaller dimensions observed like seamount rises, islands and guyots in the Indian Ocean. The Afanasy Nikitin seamount at the southern tip of the 85°E Ridge in the equatorial region, Ob, Lena and Marion-Dufresne seamounts in Crozet Basin are some of the prominent seamounts that are studied for their origin and found to be associated with hotspot volcanism.

1.4.1 Mid-ocean ridges

Mid-oceanic ridge system of the global oceans constitute around 23% of the Earth's surface extending some 70,000 km long and around 300 km wide with rough elevation of around 2000 m from adjacent ocean basin's seafloor. They typically have high heat flow, marked seismicity and rifting along the crests. In young and tectonically active Indian Ocean region, the MOR is manifested as the Central Indian Ridge (CIR) that bifurcates into Southeast Indian Ridge (SEIR) and Southwest Indian Ridge (SWIR) and meets at the Rodriguez Triple Junction (RTJ at 25°S latitude and 70°E longitude) (Schlich, 1982). In north the CIR continues further in the form of Carlsberg Ridge (CR) and truncates against the Owen Fracture Zone near the Red Sea. The CIR is extremely segmented and offset by major NE-SW trending Fracture Zones and large number of ridges, basins and plateau mark the Indian Ocean. The Southeast Indian Ridge (SEIR) separates the Indo-Australian plate from the Antarctica plate has the highest spreading rates, approximately 3.0 cm/yr. The Central Indian Ridge (CIR), which demarcates the African and Indo-Australian plate displays slower spreading rates, but complex geometry (Fisher et al., 1971; Patriat, 1987). The Southwest Indian Ridge (SWIR), which separates the African and Antarctica plate displays rough topography with large off-set fracture zones (Sclater et al., 1981) with ultra-slow spreading rates less than 1.0 cm/yr. The central Indian Ocean Triple Junction also called as

Rodriguez Triple Junction (RTJ) has been classified as ridge-ridge-ridge (RRR) triple junction (after McKenzie and Morgan, 1969).

The Central Indian Ridge extends from Rodriguez Triple junction in south and connects the Carlsberg Ridge in the equatorial region (Figure 1.1). This spreading ridge differs from the other spreading ridges of the Indian Ocean being slower in spread rates, slightly more dissected in NE-SW trend and separated by fracture zones at places. The ridge extends for about 1200 miles in length and 400 - 500 miles in width. The half spreading rate of the Central Indian Ridge calculated from the magnetic anomalies varies from north to south between 1.8 cm/yr and 2.4 cm/yr (Chaubey et al., 1991; Kamesh Raju et al., 2012).

The Southwest Indian Ridge (SWIR) extends south-westward from the Rodriguez triple junction and connects the Bouvet triple junction in South Atlantic Ocean (Figure 1.3). The ridge has specific characteristics of discontinuities and seamounts, and some of them are found even at the bottom of the basins. The ridge has ultra slow spreading rates of order of 0.8 to 1.3 cm/yr (Vine, 1966; Le Pichon and Heirtzler, 1968; Ewing et al., 1969). Detailed geophysical studies over the SWIR revealed that the ridge is dominated by a series of major fracture zones, which can be traced up to a distance of 2000 km from their active transform sections.

The Southeast Indian Ridge (SEIR) extends from the Rodriguez triple junction through Amsterdam St. Paul Island to Pacific-Antarctic Ridge south of Australia (Figure 1.3). The ridge separates the Crozet Basin to its south from the Central Indian Basin on north, and further eastward the Australian-Antarctic Basin from the South Australian Basin. Two distinct spreading rates are identified since inception of the ridge system, that is for the last 40 Ma with a half spreading rate of 3.4 cm/yr for anomalies 1 and 5 (10 Ma) and 2.5 cm/yr for anomalies 5 and 17 (40 Ma) (Le Pichon and Heirtzler, 1968; Schlich and Patriat, 1971; Schlich, 1975).

1.4.2 Oceanic fracture zones

Mid-ocean ridges are not continuous features but are cut by numerous Transform Faults(TF), which demarcate sense of relative motion of the plates. Ocean Fracture Zones (OFZ) exists on seafloor as bathymetric features, which are also considered as traces of transform fault tracks, may extend many hundreds of kilometres from the MOR. Unlike active faults, fracture zones are mostly devoid of seismic activity along their length. The

crust on one side of the fracture zone is older; hence the crust is cooler, more contracted and deeper than the other side of the fracture zone. The boundaries along the TF are often represented by deep trenches. They resemble strike-slip faults in topography and record large offsets when cut across magnetic isochrones and mid-ocean ridges. The Indian Ocean Ridge System is isotopically distinct (Mukhopadyay et al., 1999) and characterised by inconsistent presence of fracture zones. The ridge axis is more displaced south of equator than to the north. There are prominent NE-SW trending fracture zones resulting in structural dislocations of the ridges, there are large-scale offsets, often several tens of kilometres, or non-transform discontinuities, where ridge displacement is rarely more than a few kilometres. The Central Indian Basin and Wharton Basin are marked by many near N-S trending fracture zones, implying the N-S rapid drift of the Indian plate away from the Antarctic plate during the late Cretaceous to middle Eocene. Identification of fracture zones on ocean floor is extremely important as they provide explicit clues to reveal the tectonic history of the continents and oceans.

1.4.3 Ocean basins

Ocean basins are broad geomorphologic features in the oceans, which can be described as saucer-like depression on the seafloor, they cover approximately 71 percent of the Earth's surface or about 361 million square km and average water depth is 5000 m and occupy about 1.35 million cubic km volume. They are created on either side of the mid-ocean ridge system as a result of seafloor spreading. During the basin evolution, the lithosphere may occasionally experience intraplate volcanism from deep mantle, resulting in emplacement of seamounts, aseismic ridges and/ or plateaus as the case may be depending on volume of emplacement of hotspot and expansion of the basin at that point of geologic time. Other than the slow marine sedimentation in close vicinity of the passive continental margins, the ocean basins do receive terrigenous clastic sediment input brought by river delta systems at much higher rate, whereby the geomorphology of the basin changes as all the structural features get submerged. These structural and geologic features mentioned define local boundaries to broad ocean basin. The basins in the Indian Ocean are very low relief zones characterized by relatively thin homogenous sedimentary deposits. The Indian Ocean consists of a number of ocean basins and several sub basins such as central Indian Basin, Wharton Basin, Crozet Basin, Arabian Basin, Somali Basin, Enderby Basin, etc. In north-eastern Indian Ocean the ocean floor is divided into two basins by N-S trending Ninetyeast Ridge as the Wharton

Basin to the east and Central Indian Basin to the west of the Ninetyeast Ridge, which are analyzed in detail as part of the present study.

1.4.3.1 Central Indian Basin

The Central Indian Basin extends from the Central Indian Ridge to the Ninetyeast Ridge and is bounded in the south by the Rodriguez Triple Junction and northern part of the Southeast Indian Ridge. In the north, the ridge is bounded by the tip of the Indian - Sri Lanka landmass (Figure 1.1). In general the basin consists two categories of seafloor morphology, the northern region is completely free of topographic undulations as the region is covered under the Bengal Fan sediments, but the southern region is covered with numerous seamounts and abyssal hills. The basin has E-W trending magnetic anomaly isochrons34 through 22 offset by several near N-S (N5°E) trending fracture zones generally in a right lateral fashion. According to the isochron distribution the age of the basin decreases from north to south. The anomaly pattern between the 86°E fracture zone and Ninetyeast Ridge was observed to follow a complex succession. Western extension of abandoned Wharton Ridge was observed in this area up to 86°E FZ, and the spatial extent between identified mirrored anomalies on either side of this extinct ridge was not found equal, implying the possibility of multiple ridge jumps towards south at different geological ages (Krishna et al., 1995). Small ridge jumps at anomaly 30 and 26 at the northern part between the equator and 10°S (Royer et al., 1991; Krishna and Gopala Rao, 2000) and a major ridge jump at anomaly 19 towards south of it were proposed (Liu et al., 1983), resulting in a capture of Antarctic plate portions to the Indian plate spanning about 11° stretch in terms of latitude (Krishna et al., 1995). The present study had analysed the magnetic isochrons of this region with compilation of new profiles in order to understand the hotspot spreading ridge interaction in detail (Krishna et al., 2012).

1.4.3.2 Wharton Basin

The Wharton Basin lies in the northeast part of the Indian Ocean, named after William Wharton (1843-1905) and also termed as Cocos Basin and West Australian Basin (Figure 1.1). The Wharton Basin is the deepest part of the Indian Ocean, southern being deeper than the north (Heezen and Tharp, 1964). It is bounded on the west by the Ninetyeast Ridge, on the south by the Broken Ridge and east by the Java trench. This basin is divided into north and south domains by Cocos Seamount Chain trending roughly east-west along latitude 12°S. The magnetic anomaly pattern depict E-W trend similar to that of the Central Indian

Basin. Earlier analysis of the magnetic data interpreted that age of the basin decreases from south to north from late Cretaceous to late Eocene (Sclater and Fisher, 1974). Subsequent compilations of new magnetic profile data had identified the presence of fossil spreading ridge of chron 19 and its right lateral offsets in succession from the Ninetyeast Ridge at southwest to Sunda trench at northeast near equator, with the conjugate magnetic lineations on either side of the extinct ridge (Liu et al., 1983; Geller et al., 1983). The fracture zones of Wharton Basin also are trending N5°E as revealed by satellite gravity and bathymetry data similar to the fracture zones identified in the Central Indian Basin.

1.4.4 Major aseismic ridges of the Indian Ocean

Aseismic Ridges are long seamount chains found within the lithospheric plates; they are the major prominent features of the ocean besides mid-oceanic ridge features. Generally all inactive features like plateaus, island chains and seamount chains could come under this category in terms of genesis, but are different only in terms of dimensions of their structure and relief. These ridge features are found seismically inactive in spite of their volcanic origin, hence they are named as aseismic ridges. Aseismic ridges seem to be originated either by volcanism or even by breakup of continental fragments in the vicinity of lithospheric plate boundaries as well as interior of the plates. The Chagos-Laccadive and Ninetyeast ridges are the most prominent and longest aseismic ridges of the Indian Ocean. They are more or less continuous linear features traversing for few thousands of kilometres in the deep ocean floor with elevations up to 3000 m above the surrounding ocean floor. The 85°E Ridge is a less prominent aseismic ridge in the northeast Indian Ocean and its northern part is submerged under the Bengal Fan sediments, while its southern part is intermittently exposed to the seafloor (Krishna, 2003). The western Indian Ocean has relatively more aseismic ridges and plateaus, like Chagos- Laccadive Ridge, Seychelles-Mascarene Plateau complex, Madagascar Ridge, Mozambique Ridge, Crozet Plateau, Conrad Rise, etc. The Broken Ridge at the southern tip of the Ninetyeast Ridge and Naturaliste Plateau west of Australia are two such features of smaller dimensions in eastern Indian Ocean. The Kerguelen Plateau is a major bathymetric feature in the Southern Ocean. These features are studied in detail with the help of geophysical investigations and results obtained from the programmes of the Deep Sea Drilling Project (DSDP) and Ocean Drilling Program (ODP). Regarding origin of these features many hypotheses were put forth especially in cases of major linear ridges like Ninetyeast Ridge, 85°E Ridge and Chagos-Laccadive Ridge.

1.4.4.1 Ninetyeast Ridge

The Ninetyeast Ridge lying in the eastern Indian Ocean is the largest of linear aseismic ridges of the world oceans with a total length of about 5600 km. The continuous volcanic ridge trends approximately in N-S (N10°E) direction along the 90°E meridian from 34°S latitude in the south to 17°N in the north into the Bay of Bengal sediments, where it converges with the Sunda trench (Figure 1.8). The average width of ridge is 200 km and height exceeds 2 km from surrounding ocean floor (Sclater and Fisher, 1974; Udinstev, 1975; Schlich, 1982; Fisher et al., 1982). The ridge up to 10°N latitude is covered by thin sediments < 800 m and further north up to 17°N latitude the ridge is buried beneath thick sediments of Bengal Fan (Curray et al., 1982; Gopala Rao et al., 1994, 1997; Michael and Krishna, 2011) and separates the eastern Nicobar Fan from the main Bengal Fan. The morphology of the ridge varies from north to south along its stretch with linear and flat topped features at places (Sager et al., 2007, 2010). At around 15°S latitude, a broad circular bathymetric high called Osborne Knoll is situated on immediate west of the ridge. Between the latitudes 7°S and 10°N the ridge segment appears to be a complex of en-echelon blocks of individual topographic highs, with northeast-southwest elongation. The northern most part of the ridge is buried beneath the thick sediments of the Bengal Fan and the southern tip abuts against E-W trending Broken Ridge (Sclater and Fisher, 1974; Curray and Moore, 1974). At several locations the flanks of the ridge on both sides are observed to have variable topographic gradients, and specifically between 11° and 21°S is relatively deeper on the eastern flank than the western flank (Udinstev, 1975; Fisher et al., 1982; Krishna et al., 2001b). South of the Osborne Knoll, the ridge become wide and more massive than it is towards the north of the Osborne Knoll (Sclater and Fisher, 1974; Krishna et al., 1995).

Initially as the data were scarce over the Ninetyeast Ridge, several theories have been proposed for the accretion of the ridge on the Indian Ocean floor. At least six different hypotheses had been put forth in a decade's time after its discovery such as horst type feature due to an upliftment of the oceanic crust (Francis and Raitt, 1967; Laughton et al., 1970), up-thrusting caused by convergence of two fragments of the Indian plate (LePichon and Heirtzler, 1968), relict spreading ridge (McKenzie and Sclater, 1971), hotspot origin (Morgan, 1972), emplaced locally by gabbro (Bowin, 1973) and volcanism along a leaky transform fault due to relative motion of Indian and Australian plates (Sclater and Fisher, 1974). The DSDP Legs 22 and 26 and ODP Leg 121 had drilled seven wells on the ridge along its stretch (Figure 1.8) and inferred that the Ninetyeast Ridge was formed as a hotspot

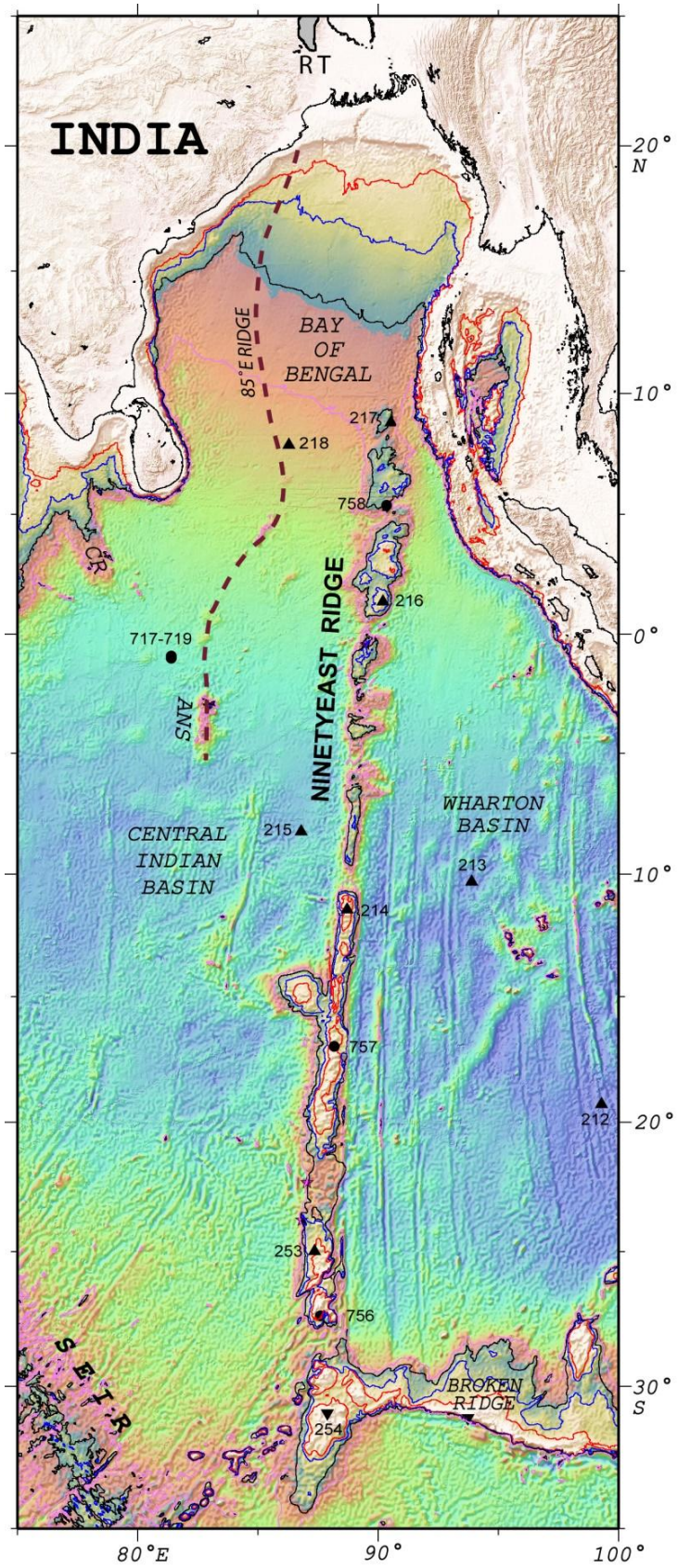

Figure 1.8: General bathymetry map of the eastern Indian Ocean showing location of the Ninetyeast Ridge between34°S and 10°N latitudes. Numbered solid triangles and circles are DSDP and ODP drill sites.

track near the spreading ridge that once separated the Indian plate from the Antarctic plate, and the volcanic trail was eventually left with the Indian plate as it drifted northward in the late Cretaceous to early Cenozoic period (Royer et al., 1991; Krishna et al., 1995, 1999, 2012). The age data from DSDP and ODP core samples show that the southernmost part of the Ninetyeast Ridge at ODP Site 756 is ~45 Ma, while the northern most part of the ridge at ODP Site 758 it is of ~77 Ma and the sites in between give a monotonous increase of age from south to north, establish the continuous emplacement of the ridge by the Kerguelen hotspot when the Indian plate moved northward over it (Weis and Frey, 1991; Klootwijk et al., 1992; Duncan, 1991; Duncan and Storey, 1992; Krishna et al., 2012).

Diffused intraplate deformation zone evolved in the central Indian Ocean around the late Miocene, encompassing the Ninetyeast Ridge in the middle of India-Australia, Capricorn-India and Capricorn-Australia diffused plate boundaries (Royer and Gordon, 1997; Royer et al., 1998). The central part of the ridge pass through the middle of diffuse deformation zone of triple junction between the plate boundaries (Petroy and Wiens, 1989; Delescluse and Chamot-Rooke; 2007), which implies the presence of the ridge being pivotal in fixing the boundaries of these three sub plates (Tinnon et al., 1995; Delescluse and Chamot-Rooke, 2007; Sager et al., 2013).The seismicity is more concentrated in the northern segment of the ridge (upto 10°S), where it undergoes NW-SE compression and vertical as well as strike slip motions occur. The seismicity is less along the southern segment of the ridge. The transition is evident from the morphology of the ridge where irregular en-echelon blocks in the north are separated from smooth flat topped highs in the south. It is also suggested that a diffuse triple junction is located in the middle of the Ninetyeast Ridge due to the deformation patterns between Indian, Australia and Capricorn sub-plates. From bathymetry, gravity and seismic data it has been concluded that northern most part of the Ninetyeast Ridge is at the final stages of indention near the Andaman fore-arc and at the same time slipping northward (Subrahmanyam et al., 2008).

1.4.4.2 Chagos-Laccadive Ridge

The Chagos-Laccadive Ridge (Ch-LR) is another prominent aseismic ridge of the Indian Ocean, extending in near N-S direction between 14°N and 10°S latitudes along 73°E meridian for about 3000 km and with a width of ~200 km (Figure 1.1).The ridge concaves to its west separates Arabian Sea from Central Indian Basin. Several deep channels trending in E-W direction separate the ridge structure into irregular blocks and the surface

topography of the ridge is abundant with shoals, coral reefs, banks and atolls with varying water depths of about 3000 - 4000 m. The Chagos, Maldives and Laccadive coral islands are summits of this ridge above sea level located in northern, middle and southern segments respectively. Seismic refraction studies over the ridge as well as the basement samples from ODP Leg 115 advocate that the ridge structure is a continuous volcanic feature with a thick crust of 14-20 km, under the Chagos Islands (Francis and Shor, 1966).

On geneses of aseismic ridges, one could come across several hypotheses proposed during the period of early 1970s to late 1980s due to the absence of sufficient geological and geophysical data. Thus even in the case of the Chagos-Laccadive Ridge, there are numerous theories depicting the ridge as a transition between continental and oceanic crust (Narain et al., 1968), emplacement over a leak transform fault during northward movement of the Indian plate during the Cretaceous-Eocene period (Fisher et al., 1971; McKenzie and Sclater, 1971), a hotspot trace (Dietz and Holden, 1970; Morgan, 1972; Whitmarsh, 1974; Duncan, 1981) and a combination of leaky transform fault and micro continent (Avraham and Bunce, 1977). But generally accepted hypothesis for origin of the ridge is of Reunion hotspot track emplacement while passage of India towards north over it. Basement samples from ODP Leg 115 Sites 713 and 715 provide age of around 49 Ma for site 713 at the south and 57 Ma for site 715 at north, which are consistent with the hotspot hypothesis (Richards et al., 1989; Duncan, 1990)

1.4.4.3 85°E Ridge

The 85°E Ridge in the northeastern Indian Ocean extends from the Mahanadi Basin in the north Bay of Bengal takes an arcuate shape off Sri Lanka and finally joins the Afanasy Nikitin Seamount (ANS) in the Central Indian Basin (Figures 1.1). The ridge elongates for more than 2500 km from 19°N to 5°S as a combination of buried, partly buried and emergent hills protruding through the distal end of the Bengal Fan (Curray and Munasinghe, 1991; Krishna, 2003; Krishna et al., 2014). In the Bay of Bengal region below the fan sediments the ridge structure appears as a double humped feature at around 13°N (Gopala Rao et al., 1994), as intrusive peak structure at around 10°N (Curray et al., 1982) and as broad basement swell (Gopala Rao et al., 1997) at 14.64°N. The northern part of the ridge is buried under the thick Bengal Fan sediments as evidenced by seismic reflection data, whereas south of 7.5°N it partly rises above the seafloor and finally culminates with the ANS at 5°S (Krishna, 2003). In the north the ridge structure, where it is buried under the

Bengal Fan sediments is associated with a significant negative gravity anomaly, whereas in the south the ridge structure is partly exposed and is associated with positive gravity anomaly signatures (Subrahmanyam et al., 1999; Krishna, 2003).

Many hypotheses have been proposed for the development of negative gravity field and the origin of the 85°E Ridge. Plate reconstruction studies of Curray and Munasinghe (1991) attribute the ridge evolution to the Crozet hotspot volcanism, suggesting that the Rajmahal Traps, 85°E Ridge and ANS were evolved in connection with the same hotspot trail. Müller et al. (1993) suggested that the 85°E Ridge segment between 10°N and ANS might have been formed by a hotspot now located underneath the eastern Conrad rise on the Antarctic plate. There were many other explanations documented in literature for origin of the ridge such as abandoned spreading centre (Mishra, 1991), volcanism through a weak zone within a short span of time (Chaubey et al., 1991), northward continuation of the 86° FZ (Kent et al., 1992), shearing and sagging of the crust due to the compressional forces at the time of major plate reorganizations (Ramana et al., 1997; Anand et al., 2009). Liu et al. (1982) modelled the flexural and gravitational response of the ridge and concluded that the ridge was formed on a weak lithosphere, which subsequently gained strength along with the sedimentation. The enigmatic gravity low of the 85°E Ridge was explained by the underplating material and crustal root at the base of the crust (Subrahmanyam et al., 1999). Subsequently Krishna (2003) and Sreejith et al. (2011) have concluded that the presence of meta-sediments and flexure of the lithosphere beneath the ridge would explain the negative gravity anomaly of the ridge. Keeping this in view they have suggested that the ridge was formed in intraplate position when the underneath lithosphere was ~35 Myr old. The major discrepancy to conclude its origin is lack of ridge crest sampling by deep drilling.

1.4.4.4 Broken Ridge

The Broken Ridge in the eastern Indian Ocean is located south of the Ninetyeast Ridge trending approximately in E-W direction between 30°S to 32°S latitudes and its western end touching the southern part of the Ninetyeast Ridge (Figure 1.8). The ridge has got an average with of 100 km and stretch E-W for about 1000 km in water depths < 2000 m. The southern flank is steeper than the northern flank. It was proposed that the central part of Kerguelen plateau and Broken ridge were emplaced by the Kerguelen hotspot volcanism during the mid-Cretaceous period, then continued to be together until rifted away in middle Eocene (Weissel and Karner, 1989; Royer et al., 1991). The results of the ODP Leg 121

have documented maximum age of 83 Ma for basalt samples of the Broken Ridge supports the mid-Cretaceous volcanic origin.

1.4.5 Oceanic plateaus and micro-continents

Oceanic plateaus are gigantic submerged features equivalent of continental flood basalts found on continental shields, the first eruptive product of a new mantle plume (Coffin and Eldholm, 1994; Campbell, 2005). They are vast in dimension ranging to as much as 2000 - 2500 km in diameter width elevated topography of 2-3 km above the abyssal ocean floor. The most prominent plateaus in the Indian Ocean are the Agulhas plateau, lies south of South Africa in the south western Indian Ocean, the Kerguelen-Heard plateau lies southwest of Australia, the Mascarene plateau lies north and east of Madagascar and the Naturaliste plateau extends from the western Australia into the Indian Ocean (Figure 1.1). Micro-continents in the Indian Ocean are nothing but small sliver fragments of the continental mass, that have been broken off from the main continent and drifted away several hundreds of kilometres from their place of rifting, and eventually the continental fragments are surrounded by newly accreted oceanic crust.

1.4.5.1 Kerguelen Plateau

The Kerguelen plateau is a typical Large Igneous Province (LIP) situated in the southern Indian Ocean adjacent to the Antarctica continent and is approximately equidistant from Australia and Africa (Figure 1.1). It is the second largest oceanic plateau in the world oceans and stretches for about 2300 km in NNW-SSE direction between 46°S and 64°S latitudes. The plateau demarcates the southern Indian Ocean into three deep ocean basins, Australian-Antarctic Basin in the northeast, Crozet Basin in the northwest, Africa-Antarctica Basin in the southwest. To the South the plateau is bordered by 3500 m deep Princess Elizabeth Trough (Schlich et al., 1988) that extends to continental shelf of Antarctica. The plateau rises for about 3700 m above the adjacent ocean basins. The Kerguelen plateau is broadly divided into 3 major morphological sectors, the northern, central and southern (Schlich, 1975; Houtz et al., 1977; Coffin et al., 1986, 2002). The northern Kerguelen plateau between 45°S and 55°S lies at water depth of about 1000 m below sea level and emerges as sub-aerial manifestations of the Kerguelen Archipelago, Heard and McDonald Islands. The tectonically more complex southern Kerguelen plateau between 58°S and 64°S is deeper lying in water depth of about1500 m with subdued topography, but it is characterized by several large basement uplifts, normal faulting, graben formation and

strike-slip faulting (Coffin et al., 1986; Fritsch et al., 1992; Rotstein et al., 1992; Royer and Coffin, 1992; Angoulvant-Coulon and Schlich, 1994; Konnecke and Coffin, 1994; Gladczenko et al., 1997). The northern and southern parts of the Kerguelen plateau between 54°S and 58°S are separated by a transition zone of complex bathymetry with a large east-west trending Elan Bank, which extends westward from the main plateau over a distance of 600 km long.

Several geophysical and petrological investigations were carried out over the plateau, leading to proposal of several hypotheses regarding the evolution of the Kerguelen plateau, which subsequently updated with the available of new geological information. Initially based on available meagre information, its origin was thought that fragment of continental piece of Gondwanaland, failed spreading ridge, product of magmatic activity related to a fault, composed of thick oceanic crust uplifted either by isostatic forces or because of thermal expansion or the result of intraplate volcanic activity related to the plume that produced the Ninetyeast Ridge, etc. Subsequently Coffin et al. (2002) proposed that the Kerguelen plateau except the Elan Bank and Skiff Bank was formed by the Kerguelen hotspot in two distinct phases. In the first phase the southern and the central parts of the Kerguelen plateau were formed during 120-100 Ma, while the northern part is being formed since 40 Ma. Multichannel seismic reflection data show numerous intra-basement reflections from the uppermost igneous crust of the Kerguelen plateau, which are interpreted as sub-aerial flood basalts (Coffin et al., 1990; Schaming et al., 1990).A group of prominent seamounts of recent age presently locate the Kerguelen hotspot underneath the northwest Kerguelen Plateau (Duncan and Richards, 1991; Curray and Munasinghe, 1991).

1.4.5.2 Elan Bank

The Elan Bank, a micro-continental fragment located in the central part of the Enderby Basin, extends westward of the Kerguelen plateau from the boundary between the central and the southern Kerguelen plateau (Figure 1.1), which stretches in E-W direction for about 900 km encompassing about ~140,000 km^2 of seafloor in water depths range from 1000 to 3500 m. The bank is asymmetric in shape with its steep slope facing south and its fairly gentle slope facing north. Geological and geochemical results from the ODP Leg 183 have revealed the Elan Bank as a micro-continent in the Southern Indian Ocean (Coffin et al., 2000; Frey et al., 2000; Nicolaysen et al, 2001; Weis et al., 2001). Wide-angle seismic

reflection studies show that the crust of the Elan Bank is at least 14 km thick (Konnecke et al., 1997; Borrisova et al., 2003) comparable to that of continental crust.

It is proposed that the east coast of India along with fragments of the Kerguelen plateau and Elan Bank were conjugate to the East Antarctica margin (Stagg et al., 2004; Krishna et al., 2009a & b). During the early phase of spreading, there was a ridge jump towards east of India, which seems to have transferred the Elan Bank from India to Antarctic plate (Frey et al., 2000) probably due to the interaction of the Kerguelen hotspot located beneath eastern edge of Indian plate, with early Cretaceous spreading centre resulting in the fragmentation of the Elan Bank and other micro-continents of the Southern Indian Ocean. The upper igneous crust of the Elan Bank consists of 2-3 km thick layer of accumulated lava flows originated from the Kerguelen hotspot (Borrisova et al., 2003).

1.5 Geological history of the Indian Ocean

The Indian Ocean has complex and unique geological history of evolution, thus formation of an exceptional structural fabric. The exploration of the ocean started since the International Indian Ocean Expedition (IIOE) during (1960-1965). Subsequently Deep Sea Drilling Project (DSDP) Ocean Drilling Programs (ODP) have drilled at selected locations for testing the hypotheses and unravelling the geodynamic history of the Ocean since the late Cretaceous. Plate reconstruction analysis based on magnetic isochron pattern of conjugate margins and ocean basins reveals the paleo-assemblage of the continental landmasses and fragments and rift situation of the eastern Gondwanaland in late Jurassic - early Cretaceous (Curray and Moore, 1971; Moore et al., 1974; Norton and Sclater, 1979; Curray et al., 1982; Royer and Coffin, 1992; Gopala Rao et al., 1997; Krishna et al., 2009a & b; Veevers, 2009). The present geomorphology of spreading ridges, continental margins, plateaus and aseismic ridges were evolved in different phases of geologic time with the activities of number of hotspots volcanism, a few plate reorganizations and ridge jumps, plate collisions, subduction and abduction, etc.

1.5.1 Phases of seafloor spreading and plate reorganisations since the breakup of eastern Gondwanaland

Pioneering research in Indian Ocean basins had envisaged the evolution of the ocean in several stages since the late Triassic/early Jurassic. These were confined to three main phases of evolution demarcated by two major plate reorganizations (Norton and Sclater, 1979; Liu, et al; 1983; Patriat and Segoufin, 1988; Royer et al; 1992). The first major

seafloor spreading phase started by opening the Indian Ocean in early Cretaceous before magnetic anomaly M11 period (~126 Ma), this lead to separation of Greater India in NW-SE direction from Australian - Antarctic plate, which subsequently ceased at around 95±5 Ma during the Cretaceous Magnetic Quiet Period. Therefore the magnetic anomalies corresponding to the first phase of spreading process are expected to be both in Bay of Bengal and Enderby Basin (Powell et al., 1988; Royer et al., 1989; Royer and Coffin, 1992; Nogi et al, 1991, 1996; Ramana et al., 1994, 2001; Gaina et al., 2007; Krishna et al., 2009a & b; Veevers, 2009).

The second phase of spreading is believed to be started in late Cretaceous as relative motion of Indian and Antarctic plates shifted from NW-SE to N-S direction. This phase is synchronous with India- Madagascar rifting and plates in eastern Indian Ocean started their reorganisation. As this phase was started during the Cretaceous Magnetic Quiet Period (120-84 Ma), a little is known about the exact time and boundary of this major plate reorganisation. The Indian lithospheric plate drifted rapidly from Antarctica with an average full spreading rate of 12cm/yr (Sclater and Fisher, 1974; Peirce, 1978) and E-W trending magnetic anomalies 34 to 20 were formed in Central Indian and Wharton basins (Liu, et al; 1983 Royer and Sandwell, 1989; Krishna et al., 1995, 2012; Krishna and Gopala Rao, 2000). During the period close to the K-T boundary age marked the eruption of Deccan Flood Basalts by the Reunion plume, leading to rifting away of Seychelles from the Western India paving the way for formation of the Carlsberg Ridge (McKenzie and Sclater, 1971; Norton and Sclater, 1979; Naini and Talwani, 1983; Royer et al., 2002; Chaubey et al., 2002). During this period the Indian and Arabian plates were moving along a fracture zone, the ancestor of Owen Fracture Zone, which connected the Carlsberg Ridge System and the Subduction zone in the Neo-Tethys region (Bhattacharya and Chaubey, 2001). The period of >10My from KT boundary to anomaly 24 is marked by maximum spread rate nearly 10 cm/yr in Indian Ocean, which is attributed to the influence of the Reunion plume eruption by some researchers (Cande and Stegman, 2011).The plate velocity reduced after this gradually and a substantial slowdown of spreading rate was observed around anomaly 22 (51 Ma) which was attributed to the check in drifting pace of the Indian plate caused later the first contact or 'soft collision' (Curray et al., 1982; Bastia et al, 2010) between continental India with southern Asian subduction zone, initiating the second major plate reorganization and mark the end of second phase of spreading (Crawford, 1974; Curray and Moore, 1974; Curray et al., 1982; Liu et al., 1983).

Consequently the E-W trending spreading ridge system in the Wharton Basin got extinct by 42 Ma and new NW-SE trending spreading started probably with a major southward ridge jump which joined the Australia-Antarctica spreading ridge to form Southeast Indian Ridge (SEIR). This marked the beginning of third phase of spreading in anomaly 19 time (42 Ma) which continues to present evidenced by NW-SE trending anomalies on both sides of the Central Indian Ridge and Southeast Indian Ridge (Sclater and Fisher, 1974; Schlich et al., 1975; Sclater et al., 1976, 1981; Liu et al., 1983).

1.5.2 Bengal Fan sedimentation and main unconformities

The Bengal Fan system is one of the largest sediment accumulations existing in the world. The fan spans of the whole Bay of Bengal bordered by continental shelf of India to the west, Bangladesh to the North, Sunda trench to the east and extending beyond the equator to about 7°S with length >3000 km and covering an area of around $3x10^6$ km^2 (Krishna et al., 2001; Curray et al., 2003; Bastia et al., 2010). The water depth varies from 1400m in the north to 5000 m towards south and the maximum sedimentation observed is of 22 km in Bangladesh shelf (Brune et al., 1990; Curray, 1994), which gradually reduces towards south.

The geological history of the Bay of Bengal starts with the breakup of India from Eastern Gondwana Land in the Early Cretaceous (~120 Ma) and sediment deposition took place since the pre-collision between India and Asia, tremendous sediment dump after the late Palaeocene/ early Eocene (~55 Ma) soft collision and subsequent Himalayan uplift in mid-Miocene, termed hard collision (Curray and Munasighe, 1989; Curray, 1990; Bastia et al., 2010). In pre-collision time rivers from the eastern margin of India probably Godavari and Mahanadi are considered as the major depositional systems prevalent. Post soft-collision period marked the onset of fan system, when rivers from the north, the Ganges and Brahmaputra started feeding the fan enormously developing a channel system evidenced by seismic time slice characteristics and post hard-collision <15 Ma increased the sedimentation rate manifold and the fan prograded further south developing many channel-levee systems (Bastia et al., 2010). Tectono-stratigraphic investigations of sediments of this geosyncline has informed of initial rift-drift history of the Indian plate, stages of Indian-Asian collisions, onset and growth of the Bengal Fan system, hydrocarbon reservoir potential and evolution history of the 85°E and Ninetyeast ridges. The major geological events had been recorded in the sediment stratigraphic sequence as periods of hiatus or erosional unconformities, which have been revealed by seismic stratigraphic studies and

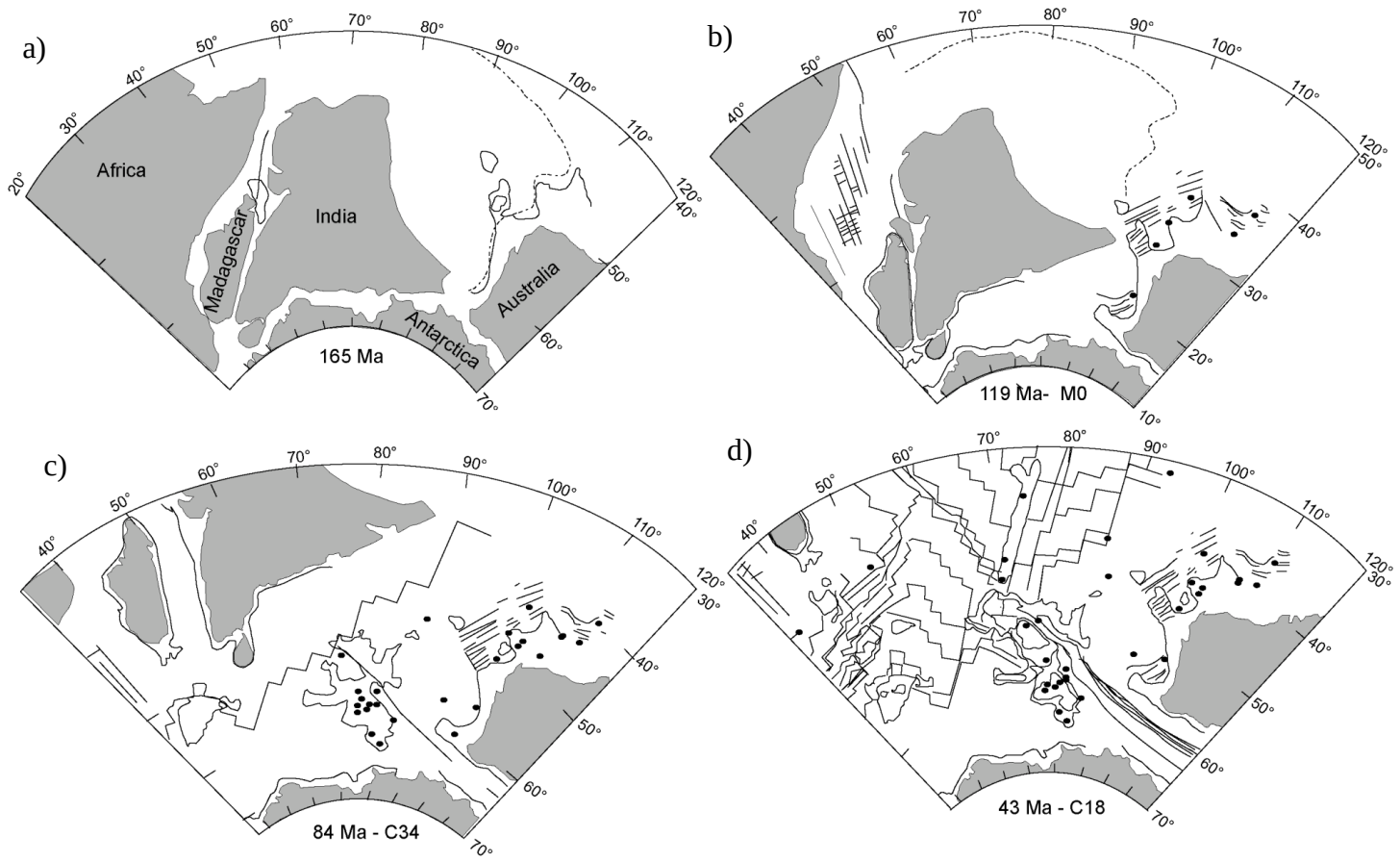

Figure 1.9: Reconstruction of the Indian Ocean since 165 Ma to 43 Ma (after Royer and Coffin, 1992). a) Plate Reconstruction at 165 Ma when Spreading has begun between East & West Gondwana and off NE Australia. b) Reconstruction at 119 Ma (M0) just before emplacement of Kerguelen Plataeu /Broken Ridge complex. Spreading between Africa & Madagascar stopped and Africa/Antarctica and India/Antarctica spreading systems got connected shortly after this. c) Reconstruction at 84 Ma after major plate boundary reorganisation around mid Cretaceous, 4 plates formed out of two plates: Africa/Madagascar, Greater India/Seychelles and Antarctica and Australia. d) Reconstruction at 56 Ma (C24). Slow spreading between Australia and Africa. Ninetyeast Ridge and northern part of the Kerguelen plateau are being constructed over Kerguelen hotspot.

Ocean Drilling Programs. The uppermost regional hiatus recorded is of late Miocene, which marks the onset of intraplate deformation and Himalayan orogeny (Shipboard Scientific Party, Site 218, 1974; Moore et al., 1974; Cochran et al., 1989, 1990; Curray and Munasinghe, 1989; Bull and Scrutton, 1992; Krishna et al., 1998, 2001b, 2009b). The older unconformity identified is of early Eocene hiatus (Shipboard scientific party, Site 218, 1974; Moore et al., 1974; Pierce and Wessel, 1990) and predicted to be associated with start of Indian-Asian continent-continent collision (Curray et al., 1982, 1989), which also demarcates the pre-collision sediments from the post-collision rapid depositions. Interpretation of high resolution E-W seismic profiles have revealed unconformities associated with lowered sea levels in the upper Oligocene, upper Miocene and upper Pleistocene (Haq et al., 1987; Gopala Rao et al., 1997).

1.6 Objectives of the Study

The present work utilizing all the available geophysical data sets like magnetic, gravity, multibeam and geochronological results, is focussed on understanding the evolution of the Ninetyeast Ridge, interactions between mid-ocean ridge and mantle plume activities and role of the ridge structure in the diffuse deformation zone of the Indian Ocean. The main objectives are:

i. Age determination of the oceanic crust on either side of the Ninetyeast Ridge through identification of seafloor spreading magnetic lineations.
ii. Using identified magnetic pattern, assign probable ages for the oceanic crust lying underneath the Ninetyeast Ridge and compare with the chronological ages of the ridge, thereby investigate the interactions between Kerguelen hotspot and spreading centres.
iii. To determine the influence of hotspot migration and absolute plate motion on stretch and paleolatitudes of the Ninetyeast Ridge.
iv. Analysis of the intraplate deformation and the magnetic response of the ridge from seismic, multibeam and magnetic data available in six close grids over the ridge.

Tectonic setting of Ninetyeast Ridge and geophysical studies on the ridge till date are discussed in chapter 2. Methods followed are discussed in chapter 3. Magnetic anomaly identifications and results follow in chapters 4 and 5. Chapter 6 is on seismic reflection

data interpretation in terms of deformation stress pattern along the ridge. Chapter 7 conclude the results.

Chapter 2

2 Structure and Tectonics of the Ninetyeast Ridge

2.1 Introduction

The Ninetyeast Ridge, one of the longest, linear, age-progressive seamount chains on the Earth extends ~5600 km in N–S direction along the 90°E meridian from the Bay of Bengal (17°N) to almost near the Southeast Indian Ridge (34°S) (Figure 2.1). Northern most part of the ridge from 10°N to 17° N in the Bay of Bengal region is entirely buried under thick Bengal Fan sediments as evidenced by seismic reflection data (Curray et al., 1982; Gopala Rao et al., 1997; Michael and Krishna, 2011), and the southern tip of the ridge intersects the E-W trending Broken Ridge. It was also reported that the ridge structure is converging upon the Andaman trench at around 17°N (Subrahmanyam et al., 2008). The ridge has an average width of 200 km and elevation of more than 2 km (Sclater and Fisher, 1974; Fisher et al., 1982; Krishna et al., 1995, 2001a). The ridge is a geographical boundary, in the Bay of Bengal and equatorial regions separating the Bengal Fan from the Nicobar Fan and farther south between Central Indian Basin and Wharton Basin.

It is widely accepted that the ridge is emplaced as a volcanic trace of the Kerguelen mantle plume (hotspot) on the northward-drifting Indian plate between ~85 and 42 Ma. The ridge is also unique because the feature is located within a diffuse deformation zone between three sub-plates, Indian, Australian and Capricorn and is associated with seismicity (Royer and Gordon, 1997; Gordon et al., 1998; Sager et al., 2010). The presence of the Ninetyeast Ridge in the Indian Ocean was first reported by Th. Stocks in 1960. Subsequently a comprehensive picture of the ocean floor emerged from the compilation of depth soundings made during the International Indian Ocean Expedition (1960–65), which emphasized the presence of this long, linear, aseismic ridge in the Indian Ocean (Bezrukov and Kanaev, 1963; Heezen and Tharp, 1965).

Structurally the ridge flanks are asymmetric in cross-section at many locations. The eastern flank between 11°S and 21°S is deeper by ~1 km (Udintsev, 1975; Fisher et al., 1982; Krishna et al., 2001a), compared to the western flank, flat topped at some locations, fractured and mountainous at other, but existing as a more or less continuous seamount chain (Figure 2.1).

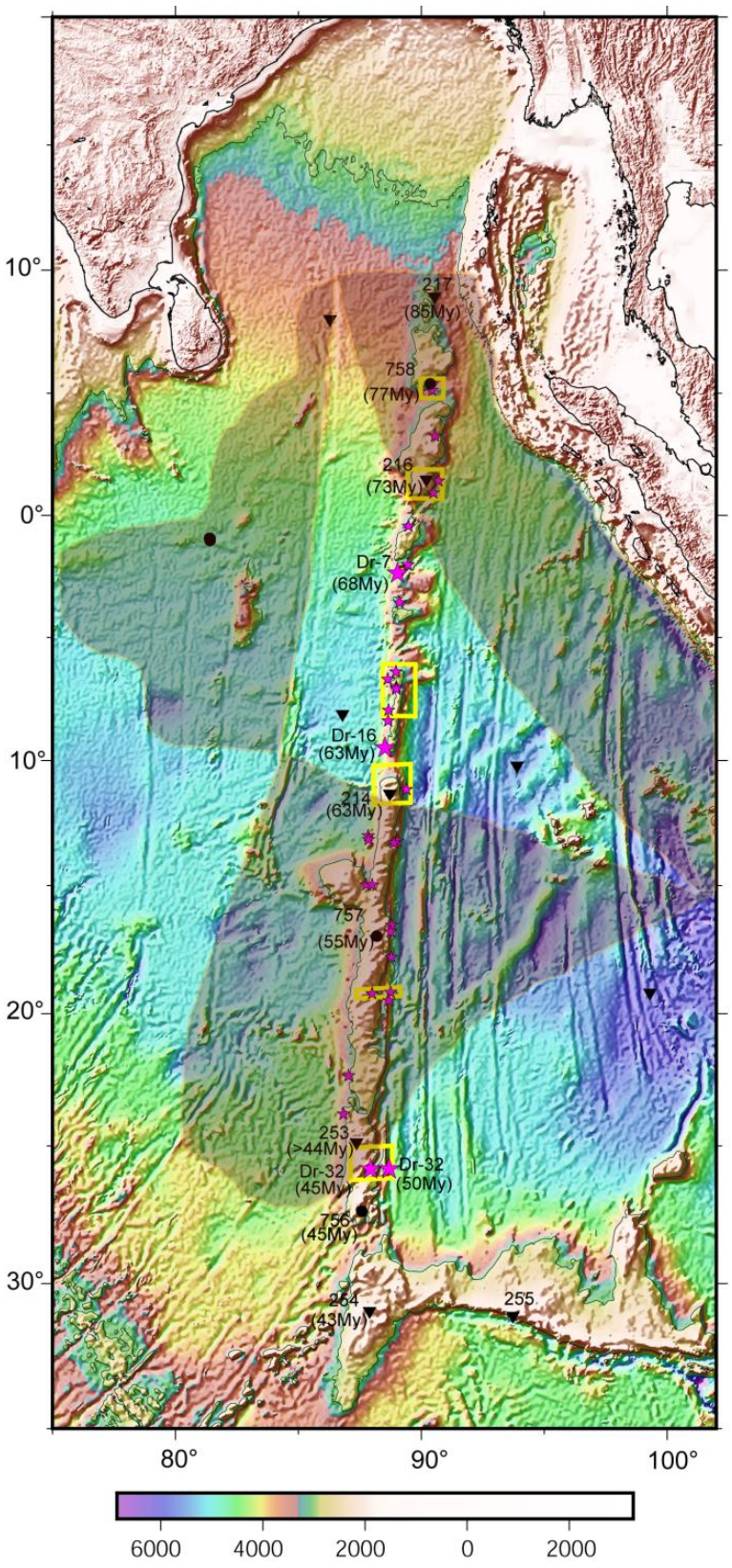

Figure 2.1: Bathymetric map of Ninetyeast Ridge with ODP (black solid circles) and DSDP (black solid triangles) sites annotated with chronology data. Shaded area and the triangular area within mark the diffused plate boundaries and diffused triple junction respectively (Royer and Gordon, 1997). Yellow boxes - grid sites, magenta solid stars - dredge sites of KNOX06RR cruise.

Between the latitudes 7°S and 10°N the ridge segment appears to be a complex of en echelon blocks of individual topographic highs, with northeast-southwest elongation. South of 7°S the ridge is a flat topped and further south as a narrow feature steeply scarping on its eastern flank by a fracture zone.

Geoscientists were curious about the origin of this dominant bathymetric feature in the Indian Ocean, and proposed many hypotheses for its origin based on its morphology details available till then, for example, a micro-continent (Heezen and Tharp, 1966), a transform fault associated with plate reorganisation (Mckenzie and Sclater, 1971) and many others. The results of Legs 22 and 26 of the Deep Sea Drilling Project (DSDP) (1974), Leg 121 of the Ocean Drilling Program (ODP) (1989) and the associated geophysical surveys have helped to establish that the Ninetyeast Ridge was originated from the Kerguelen mantle plume (Morgan, 1972, 1981; Peirce, 1978; Duncan, 1978, 1981; Curray et al., 1982). Paleomagnetic, petrological and geochronological data of the ridge suggested that the volcanic source was located beneath the northward-moving Indian plate from the late Cretaceous to the early Cenozoic period (Duncan, 1991; Klootwijk et al., 1991; Royer et al., 1991).

The studies of crustal structure and isostacy of the ridge were also supporting its hotspot origin with interactions with spreading ridge (Bowin, 1973; Detrick and Watts, 1979; Grevemeyer and Flueh, 2000; Krishna et al., 2001a; Tiwari, 2003; Sreejith and Krishna, 2013, 2015). Later TIOG (Trans Indian Ocean Geotraverse) magnetic surveys on adjacent basins of the Ninetyeast Ridge (Krishna et al., 1995, 1999), and recent KNOX06RR cruise over the ridge collecting high resolution geophysical data and basaltic dredge samples have further improved understanding of the ridge evolution (Krishna et al., 2012), northward progression of geochronology data (Pringle et al., 2007, 2008) and ongoing crustal deformation in response to active intraplate deformation of northeastern Indian Ocean since Neogene time (Sager et al., 2010, 2013).

The geophysical studies of the Ninetyeast Ridge still continue to be an important topic, mainly due to two reasons. First one is its very hotspot origin where many researchers are focussing on the implications of hotspot volcanism with plate tectonics. And secondly the on-going intraplate deformation and associated seismicity observed to be active since the Miocene in the northeastern Indian Ocean with the whole Ninetyeast Ridge is being in the

middle and act as a mechanical boundary withstanding the stress in different directions along its N-S extent. The seismicity in the area caused by this intraplate movements and role of the Ninetyeast Ridge as a bounding constraint is vigilantly monitored.

2.2 Tectonic setting of the Ninetyeast Ridge

The tectonic setting of the Ninetyeast Ridge is understood in the context of the evolutionary history of the northeastern Indian Ocean. The two major plate reorganizations of the Indian Ocean occurred at ~90 Ma and ~42 Ma, have largely contributed to restrain the position of the Kerguelen hotspot alternately beneath the Indian and Antarctic plates, respectively (Liu et al., 1983). Initially, approximately at 130 Ma, the hotspot was beneath the Antarctic plate, leading to the formation of the southern and central parts of the Kerguelen Plateau and the Broken Ridge (Coffin et al., 2002). The first major plate reorganization, at ~90 Ma, placed the hotspot beneath the Indian plate and resulted in the accretion of the world's largest linear aseismic ridge. Later (since ~42 Ma in the middle Eocene), the hotspot was again relocated beneath the Antarctic plate and has produced the northern Kerguelen Plateau, including the Kerguelen Archipelago, and Heard and McDonald Islands (Coffin et al., 2002). It is thought that during the formation of the Ninetyeast Ridge (90 - 42 Ma) the Kerguelen hotspot was mostly located north of spreading ridge-segments that were part of the western extremity of the Wharton Ridge, which separated the Indian and Australian plates and was connected to the India-Antarctica Ridge through the 86°E transform fault (Krishna et al., 1995, 1999). Concurrently with the ridge emplacement, the adjacent Wharton and Central Indian basins were also formed by the spreading of the Wharton and India-Antarctica ridges, respectively (Liu et al., 1983; Royer and Sandwell, 1989; Royer et al., 1991; Krishna et al., 1995, 1999). After the major plate reorganization at ~42 Ma, the Wharton spreading ridge has become defunct, and then the Indian and Australian plates have merged together for the formation of a single Indo-Australian plate (Liu et al., 1983; Krishna et al., 1995, 2012).

During the Neogene time, a large diffuse plate boundary has formed in the central Indian Ocean, breaking the major Indo-Australian plate into three smaller component plates - Indian, Australian, and Capricorn plates (Royer and Gordon, 1997; Gordon et al., 1998) (Figure 2.1). Almost the entire Ninetyeast Ridge resides within this zone of complex deformation. Seismic stratigraphy of the Bengal Fan sediments reveals that the lithosphere

within the boundary to the west of the ridge shows reverse faulting (5–10 km spaced faults) and long-wavelength (100–300 km) folding (Weissel et al., 1980; Bull, 1990; Chamot-Rooke et al., 1993; Krishna et al., 1998, 2001b). Subsequently using seismic stratigraphy and plate rotations, Krishna et al. (2009a) and Bull et al. (2010) have inferred that the lithospheric convergence began at 18-14 Ma within this plate boundary. Recent seismic studies of the Ninetyeast Ridge also suggested that the ridge is dissected by numerous faults and is experiencing on-going deformation activity (Sager et al., 2010, 2013). Furthermore, the ridge is thought to be a structural partition that separates different styles of deformation in the Central Indian and Wharton basins (Deplus et al., 1998; Delescluse and Chamot-Rooke, 2007).

The morphology of the Ninetyeast Ridge is complex and varies along its length (Fisher et al., 1982; Krishna et al., 1995, 2001a; Sager et al., 2010). The southern part of the ridge, south of 11°S, is tall, nearly continuous, and often highly asymmetric with a steep eastern slope and low western slope. In contrast, the ridge north of ~3°S consists of a series of mostly individual, large volcanoes with more symmetric cross-sections. In between them, the ridge is low with a combination of small linear segments and seamounts (Krishna et al., 2001a). The position of the Kerguelen hotspot with respect to the spreading centers, strike of oceanic fracture zones, plate motions, hotspot drift, variable hotspot magma output and deformation-related faults are all factors that have been implicated as controls on the morphology of the Ninetyeast Ridge.

2.3 Geophysical studies of the Ninetyeast Ridge

Various theories were postulated for the origin of Ninetyeast Ridge based on the ridge morphology, therefore a strong need was realised for detailed geophysical surveys and rock sampling from the ridge. The geophysical surveys carried out during the DSDP and ODP drilling over the Ninetyeast Ridge and adjacent Central Indian and Wharton basins and drill well results had expanded understanding on tectonic setting of the ridge and adjacent oceanic basins in terms of seafloor bathymetry and morphological intricacies (Sclater and Fisher, 1974; Udintsev, 1975; Fisher et al., 1982), crustal structure of the ridge and its isostatic behaviour (Bowin, 1973; Detrick and Watts, 1979, Grevemeyer and Flueh, 2000; Krishna et al., 2001a), sedimentation pattern and seismic stratigraphy (DSDP and ODP Shipboard Scientific Party), and seafloor spreading process on either side of the ridge (McKenzie and Sclater, 1971; Sclater and Fisher, 1974; Sclater et al., 1976; Royer and

Schlich, 1988; Liu et al., 1983; Geller et al.,1983; Patriat, 1987; Royer et al., 1991). The inferences derived from the geophysical analysis are consistent with geochronology, paleontology, petrology, paleolatitudes, and geochemistry of the basaltic rocks and overlying sediments of the ridge, advocating its volcanic origin from the Kerguelen hotspot and complex interaction with E-W Wharton spreading ridge (Peirce, 1978; Peirce et al., 1989; Royer et al., 1991). Lack of ship-borne magnetic anomaly data on immediate west and east of the Ninetyeast Ridge was a major constraint in studying the hotspot-spreading ridge interaction mechanisms in detail. The TIOG (Trans Indian Ocean Geotraverse) magnetic profiles collected in early 1990s in the Central Indian Basin, Wharton Basin and over the Ninetyeast Ridge as well on the Osborne Knoll could refine the Wharton spreading ridge dynamics near the Kerguelen hotspot with a postulation of frequent southward ridge jumps and on-spreading axis volcanism (Krishna et al., 1995, 1999).

High-resolution satellite bathymetry and free-air gravity anomaly data of the ocean floor (Sandwell and Smith, 1997), was a major advancement for geophysical studies of the Ninetyeast Ridge also. This database allowed 2D and 3D modelling of gravity flexure of the ridge to delineate its isostatic behaviour (Tiwari, 2003; Sreejith and Krishna, 2013) and precise mapping of fracture zones of the Central Indian and Wharton basins.

In 2007 an International expedition on the Ninetyeast Ridge (KNOX06RR cruise), as part of site surveys of IODP drilling, had collected high-resolution geophysical data and dredged basalt samples of the crest all along the ridge. The rock sample analysis compiling that of old DSDP and ODP core samples could reveal precise geochronology sequence along the Ninetyeast Ridge (Pringle et al., 2007, 2008). The interpretation of high resolution multibeam bathymetry and 2D reflection data collected in selected grids along the ridge depicts the original fault fabric during its emplacement and active faulting of the ridge in response to the on-going intraplate deformation (Sager et al., 2010, 2013). The compilation of new magnetic profiles with existing profile data as part of present study for identification of isochrons on either side of the ridge has modified them with more precise lateral extent by means of bounding fracture zones and has modelled the ridge hotspot interaction pattern with the help of new geochronology data of the Ninetyeast Ridge. High resolution 2D seismic reflection data and multibeam bathymetry are also analysed in the present study for analysis of fault orientations along the ridge.

2.3.1 Different hypotheses proposed for the formation of the Ninetyeast Ridge

Until the DSDP (Deep Sea Drilling Project) drilling initiated in 1972 over the Ninetyeast Ridge, many researchers have probed the ridge with meagre depth sounding observations and postulated several hypotheses for its origin such as micro-continent (Heezen and Tharp, 1966), uplifted oceanic crust like a horst structure (Udintsev,1965; Francis and Raitt, 1967; Laughton et al., 1970a), a feature resulted by convergence of two plates, when Indian plate was overriding on Australian plate (Le Pichon and Heirtztler, 1968), a locally compensated structure as free-air gravity anomaly was found low over the ridge (Bowin, 1973), as a transform fault associated with plate reorganisation during the Eocene (Mckenzie and Sclater, 1971) and even as a paleo spreading center (Veevers et al; 1971*).* Subsequently, petrological as well as paleomagnetic results of the DSDP sites confirmed its origin as volcanic emplacement (Morgan, 1972, 1981; Peirce, 1978; Duncan, 1978, 1981; Curray et al., 1982), but with different hypotheses regarding the source of volcanism including that of a fixed hotspot, like the emplacement on a leaky transform fault spreading ridge junction (Sclater and Fisher, 1974; Sclater et al; 1974), as a combination of hotspot and transform fault leaking processes (Luyendyk and Davies, 1974; Johnson et al., 1976), two hotspot origin (Luyendyk and Rennick, 1977) and excess volcanism from a fixed hotspot building the ridge progressively as the Indian plate drifted northward (Morgan, 1972, 1981; Pierce, 1978; Duncan, 1978, 1981; Curray et al., 1982). Based on the geochemical similarities of the Ninetyeast Ridge basaltic crest with that of the Kerguelen Plateau (Frey et al., 1977; Mahoney et al., 1983; Weis et al., 1987b), linearly increasing age towards north (Duncan,1978) and the fixed palaeolatitude of around 50°S, Pierce (1978) had correctly envisaged the Kerguelen hotspot as a source for emplacing the Ninetyeast Ridge. Integrative studies of ODP Legs 121,119 and 120 (1989) on Ninetyeast Ridge, Broken Ridge and Kerguelen Plateau brought consensus regarding their evolution by the Kerguelen hotspot (Duncan, 1991; Klootwijk et al., 1991; Royer et al., 1991).

2.3.2 Geophysical surveys and rock sampling over the Ninetyeast Ridge

The International Indian Ocean Expedition (IIOE) (1960-1965) was the first dedicated bathymetric survey in the Indian Ocean and over the Ninetyeast Ridge (Heezen and Tharp, 1966). Later in 1971, a part of the Ninetyeast Ridge near the equator was surveyed for acquisition of seismic, gravity and magnetic data (Bowin, 1973). Deep Sea Drilling Project (DSDP) Legs 22 and 26 have been planned in 1972 exclusively for rock sample collection

along the ridge, prior to that number of reconnaissance surveys were carried out around the proposed drill sites. Subsequently, during the 58thcruise of the RV Vityaz seismic refraction surveys were conducted in two independent polygons at 9°S and 16°S, using OBS (Ocean bottom seismometer) and also gravity and bathymetry data were collected. In 1989, ODP Leg 121 was focussed with an objective of studying the northward drift of the Indian plate from paleaomagnetic inclinations of sediment as well as rock samples (Figure 2.1). The pre-site surveys of ODP 121 by RC2708 had also collected seismic reflection, gravity and magnetic profile data near the site locations. In the early 1990s, as part of an Indo-Russian initiative, Trans Indian Ocean Geotraverse (TIOG) had collected number of magnetic profiles on and either side of the Ninetyeast Ridge. And recently in 2007, an International Expedition on the Ninetyeast Ridge was organised with its traverse spanning entire length of NER (~5°N - 25°S) for acquiring high resolution multibeam bathymetry, 48 channel seismic reflection data and magnetic profile data in six selected grids, four of them around existing DSDP (216, 214, 253), ODP (758) sites. Basaltic samples of the ridge crest were collected by dredging at 33 sites along the ridge. The 2D seismic, bathymetry and magnetic profile data of this survey are used in the present study.

2.3.2.1 Underway geophysical data

Ship-borne depth sounding, seismic refraction/reflection, gravity and magnetic profile data were acquired during the IIOE (1960-65) for mapping the seafloor features of the Indian Ocean. Later DSDP Legs 22 and 26 and ODP Leg 121 and their site surveys were conducted on and around the Ninetyeast Ridge for understanding origin of the ridge. The first attempt of the Indian Ocean plate reconstructions started using magnetic lineations and fracture zones (McKenzie and Sclater, 1971) derived from Vema-19, Circe-5 profiles and air-borne magnetic profiles of the Project Magnet of USAF (United States Air Force**).** Profile density has gradually increased with the site surveys of DSDP Legs, with magnetic surveys of RV Conrad, RV Glomar Challenger, etc., in 1972 and RC2708 and JOIDES Resolution surveys in association with ODP Legs in 1989. The Indo-Russian surveys of the Indian Ocean in early 1990s had two bilateral programmes called, viz. Trans Indian Ocean Geotraverse (TIOG) and Integrated Long-Term Programme (ILTP), which had collected several N-S magnetic profiles on either side of the Ninetyeast Ridge. The KNOX06RR survey in 2007 has acquired magnetic data over the Ninetyeast Ridge.

2.3.2.2 DSDP drill sites

The DSDP had dedicated its Legs 22 and 26 (1972) for basalt sample collection from the Ninetyeast Ridge by deep drilling with a major objective of delineating its evolution history by geochemical, petrological and paleomagnetic studies. The Leg 22 had drilled three sites: Site 217 (8.5°N), Site 216 (1.5°N) and Site 214 (11.3°S) and Leg 26 drilled the Site 253 (25.5°S). During the site surveys gravity and single channel seismic reflection data were acquired by RV Conrad during the Leg 22 and by RV Glomar Challenger during the Leg 26. The geochemistry and petrology of the collected samples were studied in detail (e.g. Heikinian, 1974, 1974b; Frey and Sung, 1974; Thompson et al., 1974) and relation with that of the Kerguelen Plateau and Broken Ridge was suggested. Paleolatitudes of all 4 sites were analysed by Pierce (1978) and basalt and sediment samples paleolatitudes were found to be between 40 - 50°S, in correlation with the Kerguelen hotspot model evolution of the ridge.

2.3.2.3 ODP drill sites

The ODP Leg 121 (1989) had drilled at three locations of the Ninetyeast Ridge with an objective of better understanding of origin and tectonic history of the ridge, to delineate its petrological relationship with the Kerguelen Plateau, documenting the northward motion of the Indian plate with better spatial and temporal resolution by studying the paleomagnetic inclinations of the sedimentary and basement rocks recovered (Pierce et al., 1988; ODP Leg 121Preliminary Report). The Leg 121 drill locations were pre-surveyed by RC2705, RC2708 and RC2707 for acquisition of geophysical data including seismic reflection. These sites together with DSDP sites on the ridge enhance the sampling density with minimum distance between two adjacent sites ~200 km and maximum as ~1400 km along the ~5600 km Ninetyeast Ridge (Figure 2.1). The geochemical, petrological and paleomagnetic inclination data of these sites brought consensus on evolution of the ridge by the Kerguelen hotspot, further constrained the northward motion of the Indian plate and tectonic setting of the Ninetyeast Ridge (Duncan, 1991; Klootwijk et al., 1991).

2.4 Seafloor spreading records in the vicinity of the Ninetyeast Ridge

In early 1970s, McKenzie and Sclater (1971) have examined the ship-borne and air-borne magnetic profile data of the Central Indian Basin, particularly close to the Ninetyeast Ridge and found that the magnetic anomalies are lineated in E-W direction. While in the eastern side of the ridge in spite of availability of numerous magnetic profiles, presence of

the Wharton Ridge was not traced. Subsequently Liu et al. (1983) and Geller et al. (1983) have identified a fossil spreading ridge with conjugate pairs of magnetic lineations in the Wharton Basin, which became extinct in the middle Eocene about chron 19 and was observed to extend from the Ninetyeast Ridge to the Sunda trench in left lateral sense. As the profile density increased in the area, E-W isochrons from 33 to 20 with right lateral offset in Central Indian Basin along with complex mirrored anomalies of two fossil ridge segments (after chrons 30 and 20) and the same sequence mirrored about fossil spreading segments (after chron 20) in the Wharton Basin, offset largely in left lateral fashion were identified (Peirce, 1978; Liu et al., 1983; Peirce et al., 1989; Royer et al., 1991; Krishna et al., 1995, 2009b; Krishna and Gopala Rao, 2000).

2.4.1 Spreading records in the Central Indian Basin

Magnetic lineations of two different trends, the E-W trending chron 34 to 20 and the N135°E trending younger sequence to the present age with a change in orientation corresponding to the middle Eocene (McKenzie and Sclater, 1971; Sclater and Fisher, 1974; Sclater et al., 1976; Patriat, 1987; Royer and Schlich, 1988) were observed in the Central Indian Basin (CIB) and on northern flank of the SEIR, the former lineations being dominant, offset by N-S trending Fracture zones. The difference in distance from anomalies 34 to 20 between the 85°E FZ and Ninetyeast Ridge compared to that west of it was noticed by Sclater and Fisher (1974) and Pierce (1978) and proposed a presence of 11° extra length of crust between these anomalies existing immediate west of the ridge, suggesting a large southward ridge jump after anomaly 30. As numerous magnetic profiles became available in subsequent years from different surveys in the area, the magnetic anomaly identifications were improved (Royer et al., 1991; Krishna et al., 1995, 2009b; Krishna and Gopala Rao, 2000). Magnetic anomaly pattern 34-20 west of the 86°E FZ (85°E FZ as per earlier nomenclature) shows a northward progression with right lateral offsets. Between 86°E FZ and 90°E FZ, complex anomaly pattern was observed with segments of two abandoned spreading ridges (ASR) after chrons < 30 and < 20 at around 2.5°N and 13.1°S, respectively (Figure 2.2). The complex ridge jumps were attributed to the hotspot influence on Wharton Ridge segments (Royer et al., 1991; Krishna et al., 1995, 1999). The identifications were carried out using geomagnetic time scale of Cenozoic (Cande and Kent, 1992). As KNOX06RR magnetic profiles became available along the ridge the scope of recompilation was realized. So in the present study new magnetic profiles are compiled with all the earlier available ship-borne profiles to improve the

anomaly identifications immediately east and west of the ridge. Geomagnetic time scale by Cande and Kent revised in 1995 is used and the extrapolation of the anomalies laterally are constrained by fracture zones delineated from satellite gravity anomaly data. The details of method followed and results are discussed in Chapters 3, 4 and 5.

2.4.2 Spreading records in the Wharton Basin

The magnetic anomalies of the Wharton Basin were baffling due to long offsets of anomalies and data gap (Liu et al., 1983; Geller et al., 1983). Increase of magnetic profiles in the basin could delineate the conjugate anomaly sequence 34 to 20 about the axis of fossil spreading ridge in left lateral succession (Royer et al., 1991; Krishna et al., 1995, 1999). Thus, the Wharton Basin is characterised by E-W trending spreading lineations similar to the Central Indian Basin, but which are largely offset in left lateral sense by N-S trending fracture zones identified at every 2° or even 1° E-W distance, so that it occurs, considerable stretch of ocean floor at its eastern end has got subducted into the Sunda trench (Figure 2.2). The oldest magnetic anomaly observed on northern part is of chron 31 near the Ninetyeast Ridge. The younger chrons till 20 are observed in sequence towards south flanking the fossil spreading ridge of chron younger than 20 followed by the mirrored anomalies till 34 progressing towards south. Anomalies are also not identified immediate east of the Ninetyeast Ridge till 11°S due to lack of suitable magnetic profiles in this area. South of 11°S between 89°E FZ and 90°E FZ the anomaly identifications are modified in this study and discussed in Chapters 4 and 5 .

2.5 Chronological data of the Ninetyeast Ridge in comparison with seafloor spreading rates

The DSDP Sites 214, 216, 254 and ODP Sites 756, 757, 758 along the Ninetyeast Ridge have provided basement ages from the studies of paleontology of basal sediments, and this revealed that the age of the ridge decreases monotonously from north to south with ~80 Ma for ODP Site 758 in the north (5°N) to ~38 Ma in the south for the DSDP Site 253 (25.5°S). These drill core samples have been re-examined along with dredge samples of KNOX06RR survey (Figure 2.1) using $^{40}Ar/^{39}Ar$ dating (Pringle et al., 2007, 2008). The determined age profile along the ridge gave linearity surprisingly even after the new samples, thus Pringle et al. (2008) had determined an emplacement rate of 118±5 km/Myr for the Ninetyeast Ridge between the northern most ODP Site 758 (77 Ma) and the southernmost site DSDP Site 253 (43 Ma) apart by ~3980 km. The length of oceanic crust

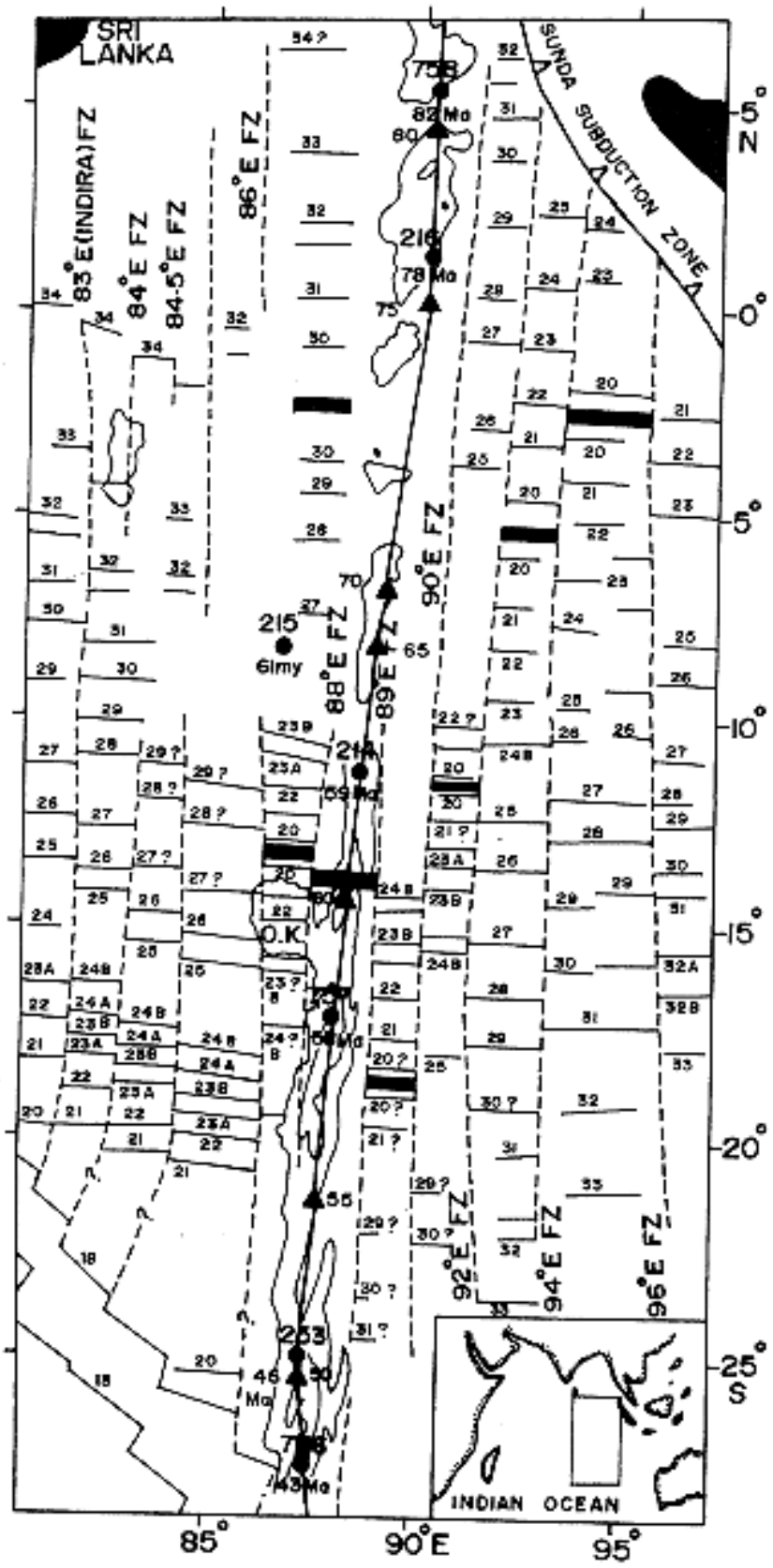

Figure 2.2: Magnetic anomaly map on adjacent basins of NER before present study (after Krishna et al., 1999).

for the same age span in the Central Indian Basin west of the 86°E FZ and east of Ninetyeast Ridge in the Wharton Basin gave a spreading rate of ~58 km/Myr, implying that the ridge emplacement rate was nearly twice the rate of seafloor spreading accretion. These are discussed in detail in Chapter 5 of this thesis report.

2.6 Elastic plate thickness (Te) of the Ninetyeast Ridge and isostatic compensation of the ridge

Isostatic study of elevated structures provide information on mechanical behaviour of underneath lithosphere at the time of crustal loading (Watts et al., 1980), which is also related to the age in the case of ocean floor. Isostatic analysis of the Ninetyeast Ridge could constrain its geological model of evolution; hence, there were many attempts in this aspect till date (Bowin, 1973; Detrick and Watts, 1989; He´bert et al., 1996; Grevemeyer and Flueh, 2000; Krishna et al., 2001a). Subsequently, advanced computing facilities gave opportunity to analyse the entire ridge track at desired intervals using spectral analysis and forward modelling of satellite gravity and bathymetry data (Tiwari et al., 2003; Sreejith and Krishna, 2013). The results of the analysis indicated average crustal thickness of ~23 km for the ridge, which is much higher than the average thickness of ~7 km for oceanic crust.

An estimation of unreasonably high crustal thickness (30-40 km) at the central part of the Ninetyeast Ridge (0-20°S) especially near the Osborne Knoll (Tiwari et al., 2003) had inferred a local compensation mechanism due to loading on young oceanic crust. Recent studies with closer intervals of satellite gravity derived profiles all along the ridge (Sreejith and Krishna, 2013, 2015) interpret that the northern part (north of 2°N) with elastic plate thickness (Te) >10 km was emplaced on intraplate setting, the southern part (south of 22°S) with Te >23 km could have emplaced on flank of the Indian plate with intermediate strength and in contrast the central part (2°N-22°S) with scattered Te values (2-22 km) might be the effect of frequent jumps of the Wharton spreading ridge due to interactions with the Kerguelen hotspot.

Magnetic anomaly data gap exist immediately west of the Ninetyeast Ridge, especially south of 15°S and immediately east of the ridge north of 14°S. On the ridge well developed anomalies are not expected due to volcanic disruptions. The ridge emplacement rate, nearly twice that of spreading rate of the Wharton spreading ridge for the same time span is a paradox especially when the Ninetyeast Ridge age is decreasing linearly

southward according all chronological sampling till date. This can be explained only by frequent, but short ridge jumps or on spreading axis emplacement. Magnetic anomaly data close to the west flank of the ridge has revealed some large ridge jumps. Existing and new anomaly data around the ridge are compiled and attempted to generate a ridge evolution model in this study and the methods, details and results are in next 3 chapters. Seismic stratigraphy at selected sites on the ridge, fault pattern and ridge deformation are discussed in 6th chapter.

Chapter 3

3 Geophysical Data and Methodology

3.1 Geophysical data investigated in the present study

For investigating the emplacement history of the long linear aseismic ridge called Ninetyeast Ridge in the eastern Indian Ocean, several geophysical data sets have been utilized in the present research work. They are enlisted below:

I. Ship-borne magnetic profile data acquired in the Central Indian Basin and Wharton Basin are extracted from all the available sources for seafloor spreading anomaly identifications.
II. Satellite derived geoid/ gravity and bathymetry data are obtained from satellite altimetry for outlining the precise locations of oceanic fracture zone as well as the ocean floor features.
III. High resolution multichannel seismic reflection data acquired during the KNOX06RR cruise in 2007 are used for seismic stratigraphy and structural analysis of the Ninetyeast Ridge.
IV. High resolution multibeam sonar data acquired during the same KNOX06RR cruise in 2007 are used for building the images of seafloor undulations and fault lineations.

These data sets are collected from various archives, then edited and processed according to the requirement of data analysis, and then used for interpretation to address the objectives.

3.1.1 Satellite bathymetry and gravity data

The invent of Satellite Altimetry has swiftly advanced the developments in the field of Earth Science, particularly seafloor topographic studies, otherwise the process of bathymetric chart preparation using ship-borne profile data is tedious and obviously less accurate. The space technology was developed in 1960s soon after the artificial satellites were launched. The ocean surface was covered, but with less track density by Seasat (Haxby, 1983) and Geosat (Sandwell and Smith, 1997) altimeters. After the ERS-1 geodetic mission (1995) the global ocean floor was able to map with spatial resolution of 1 to 12 km and gravity with 3-7 mGal (Sandwell and Smith, 1997; Smith and Sandwell, 1997). The data resolution has subsequently improved to double through retracking (Sandwell and Smith, 2009) and by compilation all existing data with higher

track density data of new altimeters installed in Cryosat-2 and Jason-1 Earth observing satellites rendering gravity data of 2 mGal accuracy and bathymetry of 1 arc minute (Sandwell et al., 2014).

Both satellite derived bathymetry and gravity data are obtained from satellite altimetry, which basically measures two-way travel time of radar signals send from them to the Earth's surface. The surface height with reference to the reference ellipsoid is the primary output (Figure 3.1). The gravity anomaly is derived from the surface slope using advanced computation methods. In the ocean floor gravity anomaly is primarily defined by topography, and the 15-200 km wavelength band is used to derive topography, with proper calibration with depth sounding data to account for regional changes of topography/ gravity ratios resulting from various factors such as sedimentation thickness and thermal effects (Smith and Sandwell, 1997).

3.1.2 Multibeam bathymetry data

Multibeam swath mapping system has been developed after World War-II for complete retrieval of seafloor image, since then research vessels have started using this technology for mapping the seafloor. Broad acoustic pulses are transmitted from the sonar transducers to the full swath across the track (Figure 3.2); the track width is generally defined by the depth to the seafloor. The depth and position of return signal are calculated from the received angle and two-way travel time. The accuracy depends on signal frequency, precision of transducer navigation and precision of sound speed in water. Multibeam system generally uses 10-500 kHZ range of frequency. Both towed and ship mounted type of multibeam systems are used for research purpose and the latter provides better navigation accuracy and flexibility as the transducers are mounted to the hull of the vessel.

High-resolution multibeam bathymetry data acquired at six selected grids over the Ninetyeast Ridge during the KNOX06RR survey are used in the present study. The research vessel Roger Revelle equipped with *Kongsberg Simrad EM120* multibeam echo-sounder was used for mapping the seafloor image in six grids of the ridge. The 12 kHz echo-sounder uses wideband, linear receiver transmitter arrays that are arranged in a Mills cross configuration on the ship's hull. The sonar electronics form 191 beams per ping in a line perpendicular to the ship’s axis. The EM120 can create a swath up to 150

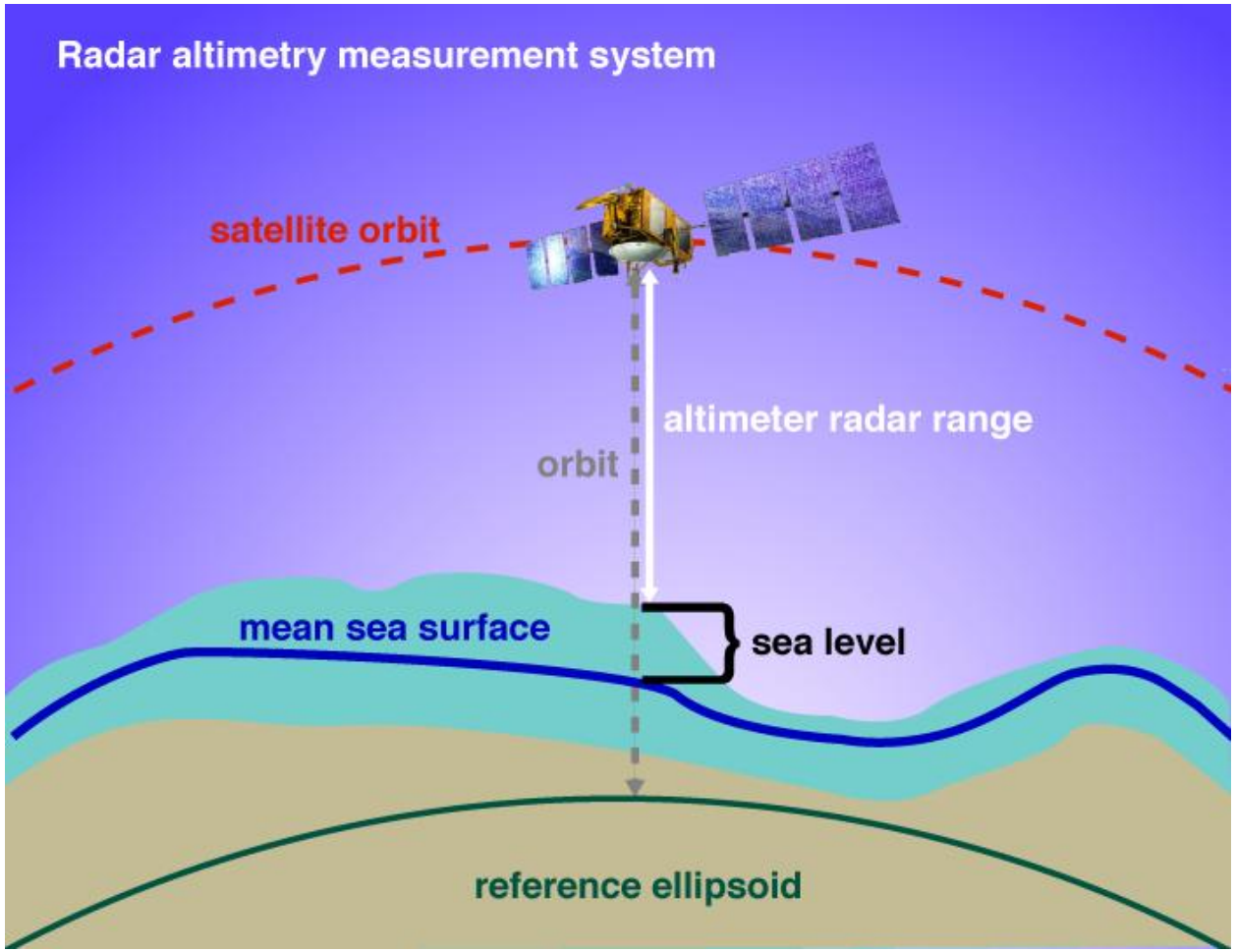

Figure 3.1: Schematic diagram showing the basic concept of satellite altimetry
(Source: http://www.star.nesdis.noaa.gov/sod/lsa/SeaLevelRise/images)

degrees wide, equivalent to 7.5 times the seafloor depth. The echo sounder achieves high accuracy independent of beam pointing angle by using a combination of phase and amplitude detection. Multibeam data were edited and processed onboard the vessel using the Mbsystem software. Corrections for variations in the sound velocity within the water column were made as the temperature structure of the water column to a depth of 1000 m at each site and these data were entered into the EM120 software (Cruise Report, KNOX06RR 2007).

3.1.3 Ship-borne magnetic profile data

Proton precession and Fluxgate magnetometers were used during the cruise for acquiring the continuous total magnetic observations. The magnetometer sensor was towed at a distance from the vessel to avoid the interference of the vessel's magnetic effect. The measured magnetic observations were corrected for Earth's main magnetic field provided by the IGRF (International Geomagnetic Reference Field).

In the present study magnetic profile segments in N-S and near N-S trend of the Central Indian Basin and Wharton Basin adjacent to the Ninetyeast Ridge are analysed. Magnetic profiles analysed in the present work are from the KNOX06RRcruise on the Ninetyeast Ridge in 2007, from ship-borne surveys of major oceanographic institutes of the world which are presently archived in National Geophysical Data Centre (NGDC), National Institute of Oceanography (NIO), database and the Trans Indian Ocean Geotraverse (TIOG) program (Figure 3.3).

3.1.3.1 Magnetic data collected during the KNOX06RR Survey

An international scientific expedition was carried out onboard R/V Roger Revelle (KNOX06RR) during the year 2007 over the Ninetyeast Ridge, wherein several researchers from different nations including India were participated. Total magnetic intensity data were continuously collected within the grid locations and as well on a track between the grids. The magnetometer used in this survey is a Marine Magnetics Sea Spy marine gradiometer with two sensors, towed 100 m apart, with the leading sensor 350 m behind the ship. The Sea Spy uses the Overhauser effect, so that it is more sensitive by two orders of magnitude than normal proton precession magnetometers. The output of both sensors was recorded to disk approximately for every second along with GPS navigation position (Cruise Report, KNOX06RR 2007). The magnetic

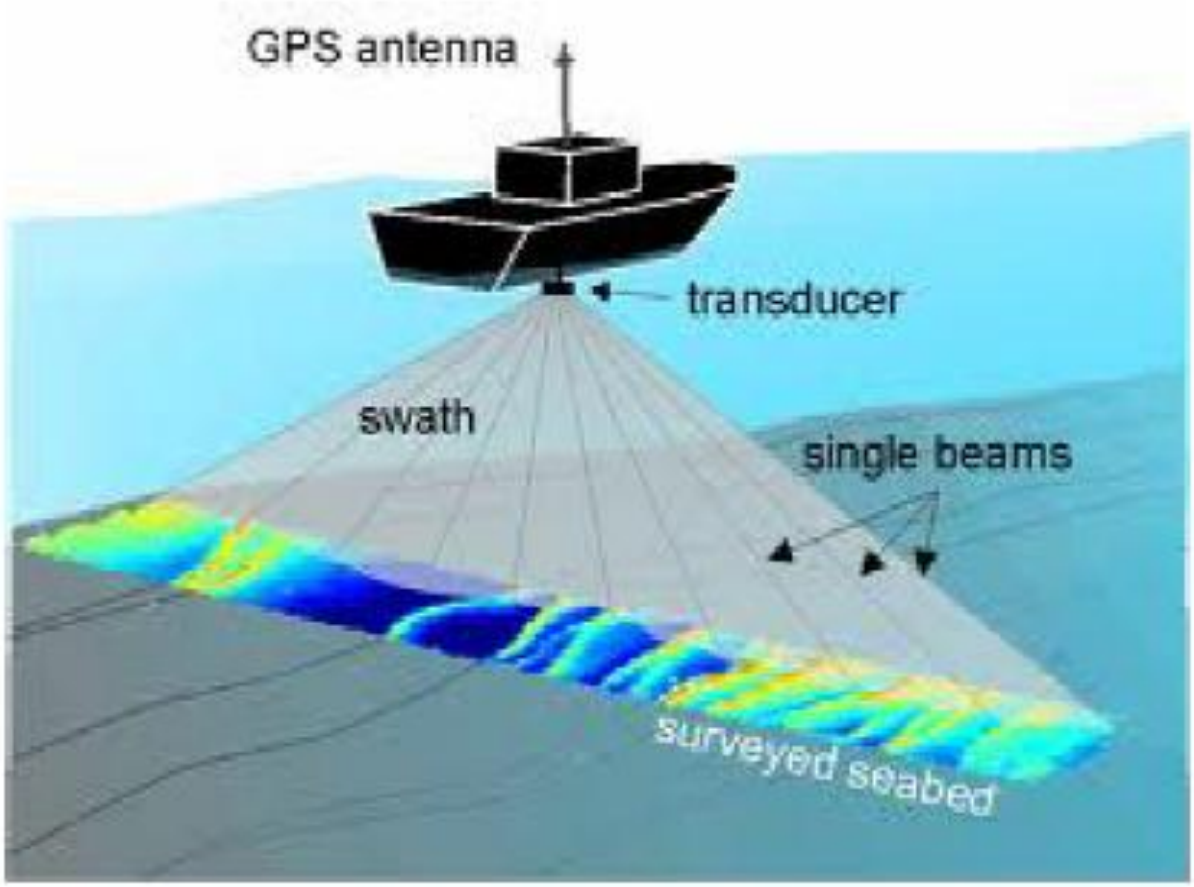

Figure 3.2: Schematic diagram showing principles of multibeam bathymetry
(Source: http://splashcos.org/sites/splashcos.org/files/2%20Multibeam.pdf)

anomalies over the ridge after corrections are found to be highly subdued and disrupted due to extensive volcanism.

3.1.3.2 TIOG Magnetic profile data

The Trans Indian Ocean Geotraverse (TIOG) project, under Indo-Russian bilateral program had acquired magnetic profile data in the central Indian Ocean between 10°S to 18°S in 1988-1989. The TIOG profiles TIOG-7 to 21, 51, 60 to 62 and constituting a total of 19 that fall in the study area are used for seafloor anomaly identifications. As these were not available in downloadable format in any archives it was digitized from the available database (Krishna et al., 1995).

3.1.3.3 NGDC Magnetic profiles

The present study further uses magnetic profiles from 22 different geophysical surveys, and 17 of them are downloaded from the National Geophysical Data Centre public archive (Figure 3.3). These surveys were carried out by research vessels of leading Oceanographic institutes of developed countries since 1960s. The details of NGDC profiles are enlisted in Table 3.1.

3.1.3.4 Magnetic Profiles from NIO database

In the northern part of the study area, total of 11 magnetic profile segments run in N-S direction are extracted from CSIR - National Institute of Oceanography (NIO) database. These data were acquired during the surveys of ORV Sagar Kanya (SK-124, SK-100 and SK-82) in north eastern Indian Ocean. The profiles fall around northern part of the Ninetyeast Ridge in the Bay of Bengal area are shown in Figure 3.3.

3.1.4 Seismic Reflection data

The seismic reflection is an efficient and widely used method for subsurface imaging of the crust and upper mantle. In multichannel marine seismic reflection surveys, an acoustic source, explosive or airgun is used as shot at regular intervals and the hydrophone array towed behind (streamer) records reflected pulses from the common mid-points in two-way travel time (Figure 3.4).

As the source receiver geometry is known, the receiver pulses are stacked with corresponding common midpoints with accurate navigation. Then the fold coverage of

reflection data is determined by number of receivers and shot used and receiver intervals. A number of processing sequences are involved from noise reduction to

Table 3.1: Details of Magnetic survey Profiles downloaded from NGDC

No.	Magnetic Profiles	Research Vessel	Data Base Source
1	CIRC05AR	R/V *Argo*	Scripps Institute of Oceanography, U S
2	CIRC03AR	R/V *Argo*	
3	LUSI7BAR	R/V *Argo*	
4	MONS03AR	R/V Argo	
5	DSDP26GC	R/V *Glomar Challenger*	
6	DSDP22GC	R/V *Glomar Challenger*	
7	INMDO6MV	R/V *Melville*	
8	ANTP11MV	R/V *Melville*	
9	ANTP12MV	R/V *Melville*	
10	84001211	R/V *Jean Chacot*	IFREMER, France
11	RC0909	R/V *Robert Conrad*	Lamont Doherty Earth Observatory, U S
12	RC1402	R/V *Robert Conrad*	
13	RC1709	R/V *Robert Conrad*	
14	C0909	R/V *Conrad*	
15	ODP121JR	*Joides Resolution*	Joint Oceanographic Institutions
16	WI34815	USNS *Wilkes*	US Navy
17	WI34907	USNS *Wilkes*	

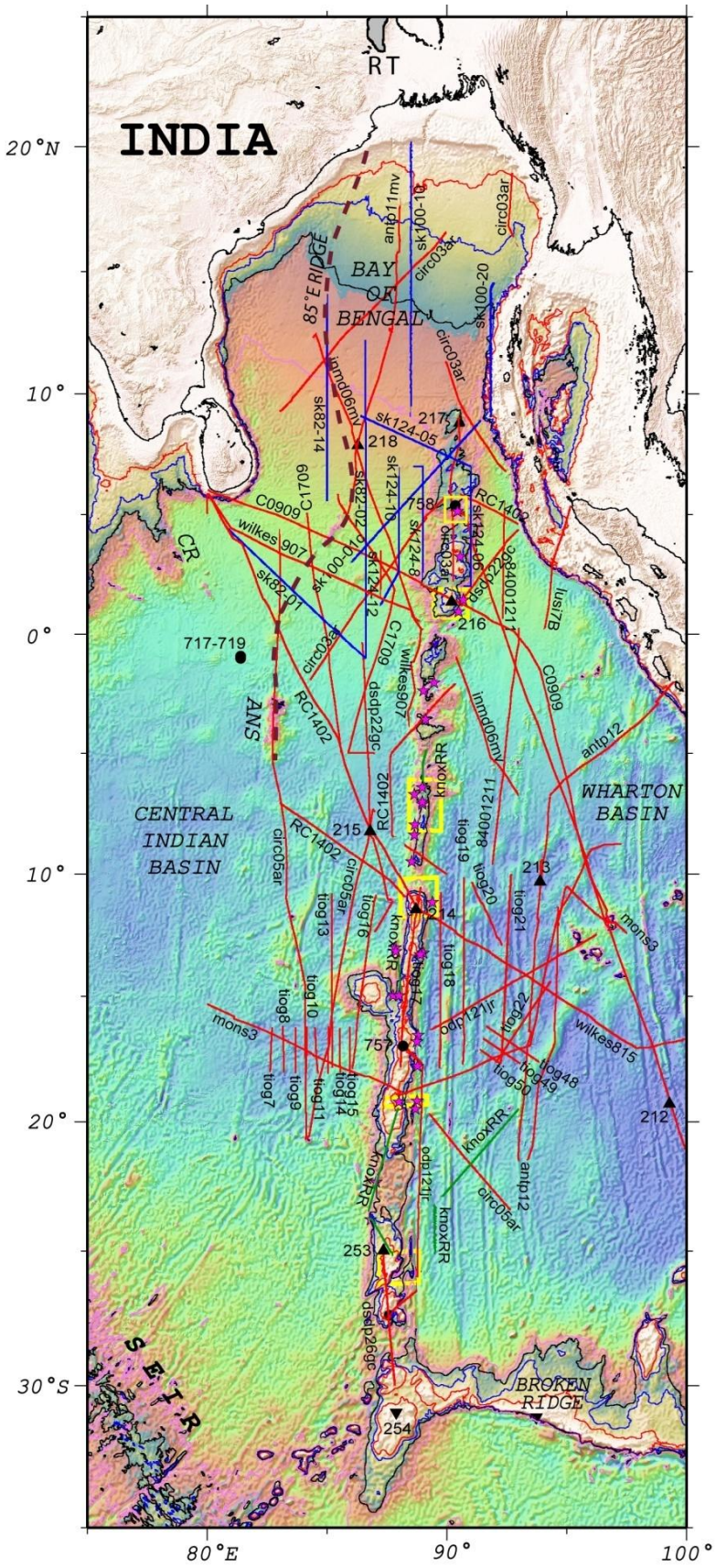

Figure 3.3: Plot of Magnetic profiles on the map of study area. Green linesKNOX06RR profiles, Red lines- NGDC profiles, Purple Lines- TIOG profiles, Blue lines- profiles from NIO data base.

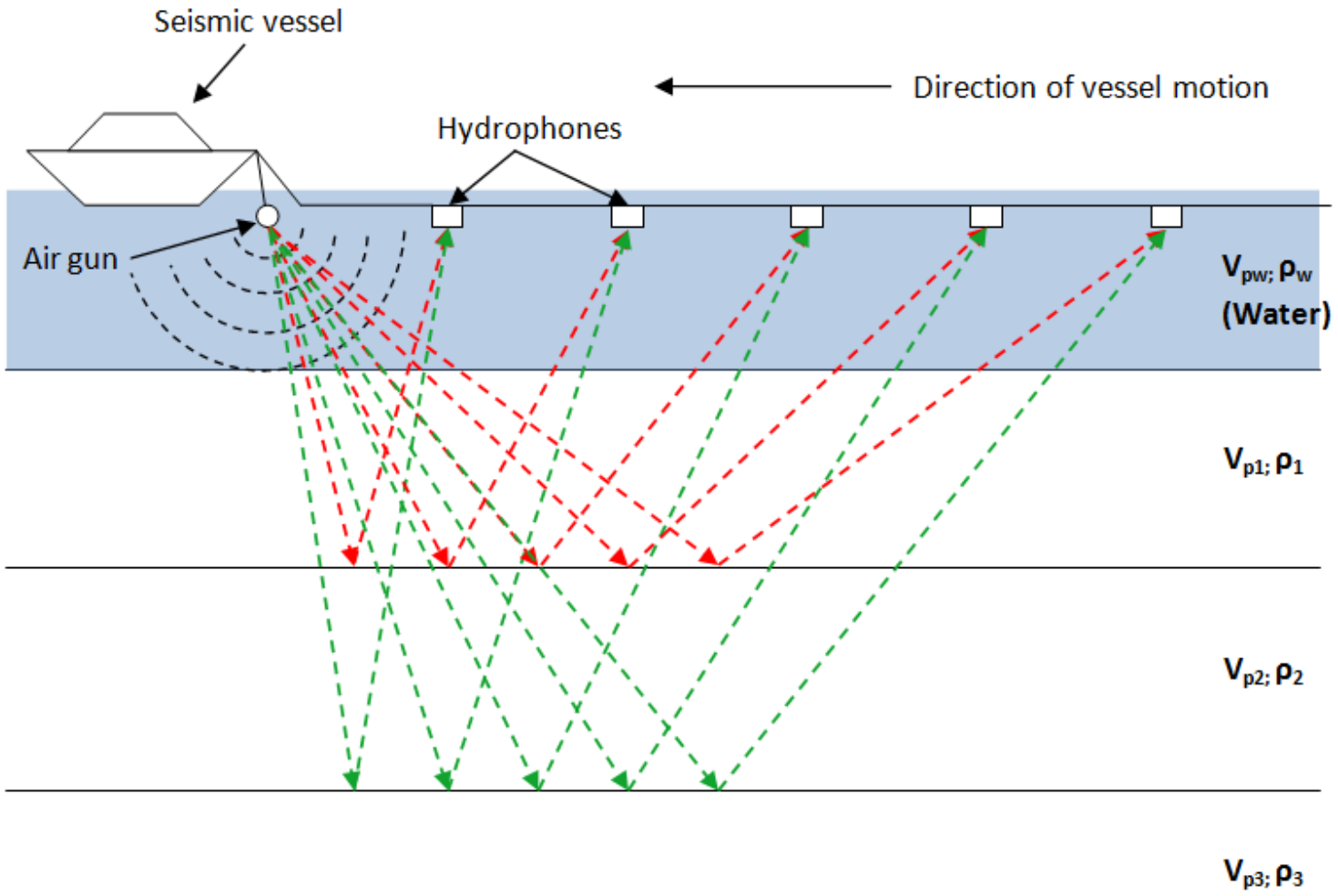

Figure 3.4: Simple schematic Figure showing marine multichannel seismic with two reflector case (Source:https://en.wikipedia.org/wiki/Reflection_seismology#/media/File:Diagram_of_a_marine_seismic_survey)

migration of signal with respect to reflector undulations, before generating the final stack of seismic traces for interpretation.

The present study uses 2D seismic reflection data collected during the KNOX06RR cruise along the Ninetyeast Ridge at six selected grid sites.

3.1.4.1 Seismic data of the Ninetyeast Ridge from KNOX06RR cruise

During the KNOX06RR cruise, 3631 line km of seismic reflection data were collected in six selected grid sites from north to south on the Ninetyeast Ridge using same configuration for all sites. The sound source was two Generator/ Injector (GI) air-guns of 45/105 in^3 volumes, respectively and the receiver was a 48-channel hydrophone array (streamer) of 12.5 m group interval. The air-guns were towed 24 m behind the stern at a depth of ~ 4 m below the sea surface. Shots were fired for every 10 seconds interval at a ship speed of 6 knots, yielding a shot point interval of 30.9 m to generate ~10 fold sub-surface coverage data, which were recorded at sampling interval of 0.5 ms. The data were processed onshore at Texas A&M University and time migrated data were kept available in NGDC digital archive. The high resolution data could image nearly 500 m sediment strata overlying the basalt flow. The data show different lithologic boundaries, different type of faults and highly deformed seismic structure of north and south part of the ridge. More details are discussed in Chapter 6.

3.1.4.2 Correlation of seismic profiles to DSDP and ODP Sites

Four out of six grid sites of KNOX06RR were surveyed around or near to the exiting DSDP and ODP Sites on the Ninetyeast Ridge. The ODP and DSDP Site surveys had seismic profiles passing through the drill locations. Hence the seismic stratigraphic results along with major lithologic boundaries and corresponding interval velocities are available in DSDP Legs 22 and 26 and ODP Leg 121 initial reports. The grids, Site 758, Site 216, Site 214 and Site 253 of KNOX06RR survey are as name indicates, around the drill locations of ODP site 758, DSDP sites 216, 214 and 253, respectively. The first three of these grids has one E-W and N-S seismic profile each passing through the well locations, so that these profiles are directly correlated at well sites, to major reflector tops identified in both KNOX06RR profile and ODP/DSDP site survey profiles. Thus, after correlating at two profiles at corresponding well sites the correlations are easily extended to all connected or crossing profiles by means of continuity and characteristic similarity. In the case of DSDP Site 253 the KNOX06RR profiles are not crossing the

drill site, but the profiles are just 50 km away from the drill site. The lithology of the sediments over the ridge crest are observed to be similar as an ooze layer on the top to a volcanic ash layer overlying the basaltic basement at the bottom with chalk and clay in between, even though the ridge has wide spatial-temporal variations from north to south. Therefore, even at sites NER2 and NER3, without nearby drilled wells, similar lithological boundaries are identified with reasonable confidence.

3.2 Methods

To investigate the evolutionary stages of the Ninetyeast Ridge as well as the northeastern Indian Ocean, magnetic anomaly data compiled and integrated from different geophysical data sets are considered as a major geophysical parameter. The seismic structure and deformation pattern of the ridge are also studied by systematic interpretation of 2D seismic reflection data interpretation for major reflectors and faults.

3.2.1 Utility of bathymetry and gravity data

The satellite bathymetry (ETOPO-2) of 2 arc minute resolution (Smith and Sandwell, 1997) and satellite free-air gravity anomaly data of 1 arc min grid (Sandwell and Smith, 1997, 2009) are used for generating base maps of topography and gravity of the study area with the help of GMT (Generic Mapping Tool) (Wessel and Smith, 1995) software. Fracture zones are delineated precisely on these maps by marking through their characteristic long linear narrow trough like features obviously seen in these bathymetry and gravity maps.

3.2.2 Utility of multibeam bathymetry data

The high resolution multibeam bathymetry data collected at all grid locations are analysed in the present study. The spatial extent of active faults appeared as narrow to wide linear troughs in multibeam data especially in northern grid locations, ODP Site 758 and DSDP Site 216. The active faults are marked in seismic profiles and overlaid on the multibeam bathymetry map along with basement contours in two-way travel time. The faults are correlated across the profiles following their similarities in type and characteristics. Scissor fault pairs of opposing and increasing throws about an axis point are also marked with the help of multibeam map.

3.2.3 Identification of isochrons from magnetic profile data

Seafloor spreading type magnetic anomalies hold their characteristic signatures in continuous succession and perpendicular to the spreading axis. The anomaly sequence is generally undisturbed except in ridge jump locations and around the intraplate volcanic regions. The anomaly lineations/ isochrons are usually found offset in the vicinity of fracture zones. The magnetic anomaly profile running perpendicular to the flank of an active or abandoned spreading axis, as the case may be, the anomaly pattern progress from younger to older chron away from the axis unless it come across with a ridge jump, when the ocean floor could consist of mirrored anomalies on opposite sides of the fossil ridge axis.

The complexities discussed above happened to be the case in the present study area, particularly on immediate west of the Ninetyeast Ridge with complex ridge jumps and their irregular anomaly patterns, so that the chron sequence progression get disrupted at short spans.

As the study area is broadly known for the presence of isochrones 34 to 20 in the Central Indian and Wharton basins, the synthetic anomaly conjugate sequences from 20 to 34 were generated about the axis of a fossil spreading ridge of age 19. The segments of magnetic profiles between the fracture zones are compared to northward progressive or southward progressive sequence to identify accurate anomaly series in succession using their characteristic signatures.

3.2.4 Seismic data acquisition and processing

Multi-channel seismic reflection profiles were acquired at seven survey grid locations on the Ninetyeast Ridge, ODP Site 758 (4.9°-5.2°N), DSDP Site 216 (0.80°-1.93˚N), Site NER2- NER3 (6.2°-8.25°S), DSDP Site 214 (10.2°-11.7°S), Site NER4 (19.1°S), and DSDP Site253 (25.1°-26.2°S) (Figure 3.3). At Site NER4 there were only two E-W profiles, but not utilized in the present work as they are not providing much information on occurrence and growth of the faults. The seismic data were recorded using a Geometrics GeoEel streamer with six active sections, each 100 m in length with 8 hydrophone groups or channels with 12 hydrophones in each channel maintaining a group interval of 12.5 m. Two identical generator/injector (GI) airguns (volumes 45/105 in^3) were used as source for generation of seismic waves. The sampling rate of digitally

recorded data was 0.5ms. The data processing was carried out at Texas A&M University with ProMax software, including geometry corrections, band pass filtering, velocity analysis, common depth point gathers, normal moveout (NMO) correction, stacking, and time migration.

3.2.5 Structural interpretation of seismic data

In seismic reflection records, prominent continuous reflectors are identified and then continued their extent all along the profile. Discontinuities/offsets of these reflectors are marked as faults. For mapping of complex geological structures such as unconformities and associated features, it needs experience and knowledge on geology of the region for effective interpretation. Features associated with unconformities like onlap, downlap, toplap or truncations can be recognized by identifying characteristic reflection patterns. Different types of faults, fold structures and even fractures can also be mapped in structural interpretation of good resolution 3D seismic data, but in the case of 2D data there are some limitations, hence interpolation and manual or computer aided contouring may be needed to generate the structural model of subsurface.

In present study, 2D seismic reflection profiles of the KNOX06RR cruise grids are interpreted for major horizons in correlation with the available DSDP and ODP drill well lithology as well as chronologic tops and faults are marked across their discontinuities. As the reflection profiles are of higher resolution the acoustic basement is easily identified on almost all the profiles of each grid site with its property of its strong seismic amplitude. Contour maps for depth to the basement in two-way travel time are prepared for all 6 grid locations, following the approach of manual interpolation between the 2D profiles for each grid with background guidance of multibeam and satellite bathymetry data, assuming that the present day bathymetry is broadly governed by the basement tectonics.

Within each grid site active faults are correlated from one profile to the other by overlaying the seismic sections on multibeam bathymetry map, so that both datasets complement each other to demarcate the deformation related features. Thus the strikes of number of active faults are obtained on each grid site. Strikes of these faults are measured on the map at regular intervals. The dips of these active faults are assumed to be higher between 80 and 85° considering the fact that faulting was initially normal, at the time of ridge formation. The values of strikes and dips are randomised between

minimum and maximum value to make nearly 30 pairs of observation per each fault in order to plot in stereonet as fault planes. Rose diagram is generated for each site with the help of stereonet software.

3.2.6 Seismic Stratigraphy

In seismic stratigraphy the interpreted seismic reflectors are correlated to drilled well chronology data, so that deposition history can be interpreted. More over seismic stratigraphy enable inferences on sediment thickness and depositional environment, burial history, paleobathymetry, paleogeography, geological history, correlation of unconformities with regional tectonic events, etc.

The sediment section within each grid location is interpreted for major lithologic reflectors, and then correlated to available drill well lithological information and geochronology for studying the evolutionary history and deformation pattern of the sediments as well basement of the ridge. The chronology data of the basement and overlying sediment deposit at each drill sites are correlated to the interpreted basement and sediment boundaries of the seismic data. This helped in analysing the fault mechanisms with age constraint over the Ninetyeast Ridge. The displacements of reflectors at suitable fault planes are measured in time and converted them to depth using appropriate interval velocities. The relative displacement with respect to the basement is noted to approximate the onset of major faulting or fault reactivation. Active faults are identified when the faults are seen continuing till near the water bottom. The lithostratigraphy changes across the sites are analysed with decrease in age from north to south.

3.3 Data editing requirements

Magnetic and seismic reflection data are needed to be edited before proceeding to modelling, analysis and interpretation. C++ codes are developed for extracting N-S magnetic profile data in desired format. Excel spread sheet is used for minor editing and preliminary data analysis. Seismic data in SEGY headers are edited using free seismic data editing tools.

3.3.1 Magnetic profile data

The marine magnetic profile data downloaded from the NGDC database and the KNOX06RR database are available in MGD77 (marine geophysical data exchange

format) format. Codes developed in C++ are used to extract latitude, longitude and anomaly data from each survey files. All available survey files are subsequently analysed in Excel spread sheets for selecting north-south segments. Geomag (Ver.6.1) a source code C program by NGDC is used for IGRF reduction for KNOX06RR total magnetic intensity profiles. Then extracted N-S segments are plotted using GMT software on background of satellite free-air gravity anomaly map with marked fracture zones for identification of magnetic isochrons.

3.3.2 Seismic reflection data

Processed 2D seismic reflection profile data of KNOX06RR survey were available in SEGY format with latitude and longitude at the byte locations for coordinates. The OpendTect software used for interpretation accepts only X, Y coordinates in meters, so that the SEGY header of each profile file was edited to change the coordinates at corresponding byte locations. This is done by a freely available seismic tool kit for SEGY header editing. After interpretation the smoothed reflector corresponding to the top of basalt flow is exported converted back to latitude longitude coordinates for plotting over multibeam bathymetric map to manually contour basement two-way travel time.

3.4 Algorithms and softwares used for modelling and interpretation

Different algorithms and software are used for magnetic anomaly modelling and identifications, and seismic data interpretation.

3.4.1 The MODMAG Algorithm for generation of synthetic magnetic model profile

The MODMAG an algorithm developed by Mendel et al. (2005) is mainly utilised for seafloor spreading related magnetic anomaly forward modelling. It is a set of scripts and functions written for use with the MATLAB software. The user interface of the program have options to feed full spreading rates against geological ages, percentage of asymmetry of spreading, width of ridge jump and parameter files of the profile as well as geological time scale to be used. Spreading direction, magnetic inclination and declination of the main field of the location, source layer characteristics such as thickness, depth to the magnetic layer and profile characteristics for its axis point can be

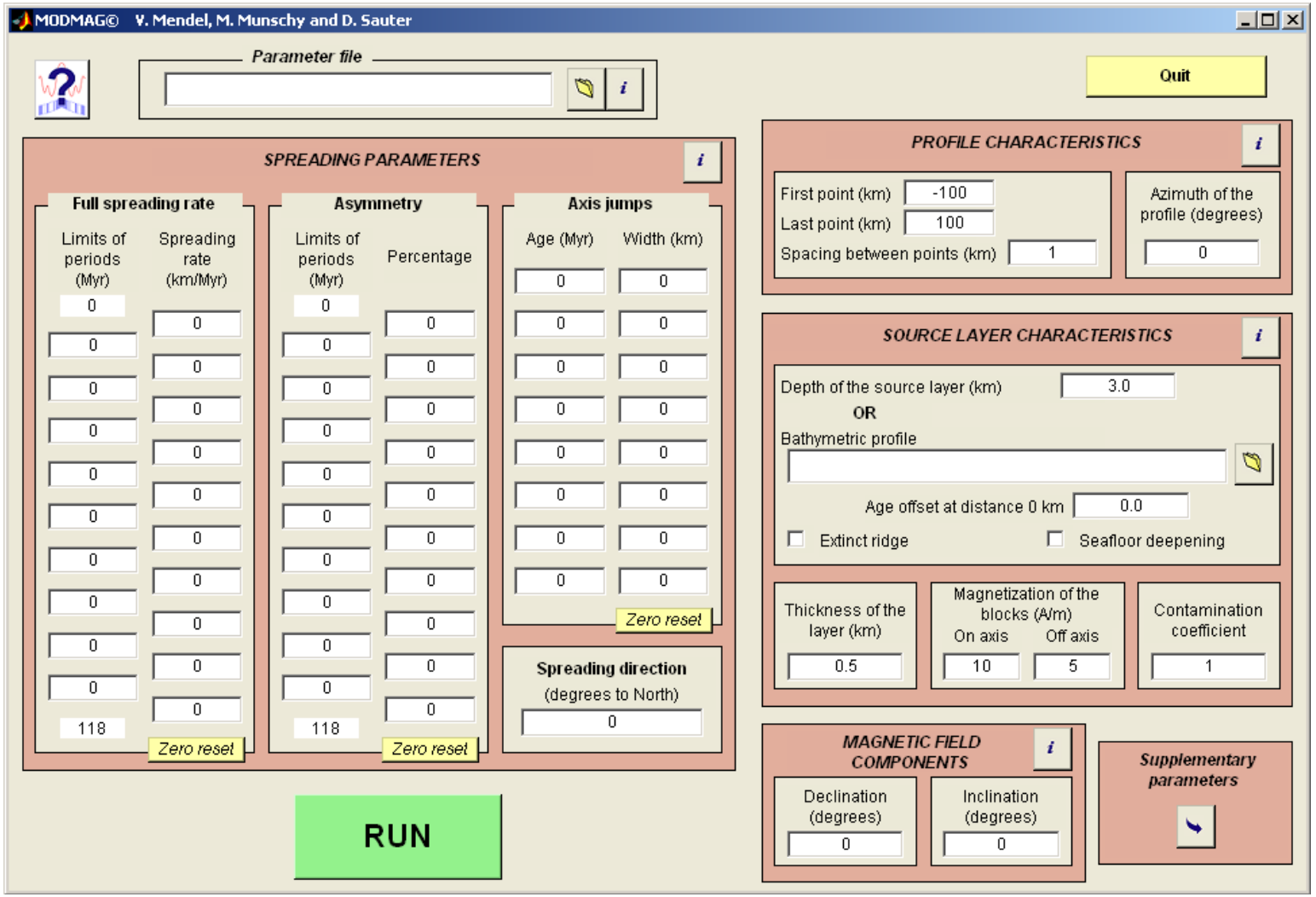

Figure 3.5: User interface of MODMAG program

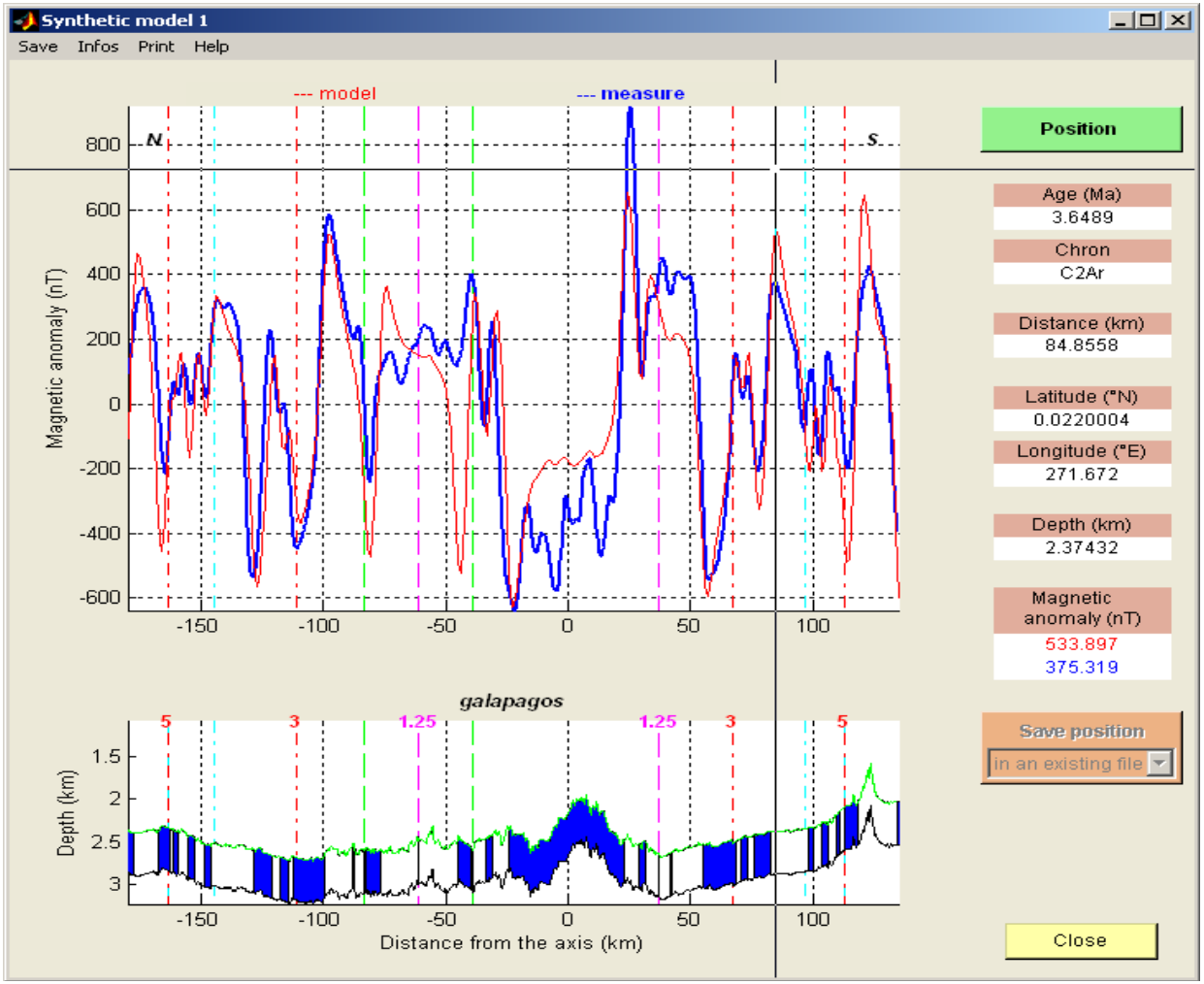

Figure 3.6: Output display of forward modelling using MODMAG program

considered as constants (Figure 3.5). When the script is run after feeding the parameters, the output of forward modelling of the anomaly with respect to given spreading rates, asymmetry percentage of spreading on either side of the spreading centre incorporating the axis jump towards north (positive width) or south (negative width), if provided, is displayed according to the given inputs. The synthetic anomalies generated with same spreading rate are displayed on the background (Figure 3.6). The input parameters of age and spreading rates can be changed iteratively until good correlation between the synthetic and observed profile is obtained.

For modelling the anomalies of the present study area, the Cenozoic time scale of Cande and Kent (1995) is used in the MODMAG algorithm. A Synthetic anomaly profile generated for the period late Cretaceous to middle Eocene (chrons 34 to 19) is used for comparison with the observed magnetic anomaly profiles, particularly the shapes and characters of the anomalies for identification of seafloor spreading sequences.

3.4.2 The OpenDtect software for seismic interpretation

OpenDtect 5.0 is free open source seismic interpretation software provided by dGB Earth Sciences (Beheer, 2013). This is used in present seismic studies for horizon and fault interpretations on all 2D reflection profiles acquired in six grid locations on the Ninetyeast Ridge. The 2D seismic data for each grid site was loaded as single project for interpretation. The software has inbuilt basic interpretation facilities like auto interpolation between picked seeds using similarity of trace amplitude selected at minimum or maximum as fixed by the interpreter, smoothening and interpolation of picked horizons, manual fault identification to put fault stick sets, etc. The interpreted horizons and fault data are exportable to other platforms for the purpose of presentation and interpretations.

3.4.3 Stereonet software for fault mapping

An updated version of Stereonet (version 8) software developed by Allmendinger et al. (2012) and Cardozo and Allmendinger (2013) is used for mapping of faults trends at each grid site. It is a freeware and is easily downloadable from the public domain for the analysis of the faults. The strike of faults measured along fault plane correlated between profiles and dips between 80-85° are randomised to obtain around 30

observations for each fault. These values of strike and dip for all faults of each grid site are populated to the software as a single file as fault planes with dip quadrant of individual faults as third parameter to generate the stereonet plot of the site. The orientation of the fault planes changes according to the strikes of faults present in the site. The software has option to plot the rose diagram of faults, which is nothing but a circular histogram, representing the frequency of fault trends along the azimuths.

Analysis of magnetic and gravity data sets discussed in this chapter are detailed in chapter 4. Chapter 5 discusses the inferences of magnetic anomaly observations. Chapter 6 exclusively describes the seismic reflection data analysis and results.

Chapter 4

4 Generation of Synthetic Magnetic Model Profiles and Correlation to observed Magnetic Profile data

4.1 Introduction

Understanding of evolution of ocean basins, particularly their temporal development has become possible after discovering the presence of Earth's past magnetic field and polarity changes within the basaltic rocks of the oceans. The magnetic fields discovered in the oceans are found as linear alternate normal and reversal bands parallel to the mid-ocean ridge system. The lava material that comes out from the rift-valley of the mid-ocean ridges undergoes through the Curie temperature, then at this point of time the solidified rocks acquire Earth's prevalent magnetic field and retain it as remanent magnetisation. As the Earth had changed its magnetic polarity several times in geological past with irregular intervals and recorded in the oceanic rocks, seafloor spreading records for the corresponding ages reveal the evolutionary history of oceans and drift of continents as well. Magnetic anomaly profiles perpendicular to the geometry of spreading axis delineate these documented fields of normal and reversals as continuous sequence of magnetic anomalies with specific characteristics associated with a specific chronology. Vine and Mathews (1963) were the first researchers to propose the synchronised magnetic lineations of ocean floor with geomagnetic reversals and seafloor spreading rates by a simple crustal block model parallel to mid-ocean ridges which is the fundamental hypothesis that paved the way to creation of geomagnetic time scales of whole Cenozoic and Mesozoic periods, reconstructions of plates and eventually to establish the theory of Plate Tectonics.

The study of evolution of the Indian Ocean has begun since the International Indian Ocean Expedition (IIOE) (McKenzie and Sclater, 1971; Fisher and Sclater, 1974; Bergh, 1977; Norton and Sclater, 1979; Liu et al., 1983; Patriat, 1983; Veevers, 1986; Royer et al., 1992) and provided three phases of spreading process following the general trends of magnetic isochrons. The evolution of the Ninetyeast Ridge in northeastern Indian Ocean has also been investigated with the help of magnetic anomaly data of the regions on either side of the ridge (Royer et al., 1991; Krishna et al., 1995) and geochronology data available for the DSDP and ODP drill sites (Pierce et al., 1989; Pringle et al., 2008). In the present study ship-borne magnetic anomaly profile data from the basinal regions adjacent to the Ninetyeast Ridge are analysed to

determine the precise magnetic pattern, and then compared with the synthetic magnetic anomaly profiles generated using geomagnetic time scale for Cenozoic period (Cande and Kent, 1995). Thus, the magnetic anomaly identifications constrained by precise locations of fracture zones led to better understanding of the Ninetyeast Ridge emplacement and interactions between the Kerguelen hotspot and Wharton spreading ridge and probable frequent ridge jumps towards the hotspot.

4.2 Geomagnetic Field and Reversals

The Earth's magnetic field is a vector with magnitude and direction, which has flipped its polarity many times in the geologic past with irregular periodicity. It is a weak dipole field through the centre of the Earth with the magnitude of the order of nano Tesla (10^{-9}T), maximum at poles and minimum at equator and presently inclined at an angle of ~5° to the Earth's axis of rotation. The main magnetic field of the Earth can be sensed by a freely hung steel needle at its center of gravity, in the absence of any other field it orients along the total field (F) at an angle D (Declination) with geographic north in horizontal plane and angle I (Inclination) with vertical plane, so that it can be resolved into X, Y and Z components (Figure 4.1). From modelling of the conductivity, temperature parameters of the Earth's liquid outer core, it is assumed that the Earth's main magnetic field is originated due to the rotation of charged core material with high electrical conductivity, as an induced magnetic field from the fluid geodynamo, ultimately caused by thermal convections in outer core. The dipole of the Earth's magnetic field is found to interchange or flip the sense of polarity during the geologic period; the change is termed as Earth’s magnetic reversals. Even though these polarity changes are not a repeatable periodical function, the observations points that, the long intervals of normal or reversed polarity (polarity epochs) typically last for 50 ka to 5 Ma and the short duration polarity changes last for 20-50 ka in between, as interruptions. Despite these the departures of magnetic poles largely from geographic polar region to even equatorial region at times, which return back to the pre-locations without resulting in a reversal, are called excursions, which may last for less than 10 ka (Lowrie, 2007).

4.3 Geomagnetic polarity time scale

The geomagnetic time scale was developed after calibration of seafloor spreading magnetic anomalies with the geochronology data and the scale has been in continuous

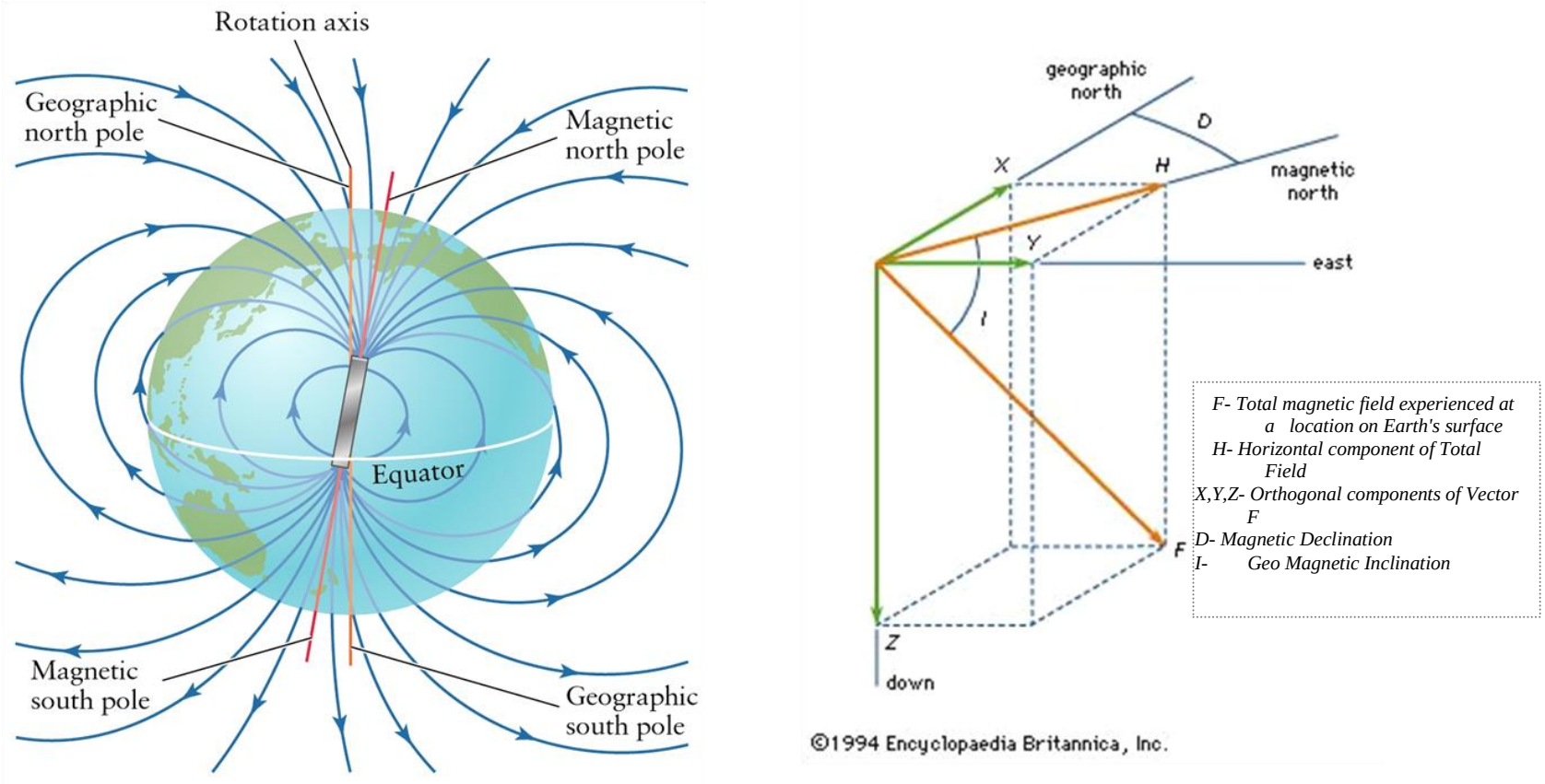

Figure 4.1: Schematic figure of Earth's geomagnetic dipole field and its major Elements
(Source: https://www.patana.ac.th/secondary/science/anrophysics/ntopic6/images/magnetic_field_earth.jpg)

improvement with addition of new datings. Using paleomagnetic studies of lava flows, the French Scientists, P. David and B. Brunhes (during 1904 - 1906) were the first to demonstrate that the geomagnetic field has changed its polarity in the past. In 1929, a Japanese Scientist M. Matuyama was the first to associate magnetic polarity of lavas to their stratigraphic ages in Tertiary. During the investigations of ocean basins, magnetostratigraphy of sediments and volcanic rocks by radiometric dating were established and magnetic anomalies of the ocean floor as alternate bands of positive and negative polarities were noticed (Heezen et al., 1953; Keen, 1963; Vine and Mathews, 1963). These observations provided sufficient supporting data to establish the geomagnetic polarity time scale with better accuracy.

Several geomagnetic time scales were evolved from paleomagnetic observations of volcanic rocks on land and magnetostratigraphic analysis of marine sediment cores with radiometric datings (Cox et al., 1963a, b, 1964, 1968; Doel and Darlymple, 1966; McDougall and Chamlaun, 1966). Pitman and Heirtzler (1966) could generate a time scale till 10 Ma based on marine magnetic anomalies across the Pacific-Antarctic Ridge and synthetic magnetic profile was calibrated according to Vine and Mathews (1963) concept with radiometric dating. Subsequently researchers utilized the seafloor spreading magnetic anomalies for expanding the geomagnetic time scale (Vine, 1968; Heirtzler et al., 1968). The geomagnetic polarity time scale for the period up to the late Cretaceous (80 Ma) proposed by Heirtzler (1968) was substantially modified with the consideration of new magnetic anomaly identifications of the world oceans (Talwani et al., 1971; Larson and Pitman, 1972; Blakely, 1974; Klitgord et al., 1975; Cande and Kristofferson, 1977), subsequently the revised time scale was published by LaBrecque et al. (1977). Deep sea sediment cores recovered from the DSDP Legs had given an opportunity for direct correlation between biostratigraphic ages and magnetic polarities of sediment strata for the entire Cenozoic period (Poore et al., 1982, 1983). The integrated approach for calibration of the polarities with radiometric and biostratigraphic chronologies had improved the accuracy of the Cenozoic polarity time scale (Ryan, 1974; Alwarez, 1981; Bergren et al., 1985). This was further updated by Cande and Kent (1992) considering the relative widths of magnetic polarity intervals from the marine magnetic profile data for entire late Cretaceous and Cenozoic, which was subsequently revised with new isotopic ages at Cretaceous-Palaeogene boundary and Pliocene (Cande and Kent,1995). The resolution of this geomagnetic time scale for

the late Cretaceous to Cenozoic is 1 kyr and the anomalies are numbered as C1 to C34 with normal, reversals and subchrons (Figure 4.2).

Generating a geomagnetic time scale for the Mesozoic period is a challenging task as the ocean floor holds magnetic anomalies only to Callovian in Jurassic (~165 Ma) as the older oceanic crust disappeared due to the subduction at convergent boundaries. Another major difficulty is assigning age to the middle Cretaceous oceanic crust as magnetic anomalies of these period (after anomaly C33r, ~ 83Ma) lack signatures due to a long magnetic normal period. Subsequently, Gradstein et al. (1994) had proposed a Mesozoic time scale extending back to 250 Ma with age estimates and error limits of few million years for each chron in the series, which involved integration of identifications by many researchers (Steiner et al., 1986; Handschtanacher et al., 1988; Channell et al., 1990; Ogg et al., 1991b) and geological as well as mathematical interpolations. Magnetic anomalies till the Callovian age (165 Ma) are annotated as M1 to M39 and the older polarity alternations are unnamed (Handschtanacheret al., 1988; Gradstein et al., 1994).

In the present study the revised time scale for the Cenozoic period (Cande and Kent, 1995) is used for forward modelling of magnetic anomaly identifications (Figure 4.2). In the present study the Cenozoic anomalies are often referred with their numbers excluding the letter C, as Mesozoic sequences (M-series) of anomalies are not dealt with, in the isochron identifications.

4.4 Magnetic lineation pattern of the ocean floor

The oceanic crust has a vertically stratified structure of two main layers as evidenced by the seismic data. On top of it, a thin cover (more in sedimentary fan regions) of slowly accumulating marine sediments constitutes Layer 1. Upper part of the oceanic crust Layer 2 is termed as Layer 2A which is strongly magnetic and mainly responsible for strong magnetic anomalies observed on ocean floor. Below is the Layer 2B weakly magnetic metamorphosed basalts contribute towards anomaly signatures, but the deeper gabbroic Layer 3 is sufficiently magnetic that adds to the skewness of the measured magnetic anomalies (Lowrie, 2007).

The magnetic anomaly pattern of the oceanic crust lie on either side of the spreading ridge is roughly in parallel trend to the ridge system as a sequence of alternating

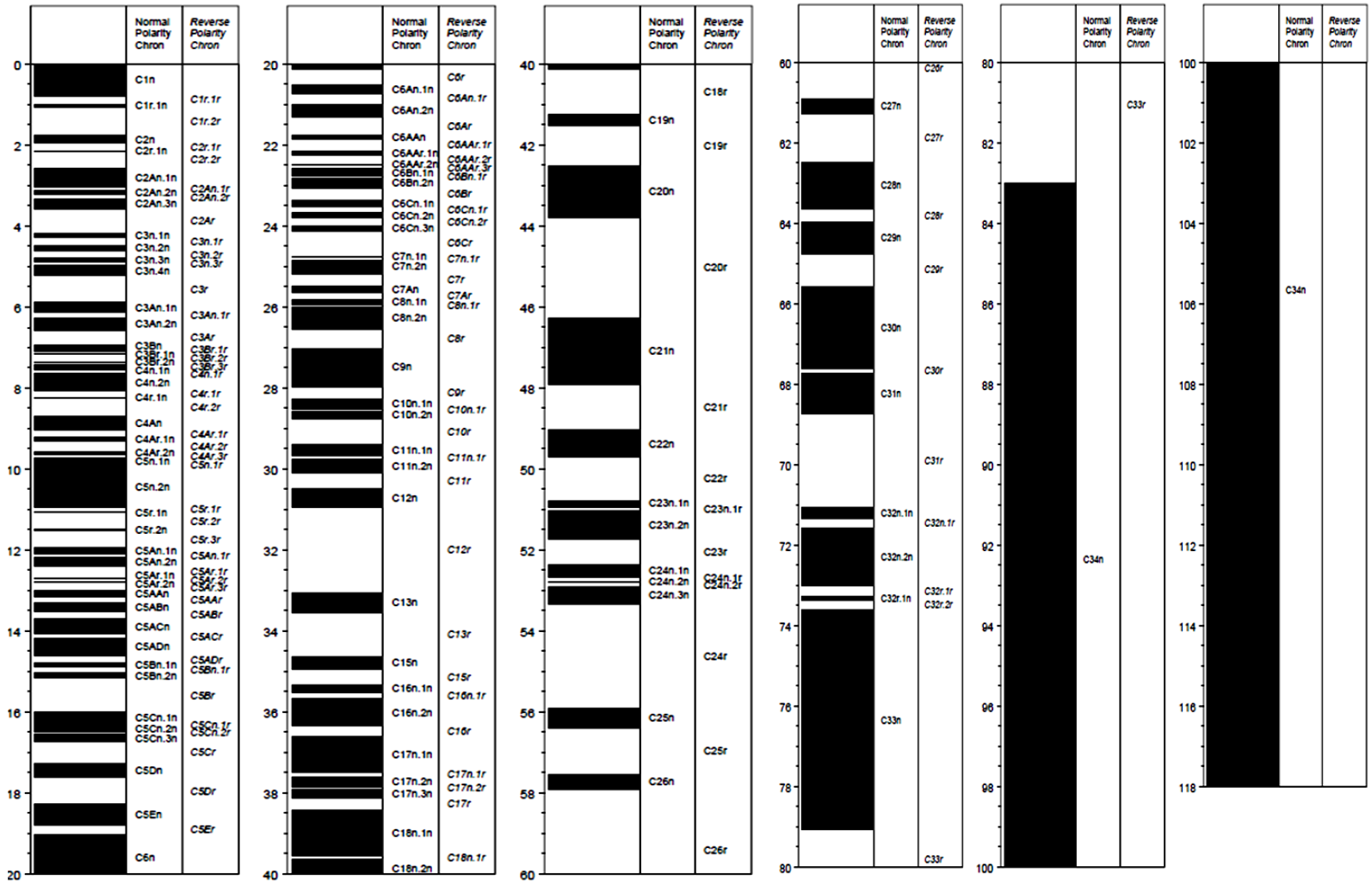

Figure 4.2: Geomagnetic polarity time scale for Cenozoic (Cande and Kent, 1995)

polarities in bands of 5-50 km width. The trend of the anomaly pattern reveals the geometry of spreading, in case of fossil spreading centers, they are assumed at the central location of conjugate anomalies. Magnetic profiles need to be run perpendicular to the spreading axis in order to record anomaly sequence with maximum amplitude. The anomaly patterns are usually observed offset at places due to transform motion at the time of spreading. Magnetic lineation patterns and their offsets are considered for outlining of transform faults, fracture zones, fossil spreading centers, ridge migration, ridge jumps, etc.

4.4.1 Magnetic anomaly lineations

The magnetic anomaly lineations defined as long magnetic stripes that run nearly parallel to the ridge crests are found as mirrored sequence on either side of the mid-ocean ridge axis. When the new oceanic material cools and solidifies, it goes through the Curie temperature on flanks of ridge, and then it acquires magnetisation along the ambient magnetic field of the Earth and remains as remnant within the rocks. The spreading progresses at a pace of few tens of km/Myr and magnetic epochs changes polarity in few million years, which results in few tens of km wide stripes of magnetised crustal blocks of alternating polarities on either side of the spreading ridge. These are called magnetic lineations or isochrons. The subchrons or events and even excursions may get recorded with shorter width decided by the half spreading rate and the time span of the polarity deviation within the linear magnetic bands parallel to the spreading center. The width of the isochron stripes are defined by half spreading rate and duration of corresponding magnetic field polarity that generally varies from 5 to 50 km. They are observed to be offset by fracture zones due to transform motions of oceanic plate at the time of formation or later. The seafloor spreading is a continuous process even though the half spreading rates change with geologic time, so that plate geometries to about 160 Ma can be reconstructed by analysis of magnetic lineation pattern of the ocean floor.

Magnetic anomaly profile data adjacent to the Ninetyeast Ridge are plotted along ship tracks and are shown in Figure 4.3. Magnetic anomalies are, in general, well developed with moderate amplitudes except over the Ninetyeast Ridge and on its immediate east side (Figure 4.3). Between the 89°E FZ and 94°E FZ, the anomalies are modestly developed with lower amplitudes (Figure 4.3). The anomalies within this corridor seem

to be subdued because of excessive seafloor undulations created by oceanic fracture zones, strike-slip displacements and vertical faulting (Pilipenko, 1996; Krishna et al., 2001a).

4.4.2 Abandoned spreading centers

The major ocean basins are generally observed to evolve in different spreading phases separated by plate reorganizations and/or ridge jumps, when a few segments of the spreading ridge system cease its activity and start elsewhere by connecting other ridge segments by means of transform faults. The ceased segments with no spreading activity are termed as abandoned/ extinct/ fossil spreading centers (ASC/FSC) or ridges (ASR/FSR). They are even developed by major or minor ridge jumps. The ceased ridge segments thermally subside and become part of the ocean floor and experience usual relative movements of the ocean floor. They may not exhibit any gravity or bathymetry anomalies, but can be identified in terms of conjugate magnetic anomaly pairs on either side of their axis.

The abandoned spreading centers (ASC) of the Indian Ocean are the result of two major plate reorganizations that the ocean had under gone and of several major and minor ridge jumps. They have been mapped at several locations in the Indian Ocean, for example the spreading centers in northwest of Australia (Wharton Basin) ceased soon after the formation of anomaly M4 (Fullerton et al., 1989), in northwest of the Madagascar after anomaly M0, in east of the Madagascar after anomaly 29, in the Wharton Basin after anomaly 19 (Liu et al., 1983; Krishna et al., 2012), on west of the Ninetyeast Ridge at the age of anomalies 30, 26 and 19 (Royer et al., 1991; Krishna et al., 1995, 2012). The ASC's ceased in the northwest of the Madagascar contributed to the first plate reorganization and those in the Wharton Basin contributed to the second major plate reorganization. The present study deals with some abandoned spreading centers (ASC's) of ~ 65 and 42 Ma age observed between the 86°E FZ and 90°E FZ and the discussion is elaborated in Chapter 5.

4.4.3 Oceanic fracture zones

The spreading rate along the mid-ocean ridge is not generally uniform along its stretch due to variable supply of lava material from the underneath magma chambers and asymmetry of spreading, this lead to segmentation of ridge system into number of ridge

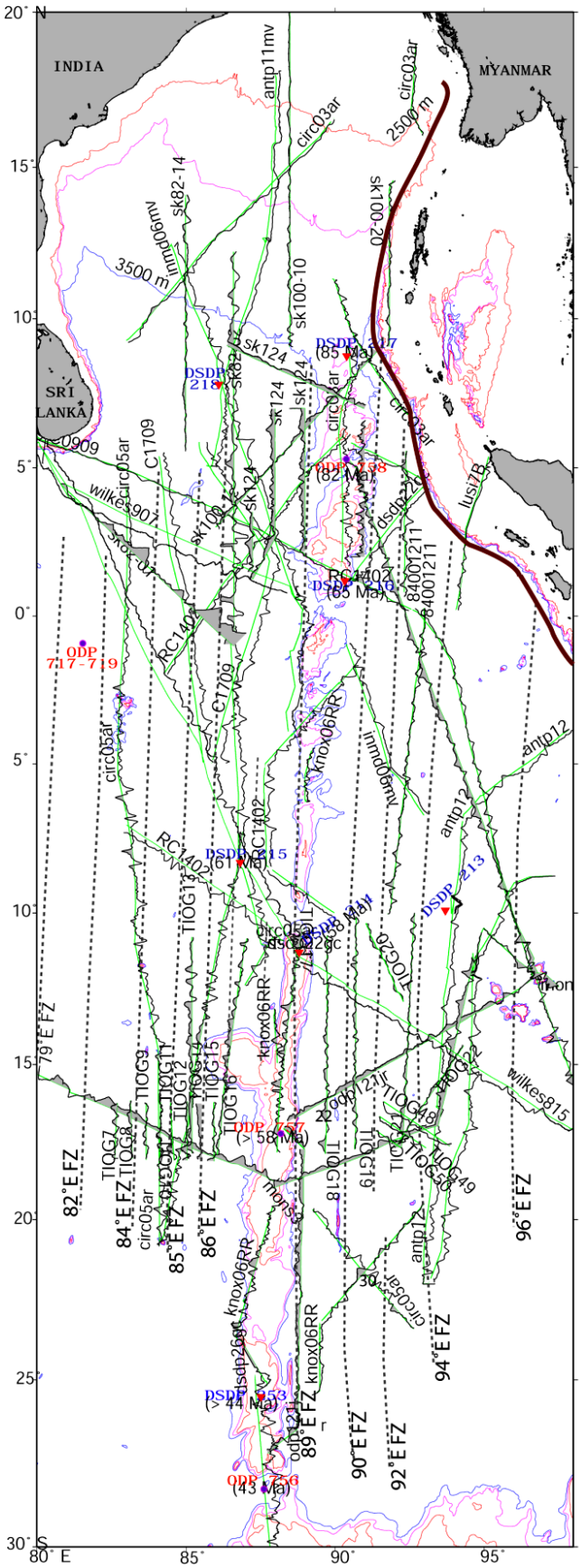

Figure 4.3: Magnetic profile data plotted in study area with profile names annotated. Dashed lines indicate fracture zones. DSDP and ODP sites of the area are annotated and along NER with corresponding ages.

segments by means of transform faults of relative strike slip motion trending perpendicular to the strike of the ridge. The ridge segments are displaced by few tens or hundreds of km length, the setting in turn offsets the magnetic lineation pattern by means of the resulting fracture zones. The magnetic lineations and fracture zones are important geophysical constraints for better understanding the tectonic fabric of the ocean floor and lithospheric plate reconstructions. The fracture zones are the marks of transform faults extending into the oceanic basins and are identified by bathymetric/gravity anomaly signatures or even by the offset of magnetic lineations in oceanic crust and they occur parallel to the spreading direction.

The magnetic anomaly data are overlaid on satellite free-air gravity data (Sandwell and Smith, 1997) in order to constrain precise positions of fracture zones (FZ) (Figure 4.4), thereby constraining extrapolation of the magnetic lineations, in this study. The satellite gravity image clearly shows the presence of a number of nearly N-S trending narrow gravity features, indicating the signatures of FZ created during the northward movement of the Indian plate. From these gravity features, we have traced ten FZ between 80° and 97°E longitudes (Figures 4.3 and 4.4). They trend in the N5°E direction, while the Ninetyeast Ridge trends N10°E, consequently the 89°E FZ crosses the NER obliquely from east to west between 15°S and 10°S latitudes (Figure 4.3, 4.4). Using both narrow gravity lineations and magnetic lineation offsets, several fracture zones have been identified in the northeastern Indian Ocean such as 80°E FZ, 83°E FZ (Indira fracture zone), 84°E FZ, 85°EFZ, 86°E FZ. Fracture zones identified on east of the Ninetyeast Ridge are 89°E FZ,90°E FZ, 92°E FZ, 94°E FZ and 96°E FZ.

4.5 Synthetic magnetic model from observed anomalies

Marine magnetic anomalies are modelled for spreading rates, following the hypothesis of Vine and Mathews (1963) depicting magnetized crustal blocks of alternating polarities symmetrical about the spreading axis. Synthetic magnetic anomaly profiles can be generated assuming magnetized blocks of constant thickness and susceptibility. Initially researchers have attempted models with varying thickness of magnetized blocks and susceptibility (Talwani et al., 1971; McKenzie and Sclater, 1971), subsequently modelling has been continued with consideration of constant thickness of 500 m crustal block and average susceptibility of 0.01cgs units for generation of synthetic magnetic profiles as relative amplitude of anomalies are immaterial. The

present study uses MODMAG algorithm, which will work as plug in module in MATLAB, developed by Mendel et al. (2007) for generating synthetic magnetic profiles, which assumes constant thickness of 500 m basaltic layer and varied magnetization away from the ridge axis. The extrusive basaltic layer can have remnant magnetization up to 25 A/m (Ravilly et al., 2001). The algorithm also accounts for varying seafloor depth as a parameter file with navigation and depth value as an input needs to be provided by the user.

Geomagnetic polarity time scale of Cande and Kent (1995) is considered for correlating radiometric ages to the magnetic reversals and for generation of several synthetic magnetic profiles for the anomalies ranging from C19 to C34 to model magnetic anomaly profiles on either side of Ninetyeast Ridge. Synthetic profiles with fossil spreading centers, ridge jumps and asymmetric spreading are modelled with MODMAG by varying parameters of relative distance of axis point, width of ridge jump with respect to input profile and percentage of asymmetry, respectively in the interactive interface of the program.

Earlier magnetic anomaly identifications from both the Central Indian and Wharton basins (Peirce, 1978; Liu et al., 1983; Peirce et al., 1989; Royer et al., 1991; Krishna et al., 1995, 2009b; Krishna and Gopala Rao, 2000) were considered to determine the spreading rates and magnetic polarity chronology for generating synthetic magnetic anomaly profiles. Hence half-spreading rates ranging from 2.3 to 8.5 cm/yr and geomagnetic polarity timescale (Cande and Kent, 1995) for the period from late Cretaceous to early Tertiary were used to create synthetic magnetic anomaly models. Following the three different anomaly patterns within the study area, west of the 86°E FZ, east of the 90°E FZ, and the region in between, three magnetic models were generated using the Matlab-based MODMAG algorithm (Mendel et al., 2005) and correlated to the magnetic anomaly profiles for identification of seafloor spreading magnetic anomalies, thereby assigning ages to the oceanic crust. The magnetic anomaly sequences in model profiles, particularly anomalies 30 through 32n.2 and 21 through 24n.2, have characteristic shapes generated by a unique arrangement of short-period geomagnetic polarity reversals. These distinctive anomaly shapes and patterns are used as reference picks for the correlation of observed anomalies to model profile data. With this approach most of the anomaly correlations have gained reasonably high confidence.

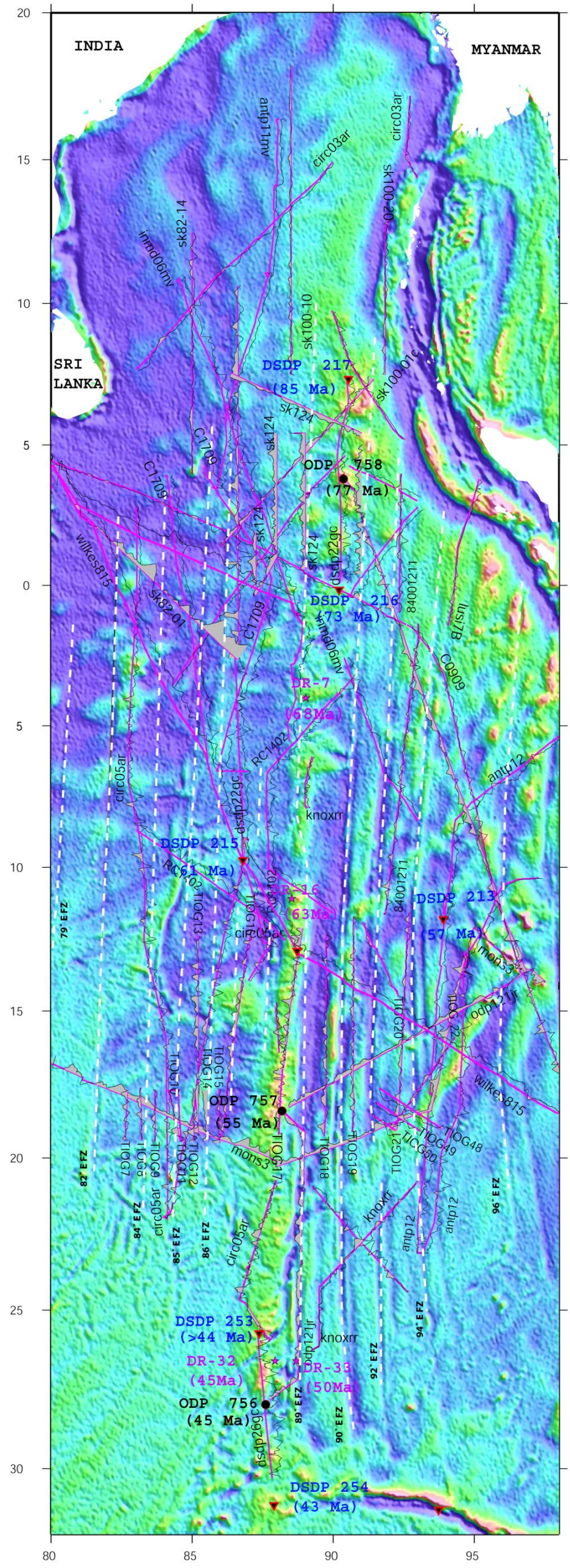

Figure 4.4: Magnetic anomaly profiles overlaid on the satellite free-air gravity image of the northeastern Indian Ocean (prepared from database of Sandwell and Smith (1997)). White dashed lines are drawn to follow narrow gravity features that define oceanic fracture zones. DSDP and ODP sites are shown by solid red triangles and solid black circles, respectively. Ages indicated at each drill site are from the geochronology data published by Pringle et al. (2008).

4.6 Correlations between synthetic magnetic model and observed magnetic anomaly profile

Considering the earlier published magnetic anomaly identifications of the Central Indian and Wharton basins (Peirce, 1978; Liu et al., 1983; Peirce et al., 1989; Royer et al., 1991; Krishna et al., 1995, 2009b; Krishna and Gopala Rao, 2000) and the difference in distribution pattern of anomaly sequences, the study area is broadly divided into three provinces such as west of the 86°FZ, east of the 92°E FZ and between the FZs for detailed anomaly identifications. Synthetic magnetic anomaly profiles are generated for each geological province with the help of MODMAG algorithm in MATLAB application using revised geomagnetic polarity time scale of Cande and Kent (1995) for Cenozoic to late Cretaceous. To start with, published half spreading rates (HSR) for anomaly 19 to 34 from Central Indian and Wharton basins are used and subsequently modelled in MODMAG for selected profiles by changing the model HSRs for a set of anomalies. For example, initially a synthetic profile of C20 to C33r is generated with constant spreading rate for sequence 20 to 23.n2, then another rate for 24.n.1 to 29 and varying again for 29 to 33r. In the process of matching synthetic profile with different magnetic profiles the spreading rates are modified interactively till reasonable match is obtained between synthetic and observed anomalies and if needed further bifurcating the sequence for different spread rates. Thus accurate half spreading rates are obtained for a selected magnetic profile along each spreading corridor separated by fracture zones, in the study area, from anomaly 19 to 34 averaged over a couple of chrons. At least one long profile in each corridor bounded by FZs is modelled against a synthetic profile for fixing its spreading rate. Then keeping the characteristic magnetic anomaly signatures in view, all nearby profiles are correlated with the anomalies of the synthetic model. Magnetic profiles of Wharton Basin and the corridor between the 86°E FZ and Ninetyeast Ridge consisting of abandoned spreading centers and conjugate anomalies on either side of ASR, are modelled with a consideration of asymmetrical spreading rates.

N-S and near N-S trending magnetic profile data are selected from database and plotted on the satellite gravity anomaly map of the study area for demarcating the fracture zones (Figure 4.3). Earlier identified anomaly sequences are directly marked on the map constrained by FZ boundaries. Anomalies identified on new profiles are attempted to correlate to similar anomalies of nearby profiles wherever they are not offset by fracture

zones. After preliminary anomaly identifications, suitable magnetic profiles with considerable N-S length between the fracture zones have been selected for forward modelling. The oblique profiles cut across fracture zones have to be fragmented for modelling, if other suitable long profiles are not available adjacent to them without crossing the fracture zones. Any ambiguity in a segment of the profile with respect to anomaly identification is solved at this stage, when synthetic profile is overlaid on the profile with best fitting half spreading rate. Any discontinuity in anomaly sequence may be identified by change in characteristic signature of the expected anomaly or any drastic change spreading rate while attempting its correlation with proposed synthetic.

4.6.1 Selected magnetic profiles on either side of Ninetyeast Ridge

Magnetic profile data from Knox06RR survey, NGDC, TIOG and NIO database as enlisted in chapter 3 are edited, and from the database N-S near N-S segments are extracted. Out of 22 different surveys total 71 profile segments are extracted for anomaly identification between 82°E FZ and 96°E FZ in Central Indian and Wharton basins (Figure 4.3). The area is characterised by N-S trending fracture zones of long offsets. 84°E FZ, 85°E FZ, 86°E FZ, 89°E FZ, 90°E FZ, 92°E FZ and 94°E FZ are the major fracture zones identified in satellite free-air gravity anomaly map, offsetting the oceanic crust. This demands a single long profile or segments of two or more profiles with all expected anomalies to be modelled in each crustal strip bounded between two fracture zones, as slight variation in spreading rates may be possible across the FZ offsets.

Between 82 and 84° E FZs profiles tiog7 and a segment of circ5a could be modelled for anomalies 23.n.1 to 24.n.2 and 28 to 34, respectively. Between 84 and 85°E FZ southern segment of circ5a for anomalies 21 to 27 and in between 85 and 86°E FZs circ5b for anomalies 22 to 27 to be used, where N-S profiles are absent in the north of 8°S to model the older anomalies (Figure 4.4).

The corridor between 86°E FZ and Ninetyeast Ridge, FZs of large offsets are absent. But the anomaly pattern is discontinuous with frequent sequence breaks due to ridge jumps. South of 10°S the available profiles are short in length and also found noisy possibly due to proximity to the volcanic ridge. The profile segments of tiog16, dsdp22gc and c1709b would together form a long N-S profile with well developed

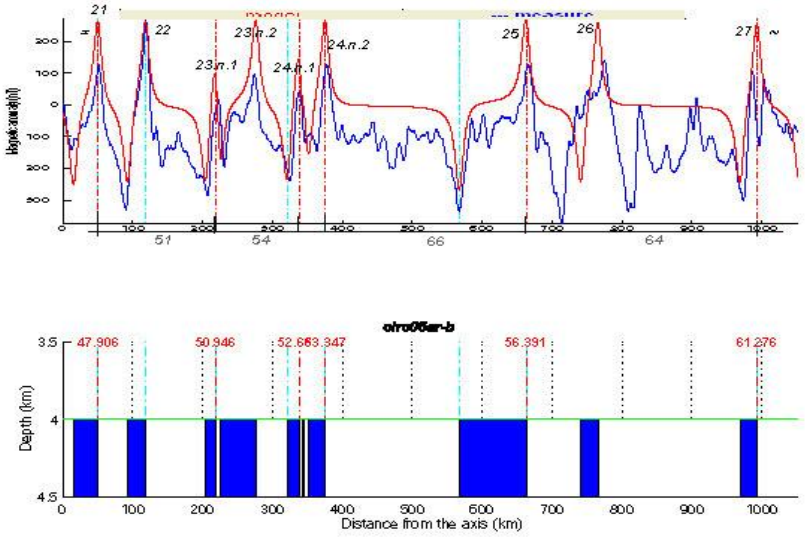

Figure 4.5 (a): Modelling of profile circ5b with anomalies 21 to 27 using MODMAG. Half spreading rates are marked (km/Myr) below the distance axis of the profile.

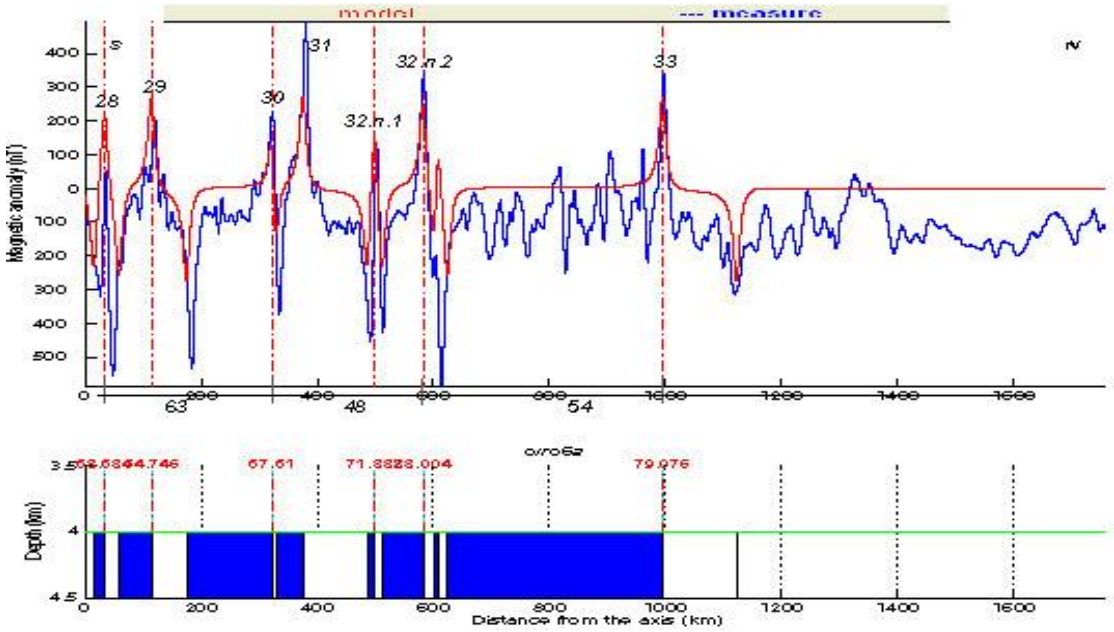

Figure 4.5 (b): Modelling of profile circ5a with anomalies 28 to 34.

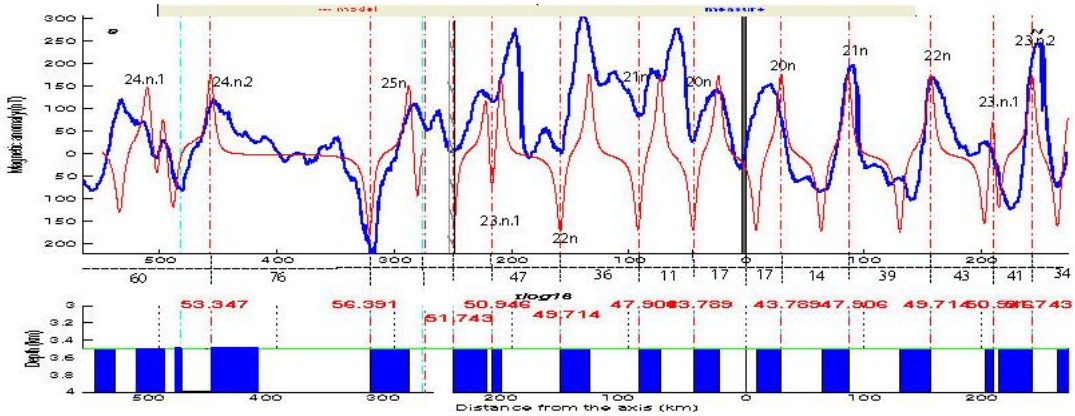

Figure 4.5 (c): Modelling of profile tiog16 with anomalies 24.n.1 to 25 followed by 20 to 23.n.2 anomalies mirrored against FSR

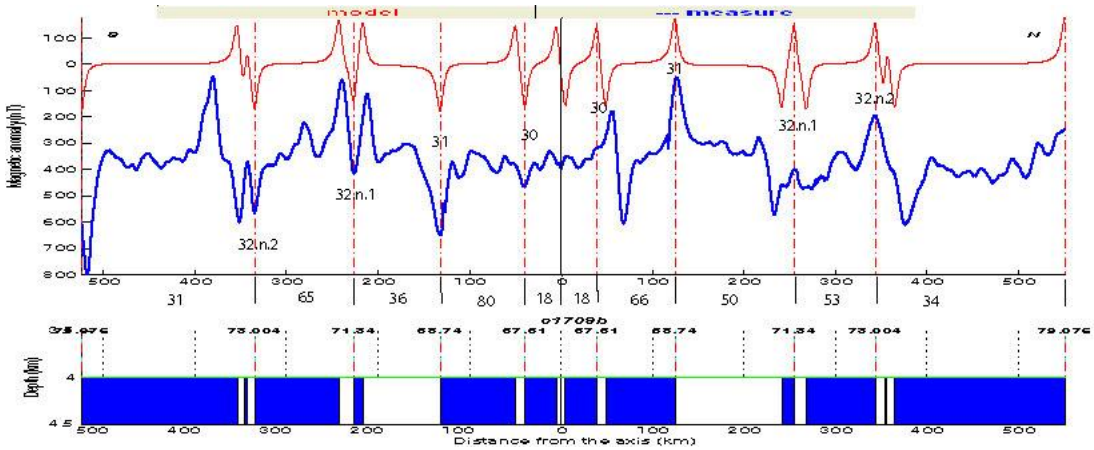

Figure 4.5 (d): Modelling of profile c1709b with anomalies 30 to 32.n.2 mirrored against FSR

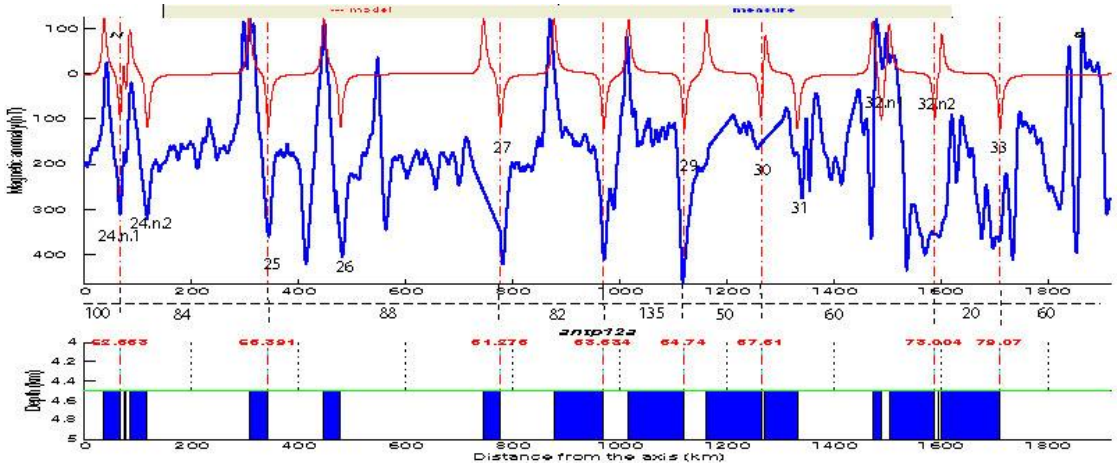

Figure 4.5 (e): Modelling of profile antp12a with anomalies 24.n.1 to 33.

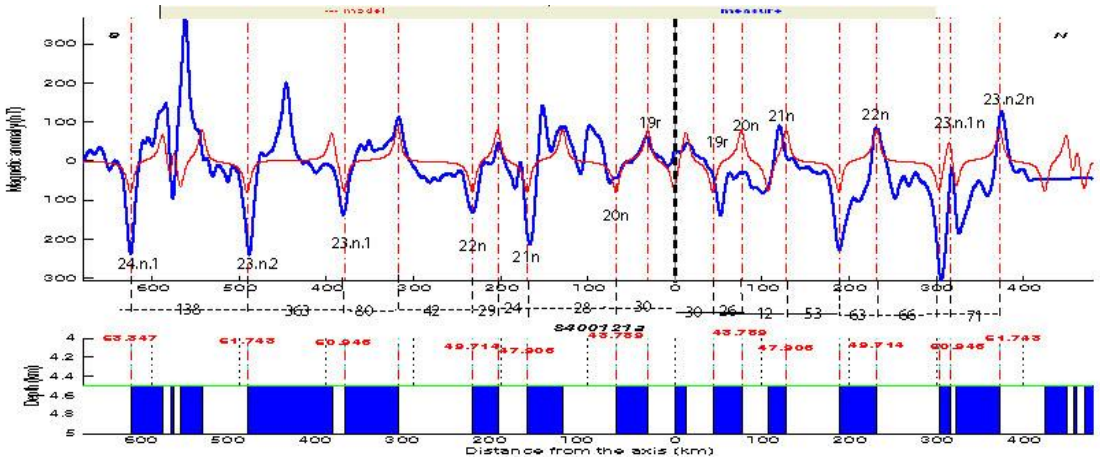

Figure 4.5 (f): Modelling of profile 8400121a with southward progressing anomalies 19r to 24.n.1, FSR and the conjugates till 23.n.2 towards north.

anomalies to generate a spreading model for this corridor (Figure 4.4).

East of the Ninetyeast ridge the oceanic crust is highly offset along the N-S FZs, ranging from 200-800 km, decreasing towards east, in left lateral manner. Fossil spreading center of age less than anomaly 20 is identified in all crustal corridors. Magnetic profile segments of odpjr121a and tiog18 in combination consist of conjugate anomalies 20 to 26 to the south and 20 to 25 anomalies to the north in between Ninetyeast Ridge and 90°FZ. Between 90 and 92°E FZs a segment of knox06RR, tiog19 and 8400121b are the profiles modelled, but with data gap of 24.n.1 to 28 anomalies in southward progressing sequence and 21 to 27 in northward progressing sequence. In between 92 and 94°E FZs tiog21and 8400121a provide complete conjugate sequence of anomaly 20 to 29 and 20 to 23.n.2 towards south and north respectively on either side of the FSR. In the corridor bounded by 94 and 96°E FZs, there are quite a few profiles with well developed magnetic anomaly profiles. Modelling antp12b and c0909 would be sufficient to correlate all the anomalies, 20 to 34 progressing south and 20 to 23.n.1 progressing towards north, across different profiles (Figure 4.4). Figure 4.5a to 4.5f shows key profiles of the study area, modelled in Modmag for half spreading rates.

After detailed modelling anomaly identifications on the map are revised where uncertain and doubtful identifications were made. For example in the profile tiog16 between 86°E FZ and Ninetyeast Ridge, after the southward progressing anomalies 20-23.n.1, 23.n.2 - 25 were identified. But while modelling spreading rates it showed unrealistic spreading rates when tried to match with synthetic and more over the characteristic signature of the sequence was not correlating. Then the possibility of older sequences due to ridge jumps were realised and trial with northward progressing 24.n.1-25 gave best fit (Figure 4.5c).

4.6.2 Identification of isochrons constrained by fracture zones

Earlier fracture zones were typically marked observing the offsets in magnetic anomalies of adjacent profiles. Presently as high resolution gravity anomaly and bathymetry maps of ocean floor derived from satellite altimetry are available, fracture zones are easily recognizable. This gives an opportunity to precisely constrain extent of extrapolation of magnetic isochrons in areas bounded by the fracture zones.

On analysis of the satellite gravity anomaly map, it is observed that the oceanic crust of the study area is highly offset by fracture zones, at every 1 to 2° intervals of longitudes, trending N5°S. Each of them is marked with dashed lines in the base map of the area. Then the magnetic profiles are overlaid for preliminary identification of anomalies in comparison with earlier identifications as well as with synthetic profiles generated in MODMAG for C19 to C34. After anomaly identifications on each profile they are extrapolated in between fracture zones on either side. Hence in the current study the lateral extent of newly and earlier identified E-W magnetic lineations are more precise (Figure 4.4).

4.6.3 Synthetic spreading models

The magnetic Profiles that include all identifiable spreading anomaly sequence are chosen from each corridor between the fracture zones and are modelled for variable half spreading rates for the purpose of correlations. As discussed in earlier sections several synthetic magnetic model profiles were generated for comparing to the observed magnetic anomalies. It is observed that the spreading rates for a particular sequence of anomalies are correlating across the fracture zones, in spite of the offsets, west of 86°FZ, east of Ninetyeast Ridge and in between, where the anomaly distribution follow a consistent pattern. This allows a single synthetic spreading model for all profiles between west of 86°E FZ, another model for profiles east of Ninetyeast Ridge and yet another one for the region between them, simplifying the case of separate models across each FZ offset. Accordingly the study area is classified into three regions based on anomaly patterns and plate velocities which are largely offset by 86°E FZ and 90°E FZ and explained with separate model for each region.

4.6.3.1 West of the 86° E Fracture Zone

West of the 86°E FZ, between 21°S and the equator, all the anomalies in sequence from 21 to 34 in northward progression are identified on the profiles with right lateral offsets of relatively lower distance varying from 45 to 90 km against offsetting fracture zones. The magnetic profiles tiog7 to 14, circ5a and 5b, wilkes815, dsdp22gc and c1709 are the major N-S profiles overlaid on gravity map and used for magnetic anomaly identification in this area. Profiles circ5b between 86°E and 85°E FZs and profiles tiog9, circ5a between 85 and 84°E FZs are modelled in this region. Similar average

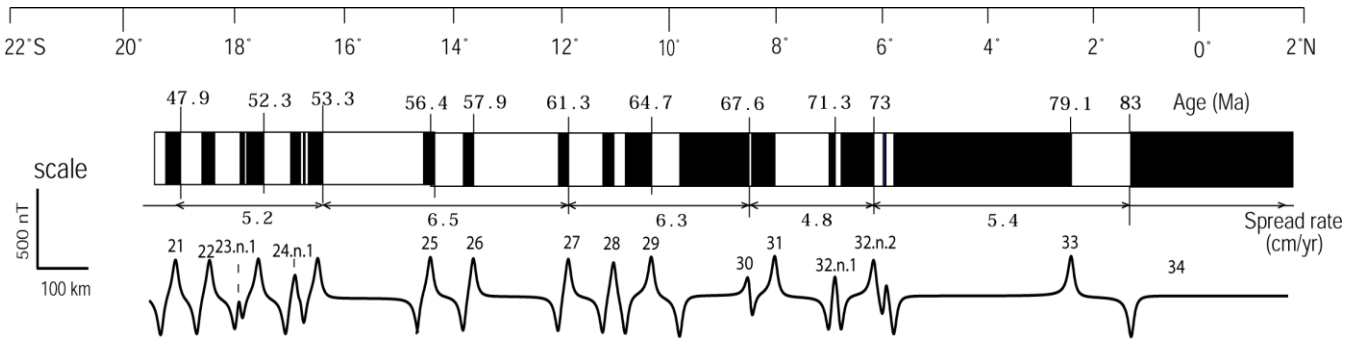

Figure 4.6a: Synthetic profiles generated with modelled half spreading rates in MODMAG program for Central Indian Basin

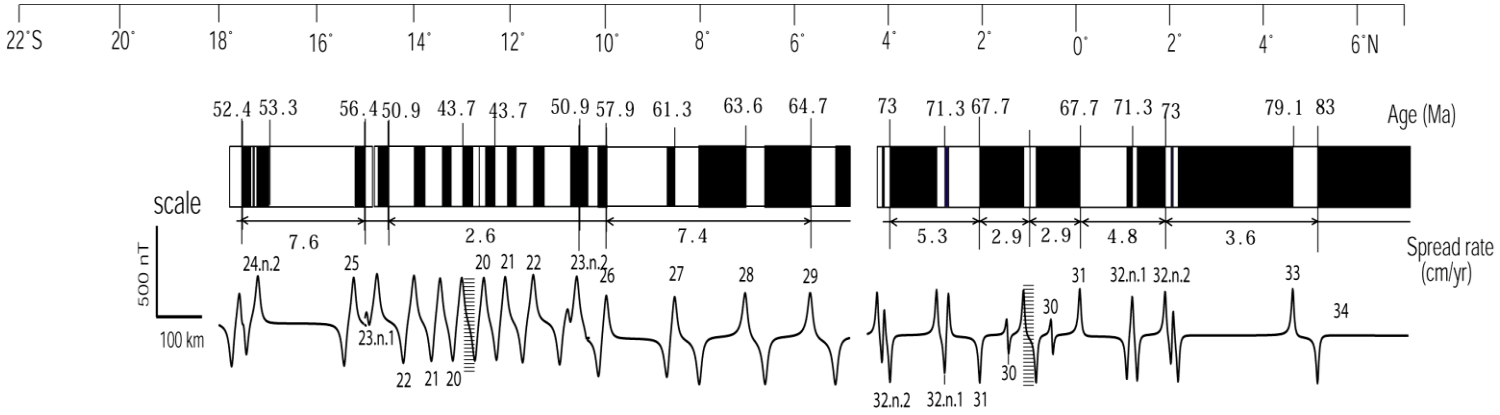

Figure 4.6b: Synthetic profiles generated with modelled half spreading rates in MODMAG program for the region between 86°E FZ and Ninetyeast Ridge.

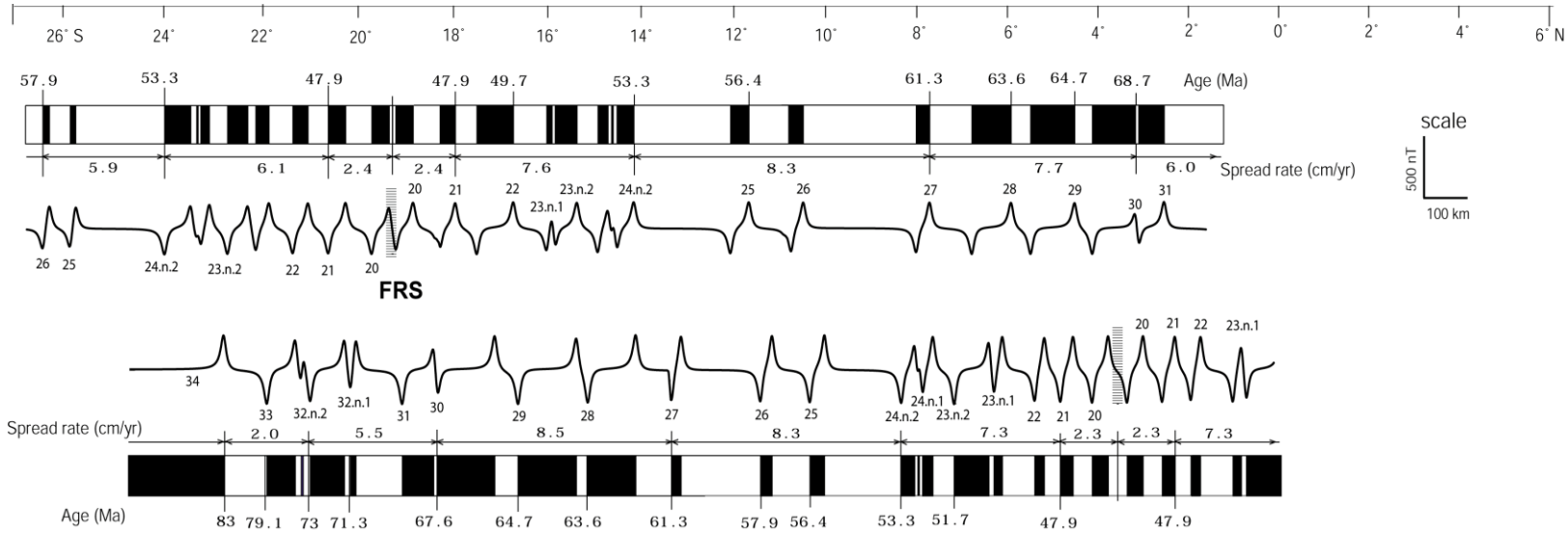

Figure 4.6c: Synthetic profiles generated with known half spreading rates in MODMAG modelling program for Wharton Basin.

plate velocities are obtained for both models, therefore a single model for anomalies 21 to 34 is generated for correlation of all profiles in the area (Figure 4.6a).

4.6.3.2 Between the 86°E Fracture Zone and Ninetyeast Ridge

With the comparison of magnetic anomalies from profiles Wilkes815, sk82–02, dsdp22gc, sk124–12, C1709, sk124–10, inmd06mv, wilkes815, circ05ar-B, tiog15, tiog16, circ05ar-C, RC1402, and Wilkes907 with the synthetic magnetic model (Figures 4.5a, b), symmetric pairs of anomaly sequences 30 through 32n.2 and 20 through 23n.1 are identified on either side of anomaly signatures presumed to be associated with fossil ridge segments. Between the anomaly pairs chrons 26 to 29 are identified and south of younger conjugate pair (20-23.n.1) northward progressing anomalies 24.n.1 to 25 are also revealed. This point out to two southward ridge jumps, at ages less than that of magnetic anomalies 30 (65 Ma) and 19 (42 Ma), and another northward ridge jump at age more than anomaly 23.n1 (51Ma) had occurred in this region. Spreading rates nearing the age of spreading cessations are found to be decreasing, ~2.9 cm/yr before ridge jump at time <30 and 2.6 cm/yr for that at <20 (Figure 4.6b).

4.6.3.3 East of the Ninetyeast Ridge

Magnetic anomalies east of the Ninetyeast Ridge in the western Wharton Basin up to 96°E FZ are analysed compiling the N-S ship-borne magnetic profiles. Segments of profiles odp121jr-a, knox06rr, tiog18-21, dsdp22gc, antp12 A, B, 8400121a, b, mons3c and c0909 are the profiles plotted over gravity free-air anomaly map for magnetic anomaly identification (Figure 4.4). The Basin crust is offset for large distance along 89°E, 90°E, 92°E, 94°E, and 96°E longitudes, forming fracture zones named after the meridian. Portions of the conjugate pairs of magnetic lineations from 34 to 20 with axial fossil ridge, broadly offset by fracture zones as whole in left lateral trend, are identified in this region (Figure 4.4).

Profile segments of odpjr121, tiog18 between the Ninetyeast Ridge and 90°E FZ, tiog19, 8400121b between 90°E FZ and 92°E FZ, tiog21, 8400121a between 92°E FZ and 94°E FZ and mon3c, c0909 between 94°E FZ and 96°E FZ are modelled for average HSRs. In this region also single model with asymmetry percentage could explain spreading rates of identified anomalies on all available profiles.

Anomaly 32n.2 to 30 was marked by moderate rate of 5.5 – 6 cm/yr. Maximum spread rates are observed between 30 - 24.n.2 in the range of 7.6 - 8.5 cm/yr and then 24.n.2-21 with 7.3 - 7.6 cm/yr. The lowest rate was near to cessation of the spreading from 21 to 20 anomalies, which gave 2.3-2.4 cm/yr in this basin (Figure 4.6c).

The magnetic profile data of each region stacked and correlated with synthetic profiles are presented in chapter 5. The modelling results and observations are further discussed and interpretation and major inferences are also enlisted in chapter 5.

Chapter 5

5 Tectonics of the Ninetyeast Ridge derived from spreading records of adjacent ocean basins and age constraints of the Ridge

5.1 Introduction

Emplacement process of the Ninetyeast Ridge by the Kerguelen hotspot was established with the help of geophysical, geological, geochemical and chronological data by early 1990s (Peirce, 1978; Peirce et al., 1989; Royer et al., 1991). The possibility of other postulations (Royer et al., 1991 and references therein) were ruled out as monotonous age progression of the linear ridge track towards north was revealed by the radiometric age data along the ridge obtained from DSDP Leg 22 and 26 and ODP Leg 121 drill sites. The age progression is of a typical of plume emplacement feature on the plate diverging away from spreading ridge system. Then the paradox aroused out of extra length of the Ninetyeast Ridge track, as the half spreading rates of the Indian plate could not account for the whole length of the ridge. Formation of extra stretch of the ridge track was explained with southward ridge jumps of the Wharton spreading ridge by transferring pieces of Antarctic plate segments along with the volcanic edifice to the Indian plate (Royer et al., 1991; Krishna et al., 1995, 1999). This was hypothesised based on identification of fossil ridge segments around anomaly 29 (~65 Ma) and 19 (~42 Ma) and some of the mirrored anomalies on either side of them on west of the Ninetyeast Ridge. But the timing, location of the hotspot, and extent of these ridge jumps are not clearer and uncertain too because the magnetic pattern near the Ninetyeast Ridge are extremely complex. Therefore, in order to improve our understanding of the processes of seafloor spreading and hotspot volcanism and their interactions in various tectonic settings, a necessity of collation of existing and new geophysical and geological data on either side of the Ninetyeast Ridge arose. The compilation carried in this work also uses new magnetic profile data collected during the KNOX06RR cruise in 2007 over the Ninetyeast Ridge. The magnetic profile data gathered from the region bounded by latitudes from 20°N to 30°S and longitudes from 82°E to 96°E (Figure 5.1).

The compiled ship-borne magnetic anomaly profile data on the Ninetyeast Ridge and adjacent Central Indian and Wharton basins (Figure 5.1) are analysed for identification of magnetic lineations caused by the Earth's past magnetic reversals. The anomaly identifications are also constrained by the locations of fracture zones marked based on the

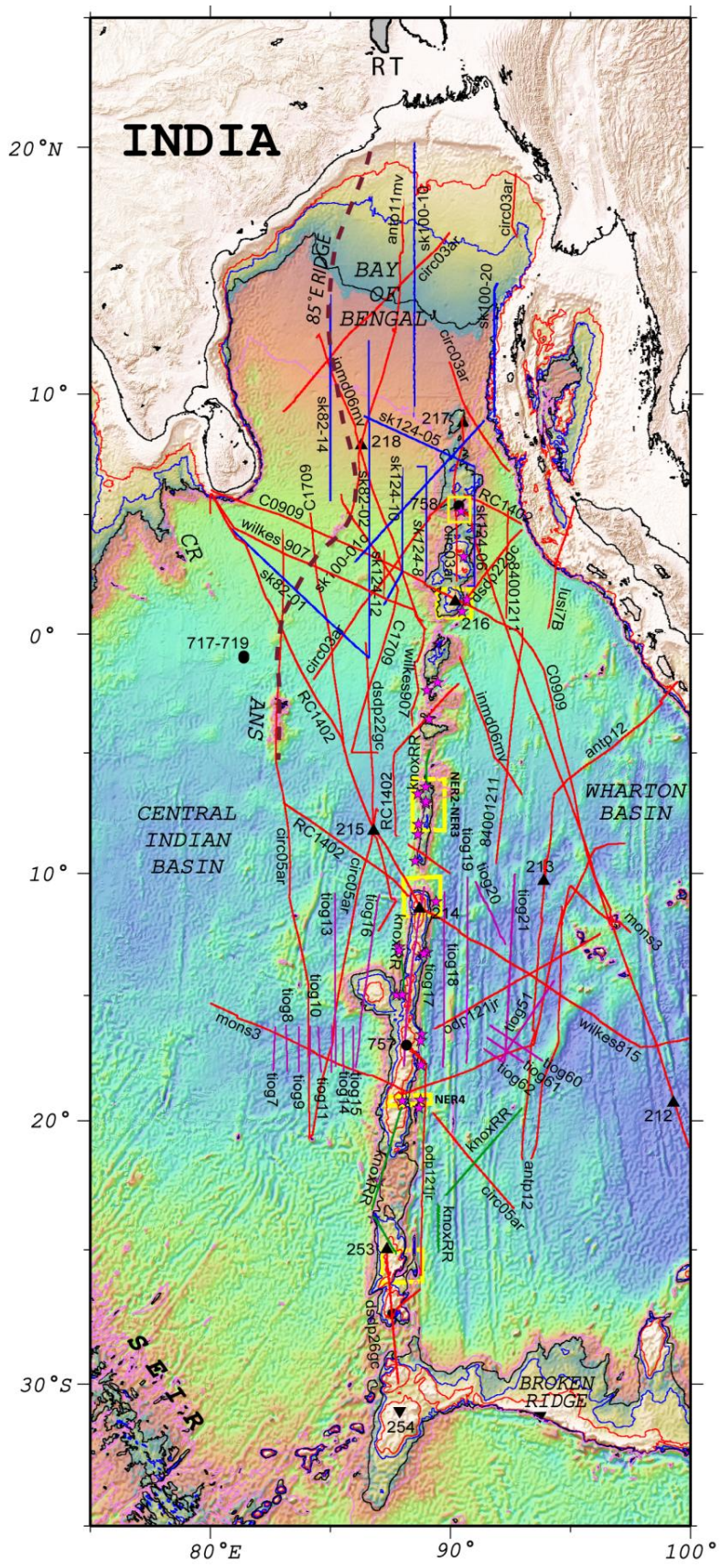

Figure 5.1: Plot of magnetic profiles on the map of study area. Green lines- KNOX06RR profiles, Red lines- NGDC profiles, purple Lines-TIOG profiles, Blue lines- profiles from NIO data base. Yellow boxes- sites of KNOX06RR seismic reflection data.

satellite gravity and bathymetry data. The newly determined geochronology data for the core samples of DSDP Leg 22 and ODP Leg 121 drill sites and KNOX06RR cruise basaltic dredge samples from the Ninetyeast Ridge (Pringle et al., 2008) are analysed to obtain a more reliable ridge emplacement rate in order to compare with the plate velocity for the same geological time period, thereby to investigate the influence of hotspot activity on seafloor spreading process of the Wharton Ridge. The mechanism that resulted in elongation of the Ninetyeast Ridge at a double the rate of Indian plate velocity is discussed to explain in terms of ridge jumps.

5.2 Chronologic data along the Ninetyeast Ridge

Deep Sea Drilling Project (DSDP) Legs 22 and 26 and Ocean Drilling Program (ODP) Leg 121 had drilled altogether 7 sites at different locations of the Ninetyeast Ridge (Figure 5.1). They are located along the latitudes of 8.5°N (DSDP 217), 5.2°N (ODP 758), 1.5°N (DSDP 216), 11.3°S (DSDP 214), 17.1°S (ODP 757), 25.5°S (DSDP 253) and 27.3°S (ODP 756) with minimum distance of ~200 km and maximum of ~1400 km between two adjacent sampling locations along the ~5600 km long Ninetyeast Ridge. The KNOX06RR cruise on research vessel Roger Revelle during the 2007 had collected enormous basaltic dredge samples at 23 sites along stretch of the ridge. Pringle et al. (2007, 2008) have investigated the dredge samples from the KNOX06RR cruise and reinvestigated the rock samples from the DSDP and ODP Sites using $^{40}Ar/^{39}Ar$ dating method for assigning age data for the Ninetyeast Ridge track. The newly determined ages along the ridge track are 77 Ma for ODP Site 758, 73 Ma for DSDP Site 216, 68 Ma for the dredge DR-7 (2.4°S), 63 Ma for the dredge DR-16 (9.5°S), 62 Ma for DSDP Site 214, 45 Ma for the dredge DR-32 (25.857°S), 45 Ma for ODP Site 756 and 43 Ma for DSDP Site 254 (Figure 5.2). The hypothesis of multiple southward ridge jumps predicts some age reversals along the ridge track, but surprisingly the dates have revealed approximately linear north-south age progression from 77 Ma to 43 Ma with a propagation rate of 118 ± 5 km/Ma. Probably the sparse sampling along the long 5600 km ridge track may not be sufficient to reveal such reversals in age.

5.3 Magnetic Anomaly pattern and Fracture zones of the study Area

The study area encompasses on either side of the Ninetyeast Ridge, towards west in the Central Indian Basin till 82°E FZ and on east in the Wharton Basin till 96°E FZ. A number of near N-S trending fracture zones which offset the magnetic lineations in the study area are demarcated along 82°E, 84°E, 85°E, 86°E, 89°E, 90°E, 92°E, 94°E and 96°E longitudes and

these interpretations are corroborated with the typical narrow trough like features identified in satellite free-air gravity map as discussed in chapter 4.

A total of 68 north-south to near north-south trending magnetic profiles (Figure 5.1) are compiled from NGDC (National Geophysical Data centre), TIOG (Trans Indian Ocean Geotraverse), NIO (National Institute of Oceanography) and KNOX06RR databases and are plotted along ship-tracks on background of free-air gravity data in order to constrain precise positions of FZs (Figure 5.2). Seafloor spreading type magnetic anomalies, in general, are well recognised with moderate amplitudes except over the Ninetyeast Ridge and on its immediate eastside (Figures 5.2 and 5.3b). Particularly in an area between the 89°E FZ and 94°E FZ, the magnetic anomalies are modestly developed with relatively lower amplitudes (Figures 5.2 and 5.3b). The anomalies within this corridor seem to be subdued because of excessive seafloor undulations created by oceanic fracture zones, strike-slip displacements and vertical faulting (Pilipenko, 1996; Krishna et al., 2001a). As earlier geophysical studies from both the Central Indian and Wharton basins have revealed the presence of anomalies from 34 to 19, it has become easier for identification of typical anomaly signatures in new compiled data. The magnetic anomaly sequences are identified in comparison to synthetic anomalies prepared using MODMAG tool (Mendel et al., 2005) in Matlab software. Following the observed magnetic anomaly pattern (Figure 5.2), the study area is divided into 3 distinct parts, as described in chapter 4 and they are discussed below.

1) west of the 86°E FZ – magnetic lineations from 22 to 34 are identified with northward progression with right lateral offsets at 84°E FZ, 85°E FZ and 86°E FZ (Figure 5.3a).

2) east of the Ninetyeast Ridge, particularly east of the 89°E FZ in Wharton Basin - mirrored anomalies from 20 to 31 in north and from 20 to 33 in south on either side of the fossil spreading ridge are identified. The sequence is found to be offset with longer left lateral offsets almost in all corridors between the fracture zones, 89°E FZ, 90°E FZ, 92°E FZ, 94°E FZ and 96°E FZ (Figure 5.3b).

3) the complex magnetic pattern is found in between 86°E FZ and 89°E FZ, where two fossil ridge segments are identified at anomalies 30 and 20 with the pairs of anomalies on either side of the fossil ridge segments. Anomalies 26 to 29 are also present in between the paired

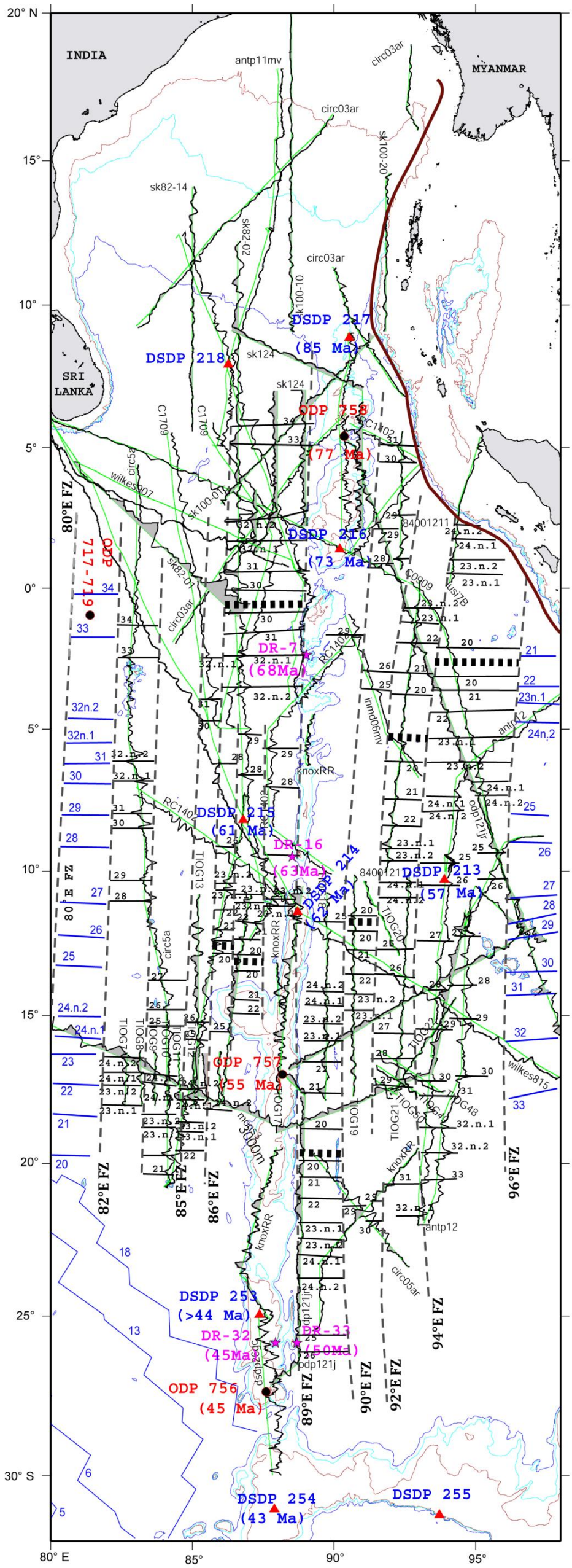

Figure 5.2: Interpreted magnetic lineations (black lines), fossil ridge segments (solid stippled line), and oceanic fracture zones (dashed lines) of the northeastern Indian Ocean. Magnetic lineations indicated with blue lines are adopted from earlier studies (Royer et al., 1991; Krishna and Gopala Rao, 2000). Magnetic profiles are shown particularly to support the anomaly identifications, correlations, and offsets. Fracture zones are tightly constrained by satellite gravity data. Bathymetric contour at 3000 m and shallower water depths are shaded to outline the physiography of the NER and other features.

anomalies. The offsets between the anomaly sequences are rather smaller comparing to those observed in the Wharton Basin (Figure 5.3c).

Considering the anomaly characteristics, particularly shapes and patterns of each magnetic profile of the study area, couple of synthetic magnetic profiles were generated using the Matlab-based MODMAG algorithm (Mendel et al., 2005). The magnetic anomaly sequences in model profiles, particularly anomalies 30 through 32n.2, and 21 through 24n.2, have characteristic shapes (Figures 5.3a – 5.3c) generated by a unique arrangement of short-period geomagnetic polarity reversals. We used these distinctive anomaly shapes and patterns as reference for initial consideration of half-spreading rates in calculation of synthetic magnetic profiles. Further the geomagnetic polarity timescale of Cande and Kent (1995) was used for the period from late Cretaceous to early Tertiary for assigning ages to the magnetic lineations. More details on input parameters and geomagnetic time scales used in this work are present in Chapter 4. Subsequently the input parameters were slightly adjusted for obtaining a best comparable synthetic model profiles with the observed magnetic profiles of the study region. Magnetic profiles are stacked region-wise (west of the 86°E FZ, east of the 89°E FZ and the region between these FZs) and synthetic model profiles (Figures 5.3a - 5.3c).

5.3.1 Magnetic Anomaly pattern in Central Indian Basin west of 86°E FZ

The magnetic profiles, tiog7 to 14, circ 5a and 5b, wilkes815, dsdp22gc and c1709 are the main N-S profiles overlaid on gravity map and used for magnetic anomaly identifications (Figures 5.2, 5.3a and 5.3b). West of the 86°E FZ between 21°S and the Equator, all the anomalies in sequence from 21 to 34 in northward progression are identified. The anomaly lineations are offset in right lateral sense at about 86°E, 85°E and 84°E longitudes, invoking the presence of fracture zones, 86°E FZ, 85°E FZ and 84°E FZ with offsets of relatively lower distance varying from 45 to 90 km (Figure 5.2).

Between 86°E and 85°E FZ anomaly sequence from 21 (~20°S) to 26 (~15°S) are identified with confidence following their characteristic signatures even though anomalies are of low amplitude. North of this, anomalies are not identified on profile tiog13 till 5°S latitude for lack of typical anomaly signatures. Further northward up to 2°S, anomaly sequence 30 to 32n.1is identified with moderate confidence. Older anomalies, particularly 33 and 34 were unable to identify in this corridor as no suitable magnetic profile is available in this region. In another corridor between 85°E FZ and 84°E FZ, anomaly identifications start from 21

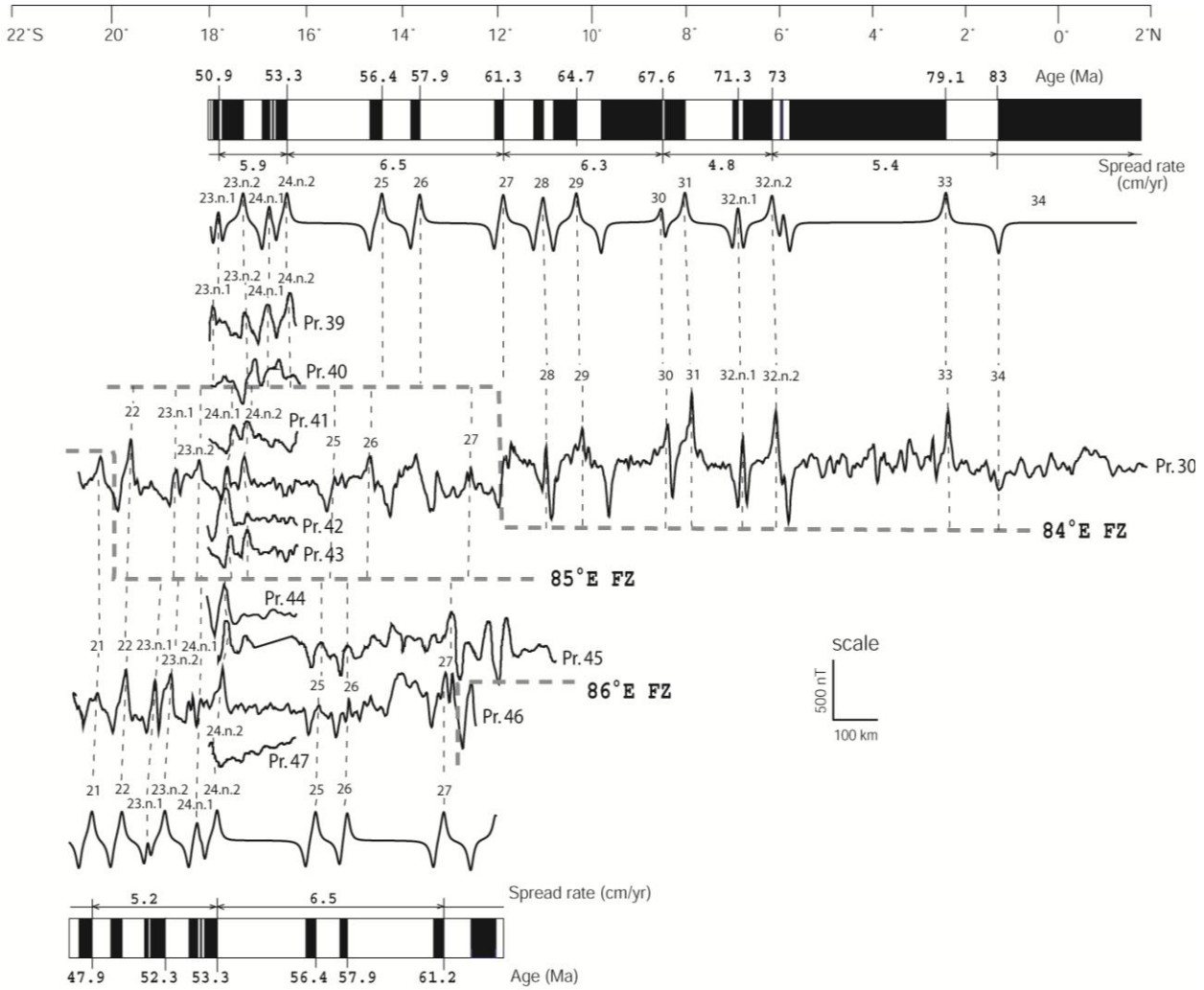

Figure 5.3 (a): Horizontal stack of magnetic anomaly profile data correlated with synthetic magnetic profiles west of the 86E Fracture Zone. Spreading-type magnetic anomalies 21–34 are identified and correlated from profile to profile. The geomagnetic polarity time scale of Cande and Kent (1995) was used for assigning the age to the magnetic lineations.

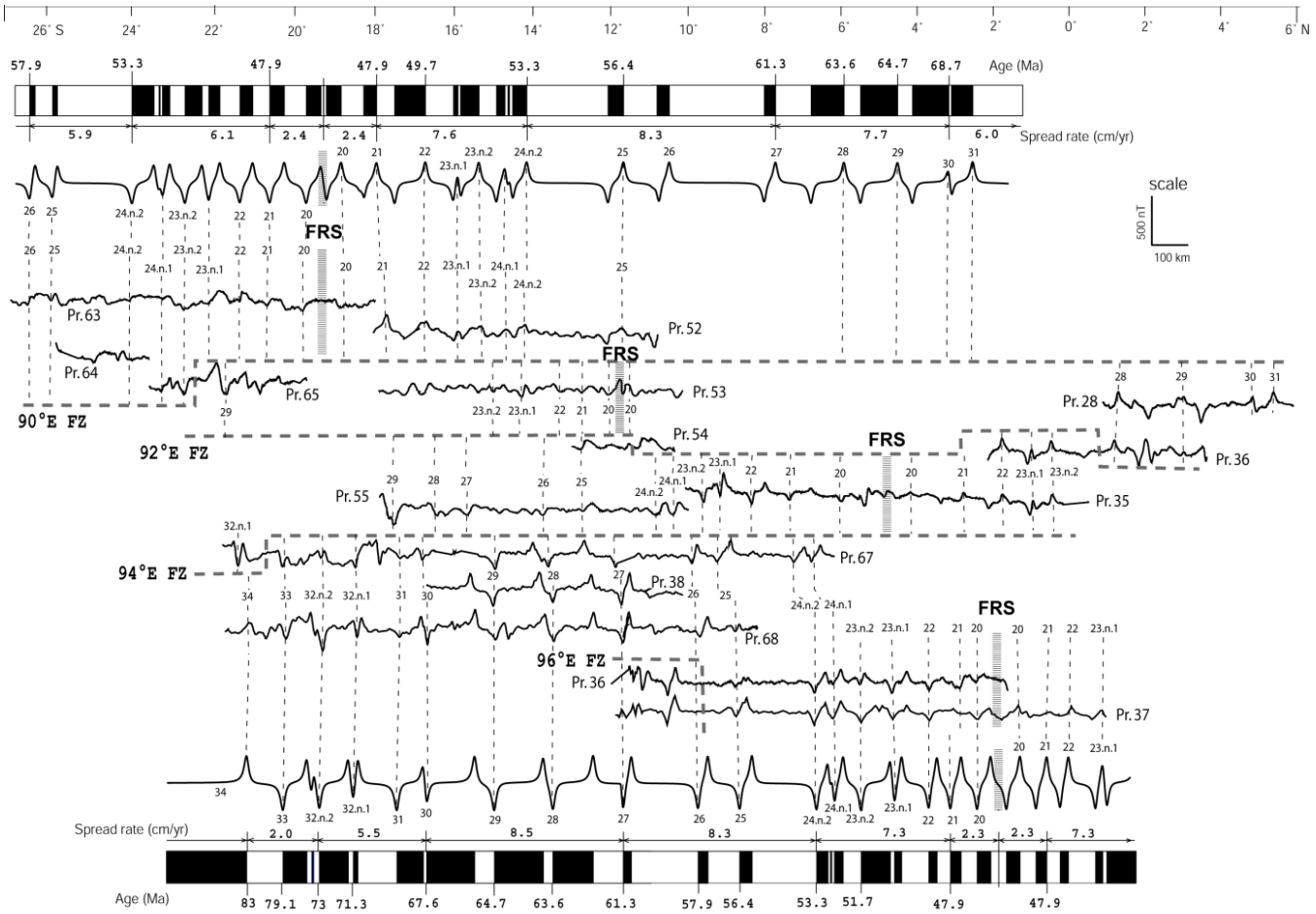

Figure 5.3 (b): Magnetic profile east of Ninetyeast Ridge. Magnetic anomalies 20–34 and fossil ridge segments (of middle Eocene age) are identified. The offsets in magnetic lineations are used to define several fracture zones. Hashed lines (FRS) denote abandoned ("fossil") spreading ridge segments.

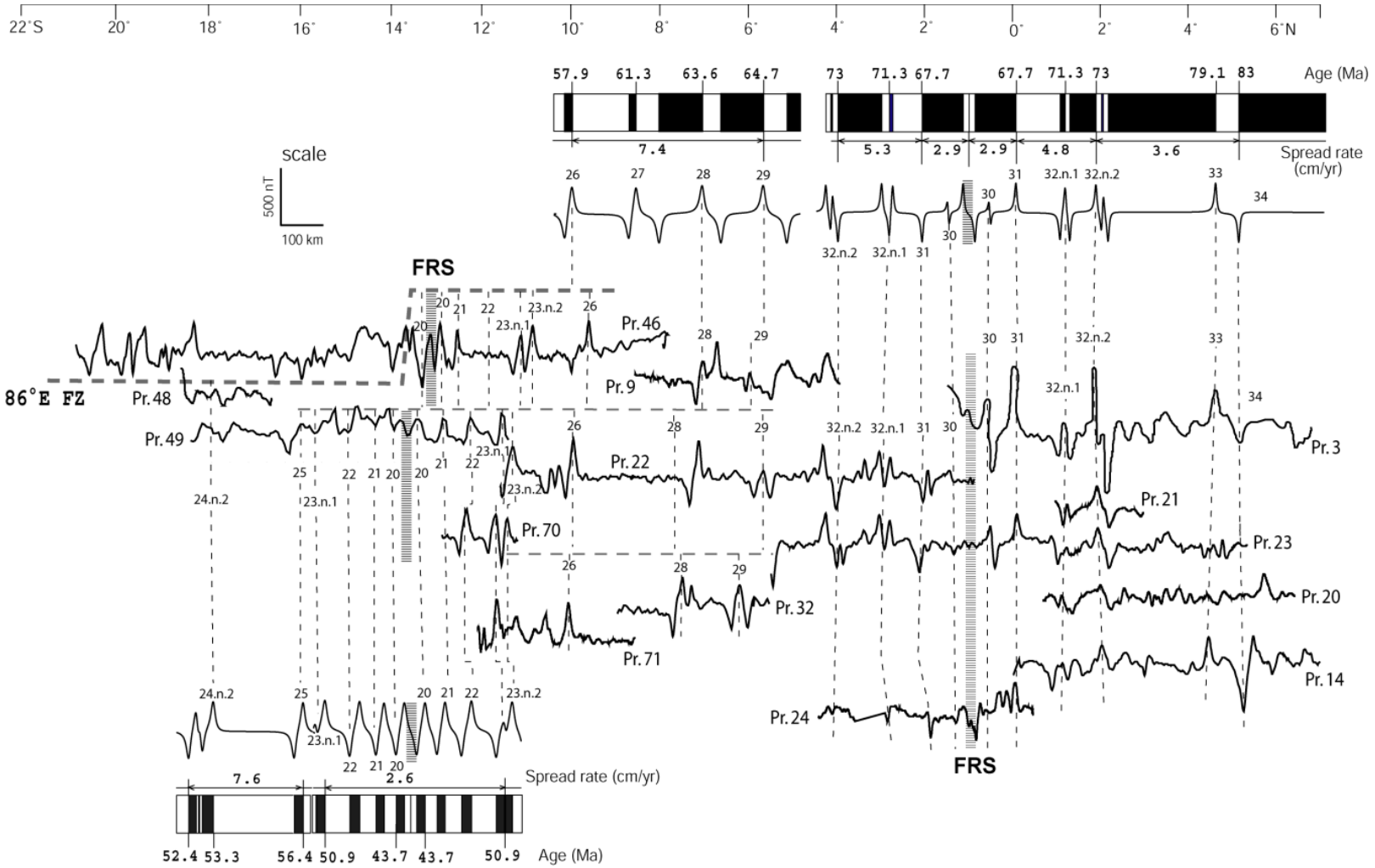

Figure 5.3 (c): Magnetic profile stack between the 86°E FZ and Ninetyeast Ridge. Anomalies 21–34 are identified and fossil ridge segments (FRS) of latest Cretaceous and middle Eocene age are identified. The magnetic lineations identified between the FRS have lost systematic continuity in anomaly sequence because of ridge jumps.

onwards from the location of slightly south of 20°S, the anomaly lineations up to 27 (~13°S) are identified with good confidence, which are offset with respect to corresponding lineations on east of the 85°E FZ with an average offset of 45 km towards north. No suitable magnetic profile is available towards north in this corridor for anomaly identifications older than 27 (Figure 5.3a).

In far western corridor bounded by 84°E FZ and 82°E FZ, magnetic anomaly lineations 23n.1 to 24n.2 between 15°S and 18°S latitudes are identified with an offset of about 90km. A data gap exists till 11°S latitude, then on further north anomalies 28 to 34 are identified with a specific characteristic anomaly signatures on single profile circ 5A (Figures 5.2 and 5.3a).

All the main regional profiles from each corridor in this area are modelled using the Matlab-based MODMAG algorithm (Mendel et al., 2005) for determining half-spreading velocities, which gave an average of 5.5 cm/yr for anomalies 21 - 24n.2, 6.4 cm/yr for anomalies 24n.2 - 30, 4.8 cm/yr for anomalies 30 - 32n.2 and 5.4 cm/yr up to anomaly 34 (Figure 5.3a).

The magnetic anomaly identifications of this area are compared with the earlier identification published by Royer et al. (1991) and Krishna et al. (1995). The contribution from the present study is demarcation of precise location of fracture zones, thereby E -W extent of the magnetic lineations and detailed modelling of half spreading rates.

5.3.2 Magnetic Anomaly pattern in Wharton Basin adjacent to the Ninetyeast Ridge

Magnetic anomalies east of the Ninetyeast Ridge in the western Wharton Basin till 96°E FZ are analysed compiling N-S ship-borne magnetic profiles (Figures 5.1 and 5.2). Segments of profiles odp121jr-a and d, knox06rr, tiog18-21, dsdp22gc, antp12A and B, 8400121a and b, mons3c and c0909 are plotted over free-air gravity anomaly image and interpreted magnetic anomaly picks are shown in Figure 5.2. Near N-S fracture zones similar to the one mapped in Central Indian Basin, are identified on gravity map along 89°E, 90°E, 92°E, 94°E and 96°E longitudes, which are named as fracture zones using same meridian names. Portions of conjugate pairs of magnetic lineations from 34 to 20 about the fossil ridge segment, broadly offset in left lateral sense by fracture zones are identified in the Wharton Basin region (Figure 5.2).

Immediately east of the Ninetyeast Ridge between 89°E FZ and 90°E FZ and between 11°S and 26°S latitudes, full sequence of conjugate anomalies from 20 to 25 are observed on either side of fossil ridge segment located around 20°S (Figure 5.2). North of 11°S, the 89°E

FZ starts obliquely cross the Ninetyeast Ridge and reaches western flank of the Ninetyeast Ridge at around 5°S and from there the fracture zone continues further north on west of the ridge. The magnetic profiles north of 11°S in this corridor fall on the Ninetyeast Ridge crest, hence the anomalies are subdued and disrupted due to volcanism, therefore no lineation pattern is identified in this area except an isolated anomaly 29 around 1°S immediately west of the 90°E FZ. The anomaly identification is supported by its signature as well the distance from the anomaly 25 identified south of it and offset is comparable with the same anomaly identified on opposite side of the 90°E FZ.

In other corridor between 90°E FZ and 92°E FZ, a fossil ridge segment (FRS) is observed around 11°S with an offset of >800 km with respect to the segment west of it. Anomaly 20 on north of the FRS and anomalies 20 to 23.n.2 to the south of it are identified, then there is a long data gap in south till 22°S, where anomalies 29 and 30 are identified (Figure 5.2). Towards north also there is a data gap till the location of anomaly identifications 25 and 26 around 3°S, on further north between 1°S and 6°N anomaly sequence 28 - 31 is identified and old oceanic crust may have subducted beneath the Sunda trench (Figure 5.2).

In another corridor between 92°E FZ and 94°E FZ, magnetic profile data are continuously available and well developed mirrored anomalies are identified north and south of the FRS located ~5°S offset by ~800 km with respect to western segment (Figure 5.2). Complete anomaly sequence from 20 to 32n.1 except anomaly 30 due to data gap around 20°S is identified, while north of the ASR anomalies 20 to 23n.2 are identified up to equatorial region, and further north data gap exists until the location of the trench.

The magnetic anomaly data in the corridor between 94°E FZ and 96°E FZ are also interpreted for identification of magnetic lineations and offsets in order to analyse the offset pattern of the ocean floor moving away from the Ninetyeast Ridge. Well-developed continuous anomaly sequence from 33 to 20 are identified south of the FSR located at ~3°S and anomalies 20 to 24n.2 except 21 and 22 are identified on north of the FSR, then the anomaly 24.n.2 nearly touches the Sunda trench at around 3°N (Figure 5.2). The offset of the fossil ridge segment with respect to the one in the corridor between 92°E FZ and 94°E FZ is around 200 km.

For the Wharton Basin region, half-spread rates range from 2.0 to 8.5 cm/yr are used for calculation of synthetic magnetic anomaly sequence 34 through 19 (Figure 5.3b) and observed that the spread rates for anomalies 34 to 19 are largely similar for the entire region

between the 89°E and 96°E longitudes except a small variation of < 5% from west to east. Half-spread rates were much slower during the formation of the anomalies 32n.2 to 34 (2.0 cm/yr) as observed in the Central Indian Basin region. Anomalies 32n.2 to 30 were formed by moderate half-spread rates of 5.5 - 6.0 cm/yr, higher spread rates are observed between the anomalies 30 - 24.n.2 ranging from 7.6 - 8.5cm/yr, and then between 24.n.2 and 21 with 7.3 - 7.6 cm/yr. The lower rates, 2.3 - 2.4 cm/yr were observed slightly before (from anomalies 21 to 20) the commencement of the cessation of spreading in the Wharton Basin.

Ages of the oceanic crust obtained from the magnetic anomaly studies (anomalies 25 and 26) in the vicinity of the DSDP Site 213 agree reasonably well with the age of oldest sediments recovered from the site (57 Ma) (Von der Borch et al., 1974b) (Figure 5.2). The anomaly identifications immediately east of the Ninetyeast Ridge especially southward progressive sequence from anomaly 20 to 25 has significantly improved compared to earlier interpretations (Royer et al., 1991; Krishna et al., 1995, 1999).

5.3.3 Magnetic Anomaly pattern in Central Indian Basin between 86°E FZ and Ninetyeast Ridge

The magnetic profiles tiog15-18, knox06rr, circ5b and 5c, wilkes907 and wilkes815, sk 82-02, sk 124-10-12, dsdp22gc, c1709b, rc1402 and inmd06mv are the N-S profiles mainly used for magnetic anomaly interpretations in the corridor between the 86°E FZ and the Ninetyeast Ridge (Figure 5.2).

The interpreted magnetic pattern between the 86°E FZ and the Ninetyeast Ridge are not in continuous sequence and thrown lot of surprises. Anomalies 33 and 34 are identified north of 5°N latitude, but towards south whole mirrored sequence of anomalies 32.n.2 to 30 are identified along with the fossil spreading centre (Figure 5.2). Immediately south of the conjugate anomaly sequence 30-32.n.2, anomaly 29 and younger sequence till 26 are identified, implying a southward ridge jump of considerable distance >300 km at the time of anomaly 30 (~65 Ma). Anomaly 27 is not identified due to profile break in the northward progressive sequence from 26 to 29, but assumed to be present according to the proportionate distance between 26 and 28 (Figure 5.2). Towards south, continuity of this sequence is also broken and a lineation pattern of 23.n.2 to 20 with fossil ridge centre near 13°S and the conjugate anomalies 20 and 21 are identified before reaching the Osborne knoll. Minor right lateral dislocations, <50 km at two locations offsetting the anomalies from 26 to 29 and younger anomaly conjugates to its south are noted, and this led to recognition of smaller

second-order fracture zones, whose continuation is not observed in anomalies older than 30. This suggests that these two fracture zones may have originated after magnetic anomaly 30 and continued up to anomaly 19. On south of the Osborne knoll, there is a data gap and further south anomalies 25 and 24.n.2in the vicinity of 19°S latitude are identified, which should be the continuation of the older northward progressive sequence broken after anomaly 26 by the younger anomaly conjugates, implying a northward ridge jump after anomaly 24n.2.

Ages of the oceanic crust obtained from interpretation of magnetic lineations agree obviously well with the ages of rock samples recovered at DSDP Site 215 in the region of Central Indian Basin, giving confidence in magnetic anomaly interpretations in this region. The rock samples at DSDP Site 215 shows 61 Ma age oceanic crust (Von der Borch et al., 1974a), which corresponds to magnetic anomaly 27 following the geomagnetic polarity timescale of Cande and Kent (1995). This is in good agreement with anomalies 26 and 28-29 in the vicinity of the DSDP Site 215.

The determined half-spread rates for magnetic anomaly pattern east of the 86°E FZ show average value of 5.3 cm/yr for anomalies younger than 24.n.2, 6.4 cm/yr for anomalies between 24.n.2 - 30, 4.8 cm/yr for anomalies between 30 and 32.n.2 and 5.4 cm/yr for older age anomalies 32.n.2 and 33 (Figure 5.3c). In the corridor between the 86°E FZ and the Ninetyeast Ridge, ages between the conjugate pattern 30-32.n.2 and the younger pattern 20-23.n.2 are recorded with slower average velocities of 4 cm/yr and 2.6 cm/yr, respectively, while the sequence of 32.n.2-33, 26-29 and 24.n.2-25 are marked with half-spread velocities of 3.6, 7.6 and 7.4 cm/yr, respectively.

Magnetic anomaly pattern in the central corridor (on immediate west of the Ninetyeast Ridge) is quite unsystematic and complex in comparison to that of other regions west of the 86°E FZ and east of the Ninetyeast Ridge. The pattern was controlled by a series of ridge jumps as well as second order fracture zones, the reason for such pattern could be the influence of the Kerguelen hotspot emplacement in proximity of the spreading centre and their thermodynamic interactions. Previous studies have also noted complex magnetic patterns west of the Ninetyeast Ridge (Royer et al., 1991; Krishna et al., 1995; Krishna and Gopala Rao, 2000) and in the Wharton Basin (Liu et al., 1983) in broader perspective. In this study we generated more accurate magnetic anomaly maps for the basinal regions on both sides of the Ninetyeast Ridge using up-to-date available magnetic anomaly profile data and

satellite gravity anomaly data, providing tighter constraints on the evolution of the Ninetyeast Ridge and the interaction of the hot spot with spreading ridge segments.

Analysis of magnetic pattern and precise locations of fracture zones of all three crustal domains of the study area, reveals that the age of the oceanic crust to the west of the 86°E FZ increases towards the north from early Cenozoic to late Cretaceous with minor right lateral offsets, while the crust to the east of the 89°E FZ increases its age in both north and south directions symmetric about the middle Eocene fossil Wharton Ridge segments with large left lateral offsets (Figure 5.2). Contrasting to these trends, the crust in between these FZs shows a complex age succession with different age (65 and 42 Ma) fossil ridge segments. The ridge segments abandoned at anomaly 30 and at anomaly 19 by ridge jumps are identified in the equatorial region and in the area between 12° and 14°S latitudes, respectively. It is observed that half-spreading rates are significantly reduced, as low as 2.9 and 2.3 cm/yr, close to the end-phase of ridge segments at anomalies 30 and 19, respectively (Figures 5.3b and 5.3c). The ridge segments that ceased at anomaly 19 were part of the cessation of the entire Wharton spreading ridge, thereby contributing to the second major plate reorganization in the Indian Ocean and unification of Indian and Australian plates into a single major lithospheric plate. This event is thought to be a result of continent-continent collision between India and Asia (Liu et al., 1983; Patriat and Segoufin, 1988).

5.4 Tectonic evolution of the Ninetyeast Ridge

Magnetic isochron analysis of the study area surrounding the Ninetyeast Ridge clearly points to the possibility of several southward ridge jumps, which can result in some age reversals at places along the continuous ridge track. But geochronology analysis of the Ninetyeast Ridge based on new high precision $^{40}Ar/^{39}Ar$ radiometric dating from basalts recovered at DSDP Sites 214, 216, 254 and ODP Sites 756-758 reveal that the portion of the Ninetyeast Ridge that was emplaced from north to south for a distance of ~3980 km, during the period from 77 to 43 Ma follows a monotonous linear pace with geological time (Pringle et al., 2007, 2008). These new ages are more accurate and precise than previous age determinations (Duncan, 1978, 1991). A plot of age versus location along the ridge displays remarkable linearity (Figure 5.6), with age decreasing to the south at a rate of 118$\pm$5 km/Myr (Pringle et al., 2008). This contrasts with earlier dates that implied a significantly slower rate of 86$\pm$12 km/Myr (Duncan, 1991). The new propagation rate for the Ninetyeast Ridge indicates that the ridge formation was completed in a period less by ~10 Myr than previously thought.

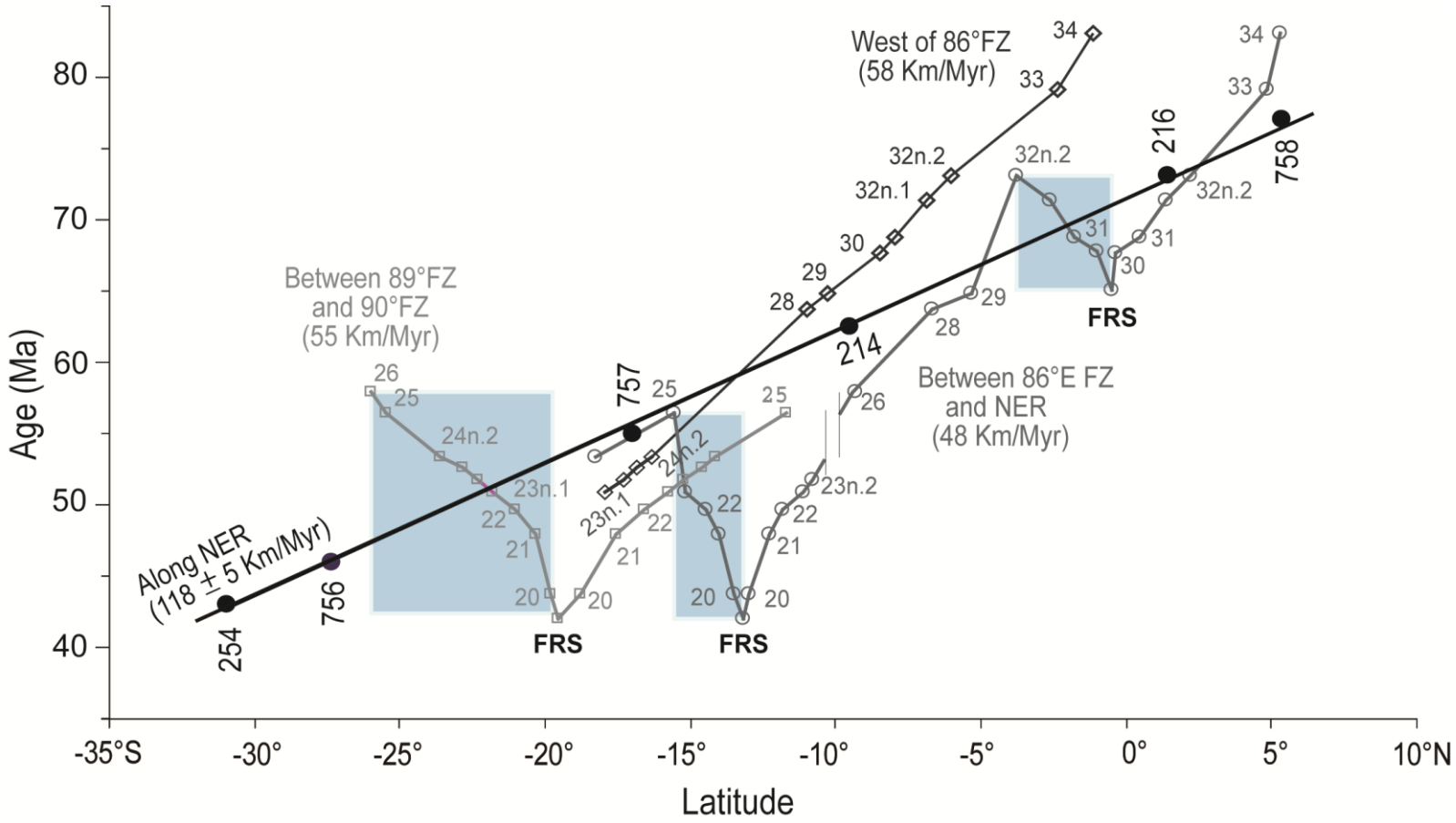

Figure 5.4: Comparison of rates of ocean crust creation in different spreading corridors and the volcanic propagation rate on the NER. Radiometric ages from DSDP and ODP sites along the NER, seafloor created immediately to the west between the 88°E and 89°E fractures zones, and seafloor created immediately to the east between the 89°E and 90°E fracture zones. Black dots show ages of drill core samples (Pringle et al., 2008); open symbols denote seafloor spreading magnetic anomalies of corresponding regions. FRS indicates fossil ridge segment. Shaded portions indicate Antarctic plate crust transferred to Indian plate through ridge jumps.

Moreover comparison of the age progression along the Ninetyeast Ridge with that in adjacent oceanic basins (Figure 5.2 and 5.4) indicates that the Ninetyeast Ridge lengthened much more rapidly than adjacent lithosphere. In basinal regions west of the 86°E FZ and east of the 90°E FZ, magnetic lineations 33 and 20, corresponding approximately to 77 and 43 Ma, respectively, are separated by ~2000 km (Figures 5.2 and 5.4), revealing that the oceanic crust was created at a rate of ~58 km/Myr. In other areas closer to the Ninetyeast Ridge (between 86°E FZ and Ninetyeast Ridge; between 89°E FZ and 90°E FZ), the oceanic crust was formed at comparable rates ranging from 48 to 55 km/Myr. This discrepancy between the lengths of the Ninetyeast Ridge and adjacent oceanic crust formed during the same period is inconsistent with previous studies, which advocated that the Ninetyeast Ridge formed simply as the rapidly northward moving Indian plate drifted over the hotspot. Now that the difference between relative plate velocity, recorded by seafloor magnetic lineations, and the volcanic propagation rate of the Ninetyeast Ridge, which reflects the velocity of the Indian plate relative to the hotspot are revealed with more precision.

The propagation rate of the Ninetyeast Ridge volcanism is about twice that of the half-spreading rates recorded on the Indian plate, or similar to the full-spreading rate between the Antarctic and Indian plates. The motion of the Antarctic plate relative to the hotspot reference frame at this time was slow (Acton, 1999; Besse and Courtillot, 2002). Thus, relative to a nearly fixed Antarctic plate, the Indian plate was moving northward at about the full spreading rate, and the Wharton spreading center itself was migrating northward at about the half spreading rate. It would thus seem that the Ninetyeast Ridge volcanic propagation simply records this full spreading rate as postulated previously (e.g. Royer et al., 1991). Because of its rapid northward drift relative to the Ninetyeast Ridge hotspot, the Wharton spreading ridge should have crossed over the hotspot, and subsequent volcanism would have occurred on the Antarctic plate. However, the eruption ages for the Ninetyeast Ridge core samples are similar to the nearby magnetic anomalies indicating that the Wharton spreading ridge remained relatively close to the hotspot throughout much of the Ninetyeast Ridge history (Figure 5.4). This circumstance required that some tectonic mechanism acted to keep the spreading ridge close to the hotspot and in this study it hypothesised by the mechanism of hotspot interaction with Wharton spreading ridge which resulted in multiple jumps of a portion of spreading ridge in immediate vicinity, towards the hotspot.

5.5 Wharton ridge segments and interaction with the Kerguelen hotspot

The fossil spreading ridge segments observed west of the 89°E FZ (Liu et al., 1983) are found to be continuing till 86°E FZ as portions of Wharton fossil ridge (Krishna et al., 1995, 1999). Using an updated magnetic data set in this region an improved interpretation of magnetic anomalies, particularly immediately to the east and west of the Ninetyeast Ridge (Figure 5.2), supersedes earlier anomaly identifications (Sclater and Fisher, 1974; Liu et al., 1983; Royer et al., 1991; Krishna et al., 1995). From the trends of the FZs and the Ninetyeast Ridge and its morphology, it is found that the 89°E FZ crosses the Ninetyeast Ridge obliquely between 15°S and 10°S latitudes (Figure 5.2). Consequently the Ninetyeast Ridge was formed in two different spreading corridors of oceanic crust: the north part of the ridge emplaced before ~62 Ma is situated between the 89°E FZ and the 90°E FZ, while the south part of the Ninetyeast Ridge is located between the 86°E FZ and the 89°E FZ. As described in section 5.3.3, the oceanic crust between the 86°E and 90°E FZs shows non-monotonic sequences of magnetic lineations caused by ridge jumps, with two major jumps occurring at 65 and 42 Ma. In the northern part there is a data gap immediate east of the ridge between the 86°E FZ and the 89°E FZ (Figure 5.2).

At ~90 Ma, the Indian plate was bounded on the southwest side by the Wharton and India-Antarctica ridges, which were connected through the 86°E transform fault (Krishna et al., 1995) and the Kerguelen hotspot was located beneath the Indian plate at a moderate distance from the Wharton Ridge segments. During the first spreading reorganization during the late Cretaceous, a ridge segment immediately west of the Ninetyeast Ridge ceased its activity at ~65 Ma and jumped southward to a place between the locations of magnetic anomalies 33 and 32n.2. This spreading segment also broke into three smaller sub-segments. The ridge jump created a fossil ridge segment, now located near the equator (Figure 5.2), and transferred oceanic crust from the Antarctic plate formed between magnetic anomalies just younger than 30 to older than 32.n.2 to the Indian plate (Figures 5.2 and 5.3c). During the second spreading jump at ~52 Ma, two sub-segments to the west of the Ninetyeast Ridge jumped northward to the crust formed between anomalies 25 and 26 (Figure 5.3c), and transferred oceanic crust from the Indian plate formed between magnetic anomalies just younger than 24n.2 to just older than 25 to the Antarctic plate (Figures 5.3c and 5.5d), while a third sub-segment closer to the Ninetyeast Ridge appears to have jumped southward into pre-anomaly 34 oceanic crust. Finally, in the third spreading reorganization the entire Wharton Ridge system, including all three sub-segments, ceased spreading soon after middle

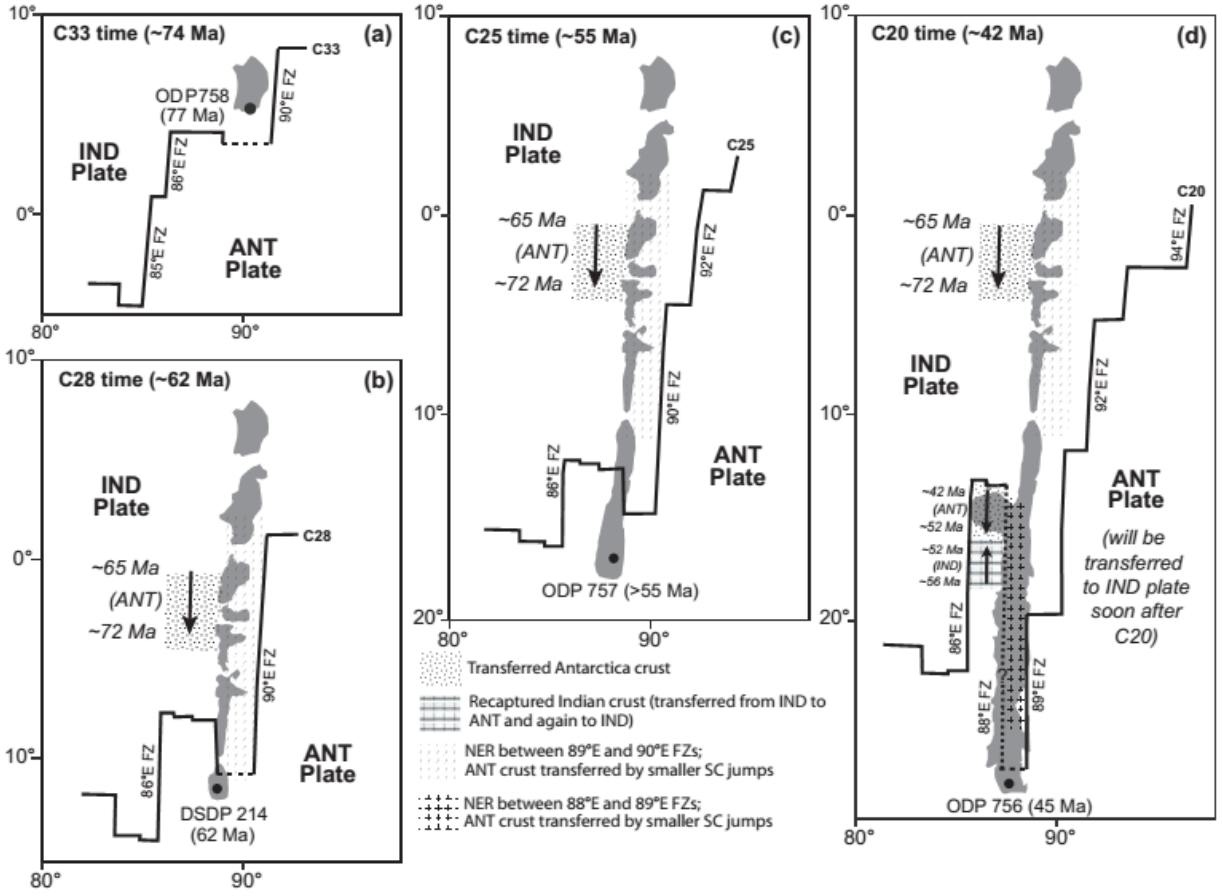

Figure 5.5: Tectonic evolution of the NER with respect to adjacent spreading ridge segments for four different ages from the Late Cretaceous to early Cenozoic. Solid lines show the relatively well constrained location of the Wharton spreading centers and transform faults on either side of the NER. Dashed lines represent the Wharton spreading segment active directly under the NER at that time; its location is only approximate because the complex volcanic history of the crust directly under the NER did not allow the formation of discernable magnetic anomaly patterns. Two episodes of spreading center jumps and transferred crust can be specifically identified directly to the west of the NER. The more frequent, smaller spreading center jumps proposed for the corridor directly under the NER cannot be specifically identified, but those corridors should include about 50% crust transferred from the Antarctic (ANT) to Indian (IND) plates.

Eocene anomaly 19. This process eventually led to unification of the Indian and Australian plates into a single Indo-Australian plate.

Based on the complex magnetic anomaly pattern with the age progression of ocean floor derived from magnetostratigraphy on either side of the Ninetyeast Ridge in comparison with the progression of ages determined from drill core samples (Figures 5.2 and 5.4), and proximity of the hotspot to spreading centres, two possible explanations for the ridge jumps with respect to the Kerguelen hotspot are suggested. With the observation of a few large ridge jumps to the west of the Ninetyeast Ridge and the apparent continuity of the hotspot track, evolution of the Ninetyeast Ridge may be explained by the positioning the Kerguelen hotspot beneath the Indian plate continuously from 77 to 43 Ma. This model requires a large amount of Antarctic plate lithosphere to be transferred to the Indian plate via spreading center jumps to the south away from the hotspot. Although this model appears to be simple because it allows the Ninetyeast Ridge to form simply and with a monotonic age progression, the jumping of the ridge away from the hotspot appears counter to the widely held idea that the excess heat and dynamic uplift over the hotspot weakens the lithosphere, causing the spreading center to jump toward the hotspot position. Observations on ridge-hotspot interactions at other locations led several researchers (Brozena and White, 1990; Small, 1995; Hardarson et al., 1997; Mittelstaedt et al., 2011) to conclude that ridge segments jump repeatedly toward a hotspot, even when the overall motion of the ridge may be away from the hotspot. It is thought that warm upper mantle temperatures weaken the lithosphere and the hotspot-imposed stress field provides necessary conditions for rifting. A possible explanation for the unusual behaviour of the ridge jumps near the Ninetyeast Ridge is that regional stress changes caused these ridge jumps, overriding local stresses caused by the hotspot.

An alternative model, which fits the notion of the spreading ridge jumping toward the hotspot, has the Wharton Ridge system drifting northward of the hotspot and the ridge segment beneath the Ninetyeast Ridge repeatedly jumping back to the hotspot location, thereby accreting bits of the Ninetyeast Ridge from the Antarctic plate to the Indian plate. Ninetyeast Ridge components formed on the Antarctic plate should have reverse age progressions (i.e. younger toward the north). The existing, reliable age data (Figure 5.4) are sparse, but remarkably consistent with a simple, linear age progression. Thus, if this explanation is true, reverse age segments must occur in the gaps between dated samples or the ridge jumps were frequent and small enough that the reversed age trends are not resolvable (Sager, et al., 2010). Although it requires the added complexity of additional ridge

jumps, this hypothesis is preferred because it allows the ridge segment to jump to the hotspot and it fits the observed hotspot-ridge offsets interpreted from magnetic lineations, which fix the hot spot to the south of the Wharton Ridge during the Cenozoic.

Various stages of possible interactions between the spreading center and the Kerguelen hotspot during the formation of the Ninetyeast Ridge are presented in Figures 5.5a-d. Initially the hotspot was beneath the Indian plate and possibly at some distance from the spreading centre, resulting in intraplate volcanism on the Indian plate now in the Bay of Bengal region (Figure 5.5a). This postulation is supported by the presence of regional lithospheric flexure determined beneath the Ninetyeast Ridge in the Bay of Bengal region (Gopala Rao et al., 1997; Tiwari et al., 2003; Sreejith and Krishna, 2013, 2015). Subsequently, rapid northward migration of the Wharton spreading ridge allowed it to coincide with the hotspot for on-axis volcanism (Figure 5.5b), which may have emplaced sections of the Ninetyeast Ridge simultaneously on both plates (with much of that formed on the Antarctic plate eventually captured via ridge jumps). Evidence of the Kerguelen hotspot volcanism on the Antarctic plate during the formation of the Ninetyeast Ridge is basalts from Skiff Bank (Kerguelen Plateau) dated at 68 Ma (Coffin et al., 2002).

Further spreading centre migration would have placed the hotspot beneath the Antarctic plate for near-ridge or ridge-flank volcanism (Figure 5.5c). With continued ridge migration, the hotspot moved farther from the spreading ridge beneath the Antarctic plate. The stress field created by the hotspot may have caused uplift and weakening of the overlying oceanic lithosphere, resulting in the initiation of rifting and spreading within the Antarctic plate and leading to southward ridge jumps. It is possible that hotspot material flowed along the base of the lithosphere to reach the spreading centre for on-axis volcanism (Figure 5.5d), even when the hotspot was not located in the vicinity of the spreading ridge crest. This mechanism has been called upon to explain some features of the Amsterdam‐St. Paul plateau, which is nearby and had a similar history of construction (Maia, 2011). In addition, the magnetic anomalies suggest that the Ninetyeast Ridge formed within a relatively narrow spreading center corridor with long-offset FZ segments (Figure 5.2), and some Ninetyeast Ridge volcanism may have occurred along the FZ or the long offsets may have encouraged small bits to break off of the Antarctic plate (i.e. micro-plates or ridge jumps). The continuous process of hotspot-spreading ridge interaction may have provided necessary conditions to cause multiple ridge jumps. This behaviour is also consistent to ridge -hotspot interaction in which ridge jumps are promoted by hotspot heating of the lithosphere and

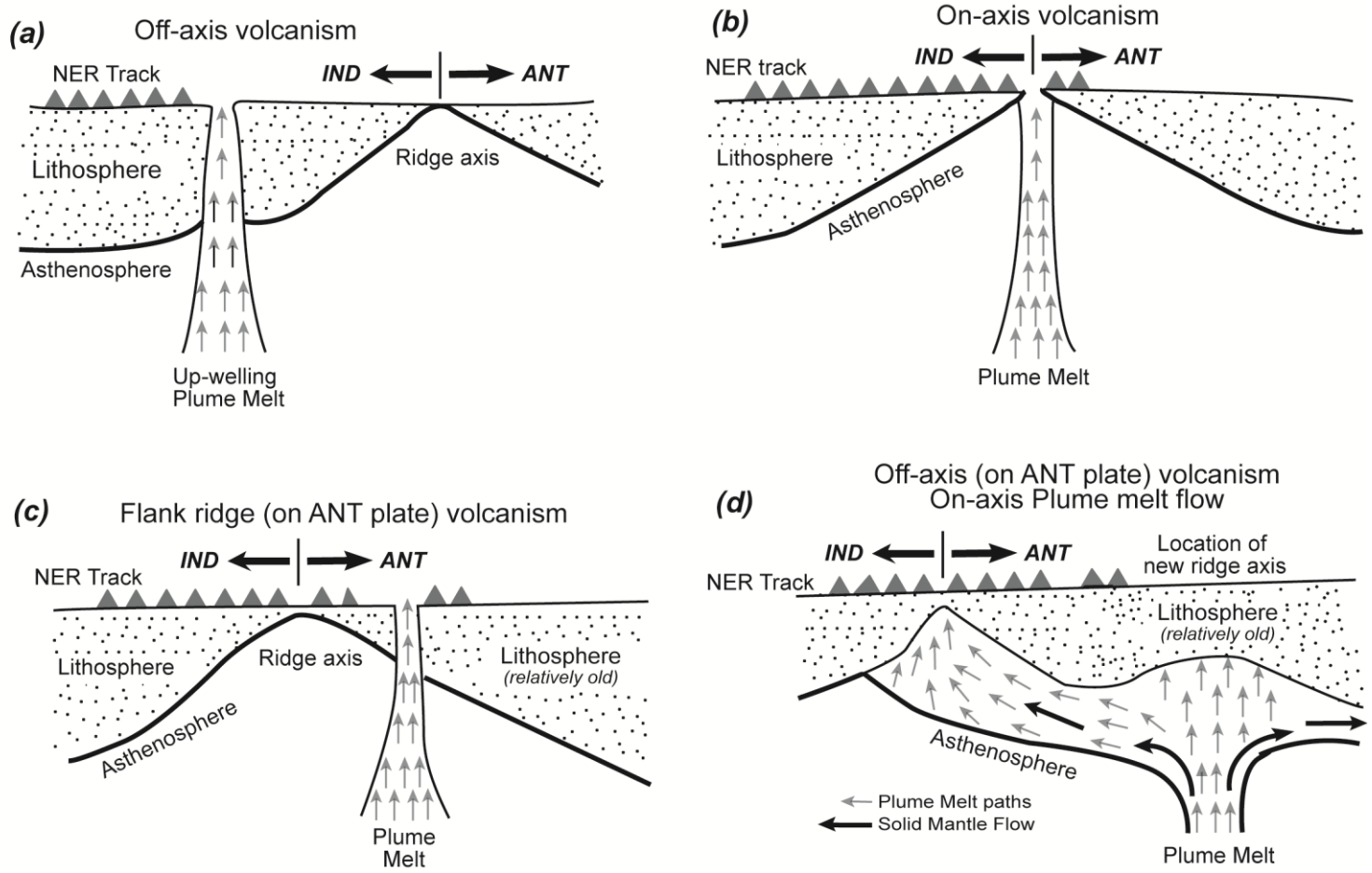

Figure 5.6: Sketch model showing possible interactions between the Kerguelen hot spot, proximal ridge segments, and oceanic lithosphere during the formation of the NER. The model is developed on the basis of the conceptual model of Mittelstaedt et al., 2011 and the results obtained from the present study. (a) Off-axis volcanism when the hot spot was located north of the spreading ridge segments. (b) On-axis volcanism when the hot spot was located at the spreading ridge after northward migration of the plate boundary (Wharton Ridge) with respect to a nearly fixed Antarctic plate. (c) Volcanism on the ridge flank when the hot spot was located beneath the weak lithosphere of the Antarctic plate. (d) On-axis melt flow when the hot spot was located off-axis beneath older lithosphere of the Antarctic plate.

perturbations of the local stress field, and form preferentially in younger lithosphere in systems with relatively fast plate velocity (Mittelstaedt et al., 2008, 2011).

Earlier research on magnetic anomaly data around Ninetyeast Ridge (Krishna et al., 1999; Desa et al., 2009) have proposed a model for southward ridge jump at anomaly <30 and have identified ridge jumps at anomalies <24.n.2 and <19, immediately west of the ridge. In present study based on a new identication of anomalies in between 86°E FZ and Ninetyeast Ridge with short right lateral offsets (Figures 5.2 and 5.3c) and new chronological data on the ridge a new ridge evolution model is proposed till anomaly 20 (42 Ma), in four stages (Figures 5.5a-5.5d), considering thermodynamic constraints, which is most plausible within the limitations of presently available data.

5.6 Implications of Magnetic pattern analysis under the constraints of chronologic data

It is obvious from age data of the Ninetyeast Ridge and adjacent oceanic crust evolved within the same time frame (77 to 43 Ma) that the length of the Ninetyeast Ridge is much greater than the stretch of the oceanic crust evolved on the Indian plate (Figure 5.5). The Ninetyeast Ridge emplacement rate was almost a factor of 2 faster than the rate of accretion of oceanic crust. The extra length of the Ninetyeast Ridge track is ~2000 km, and because the Wharton spreading ridge would have quickly passed the hotspot, it is necessary to postulate other explanations than simple plate drift. Furthermore, the linear trend of the Ninetyeast Ridge ages (Pringle et al., 2008) implies that significant slowing of the Indian plate, considered as a response of the continental collision between India and Asia, did not start until completion of construction of the entire Ninetyeast Ridge (~42 Ma). Slow spreading rates (2.4 - 2.9 cm/yr) observed in the present study (Figures 5.3b and 5.3c), particularly in two phases (anomalies 31 to 30 and again from 21 to 19) appear to indicate waning stages of ridge segments in the process of abandonment, but not a response to the slowing of the Indian plate motion.

As discussed in section 5.4, the Kerguelen hotspot was initially in an off-ridge position during the formation of the Ninetyeast Ridge in the Bay of Bengal region (Figure 5.5a), therefore the Wharton spreading ridge may have taken considerable time to reach the position of the hotspot and to move away towards north. In the process, the northern part of the Ninetyeast Ridge, at least down to 5°N latitude, was created by two different plate motions, viz., by plate motion relative to the hotspot and by a plate boundary (Wharton spreading ridge) migration. The latter activity may have added some additional length of volcanic

constructs to the Ninetyeast Ridge track. During the emplacement of the central part of the Ninetyeast Ridge, particularly from 5°N to 11°S latitudes, the hotspot and ridge segments were often in close proximity and this may have allowed the hotspot to form components of the Ninetyeast Ridge on the Antarctic plate that were subsequently transferred to the Indian plate through southward ridge jumps (Figures 5.5b - 5.5d). Isostatic studies of the Ninetyeast Ridge and its magma rate productions do clearly suggest the interactions between the ridge segments and Kerguelen hotspot and multiple southward ridge jumps (Sreejith and Krishna, 2013, 2015).

A critical question for the Ninetyeast Ridge evolution is how many such ridge jumps occurred. Our interpretation of the magnetic data set in basins adjacent to the Ninetyeast Ridge is a small number of larger ridge jumps. However, both Krishna et al. (1999) and Desa et al. (2009) have mapped smaller southward ridge jumps near the Ninetyeast Ridge at ~76 and 54 Ma, respectively. Sager et al. (2010) concluded, on the basis of identification of extensive faulting within the Ninetyeast Ridge structure, that numerous small-scale ridge jumps may have occurred and that the hotspot and Wharton spreading ridge may have remained in close proximity. Small ridge jumps are an attractive solution to the paradox that large ridge jumps would result in long segments of reversed age trend yet existing age data are remarkably linear (Figure 5.4). Such ridge jumps may also explain the apparent increased FZ offsets during the Cenozoic on the Wharton Ridge near Ninetyeast Ridge (Figure 5.5).

Although it is true that existing Ninetyeast Ridge age data are sparse and might not detect a reversed age segment, the deviant segment could be hiding in the gaps of the current data. Further, magnetic anomalies near the Ninetyeast Ridge are very difficult to interpret (Figure 3) presumably because the extended history of hotspot and spreading center volcanism does not result in simple magnetization of the ocean crust and discernable patterns of magnetic anomalies. Another factor is that small ridge jumps can be difficult to detect because this requires the recognition of a repeated anomaly pattern that may not be clear unless there are several mirrored anomalies (i.e., a seafloor spreading for a significant time). Thus, despite the improvement with the current magnetic data set over prior compilations, it is not surprising that small ridge jumps are not recognized in the pattern of magnetic anomalies along the Ninetyeast Ridge. More detailed magnetic surveys with closely spaced data would be needed to recognize of small jumps, as shown, for example, at Amsterdam‐St. Paul Plateau (Maia et al., 2011).

Besides the processes discussed above, absolute hotspot movement also may have contributed to the lengthening of the Ninetyeast Ridge. Paleomagnetic analyses and mantle flow models have been used to infer 7 - 10° (800 - 1100 km) of southward motion of the Kerguelen hotspot during the past 120 Ma (Klootwijk et al., 1991; Antretter et al., 2002; O'Neill et al., 2003). Such southward motion would also lengthen the Ninetyeast Ridge, but we cannot quantify the north-south hotspot motion because our data set only shows the relative motions of the hotspot and spreading centre.

This chapter concludes the results of magnetic profile data analysis with a model of Ninetyeast Ridge evolution. Next chapter discuss 2D seismic reflection data interpretation at selected grids on the ridge and the inferences.

Chapter 6

6 Seismic structure and fault activity along the Ninetyeast Ridge

6.1 Introduction

The Ninetyeast Ridge was widely believed to be emplaced by the Kerguelen hotspot volcanism (Peirce, 1978; Peirce et al., 1989; Royer et al., 1991) during the period ~80 - 40 Ma (Pringle et al., 2008). The ridge accretion was completed approximately between the events of first and second major plate reorganisations of the Indian Ocean, coinciding with the period of northward migration of the Indian plate. The ridge was emplaced when the north-south seafloor spreading along the Wharton Ridge and India-Antarctica Ridge was dominantly prevalent. It was also believed that the Kerguelen hotspot activity was in close proximity to the spreading centers of the Wharton Ridge during the Ninetyeast Ridge evolution (Royer et al., 1991; Krishna et al., 1999, 2012). An extensional regime along both the Wharton Ridge and India-Antarctica Ridge led to form E-W gravity lineations, horst-graben structures as well as normal faults from north to south across the Ninetyeast Ridge (Sager et al., 2010, 2013). Later, during the Miocene period an intraplate lithospheric deformation was initiated and is currently underway in the central Indian Ocean (Weissel and Anderson, 1980; Weins et al., 1985; Bull and Scrutton, 1990; Cochran et al., 1990; Chamot-Rooke et al., 1993; Krishna et al., 1998, 2001, 2009a). Further the deformation zone has divided the single Indo-Australian plate into three sub-plates: India-Australia, Capricorn-India and Capricorn-Australia (Royer and Gordon, 1997; Gordon et al., 1998) (Figure 6.1). As a result most part of the Ninetyeast Ridge locates within a deformation zone and central part of the ridge lies within the zone of diffuse triple junction between the sub-plates boundaries, which implies the chance of the ridge being pivotal in fixing the boundaries of these plates (Tinnon et al., 1995; Delescluse and Chamot-Rooke, 2007; Sager et al., 2013). Therefore, the Ninetyeast Ridge as a whole is under different deformation-related stress fields active on either side of the ridge and also the stress directions vary along its stretch from north to south gradually and different for its southern and northern parts. High magnitude seismicity generally attributed to the lithospheric plate boundaries is found associating with the most part of the northern Ninetyeast Ridge (Weins et al., 1986). With the identification of variety of faults on KNOX06RR 2D (two dimensional) seismic profile data and multibeam data, Sager et al. (2013) have demarcated the spatial

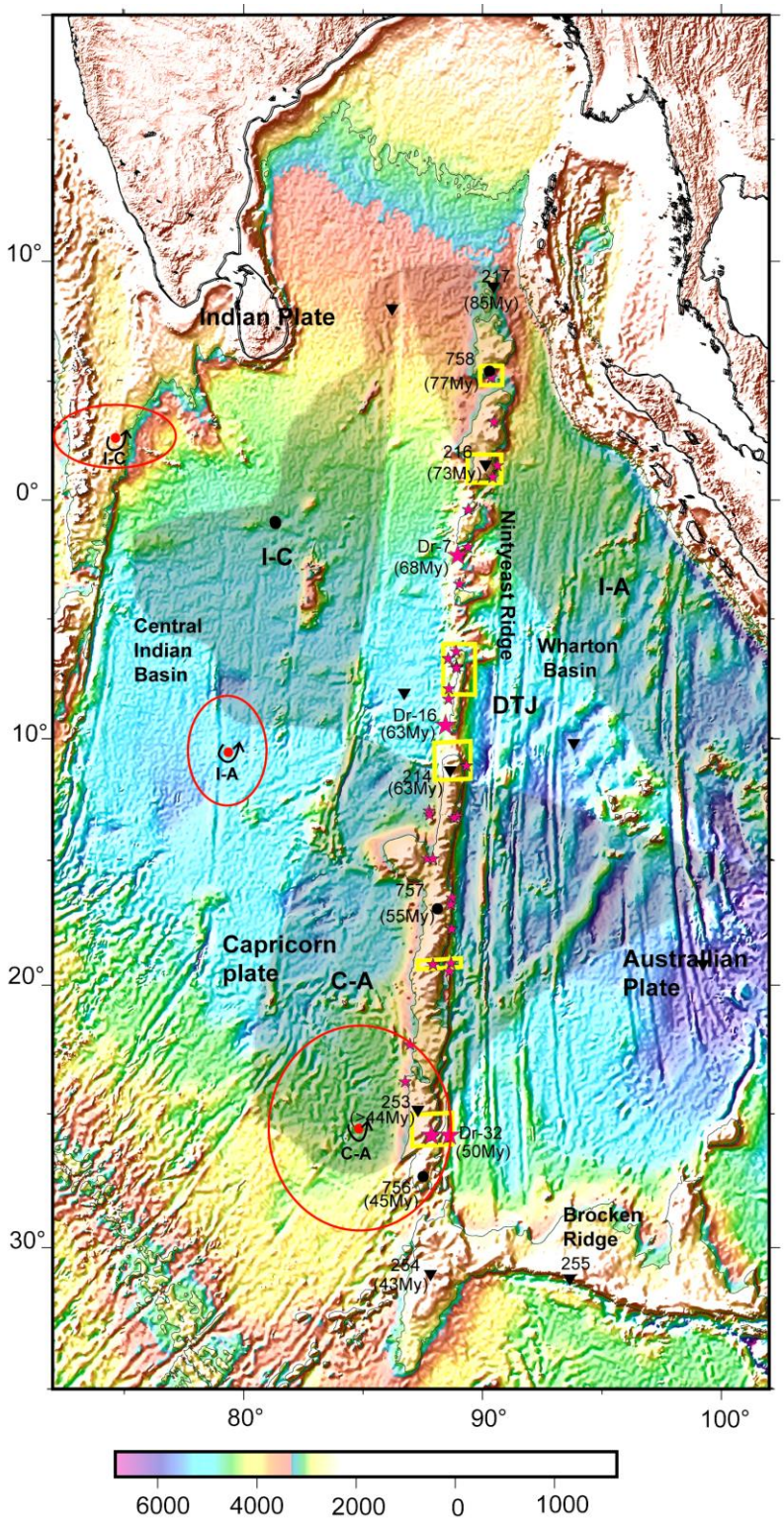

Figure 6.1: Ninetyeast Ridge environs and tectonic setting. Background plot is satellite-predicted bathymetry (Smith and Sandwell, 1997). Shaded areas around the NER represent diffuse plate boundaries (I-C = India-Capricorn, C-A = Capricorn-Australia, I-A = India-Australia; DTJ=diffuse triple junction) (Royer and Gordon, 1997). Yellow boxes show study sites. Red-filled circles denote Euler poles: IN-CP - India-Capricorn, IN-AU - India-Australia, CPAU - Capricorn-Australia (DeMets et al., 2010). Red ellipses show pole 95% confidence regions. Magenta stars KNOX06RR dredge sites. Black triangles DSDP sites. Black circles ODP drill sites.

changes of compression, transpression and extension along the Ninetyeast Ridge. The dataset is re-examined in the present study for the detailed interpretation and for mapping of major seismic reflectors and faults in order to bring out fault-related tectonic styles, re-activations or cessation. As the ridge got emplaced near a divergent plate boundary, normal faults would have formed and remained active awhile till the volcanic edifice got moved away from the spreading center. Later stress changes caused by the plate movements may have reactivated the same faults in different characters from strike slip, compression to extension according to their locations with respect to direction of deformation stress. But, at the same time it is quite possible that some of the initial normal faults did not get reactivated and remained as dead faults in spite of changes in deformation style especially when the stress magnitude is comparably low. So, reactivated normal faults are expected in all the grid sites and throws can be measured along the reflector displacement for the fault analysis. Therefore, the present study is used to detail the active stress directions by means of fault strike analysis delineated by correlation of active faults between 2D seismic reflection profiles with the help of multibeam bathymetry data of the area.

6.2 Seismic reflection and multibeam bathymetry data on Ninetyeast Ridge

During the KNOX06RR cruise, high resolution 2D seismic data were acquired at six grids located from north to south over the Ninetyeast Ridge (Figure 6.1). The seismic data were acquired using 48 channel hydrophone streamer and 2 identical generator injector air guns as sound source, so that the geometry generated ~10 fold 2D seismic data with a CDP interval of 6.25 m and is recorded at 0.5 ms sampling interval (Cruise Report KNOX06RR, 2007). Subsequently, the data were processed at Texas A&M University, College Station and time migrated data were stored in NGDC database (Sager et al., 2010) for the purpose of other users. Along the seismic profiles 12 KHz bathymetric data were also collected with EM120 multibeam echo sounder. The data processing was done on board using MB-System software. Older single channel seismic reflection data collected during the DSDP 22 and 26 and ODP 121 Legs were of low resolution, hence they were not used for retrieving the finer details of the ridge structure.

Seismic data interpretation was carried out using OpendTect 5.0 free open source software by dGB Earth Sciences for mapping of horizons and faults on all 2D profiles recorded at six grid sites of the Ninetyeast Ridge. The 2D lines for each grid site were loaded as single project. Generic Mapping Tools (GMT) is used for all bathymetric mapping and free open source photo editing software was used for image editing.

6.3 Interpretation of KNOX06RR grid site seismic reflection profiles and fault correlation with multibeam data

The KNOX06RR seismic profiles are interpreted for major reflectors and correlated to lithologic or stratigraphic markers of available DSDP and ODP Sites at each grid location. As the seismic profiles are of higher quality, the acoustic basement is easily identified on almost all profiles with its property of strong seismic amplitude against that of overlying sedimentation. Contour maps of the basement (in two-way travel time) are prepared by manual interpolation between 2D lines within each grid location following the multibeam and satellite bathymetry trends as guidance, assuming the bathymetric observations are broadly governed by the basement tectonics, and on ridge peaks the basement gets shallower and on troughs basement goes deeper.

In second stage of interpretation, faults are identified as discontinuity of reflectors starting from acoustic basement to overlying sediment sequence till the least visible displacement and the sequence above become horizontally continuous. Faults are analysed in seismic section for their typical characteristics to categorise them to strike slip or dip slip as well as to make out the component of compression, if present. The displacement of reflectors at major dip slip faults are measured in time and converted them into depth using interval velocities available from nearby wells. The relative displacements with respect to the basement are noted to approximate the onset of major faulting or fault reactivation. Active faults are identified when the fault stick continued till near the water bottom.

The multibeam bathymetry map of each grid site is analysed for describing seafloor morphology and identification of seafloor/ tectonic lineations. The 2D seismic profiles are drawn on bathymetry map along with annotation of two-way travel time to basement, at every 500 trace number, and then contour maps are made manually with interpolation between the profiles broadly following the bathymetry trends. The interpreted seismic profiles are then overlaid on bathymetry map with basement time

contours, and faults of nearby N-S profiles are joined with the guidance of throw direction, type and also considering the associated seafloor lineations on bathymetric map as troughs or offsets of bathymetric contours. Thus, the strikes of number of active faults are determined at each grid location.

The dips of these active faults are assumed high ranging from 80° to 85° and strikes are measured on the map at regular intervals. The values of strikes and dips are randomised between minimum and maximum of observed values to make 30 pairs of observations per each fault in order to plot on stereonet as fault planes. Rose diagram is also generated for each grid site with the help of stereonet software.

6.3.1 Site 758 (5°N latitude)

During the KNOX06RR cruise, 9 seismic profiles were acquired in the vicinity of the ODP Site 758 location covering a grid area from 4.95˚ N to 5.52˚ N latitudes and from 90.10˚E to 90.65˚E longitudes (Figure 6.2). The profile configuration consists of 4 north-south and 5 east-west direction profiles. Both line-4 (N-S profile) and line-2 (E-W profile) passed through the location of ODP Site 758 that had a total penetration of about 676 m, reaching below the basaltic basement beneath the Ninetyeast Ridge. The drill well results on correlation to interpreted seismic profile RC2705 reported 5 major lithologic units with several subunits and varying interval velocities within each unit. Accordingly a total of 10 reflector tops were identified along all these profiles (Table 6.1) from top of basalt basement to the seafloor (Peirce et al., 1989). All these lithologic/ stratigraphic tops are marked on profiles line-2 and line-4, and prominent four of them found continuous all along the profile are extended to other profiles of the grid and named them as R1 to R4 from top to bottom (Figure 6.3).

The four prominent interfaces are correlated to the ooze-chalk boundary of middle Miocene age (R1), the large unconformity within chalk layer where Eocene hiatus was observed and mark early Palaeocene (R2), Chalk-Clay boundary of Companion age of late Cretaceous (R3) and the top of lava flow/ pillow lavas assumed as the acoustic basement (R4). The KT boundary about 65 ms below R2 is continuous on either side of well site for a short length and similarly present in few other profiles with a unique erosional seismic characteristics, but is not marked as a reflector as it becomes vague in regions of compressional forces (Figure 6.3). All profiles are interpreted with reflectors

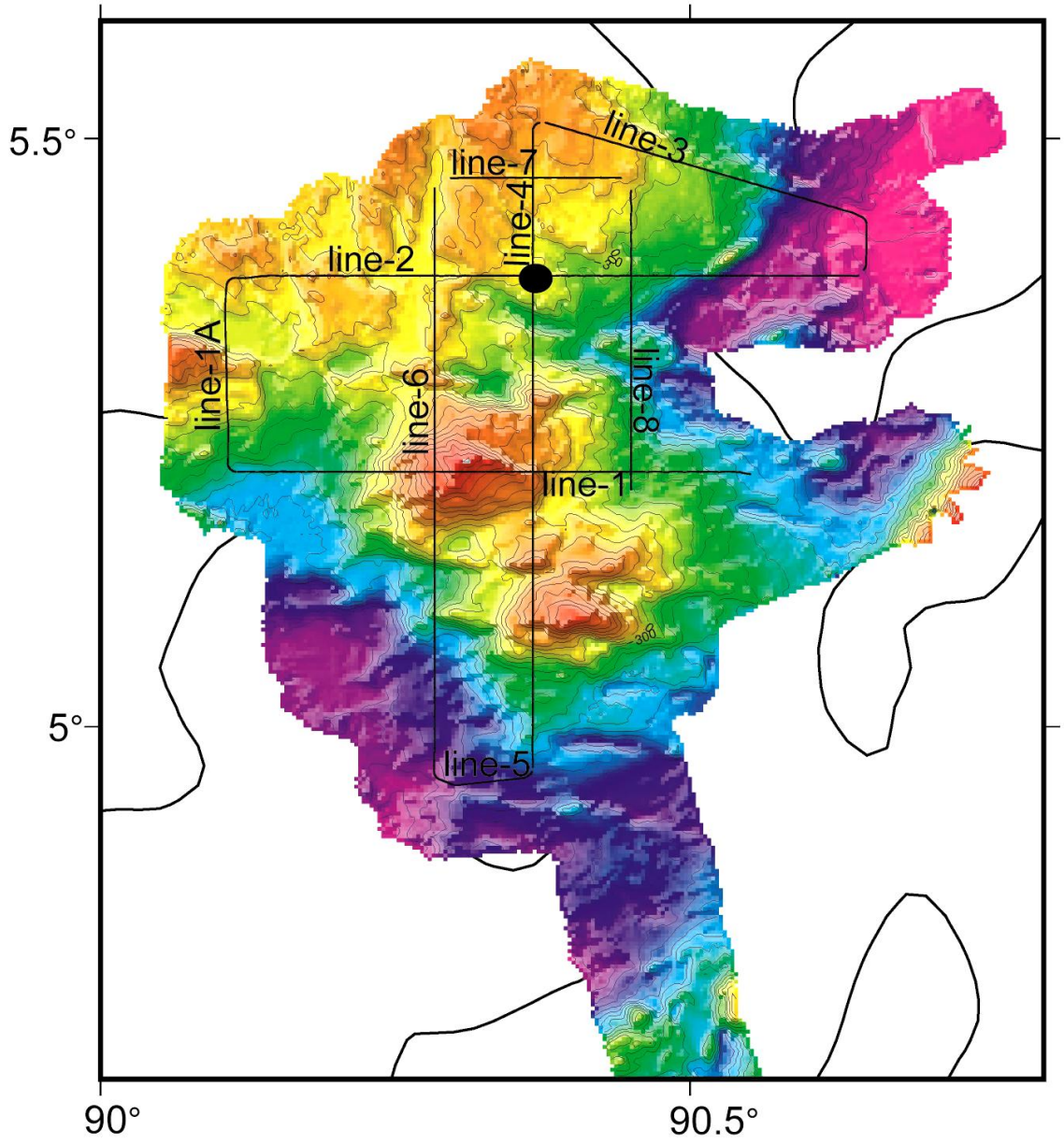

Figure 6.2: Multibeam bathymetry of KNOX06RR grid Site 758. Seismic profile tracks are overlaid with annotation of line numbers. Bathymetric contour in multibeam map is of 50 m and in the regional area of 500 m interval. ODP 758 well site is marked with solid black circle.

R1 to R4, except on elevated peaks of the ridge. Faults are marked against displacements of reflectors. Some of the interpreted profiles of the site with major reflectors and faults are presented in Figure 6.4. N-S profiles are having higher population of faults than on E-W profiles as expected. The configuration of fault fabric observed at ODP Site 758 implies that the location is highly fractured. Compression is obviously noted from the reverse geometry of reflectors at some faults (F_9), up-warp of reflectors (e.g. between F_8 and $F_{10,}$ F_6 and F_7) and kink of layers between major faults (F_8 and F_9) (Figures 6.4 and 6.6). Many faults in 2D seismic sections reveal strike slip displacements by typical characteristics, like abrupt change in thickness of seismic facies across the fault (F_{10}, F_7) or flower structures (F_7) (Figures 6.4 and 6.6).

Measurement of displacements along major dip slip faults which are not deformed by strike-slip, could reveal their probable period of major activity and the time of cessation. On line-4, a fault annotated as f1 appears to be of dip slip type. The displacements measured indicate that the fault could have originated at basement level at the time of accretion of the ridge, and then reactivated much later in geological time implied by the larger throw only at basement while the other 3 reflectors have suffered similar but lower displacements in terms of depth (Figure 6.4). Above the middle Miocene boundary (R1) another three horizons (h3, h2 and h1) are marked to fix the boundary corresponding the onset of faulting where displacement should be similar to R1 and lower sequence faulted by reactivation stress. Line-4 of grid Site 758 becomes a good example of faulting (Figure 6.4), where boundary h3 around 70 ms above R1 is identified as the boundary corresponding to fault reactivation time with fault throw similar to reflectors R1 to R2, above which the fault displacement gradually decreases (h2 and h1) till water bottom and onlapping sedimentation is observed (Figure 6.5).

Assuming average sedimentation above R1 (middle Miocene ~13 Ma), rate of sedimentation is calculated using two way travel time and interval velocity available at ODP 758 well site. According to that, age of h3 could be roughly around 8 - 9 Ma (Table 6.2), which means the onset of stress change leading to the fault reactivation within the location of Site 758 was around late Miocene age and the faults are still active (buried under sediments) with less ambient stress regime at present time .

Table 6.1: Correlation of seismic stratigraphy of line-4 of KNOX06RR Site 758 with seismic and lithostratigraphy of ODP Site 758

Unit	***Reflector***	***ODP 758***		***KNOX06RR 758***	***Lithologic /Stratigraphic demarcation***	***Age***
		Int.velocity (m/s)	***twt (ms)***	***twt (ms)***		
0	-	1500	3900	3935	water bottom	Holocene to Middle Miocene
1	-	1540	3952	3984	-	
2	R1	1540	4058	4087	Ooze /pale chalk Boundary	
3	-	1890	4174	4202	Probable-Unconformity	Mid. Miocene to early Palaeocene
4	R2	1890	4200	4224	Large-Unconformity	
5	-	1890	4242	4269	KT boundary	
6	-	2330	4303	4325	Green chalk/clay boundary	Late Maastrichtian to Campanian
7	R3	1800	4374	4386	Clay/tuff boundary	Campanian
8	R4	2130	4432	4470	Tuff-basalt boundary	Campanian
10	-	4600	4514	4549	Drilled depth	Early Camapanian

Several seafloor lineations, trending WNW-ESE are observed in multibeam bathymetry map and found associated with fault troughs (Sager et al., 2013) (Figure 6.2). On correlation of seismic results with bathymetry data, 11 faults could be marked on the basement map (Figure 6.6). The general trend of faults is near E-W, but on closer examination it reveals that there are few WNW- ESE trending faults and the rest are in their conjugate direction, i.e. in ENW- WSW strikes. The faults F2, F3 form a pair of scissor fault, which seem to be generated when the stress in opposite direction or compression is present. Fault F7 strikes in WNW- ESE, is a major one with a maximum slip and surface expression as seen in multibeam background data. The possibility is that the strike of F7 is the net strike slip direction at present time and the rest sub-parallel faults could be due to reactivation in the direction of Reidel shears associated

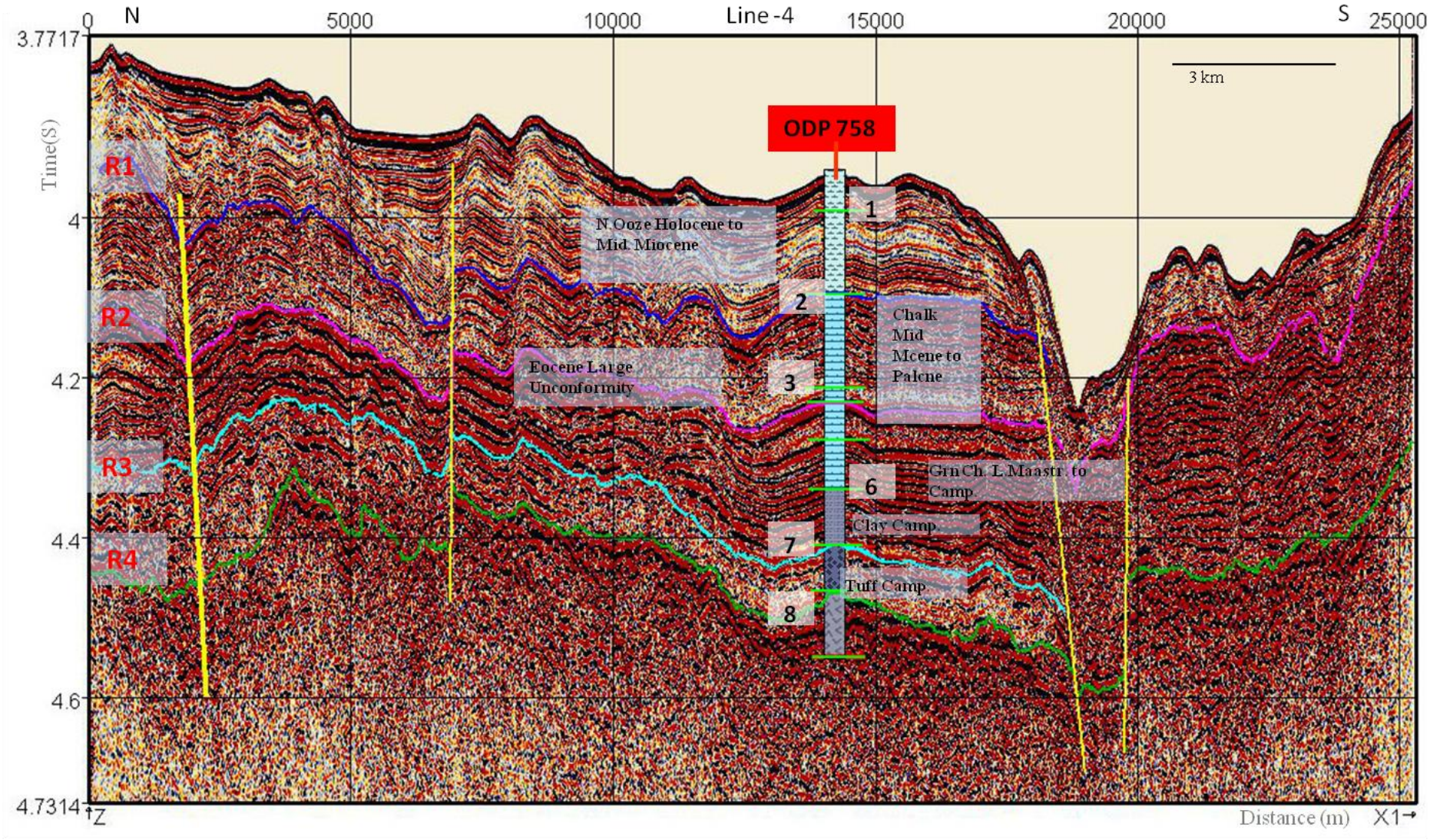

Figure 6.3: Site 758-Line-4 correlated with ODP 758 well site stratigraphy

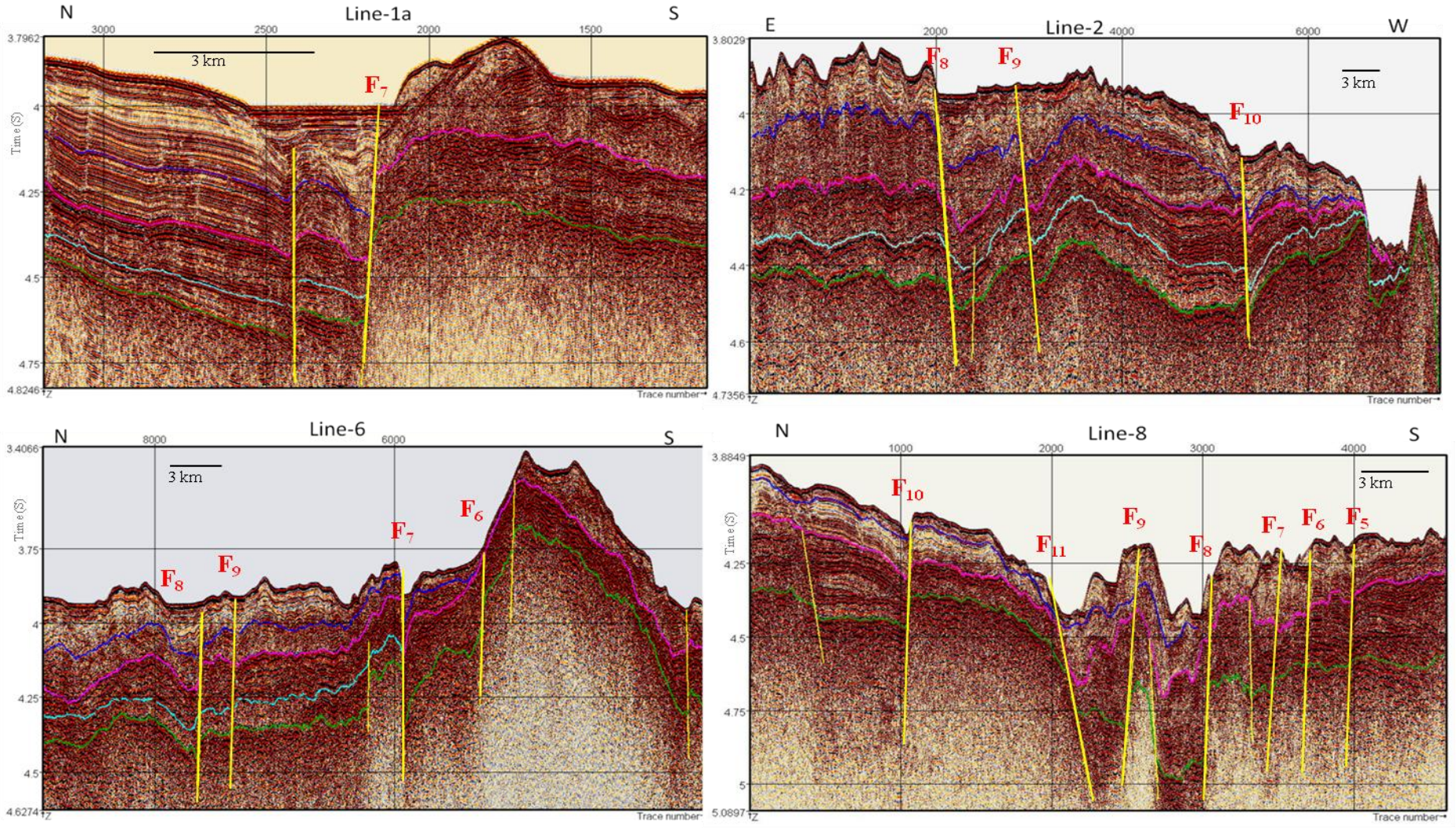

Figure 6.4: Interpreted profiles of Site 758. Lines 1a, 6 and 8 are N-S and 2 is E-W. Faults are names are with reference to the correlation presented in map of Figure 6.6.

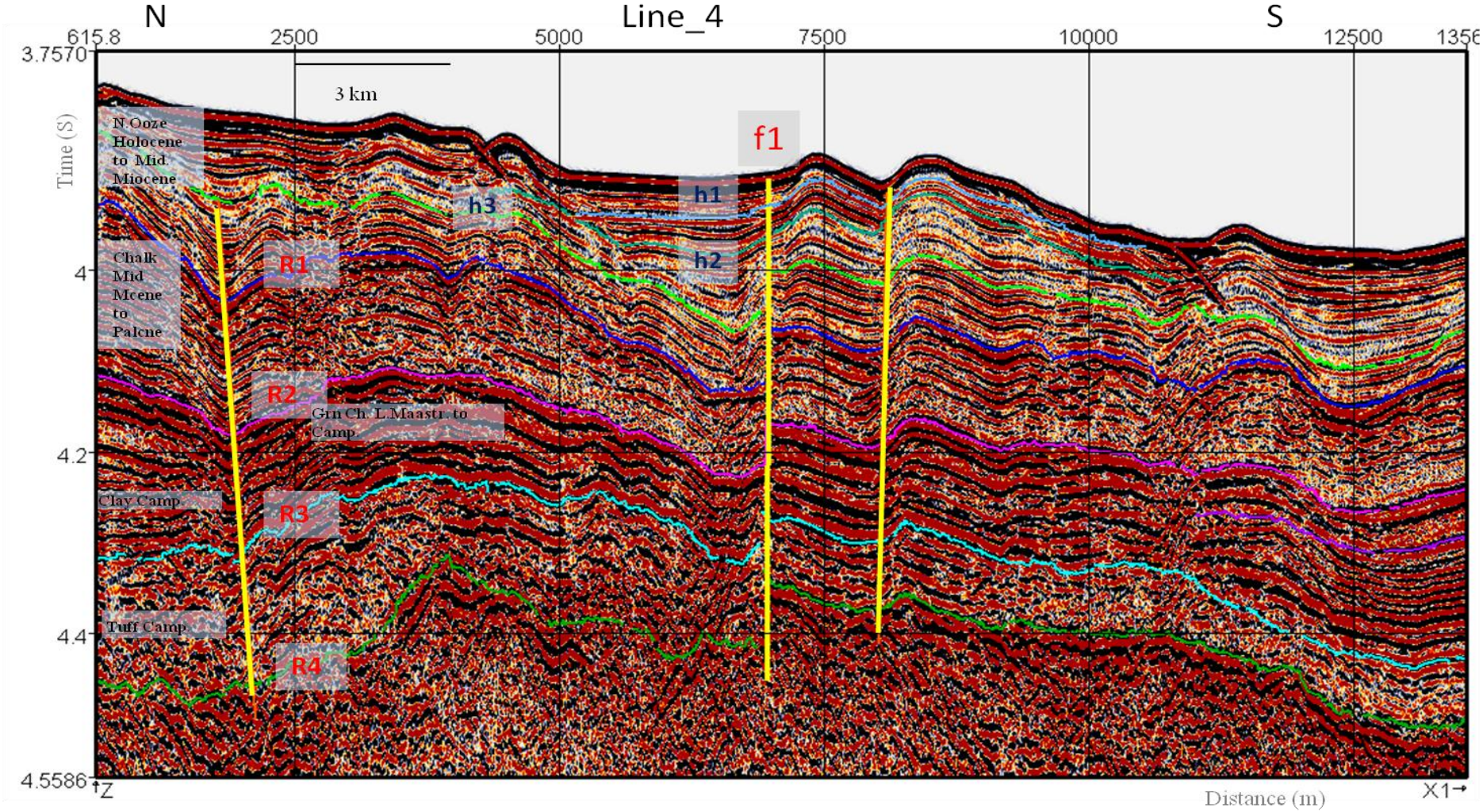

Figure 6.5: Site 758 - Line-4 interpretation with reflectors and faults. Lithology is annotated. Fault displacement against fault marked f1are measured. h1, h2 and h3 are three horizons marked only to compare the variation in fault displacement.

Table 6.2: Fault displacements measured against active fault f1 in line-4 ODP Site 758 grid and age calculation for onset of fault corresponding to horizon marked h3. P1 - Shallower point against fault. P2 - deeper point against fault.

Reflector	***TWT (ms) @***		***Displ. TWT (ms)***	***Int.Velocity (km/s)***	***Depth to the reflector (m)***		***Age known/derived (Ma)***		***Sedimenation Rate (m/Ma)***	
	P1	**P2**			**P1**	**P2**	**P1**	**P2**	**P1**	**P2**
W.B	3868	3891	23	1.5	0	0			11.08	13.62
h1	3896	3933	37	1.5	21	31	1.90	2.28	11.08	13.62
h2	3930	3974	44	1.5	46	62	4.15	4.55	11.08	13.62
h3	**3988**	**4057**	**69**	**1.5**	**90**	**124**	**8.13**	**9.11**	**11.08**	**13.62**
R1	4060	4128	68	1.5	144	177	13	13	11.08	13.62
R2	4168	4218	50	1.89	283	309				
R3	4270	4317	47	1.89	379	402				
R4	4347	4408	61	2.1	502	542				

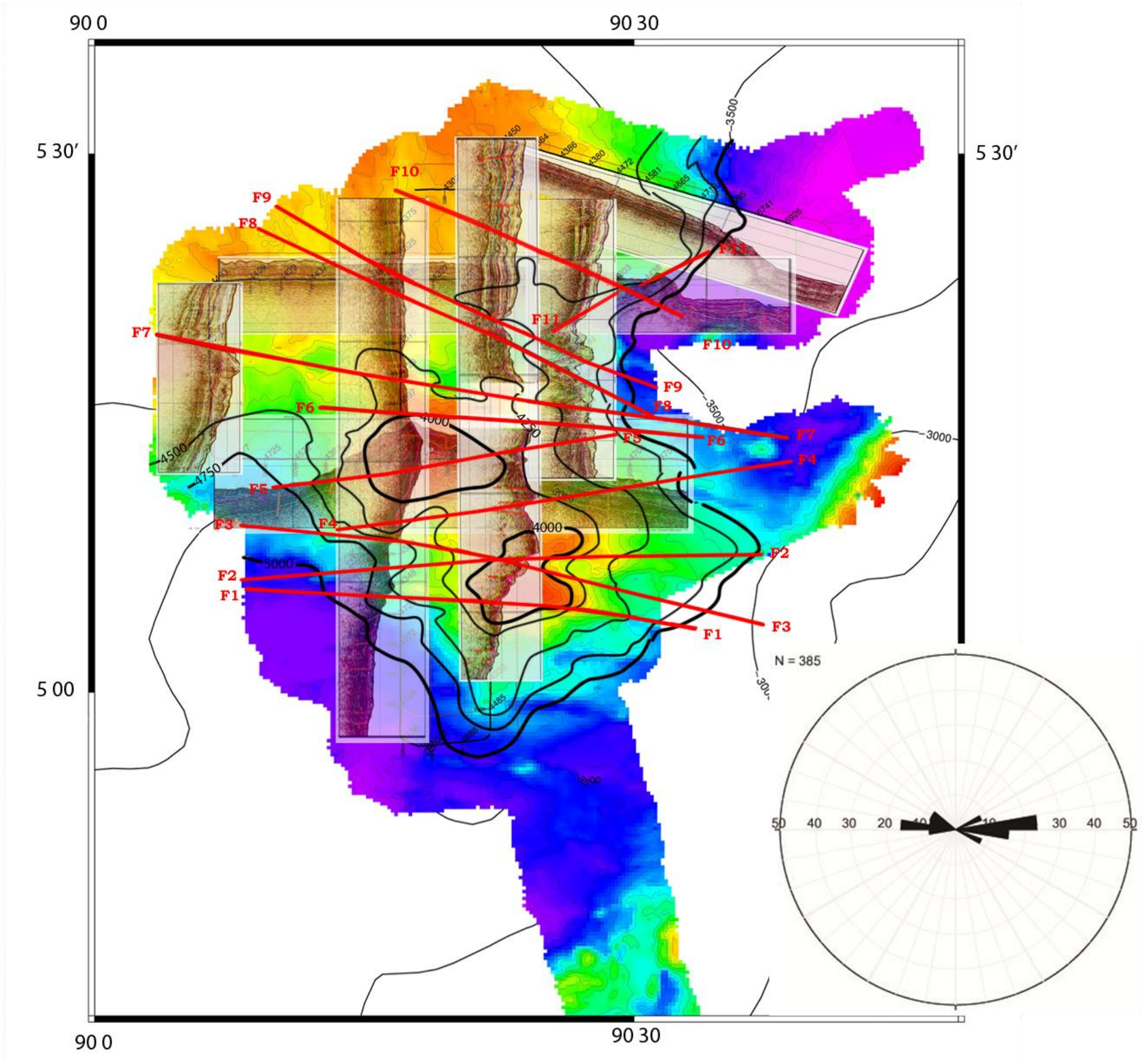

Figure 6.6: Site 758 Fault strike analysis with interpreted seismic profiles overlaid on bathymetry. Rose diagram in stereonet of all the faults drawn is inserted.

Table 6.3: Fault strike and dip measurements at Site 758: Data input for Rose diagram. Sc.F-Scissor fault which changes throw to opposite direction about an axis.

Fault Name	***Angle of Strike (°)***	***Dip (°)***	***Direction of throw***
F_1	92 - 94	80 - 85	S
F_2	84 - 89	80 - 85	Sc.F
F_3	96 - 104	80 - 85	Sc.F
F_4	80 - 82	80 - 85	S
F_5	80 - 82	80 - 85	S
F_6	94 - 95	80 - 85	N
F_7	97 - 99	80 - 85	N
F_8	114 - 116	80 - 85	N
F_9	116 - 119	80 - 85	S
F_{10}	121 -122	80 - 85	S
F_{11}	60 - 62	80 - 85	S

with the main strike-slip movement. The dominant type of stress at this site is of strike slip and compression (Royer and Gordon, 1997). The net ambient stress of this location can be the resultant of the Euler poles corresponding to the three pairs of diffused plates. Out of the three diffused tectonic plates of the Indian Ocean, the Indian-Australian relative plate movement has been observed to be maximum (Royer and Gordon, 1997). The effective stress due to the other two plates must be negligible at location of ODP Site 758. Hence as implied by the Euler pole of Indo-Australian plate boundary, the active stress here is compression along 45° and E-W striking active faults and associated bathymetric lineations are due to reactivation of original normal faults (Sager et al., 2013) along as well as the Reidal shear direction of the effective stress. From the observed fault pattern, it is found that majority of original E-W faults are reactivated and scissor faults are formed due to compression. The faults lay in NW-SE and WNW-ESE direction are reactivated with higher offsets and also

there is a strike-slip component associated with many of them so that they have generated seafloor lineations or troughs.

Rose diagram of the faults shows that density of faults are more in E-W azimuth than WNW-ESE (Figure 6.6), indicating dominance of compressive stress over transform stress at this site.

6.3.2 Site 216 (1.5°N latitude)

Around the location of DSDP Site 216, the KNOX06RR cruise acquired 9 seismic profiles, in a random grid of 3 profiles in north-south direction, 3 in east-west direction and 2 in NW-SE direction covering an area from 1.93˚N to 0.80°N latitudes and from 89.56°E and 90.73°E longitudes. A total of 632 km seismic reflection data were acquired in this grid. Two of the profiles, line-1b and line-5, run in N-S and E-W direction pass through the DSDP Site 216 well location (Figure 6.7). Total depth of penetration of the well is 477m.

The drilled well results reported 3 major lithologic units and 3 and 2 subunits each in top two major units from late Pleistocene nanno fossil ooze on top to late Maastrichtian beds of micarb chalk ash at the bottom (Von der Borch et al; 1974d) (Table 6.4). Pre-site seismic profiles survey over the location had identified 3 prominent reflectors, which were not correlated to any lithologic boundary except basalt following the report (Shipboard Scientific party, Site 216, 1972). But acoustic basement mapped in new seismic profiles is deeper by 90 ms, this means the DSDP 216 well was probably penetrated only till the basaltic tuff layer (Figure 6.8). The low velocity, 2.l km/s is reported for the tuff layer also supports this possibility.

Keeping the DSDP 216 well lithologic markers in view, the seismic profile data connecting the drill site are interpreted to correlate the reflectors. The ooze/ chalk boundary of the late Oligocene, boundary of nanno chalk with Gluconitic clay rich micarb chalk of the late Maastrichtian and the boundary immediately below demarcating this micarb chalk with volcanic micarb chalk identified in late Maastrichtian itself are the sequences correlated. Similar sedimentation of 0.5 to 0.8 s is observed along the ridge crest till sharply deepening eastern flank (Figure 6.8). Interpreted 3 seismic reflectors and acoustic basement in the vicinity of drill well are extended to all seismic profiles of the grid.

Faults marked at this site also are combination of compression and strike-slip type similar to those identified at ODP Site 758 but with reduced density in number of faults (Figure 6.9).

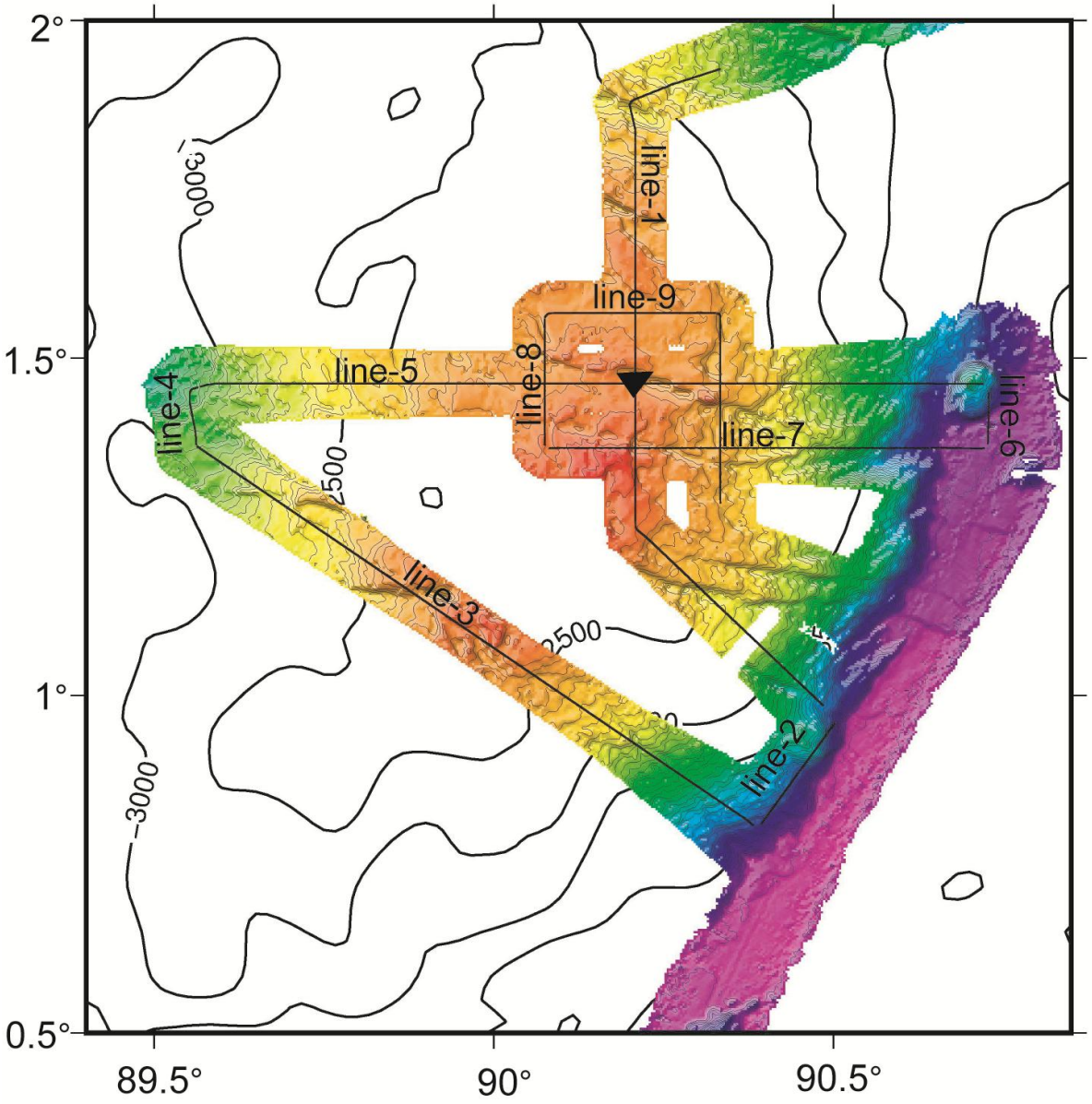

Figure 6.7: Multibeam bathymetry of KNOX06RR grid Site 216. Seismic profile tracks are overlaid with annotation of line numbers. Bathymetric contour in multibeam map is of 50 m and in the regional area of 500 m interval. DSDP 216 well site is marked with solid black triangle.

Table 6.4: Correlation of seismic stratigraphy of line-1 of KNOX06RR Site 216 with seismic and lithostratigraphy of DSDP Site 216. Shallower point against fault. P2 - deeper point against fault.

Unit	***Reflector***	***depth***	***Avg. int. Vel***	***TWT***	***lithology/stratigraphy***	***Age***
0	-	0	1500	2998	water bottom	Pleistocene to Late Oligocene
1	R1	187	2100	3176	Nanno Ooze	
2	-	332	2100	3314	Nanno chalk	Late Oligocene to Paleaocene
3	R2	348	2000	3329	Gluconitic clay rich micarb chalk	Late Maastrichtian.
4	R3	396	2000	3375	Gluconitic clay rich volcanic micarb chalk	Late Maastrichtian.
5	-	457	2000	3433	volcanic clay micarb chalk with ash beds	Late Maastrichtian.
6	-	477	2000	3452	drilled depth/ basaltic tuff?	Camapanian
7	R4	537	2000	3528	basalt top	Campanian

Few of the original faults have got reactivated during the onset of deformation activity and active faults are observed to be continued till the seafloor indicating the current activity (Figures 6.8 and 6.9).

The topmost reflector identified (R1) in profiles of this site is of late Oligocene age. The north-south profile line-1 itself is selected for active fault displacement analysis, as the section is otherwise undisturbed, with thick sedimentation and the reflectors are propagated with confidence near the well location.

Above R1 another three horizons - h3, h2, h1 and one below - h4 are marked to fix the boundary corresponding the onset of faulting by comparison of displacements (Figure 6.8). Layers R2 to R4 suffer more throw as expected due to earlier episodes of faulting since ridge formation. Horizon h4 has slightly higher displacement due to the active fault termed f1 (for convenience) compared to that of R1 and h3 by 6 ms which could be real due to an earlier age fault activity (Table 6.5). Horizons h2 and h1 have similar throw less by only 5ms to that

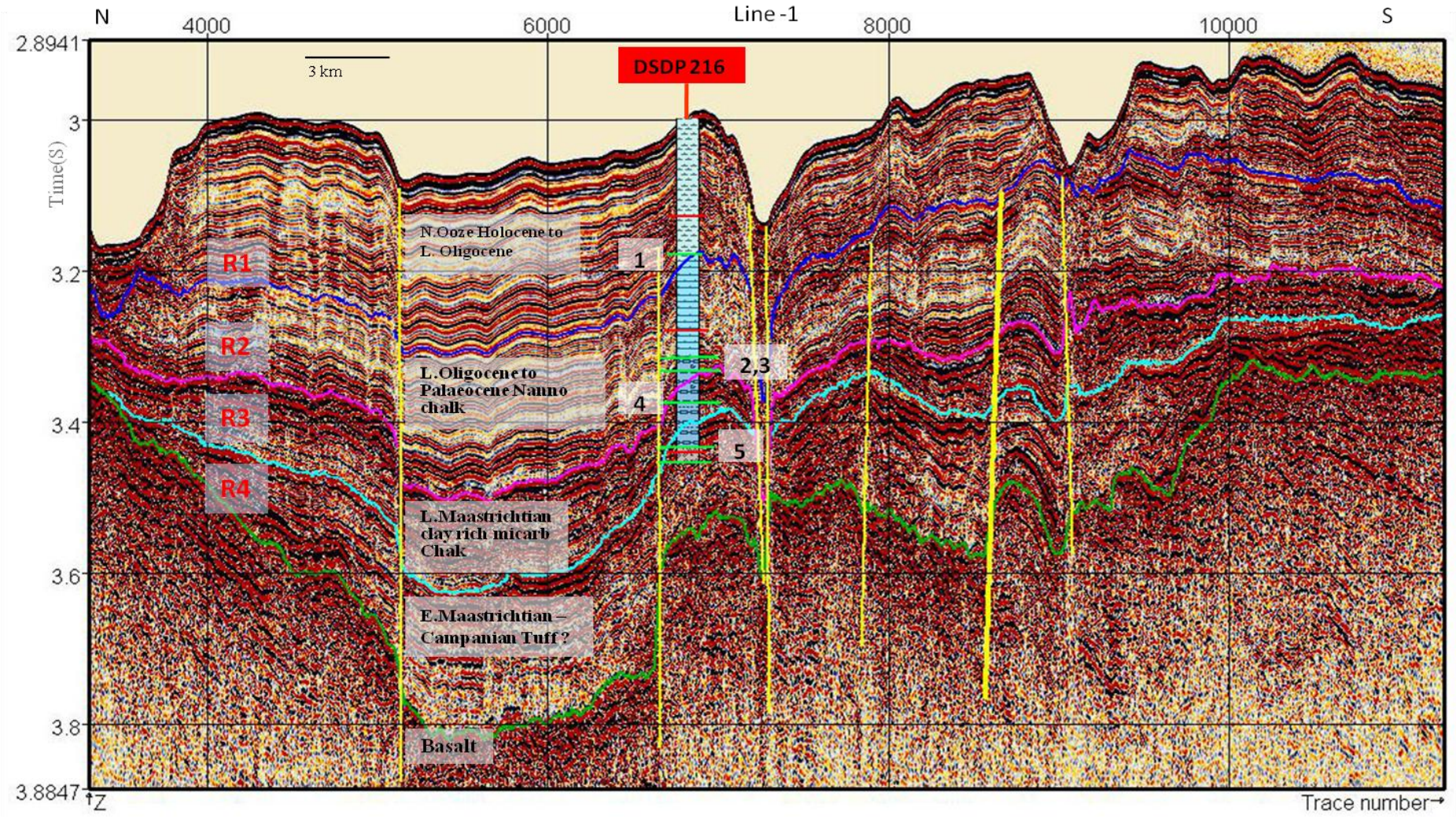

Figure 6.8: Site 216-Line-1 correlated with DSDP 216 well site stratigraphy

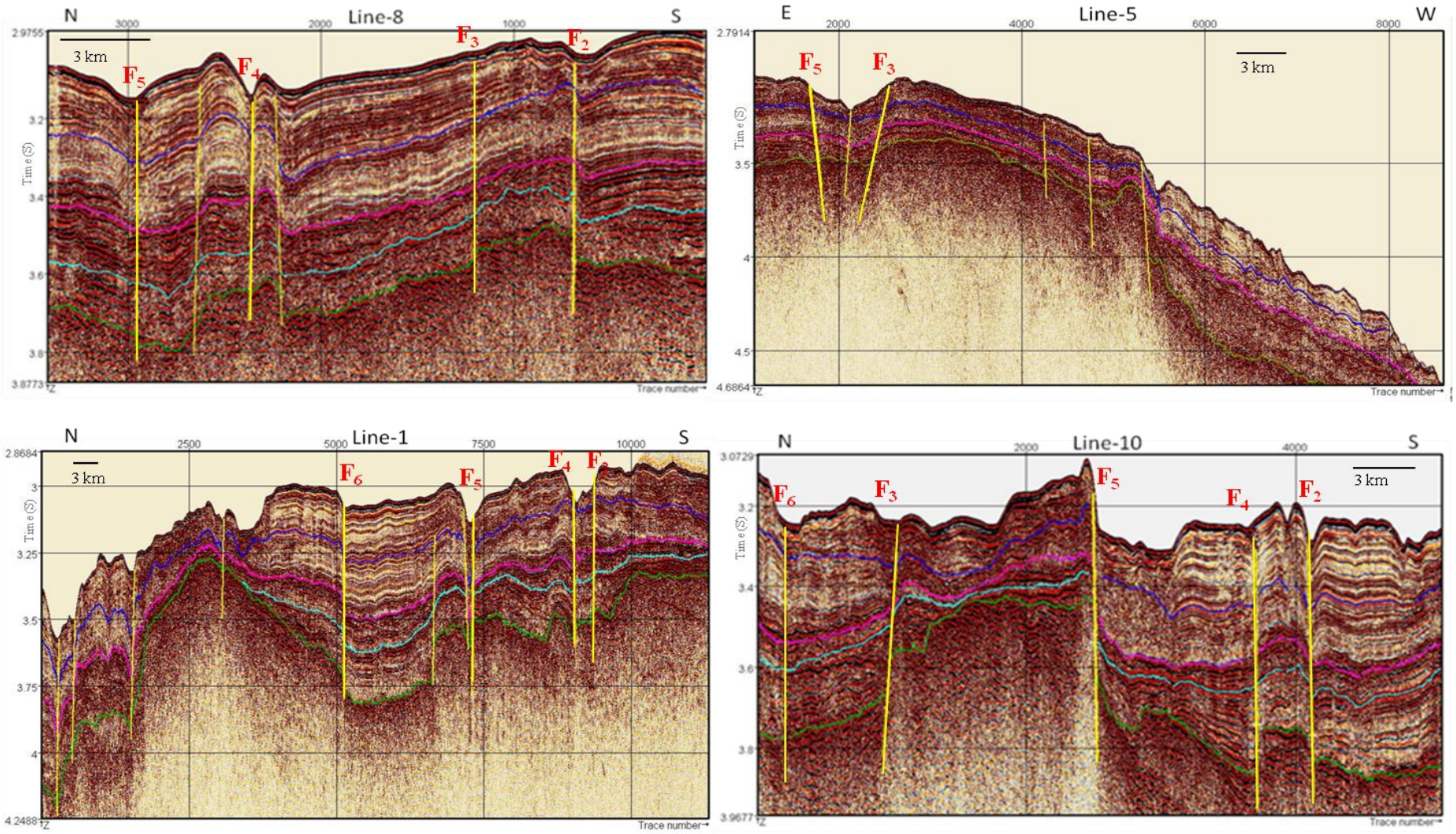

Figure 6.9: Interpreted profiles of Site 216. Lines 1, 8 and 10 are N-S and 5 is E-W. Faults names are with reference to the correlation presented in map of Figure 6.10.

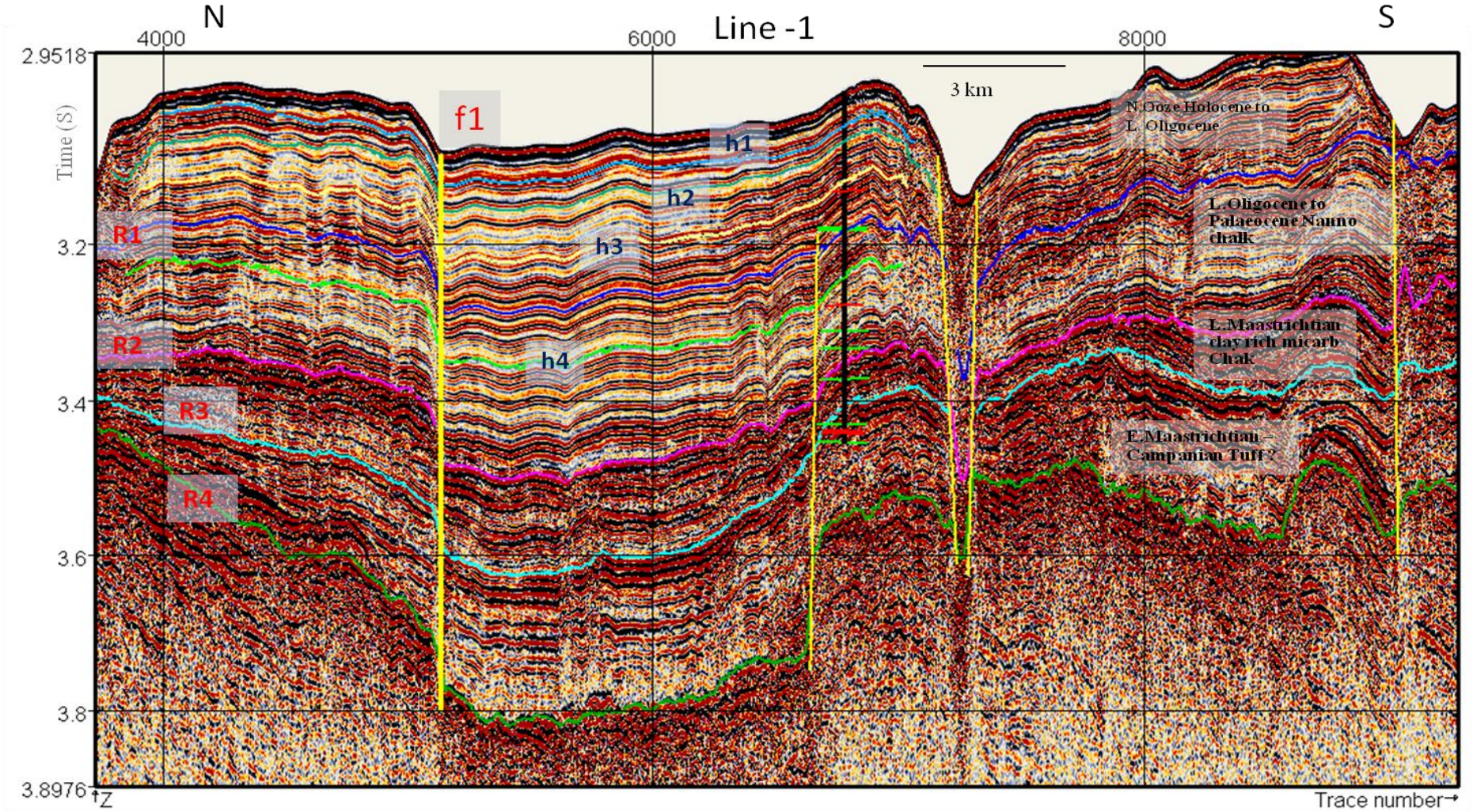

Figure 6.10: Site 216 - Line-1 interpretation with reflectors and faults. Lithology is annotated. Black vertical line shows drill site with lithology/ reflector tops identified at DSDP site 216. Fault displacement against fault marked f1are measured. h1,h2, h3 are three horizons marked only to compare the variation in fault displacement.

Table 6.5: Fault displacements measured against active fault f1 in line-1 Site 216 grid and age calculation for onset of fault corresponding to the horizon marked h2. P1 - Shallower point against fault. P2 - deeper point against fault.

Reflector	***TWT (ms) @***		***Displ. TWT (ms)***	***Int.Velocity (km/s)***	***Depth to the reflector (m)***		***Age known/derived (Ma)***		***Sedimenation Rate (m/Ma)***	
	P1	***P2***			***P1***	***P2***	***P1***	***P2***	***P1***	***P2***
W.B	3017	3070	53	1.5	0	0				
h1	3055	3118	63	2	38	48	5.27	6.17	7.21	7.79
h2	**3084**	**3146**	**62**	**2**	**67**	**76**	**9.29**	**9.76**	**7.21**	**7.79**
h3	3147	3214	67	2	130	144	18.02	18.50	7.21	7.79
R1	3210	3278	68	2.1	202	218	28	28	7.21	7.79
h4	3269	3343	74	2.1	264	286				
R2	3383	3483	100	2.1	384	433				
R3	3506	3608	102	2.1	513	564				
R4	3656	3798	142	2.1	670	764				

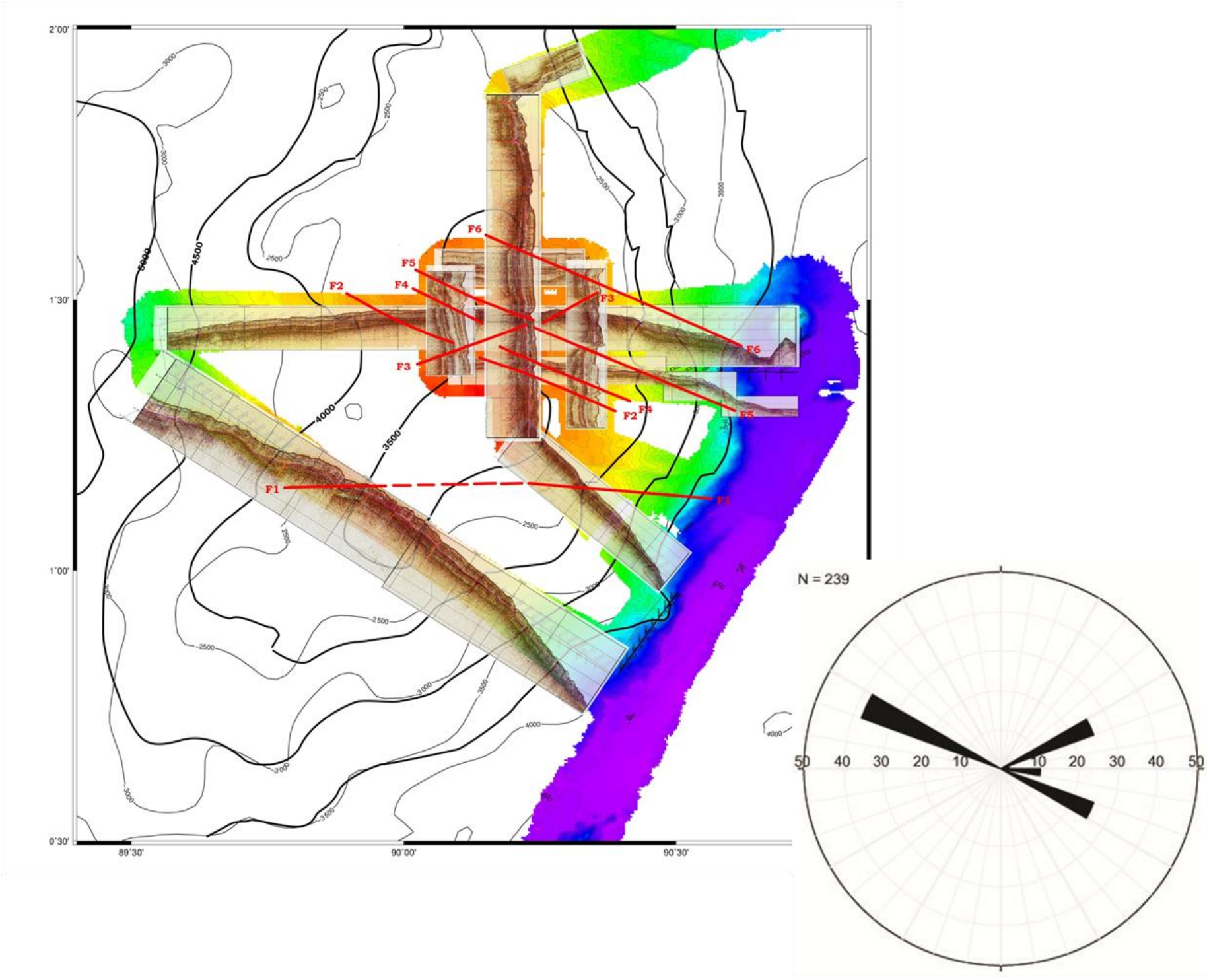

Figure 6.11: Site 216 Fault strike analysis with interpreted seismic profiles overlaid on bathymetry. Rose diagram in stereonet of all the faults drawn is inserted.

Table 6.6: Fault strike and dip measurements at Site 216: Data input for Rose diagram. Sc.F- Scissor fault which changes throw to opposite direction about an axis.

Fault Name	***Angle of Strike (°)***	***Dip (°)***	***Direction of throw***
F_1	89 - 95	80 - 85	S
F_2	110 - 112	80 - 85	S
F_3	68 - 69	80 - 85	S
F_4	113 - 115	80 - 85	Sc.F
F_5	111- 112	80 - 85	Sc.F
F_6	112 - 114	80 - 85	N

of R1 which reduces by 10 ms by the fault reaches water bottom. Above the h2 horizon sediment wedge out features are identified so that this can be marked as the onset of an impulsive faulting of short time period after which the stress has reduced. By averaging the sedimentation rate after late Oligocene at R1, h2 correspond to an average age of ~9.5 Ma (Table 6.5) indicating the fault reactivation time at this site.

A major strike-slip fault is observed on line-10 with an offset of sedimentary packages on either side of it, which is associated with a typical bathymetric trough and contour offset and found to be continued between the parallel N-S lines, line-1b and line-8 (marked as F_5 in Figure 6.9). The azimuth of strike-slip is WNW-ESE similar to the one observed at Site 758, and there are 3 other faults identified parallel to F_5 correlating through seismic profiles and to the bathymetric map, which are marked as F_2, F_4 and F_6 (Figure 6.9, 6.11). Fault F3 is in conjugate direction to these faults in ENE-WSW azimuth, with compressional features on profiles line-8, line-1b, line-5 and line-10. Fault F_1 correlated between line-1c and line-3, in near E-W trend also have strike slip as well as compressional components. All the six faults are plotted in stereonet and Rose diagram shows WNW-ESE as the main azimuth of active stress at this location, which means transform type but with a component of compression in near E-W as well as ENE-WSW direction with less density. The analysis further proved that major change in stress

regime from the ODP Site 758 to DSDP Site 216 in terms of relative motion even though types of stress present at both sites are similar.

6.3.3 Sites NER2 and NER3 (6 - 8°S latitude)

These two grid sites are located nearby between 6.25° S and 8.2° S latitudes on central part of the Ninetyeast Ridge track and falls within the diffused triple junction zone of the intraplate deformation (Figure 6.1). There are no drill sites available in this grid location, but about 600 km away from the DSDP Site 216 (73 Ma) and 250 km away from the DSDP Site 214 (62 Ma). Considering the average emplacement rate of 118 km/Ma (Pringle et al., 2008; Krishna et al., 2012), the age of the ridge crest at the sites should be around 65 Ma (Figure 6.12), assuming monotonous increase of age from south to north along the ridge track.

Considering the comparison of seismic characteristics of these grid sites with other sites, it is found that general lithology of the sites also could be of nanno ooze, chalks carbonates and volcanic ash overlying the basaltic basement, similar to the sedimentation process observed at other sites on the Ninetyeast Ridge. Assuming 65 Ma age for the basement, the overlying sedimentation of ooze to ash must be of recent to early Palaeocene, if any hiatus at the bottom is ruled out. The volcanic ash had settled down at a faster rate as observed at all the DSDP/ODP drill sites, as basement ages at these sites are known presently. At both ODP Site 758 (77 Ma) and DSDP Site 216 (73 Ma) the ash layer of about 100 m thick have taken around 10 My of maximum settling time for its deposition. For the DSDP Site 214 (62 Ma), ash layer is about 100 m thickness again at well site and settling time span for the layer could be less than 7 My, as the carbonate silt layer above also is of Palaeocene. At the DSDP Site 214 it is documented to be > 4 My in Palaeocene. Following these observations it can be assumed that the ash layer within the grids NER2 and NER3 may have formed during the Palaeocene age. Then the ooze, chalk and clay would range from Recent to late Palaeocene or early Eocene.

6.3.3.1 NER2

A total of 13 seismic profiles were acquired in the grid NER2, 7 of them in N-S and 6 in E-W direction, falling between 6.25°S and 7.2°S latitudes (Figure 6.13). Four seismic horizons R1 to R4 are identified reflecting general sedimentation pattern on the ridge crest with total sediment thickness of around 0.5 to 0.7s (Figure 6.14). Interpretations of

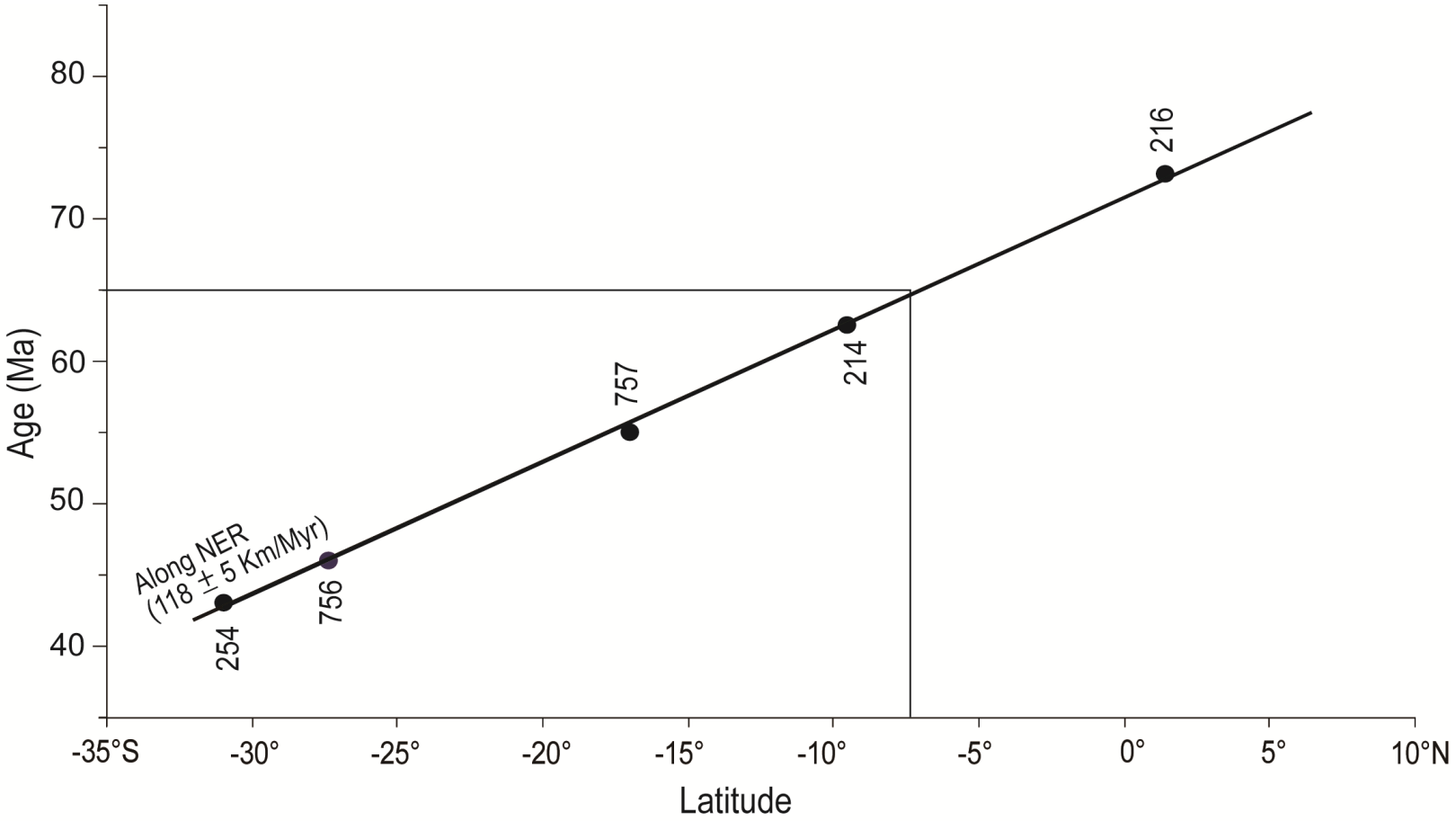

Figure 6.12: Age interpolation at NER2 and NER3 from linear chronology plot of NER (Pringle et al., 2008)

major N-S profiles are shown in Figure 6.13. The displacements of active faults are low compared to northern sites. Many profiles are analysed and profile of line-11 is selected for throw measurement. An active dip slip fault marked f1 in line-11 is observed suitable for the purpose. Two horizons h2, h1 are marked above R1 for comparison of faulting extent. R1 and h2 have same displacement over the basement reaching fault marked as f1 (Figure 6.15), and sediment onlaps are observed above h2, marking the cessation of fault impulse later to h2 age. Assuming R3 at late Palaeocene, sedimentation rate of 7 to 8 m per Myr is obtained comparable to that of Site 216, indicating age of 10-11 Ma (Table 6.7) at h2 corresponding to fault reactivation.

The grid site is located within the diffused zone of triple junction between the sub-plates and there is no recorded evidence of seismicity revealing the type of stress in this area, except presence of some weak E-W thrust faults (Sager et al., 2013). Analysing the interpreted seismic profiles it is observed that only few of the original faults have reactivated due to mild stress, resulting sediment up-warps and kinks despite few fault throws. On line-7 a typical strike-slip fault in WNW-ESE trend is noticed (F_{10}), which continued to nearby N-S profiles, line-9 and line-11, where same type of fault characteristics are observed (Figure 6.14). On bathymetry map the fault is not observed as a narrow lineation, but as a wider trough of asymmetric shape (Figures 6.13 and 6.16). By plotting all major faults on N-S and E-W profiles and making correlations, total of 10 faults are identified within the grid NER2 and numbered F_1 to F_{10} including the strike-slip fault F_{10}. Faults F_6 to F_9 are distributed on either side of F_{10} and probably would have resulted as consequence of F_{10}. The throws of these adjacent faults are in opposite directions, forming a scissor fault complex with their apex along a region of fault F_{10}. The faults F_4 and F_5 also act as a pair with opposite throws sub-parallel in the grid and nearing each other as they approach the fault F_{10}. Faults F_1 to F_3 trending near E-W but in 3rd quadrant, are nearly parallel to each other, but in Reidel direction to F_{10} and associated strike-slip cum compression components are obvious in corresponding profiles. The Rose diagram of F_1 to F_{10} shows the near E-W to ENE-WSW trending fault population.

Strike-slip faults with considerable offsets are clear in this grid with associated scissor fault movement which were generated out of the compressional stresses. The number of strike-slip faults are less compared to northern sites ODP 758 and DSDP 216 and

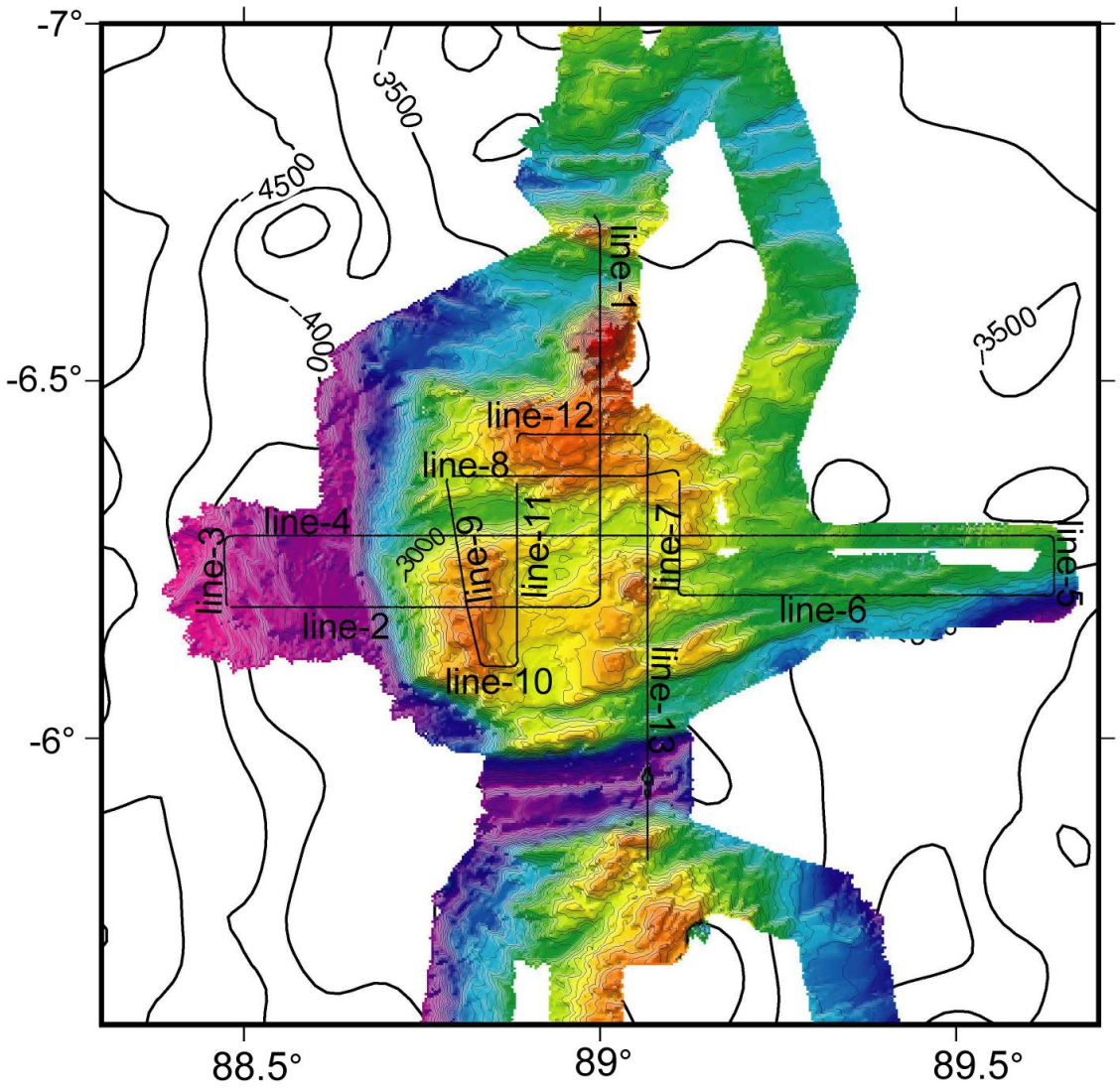

Figure 6.13: Multibeam bathymetry of KNOX06RR grid NER2. Seismic profile tracks are overlaid with annotation of line numbers. Bathymetric contour in multibeam map is of 50m and in the regional area of 500m interval.

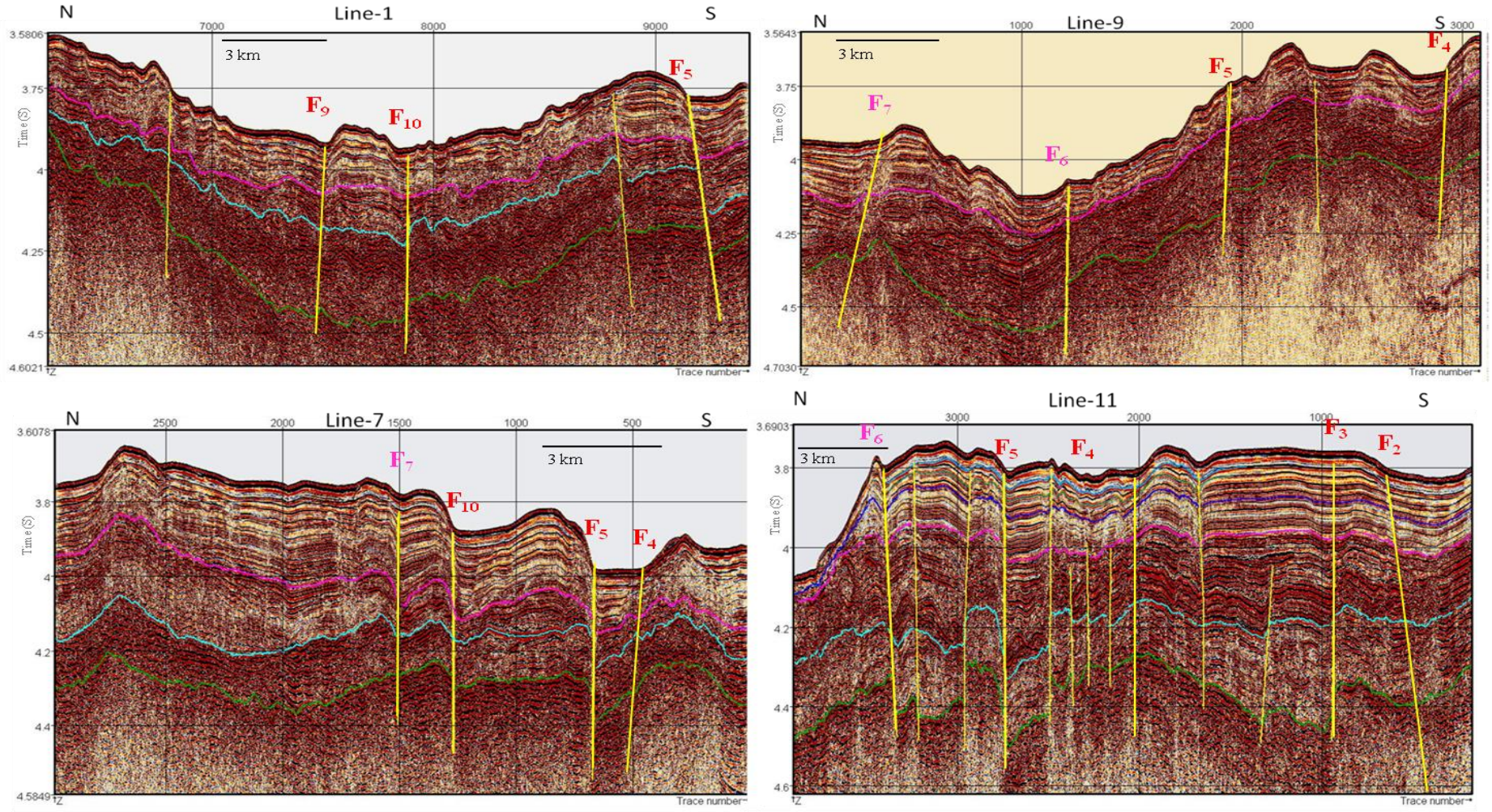

Figure 6.14: Interpreted profiles of Site NER2. Lines 1, 7, 9 and 11 are in N-S direction. Fault names are with reference to the correlation presented in map of Figure 6.15.

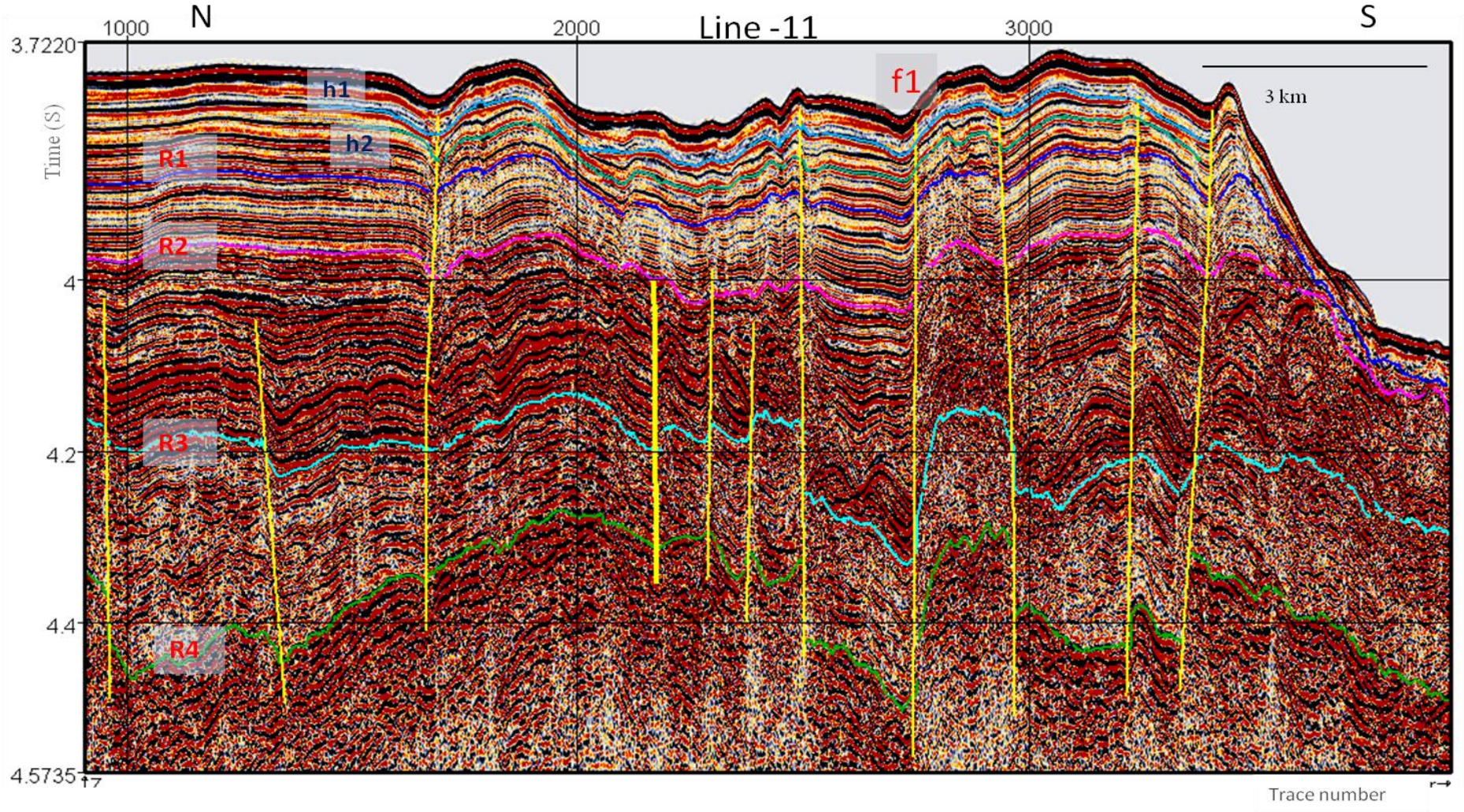

Figure 6.15: Site NER2 - Line-11 interpretation with reflectors and faults. Fault displacement against fault marked f1are measured. h1and h2 are two horizons marked only to compare the variation in fault displacement.

Table 6.7: Fault displacements measured against active fault f1 in line-11 Site NER2 grid and age calculation for onset of fault corresponding to horizon marked h2. P1 - Shallower point against fault. P2 - deeper point against fault.

Reflector	***TWT (ms) @***		***Displ. TWT (ms)***	***Int. Velocity (km/s)***	***Depth to the reflector (m)***		***Age known/derived (Ma)***		***Sedimentation Rate (m/Ma)***	
	P1	***P2***			***P1***	***P2***	***P1***	***P2***	***P1***	***P2***
W.B	3777	3786	9	1.5	0	0				
h1	3819	3829	10	2	42	43	5.98	5.00	7.02	8.60
h2	**3854**	**3872**	**18**	**2**	**77**	**86**	**10.97**	**10.00**	**7.02**	**8.60**
R1	3893	3911	18	2	116	125	16.53	14.53	7.02	8.60
R2	3995	4020	25	2	218	234	28	28	7.02	8.60
R3	4163	4259	96	2	386	473	55	55	7.02	8.60
R4	4327	4420	93	2	550	634				

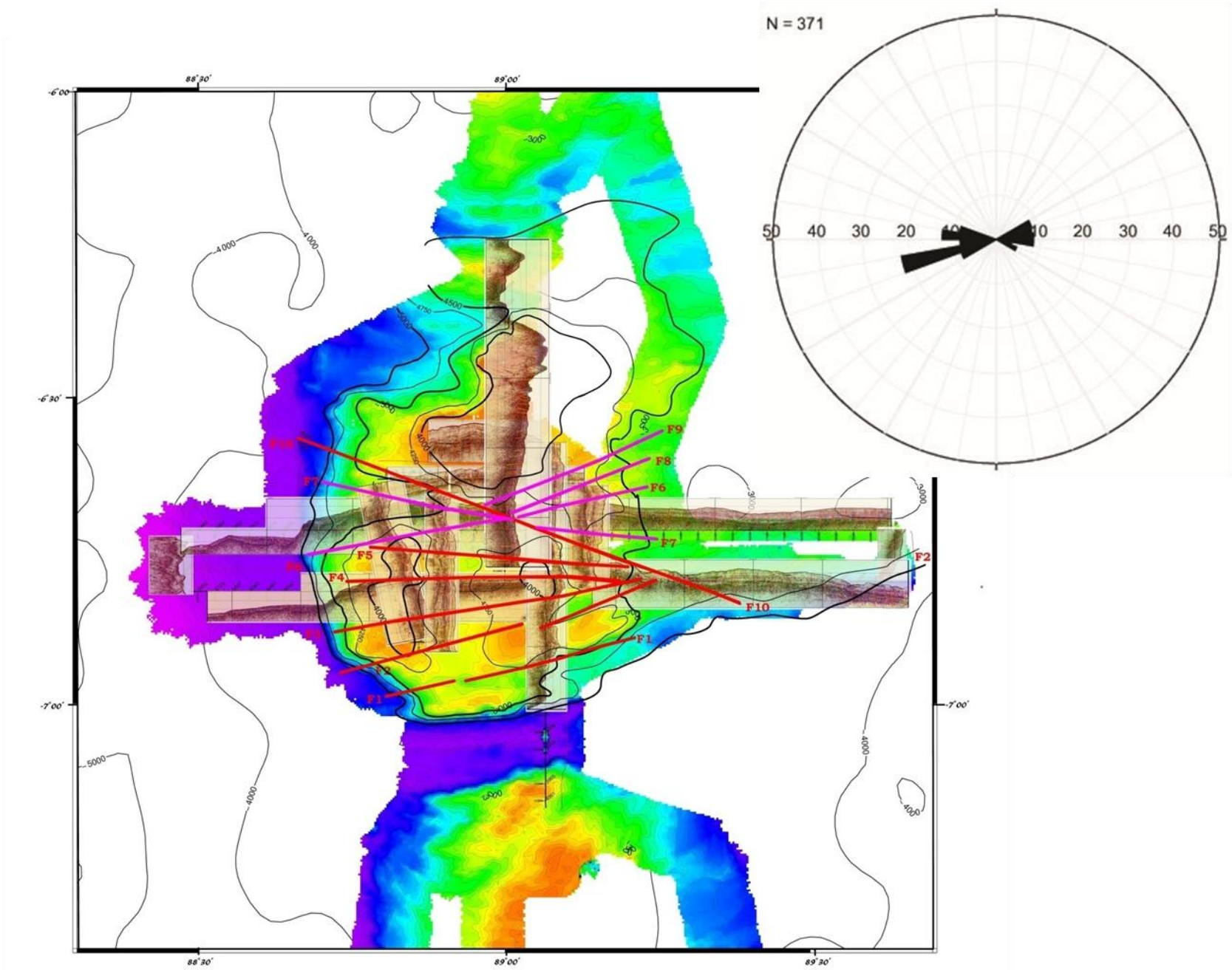

Figure 6.16: Site NER2 Fault strike analysis with interpreted seismic profiles overlaid on bathymetry. Rose diagram in stereonet of all the faults drawn is inserted.

Table 6.8: Fault strike and dip measurements at Site NER2: Data input for Rose diagram. Sc.F- Scissor fault

Fault Name	Angle of Strike (°)	Dip (°)	Direction of throw
F_1	76 - 78	80 - 85	S
F_2	75 - 77	80 - 85	N
F_3	80 - 81	80 - 85	S
F_4	88 - 91	80 - 85	N
F_5	94- 95	80 - 85	S
F_6	76 - 80	80 - 85	Sc.F
F_7	95 - 102	80 - 85	Sc.F
F_8	68 - 69	80 - 85	N
F_9	67 - 68	80 - 85	S
F_{10}	109 - 110	80 - 85	S

compressional-related reactivation is weak. The overall direction of relative movement is near E-W.

6.3.3.2 NER3

The grid NER3 consists of 9 seismic profiles, 4 in N-S and 5 in E-W or near E-W directions between 6.9° S and 8.2° S latitudes (Figure 6.17). Basaltic basement, ash layer overlying it and 2 sedimentary sequences are able to identify, constituting from R1 to R4. The ash layer boundary, R3 is resolved only in few profiles (Figure 6.18).

Measured displacements along the faults reveal that few of them are recently originated other than the one reactivated. On some faults the displacement from basement to Recent is found similar. Minor reactivations are also observed in recent sediments in comparison to the Eocene or older fault activity (Figure 6.19). On a broader scale the fault pattern of NER3 appears to be similar to that of NER2. The E-W faults observed are more frequent with offset at basement level probably formed at the time of evolution by extension. The number of reactivated faults by compression is higher with larger displacements than NER2.

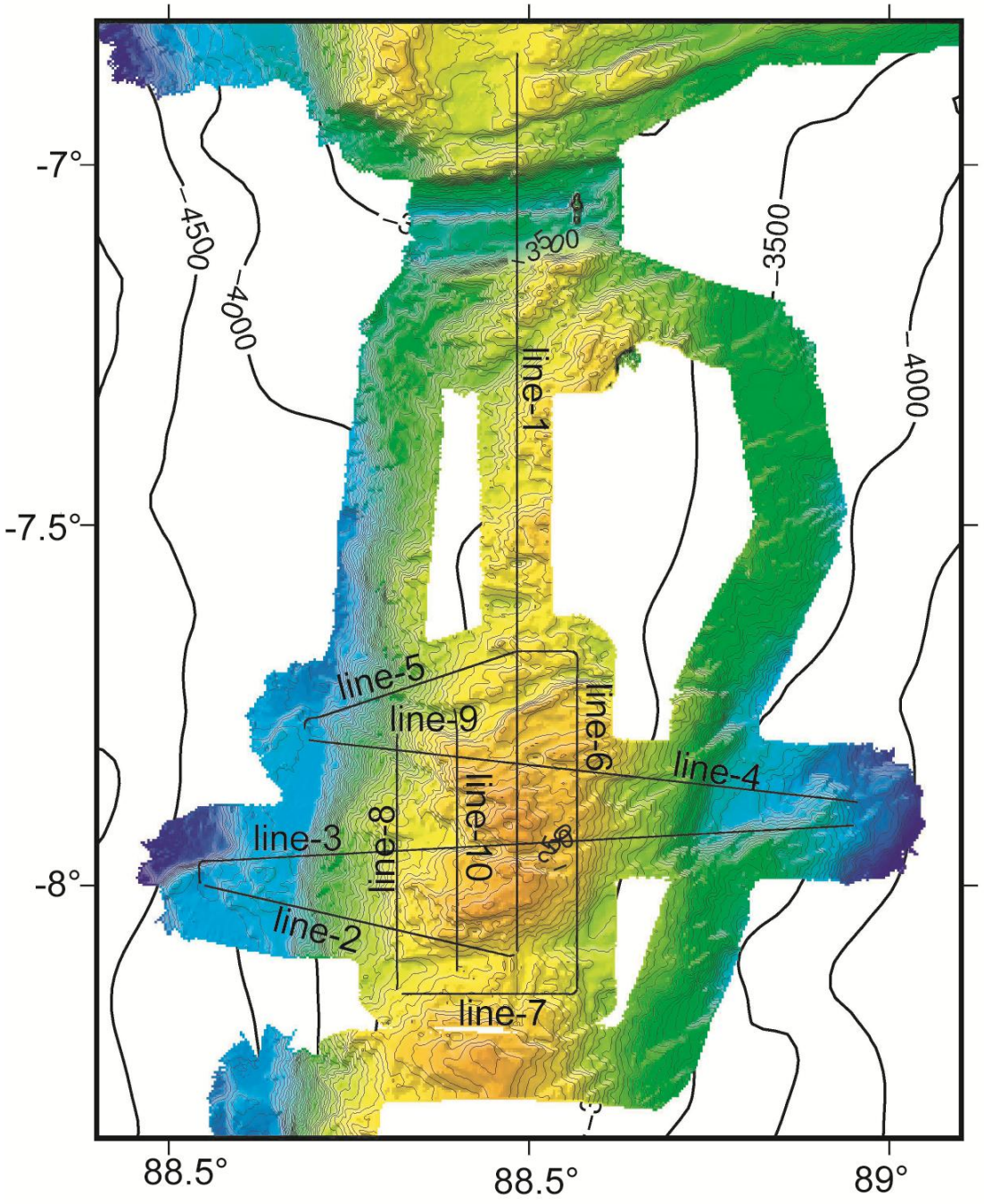

Figure 6.17: Multibeam bathymetry of KNOX06RR grid NER3. Seismic profile tracks are overlaid with annotation of line numbers. Bathymetric contour in multibeam map is of 50m and in the regional area of 500m interval.

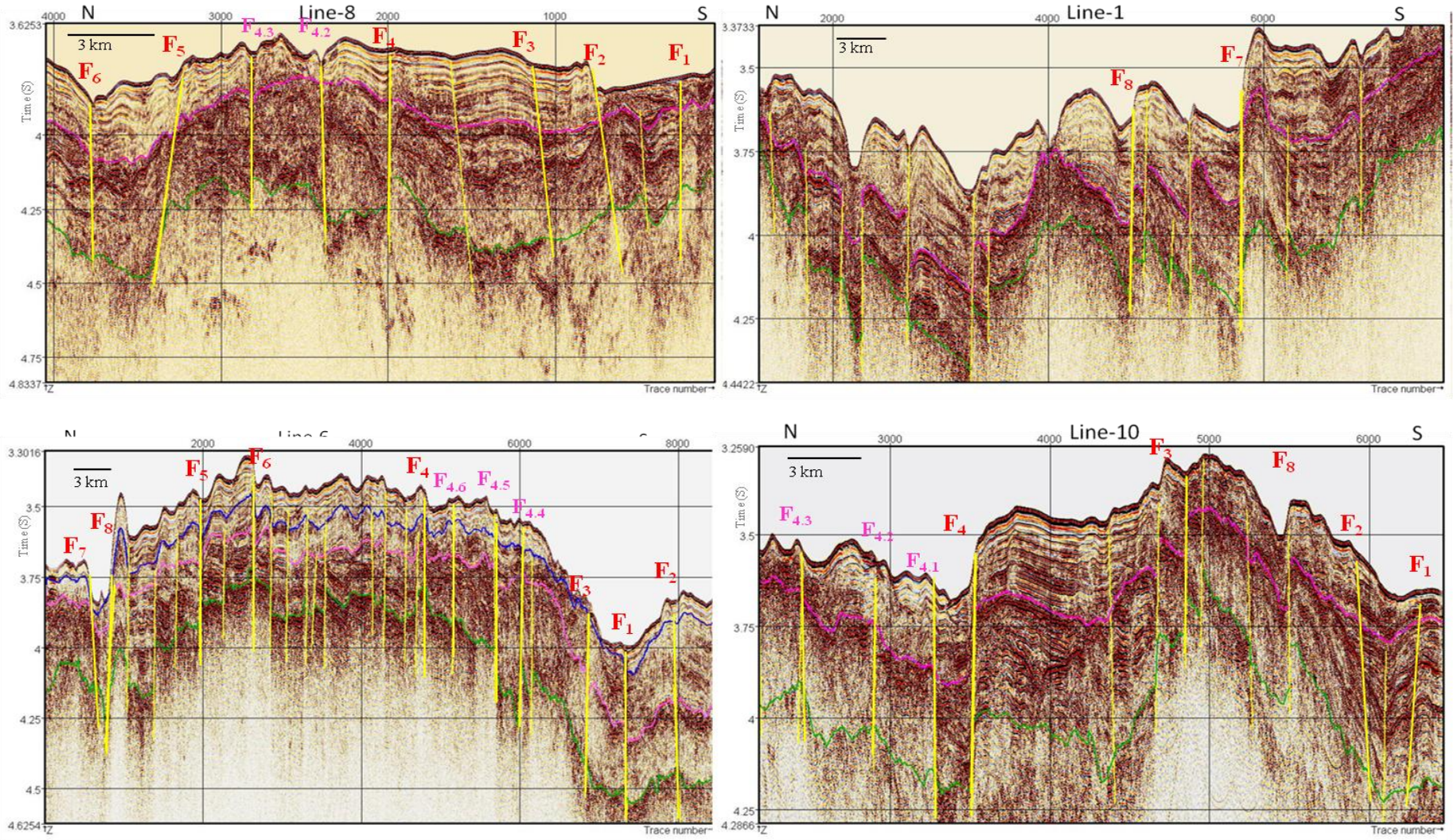

Figure 6.18: Interpreted profiles of Site NER2. Lines 1, 6, 8 and 10 are in N-S direction. Fault names are with reference to the correlation presented in map of Figure 6.19.

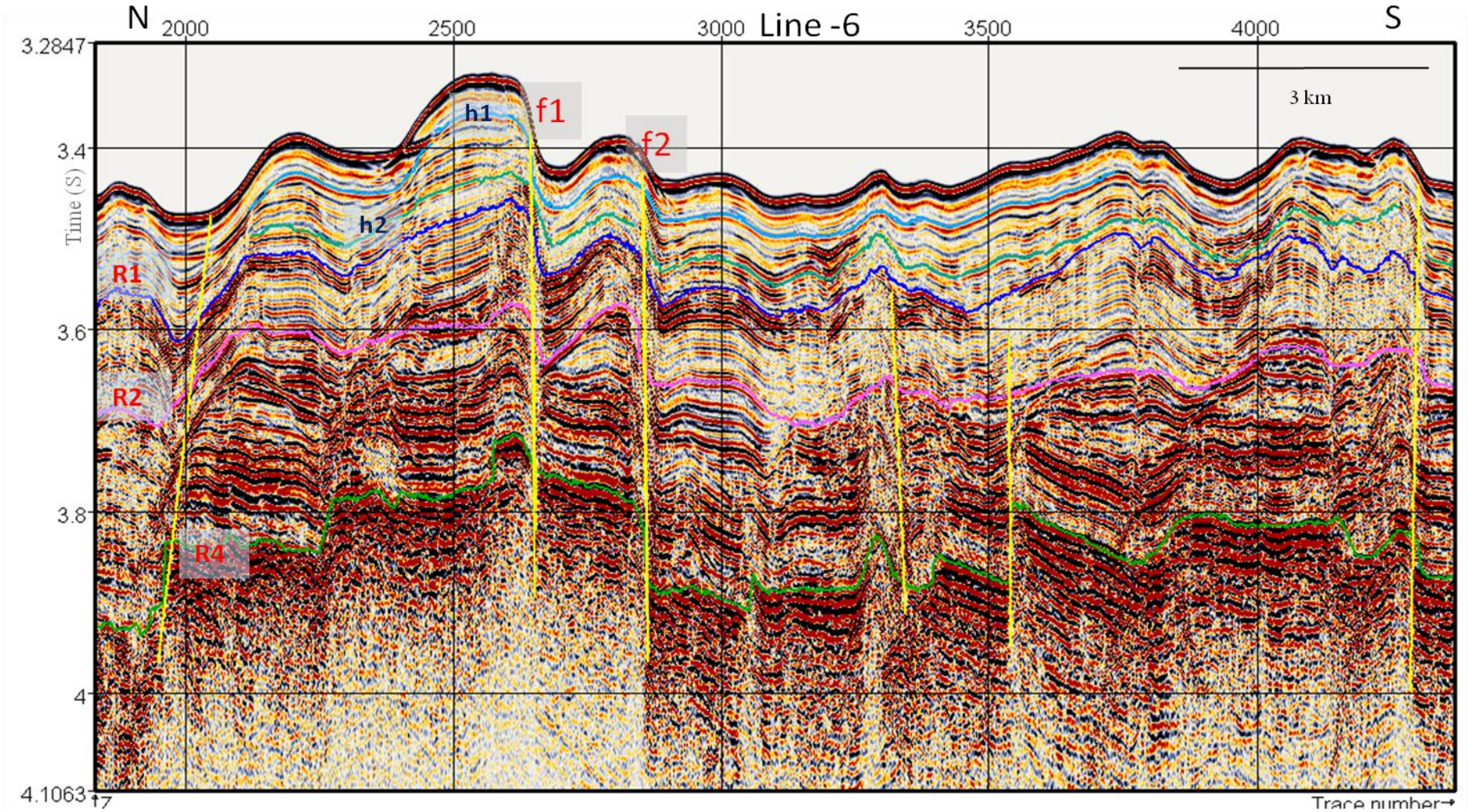

Figure 6.19 Site NER3 - Line-6 interpretation with reflectors and faults. Lithology is annotated. Fault displacement against fault marked f1 are measured. h1 and h2 are two horizons marked only to compare the variation in fault displacement.

Table 6.9 (a), (b): Fault displacements measured against active fault f1, f2 respectively in line-6 of Site NER3 grid and age calculation for onset of fault corresponding to horizon marked h2. P1 - Shallower point against fault. P2 - deeper point against fault.

(a)

Reflector	***TWT (ms) @***		***Displ. TWT (ms)***	***Int.Velocity (km/s)***	***Depth to the reflector (m)***		***Age derived (Ma)***		***Sedimenation Rate (m/Ma)***	
	P1	***P2***			***P1***	***P2***	***P1***	***P2***	***P1***	***P2***
W.B	3321	3406	85	2						
h1	3363	3450	87	2	42	44	5.98	6.27	7.02	8.6
h2	**3425**	**3490**	**65**	**2**	**104**	**84**	**14.82**	**11.97**	**7.02**	**8.6**
R1	3454	3516	62	2	133	110	18.95	15.67	7.02	8.6
R2	3568	3620	52	2	247	214	35.19	30.49	7.02	8.6
R4	3711	3758	47	2	390	352	55.57	50.16	7.02	8.6

(b)

Reflector	**TWT (ms) @**		**Displ.TWT (ms)**	**Int. Velocity (km/s)**	**Depth to the reflector (m)**		**Age derived (Ma)**		**Sedimenation Rate (m/Ma)**	
	P1	**P2**			**P1**	**P2**	**P1**	**P2**	**P1**	**P2**
W.B	3385	3434	49	2					7.02	8.6
h1	3428	3477	49	2	43	43	6.13	5.00	7.02	8.6
h2	**3472**	**3526**	**54**	**2**	**87**	**92**	**12.40**	**10.70**	**7.02**	**8.6**
R1	3498	3555	57	2	113	121	16.10	14.07	7.02	8.6
R2	3572	3653	81	2	187	219	26.65	25.47	7.02	8.6
R4	3778	3873	95	2	393	439	56.00	51.05	7.02	8.6

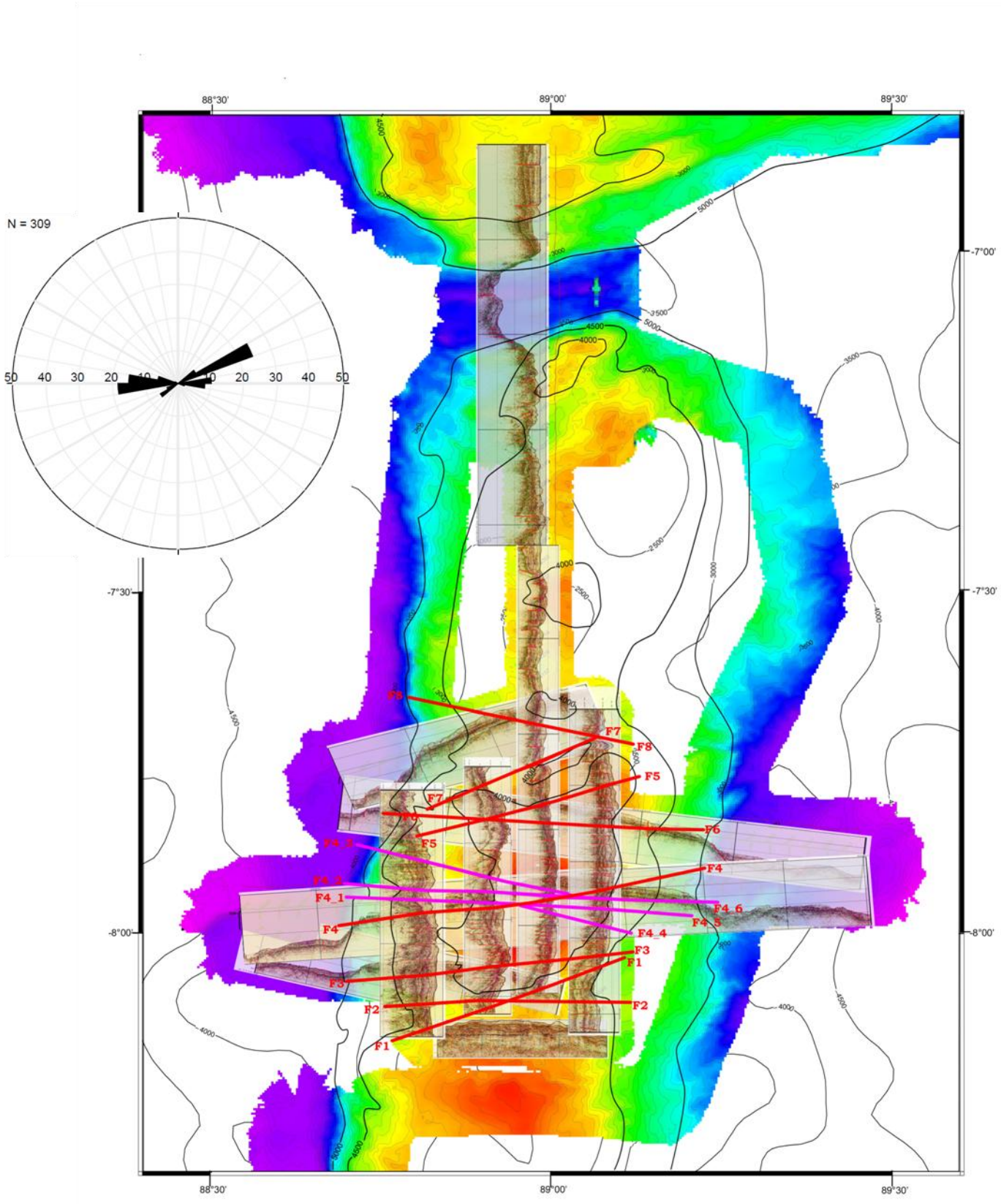

Figure 6.20: Site NER3 Fault strike analysis with interpreted seismic profiles overlaid on bathymetry. Rose diagram in stereonet of all the faults drawn is inserted.

Table 6.10: Fault strike and dip measurements at Site NER3: Data input for Rose diagram.For scissor faults (Sc.F) throw direction changes from north to south about its axis.

Fault Name	***Angle of Strike (°)***	***Dip (°)***	***Direction of throw***
F_1	70 - 71	80 - 85	Sc.F
F_2	87 - 91	80 - 85	Sc.F
F_3	82 - 85	80 - 85	S
F_4	78 - 84	80 - 85	Sc.F
$F_{4.1}$	91- 92	80 - 85	S
$F_{4.2}$	93 - 96	80 - 85	S
$F_{4.3}$	93 - 96	80 - 85	S

Fault Name	***Angle of Strike (°)***	***Dip (°)***	***Direction of throw***
$F_{4.4}$	103 - 104	80 - 85	N
$F_{4.5}$	94 - 95	80 - 85	N
$F_{4.6}$	90 - 91	80 - 85	S
F_5	73- 75	80 - 85	S
F_6	92 - 94	80 - 85	N
F_7	66 - 67	80 - 85	N
F_8	100 - 101	80 - 85	N

Fault displacements are measured against two adjacent faults on line- 6 of the site. Two horizons are marked above R1 for throw comparison. At fault marked as f1, R1 and h2 have similar displacements but h1 and water bottom mark larger displacements probably due to a period of erosion after major fault activity at the time of h2. Assuming same sedimentation rate as NER2 at this location also, as the ash layer is not identified here for reference, age at h2 are generated in the range 10.5−14 Ma from measurements at f1 and f2 (Tables 6.9.a, b). This is too wide a range and to consider for any inference.

On correlation of seismic results 9 faults, F_1 to F_8 are identified in near E-W conjugate trends, i.e. WNW-ESE and ENE-WSW directions (Figure 6.20). At least 3 pairs of scissor fault systems are present in this grid, where the middle one about F_4 forms a scissor fault complex similar to the one in NER2. This is a clear indication of currently on-going compressional stresses in the location. Following the principles of structural geology this situation can be interpreted as presence of two types of compressions of near opposing nature, but not exactly opposing on a single line are active at a location for long span of time. This is in agreement with near N-S compressive stresses exerted by India-Australia and India-Capricorn plates at this location and the subtle strike slip component by E-W stress of Capricorn-Australia plates. The Rose diagram depicts the distribution of faults in conjugate direction about E-W azimuth.

6.3.4 Site 214 (11°S latitude)

In the KNOX06RR grid around DSDP Site 214, a total of 11 seismic profiles are collected, but the profiles 4 and 6 are being curved and too shorter in length are excluded from the analysis (Figure 6.21). The basement at site 214 is post-Cretaceous of 62 Ma (Pringle et al., 2008). The biostratigraphy of site 214 have documented ages from Holocene to late Palaeocene continuously in the sediments of about 500 m thickness overlying the basaltic basement without any unconformities in between (Von der Borch et al; 1974b).. The N-S seismic line-1 and E-W line-7 passed through the drill site 214 (Figure 6.21). The reflectors identified in old seismic data collected during the DSDP drilling do not match with the reflectors of KNOX06RR profiles interpreted based on major impedance contrasts, except the top of basaltic basement (Figure 6.22).

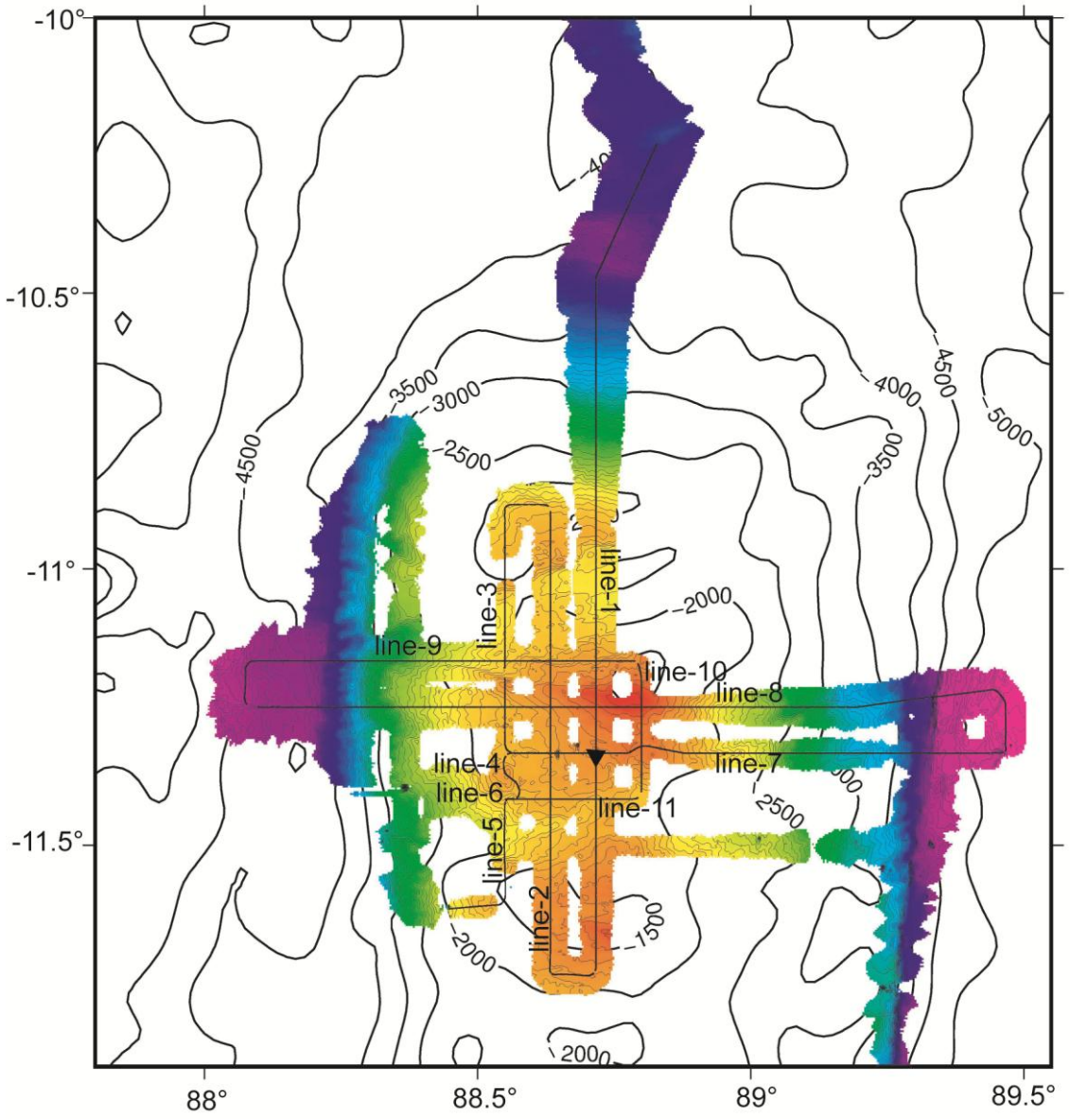

Figure 6.21 Multibeam bathymetry of KNOX06RR grid Site 214. Seismic profile tracks are overlaid with annotation of line numbers. Bathymetric contour in multibeam map is of 50 m and in the regional area of 500 m interval. DSDP Site 214 location is marked with solid black triangle

Table 6.11: Correlation of seismic stratigraphy of line-1 of KNOX06RR Site 214 with seismic and lithostratigraphy of DSDP Site 214.

Unit	***Reflector***	***Depth (m)***	***Avg. int. Vel***	***TWT (ms)***	***Lithology /stratigraphy***	***Age***
0	-	0	1500	2254	water bottom	
1	R1	162	1700	2444	ForamNanno Ooze	Pleistocene to upper Mid.Miocene
2	-	219	1900	2504	Foram rich Nanno Ooze	Mid to Early Miocene
3	R2	323	1900	2613	Nanno Ooze	Late Oloigocene to Early Eocene
4		333	1900	2623	Glauconitic foaram rich oze and chalk	Early Eocene to Palaeocene
5		366	2150	2653	Glauconitic carbonate silt and sand	Palaeocene
6	--	390	2150	2675	Glaucon. Shelly silt and limestone with volc. components carbonate silt and sand	Palaeocene
7	R4	490	2150	2768	Lignite Volc. Clay tuff with interlayered rocks	Palaeocene
8		500	2150	2777	Basalt	Early Palaeocene-Danian

Two of the lithologic boundaries identified in core analysis of the DSDP Site 214 matches with the two major acoustic reflectors interpreted above basement in KNOX06RR profiles (Table 6.11, Figure 6.22), the mid-Miocene boundary in the ooze layer and ooze chalk boundary of the early Eocene. The ash layer at and the vicinity of drill site does not have any impedance contrast as observed it on many other profiles.

The effective stresses caused by the diffused plate boundary change the style of deformation activity from compression to extension towards the southern Ninetyeast Ridge. Changes in type of fault activity as observed by Sager et al. (2013) corroborate this fact. Bathymetric lineations at this location are not very clear along any specific orientation. Most of the major faults are of extensional type (F_3, F_5, F_6, F_7, F_8, F_9) but compressional bending of sediment layers are observed in between (F_5 - F_6, north of F_9) them (Figure 6.23, 6.25). The correlation between the faults helps in identifying the net direction of extension within this grid. Following the similar procedure of other grids, 9 active faults F_1 to F_9 are correlated in near

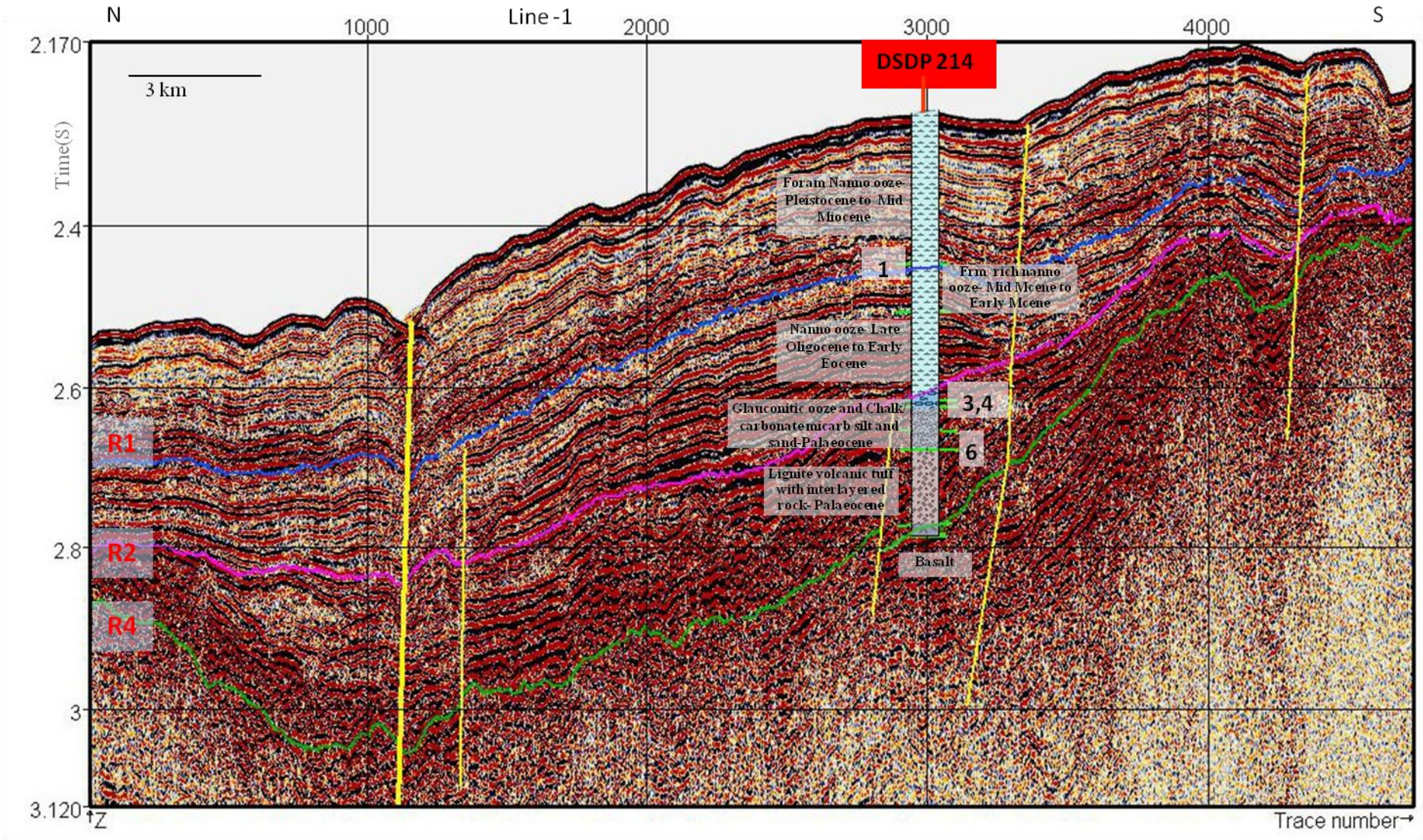

Figure 6.22: Site 214-Line-1 correlated with DSDP 214 well site

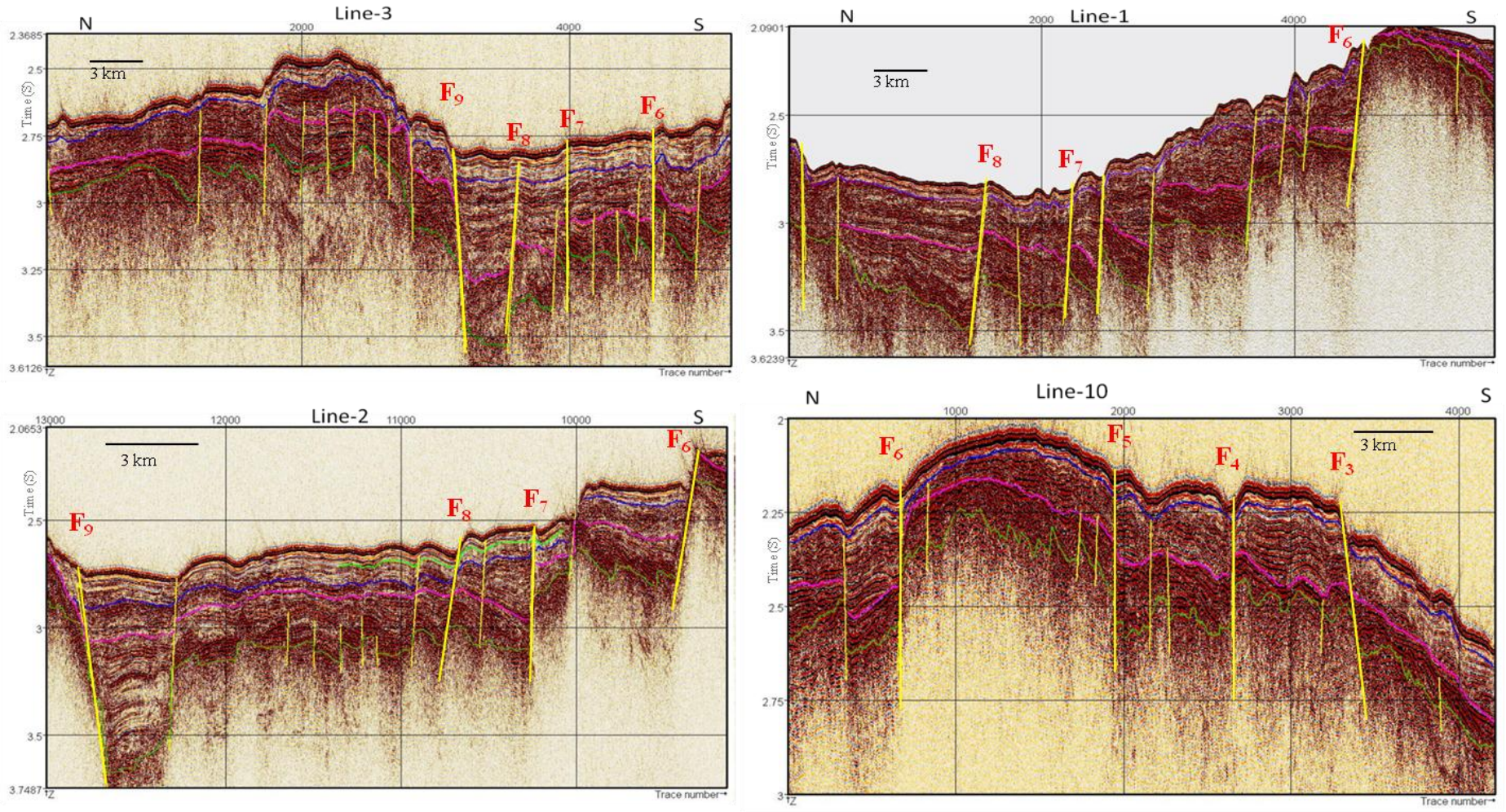

Figure 6.23: Interpreted profiles of Site 214. Lines 1, 2, 3 and 10 are in N-S direction. Fault names are with reference to the correlation presented in map of Figure 6.24.

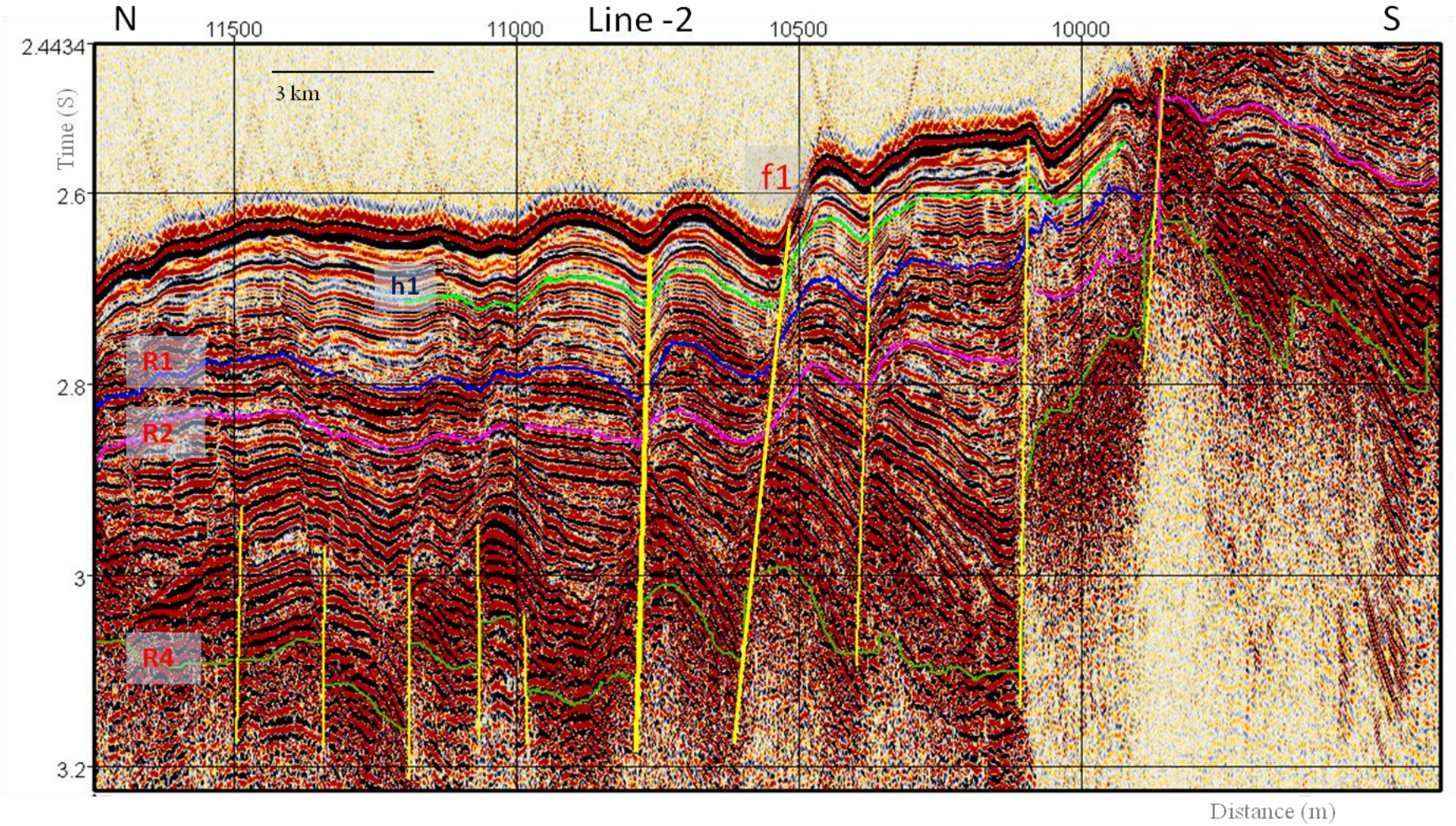

Figure 6.24: Site 214 - Line-2 interpretation with reflectors and faults. Fault displacement against fault marked f1 are measured. A horizon h1 is marked on to compare the variation in fault displacement while measurement.

Table 6.12: Fault displacements measured against active fault f1 in line-2 of Site 214.

Reflector	***TWT (ms) @***		***Displ.TWT (ms)***
	P1	***P2***	
W.B	2560	2648	88
h1	2623	2710	87
R1	**2687**	**2777**	**90**
R2	2778	2846	68
R4	2991	3086	95

Table 6.13: Fault strike and dip measurements at Site 214: Data input for Rose diagram

Fault Name	***Angle of Strike (°)***	***Dip (°)***	***Direction of throw***
F_1	57 - 61	80 - 85	N
F_2	55 - 62	80 - 85	S
F_3	83 - 85	80 - 85	S
F_4	80- 90	80 - 85	N
F_5	98- 100	80 - 85	S
F_6	97 - 110	80 - 85	N
F_7	83 - 84	80 - 85	N
F_8	90 - 92	80 - 85	N
F_9	63- 64	80 - 85	S

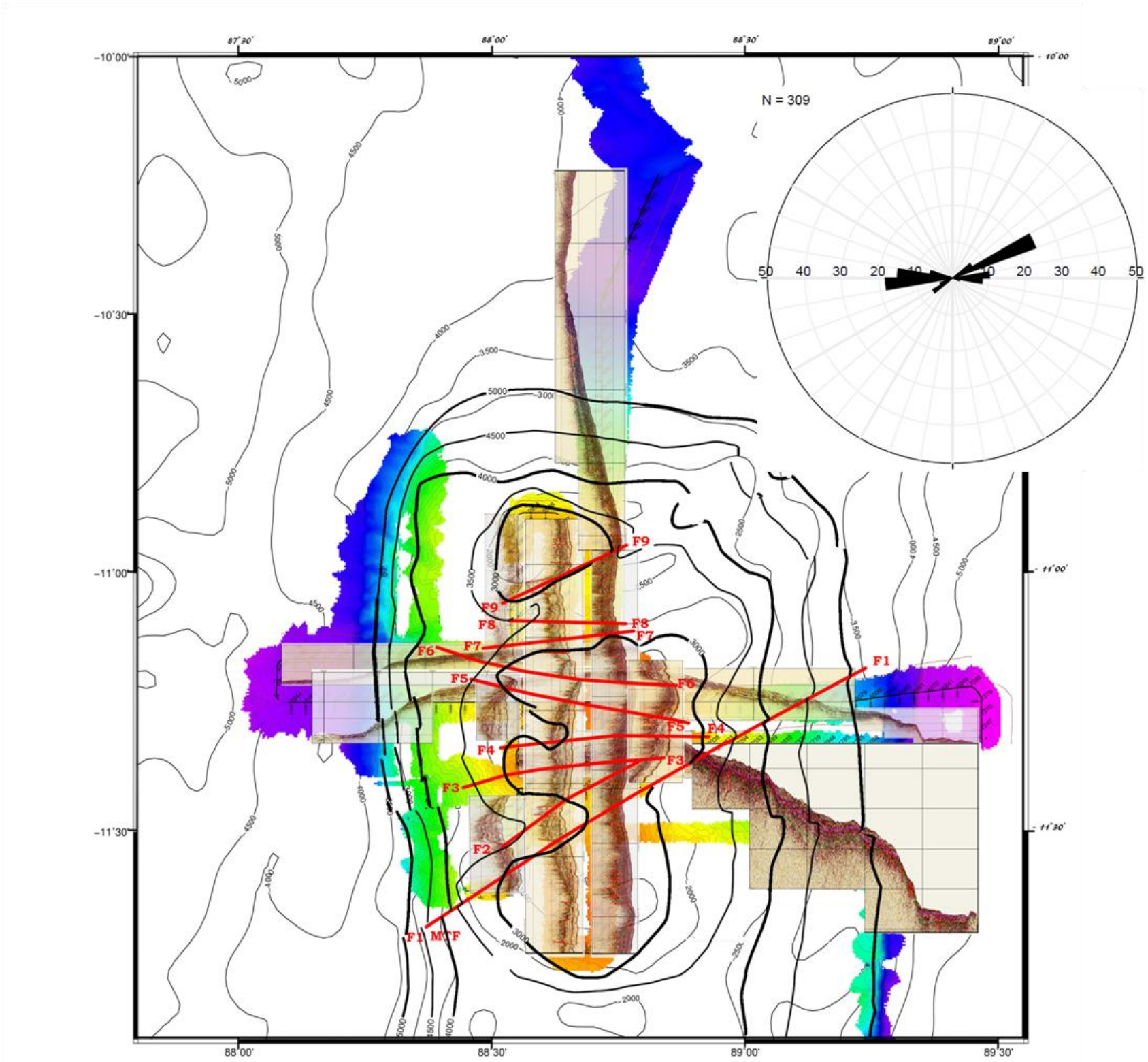

Figure 6.25: Site 214 fault strike analysis with interpreted seismic profiles overlaid on bathymetry. Rose diagram in stereonet of all the faults drawn is inserted.

E-W to ENE-WSW are identified in this grid, indicating the on-going major extensional stress in WNW-ESE azimuth (Figure 6.25). Minor compression and strike-slip components are inferred on near E-W (F_4) trending faults as they are associated with compressive stress in near N-S direction. The rose diagram explains this fact with higher population in ENE-WSW direction and the rest in E-W direction.

Displacements are measured at an active fault marked f1on line-2 of grid 214 (Figure 6.24, Table 6.12). The stress reactivations of the area upwarp the sediment layers faulted with extensional stress in previous episode of activity to give an appearance of short wavelength folds. Approximately similar displacements are observed at reflector R1 and horizons marked above. Onlapping type of features is not observed above these reflectors, indicating continuation of the fault activity. R1 and R2 are different in terms of displacement. It can be inferred that the fault activity had started around age corresponding to R1 boundary which is in mid Miocene (~13 Ma) and continuing to present with similar but weak stress regime, reactivating the extensional faults of origin.

6.3.5 Site 253 (26°S latitude)

The grid in the vicinity of DSDP Site 253 bounded by 25°S and 26.2°S latitudes has total 13 seismic profiles with 5 N-S, 6 E-W and 2 in oblique directions (Figure 6.26). The DSDP Site 253 (24.88°S, 87.37°E) is about 50 km away from the KNOX06RR Site 253 grid, so that direct correlation of seismic reflectors to well data cannot be attempted, but the lithology can be interpreted similarly. Three reflectors are identified in all profiles of the new survey. The lithology in this site also varies from nanno ooze and chalk to volcanic ash with a thin vesicular basaltic layer within the ash (Von der Borch et al; 1972). Out of 559 m penetration the ash layer is thickest here about 400 m while the top ooze- chalk sediment is of only 153 m and the ages varies from the Quaternary to late Eocene continuous except a small hiatus within the late Eocene, according to biostratigraphy the basement age at this site is 46±3 Ma old and the ash layer had settled in less than 4 Myrs of time (Shipboard Scientific Party, DSDP Site 253).

Interpretation of seismic reflection profiles of the grid could map 3 reflectors including the basement and top of the volcanic ash layer. The top most one corresponds to some impedance change in the ooze - chalk layer (Figure 6.27, 6.28). Above the ash layer only two sediment layers are observed unlike the three sediment layer interpretations in northern grid locations. Sharp elevations cutting through even the top most reflector

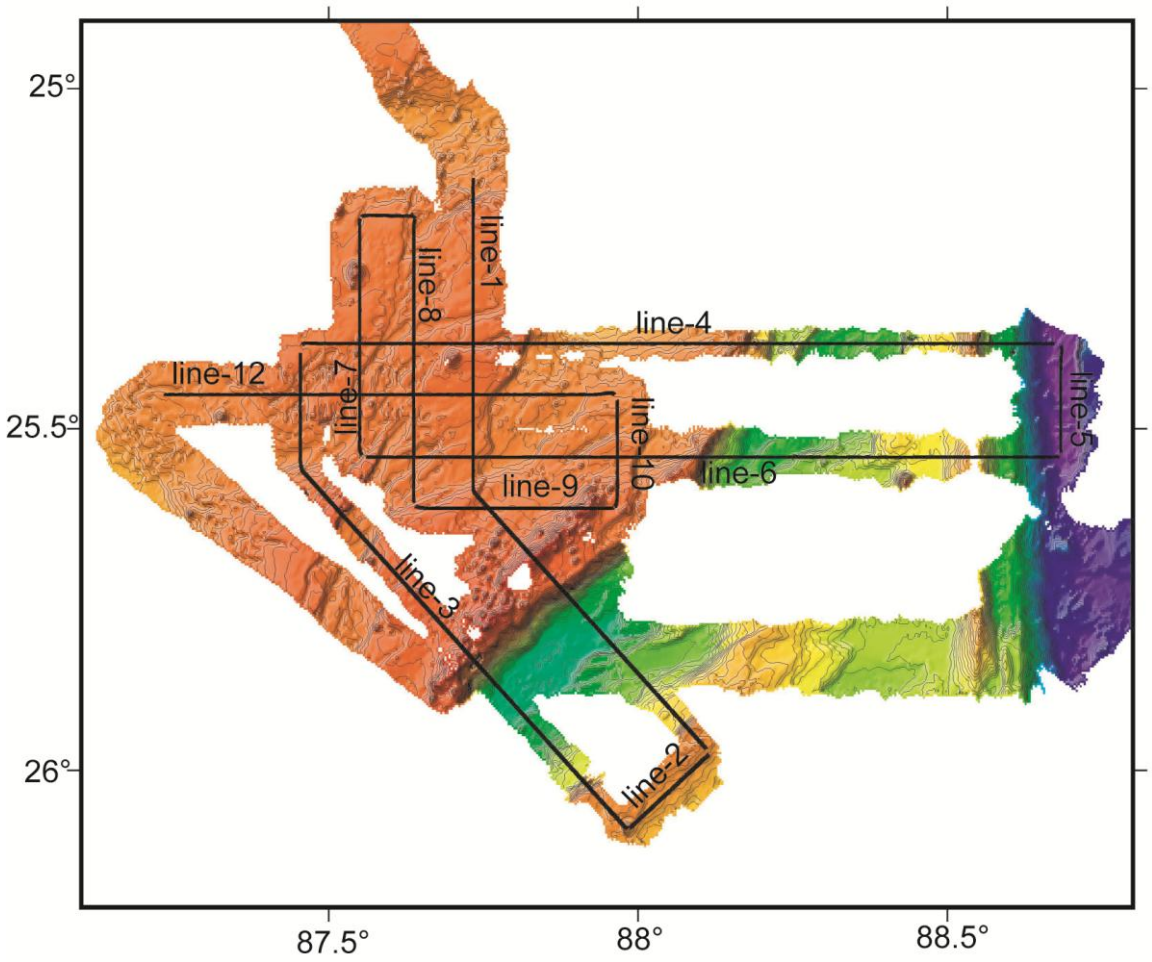

Figure 6.26 Multibeam bathymetry of KNOX06RR grid Site 253. Seismic profile tracks are overlaid with annotation of line numbers. Bathymetric contour in multibeam map is of 50m and in the regional area of 500 m interval.

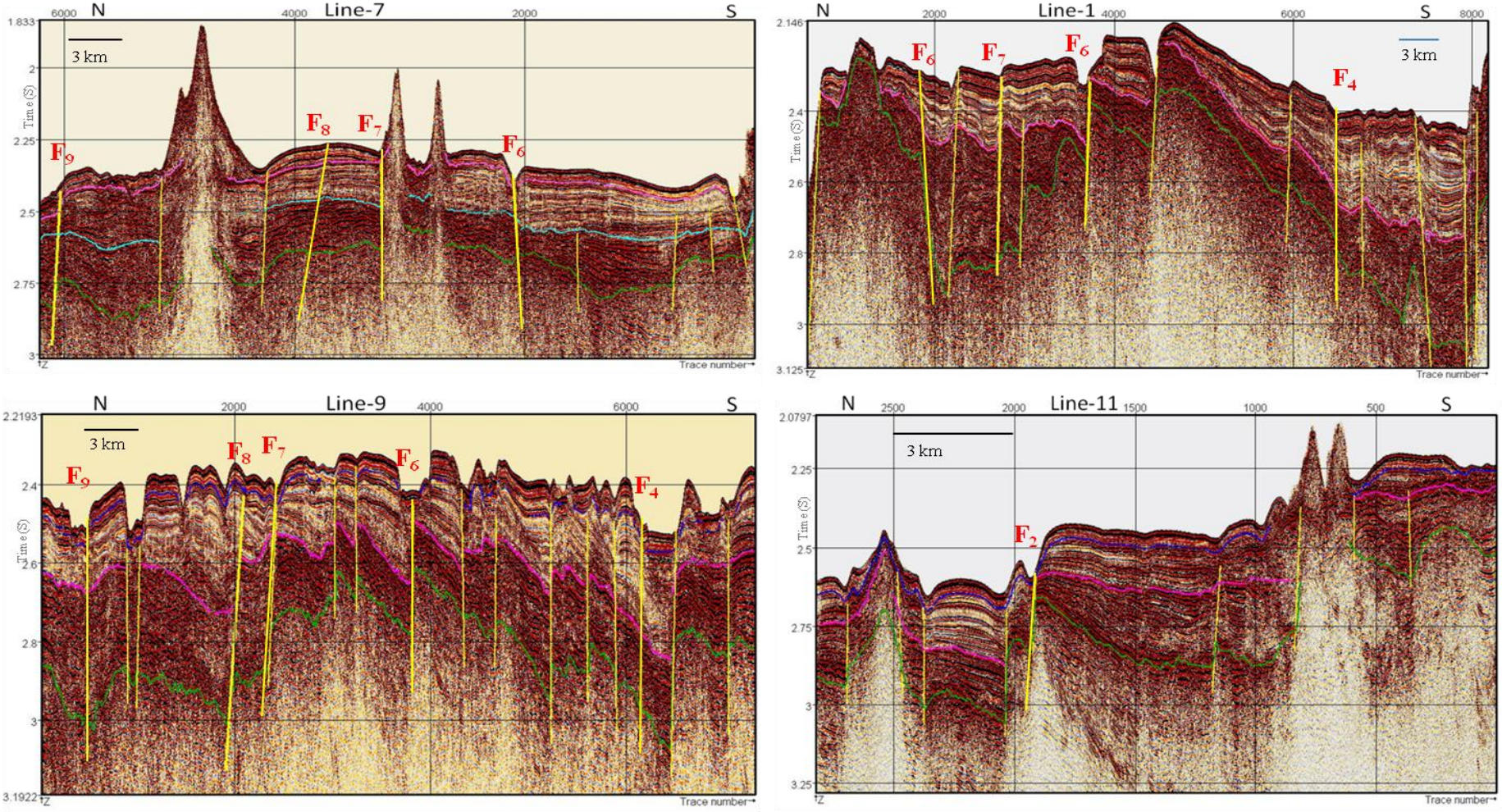

Figure 6.27: Interpreted profiles of Site 253. Lines 1, 7, 9 and 11 are in N-S direction. Fault names are with reference to the correlation presented in map of Figure 6.28.

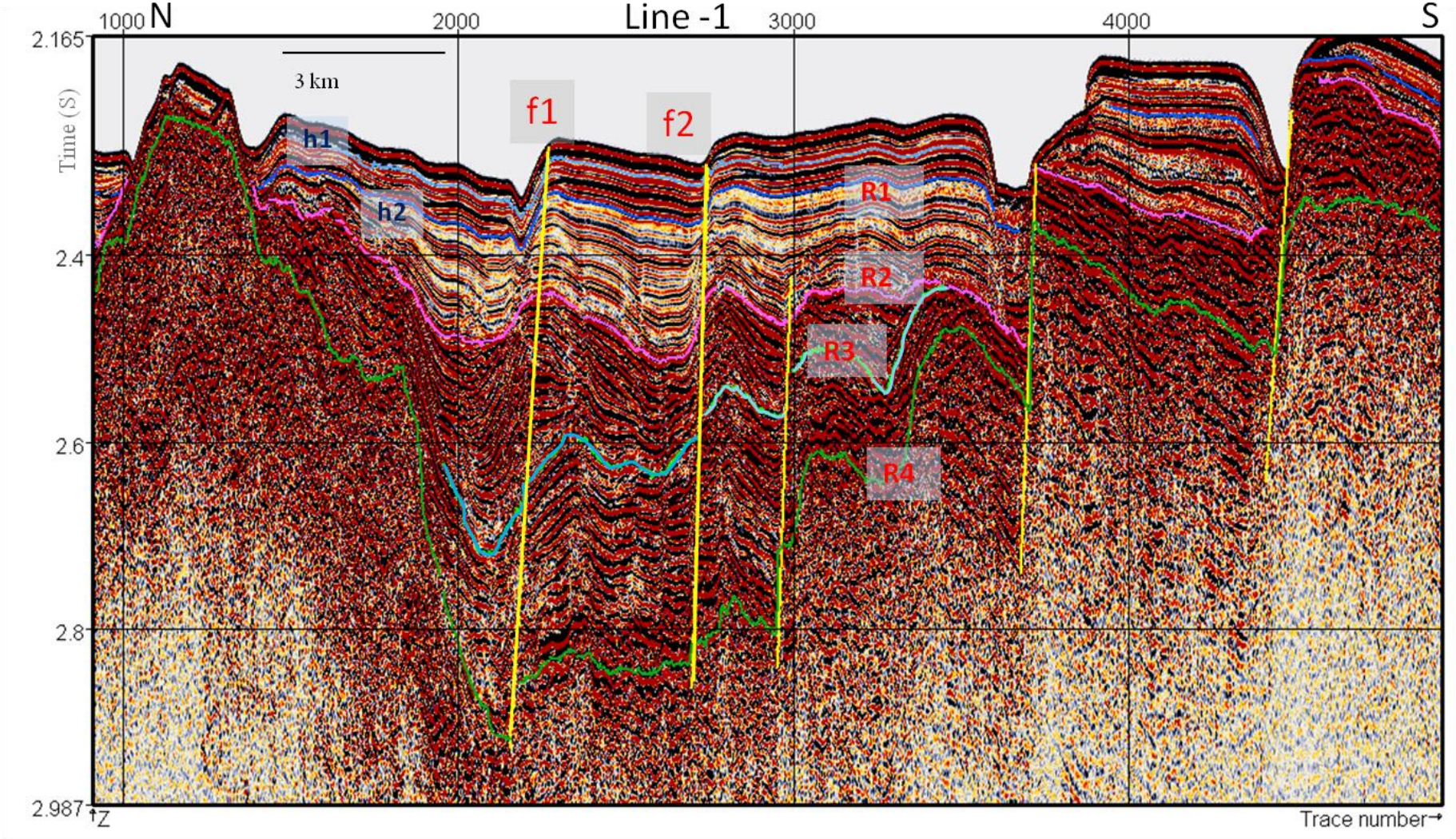

Figure 6.28: Site 253 - Line-1 interpretation with reflectors and faults. Fault displacement against fault marked f1 and f2 are measured. h1 and h2 are two horizons marked only to compare the variation in fault displacement.

Table 6.14 (a): Fault displacements measured against active fault f1 in line-1 of Site 253

Reflector	***TWT (ms) @***		***Displ.TWT (ms)***
	P1	***P2***	
W.B	2274	2319	45
h1	2294	2339	45
R1	**2331**	**2381**	**50**
R2	2433	2501	68
R3	2592	2716	124
R4	2831	2899	68

Table 6.14 (b): Fault displacements measured against active fault f2 in line-1 of Site 253

Reflector	***TWT (ms) @***		***Displ.TWT (ms)***
	P1	***P2***	
W.B	2271	2296	25
h1	2294	2319	25
R1	**2323**	**2359**	**36**
R2	2431	2501	70
R3	2539	2621	82
R4	2777	2837	60

Table 6.15: Fault strike and dip measurements at Site 214: Data input for Rose diagram

Fault Name	***Angle of Strike (°)***	***Dip (°)***	***Direction of throw***
F_1	43 - 44	80 - 85	S
F_2	35 - 51	80 - 85	N
F_3	35 - 47	80 - 85	N
F_4	36 - 49	80 - 85	S
F_5	104- 106	80 - 85	S

Fault Name	***Angle of Strike (°)***	***Dip (°)***	***Direction of throw***
F_6	52 - 53	80 - 85	S
F_7	56 - 60	80 - 85	N
F_8	59 - 61	80 - 85	S
F_9	64 - 65	80 - 85	S

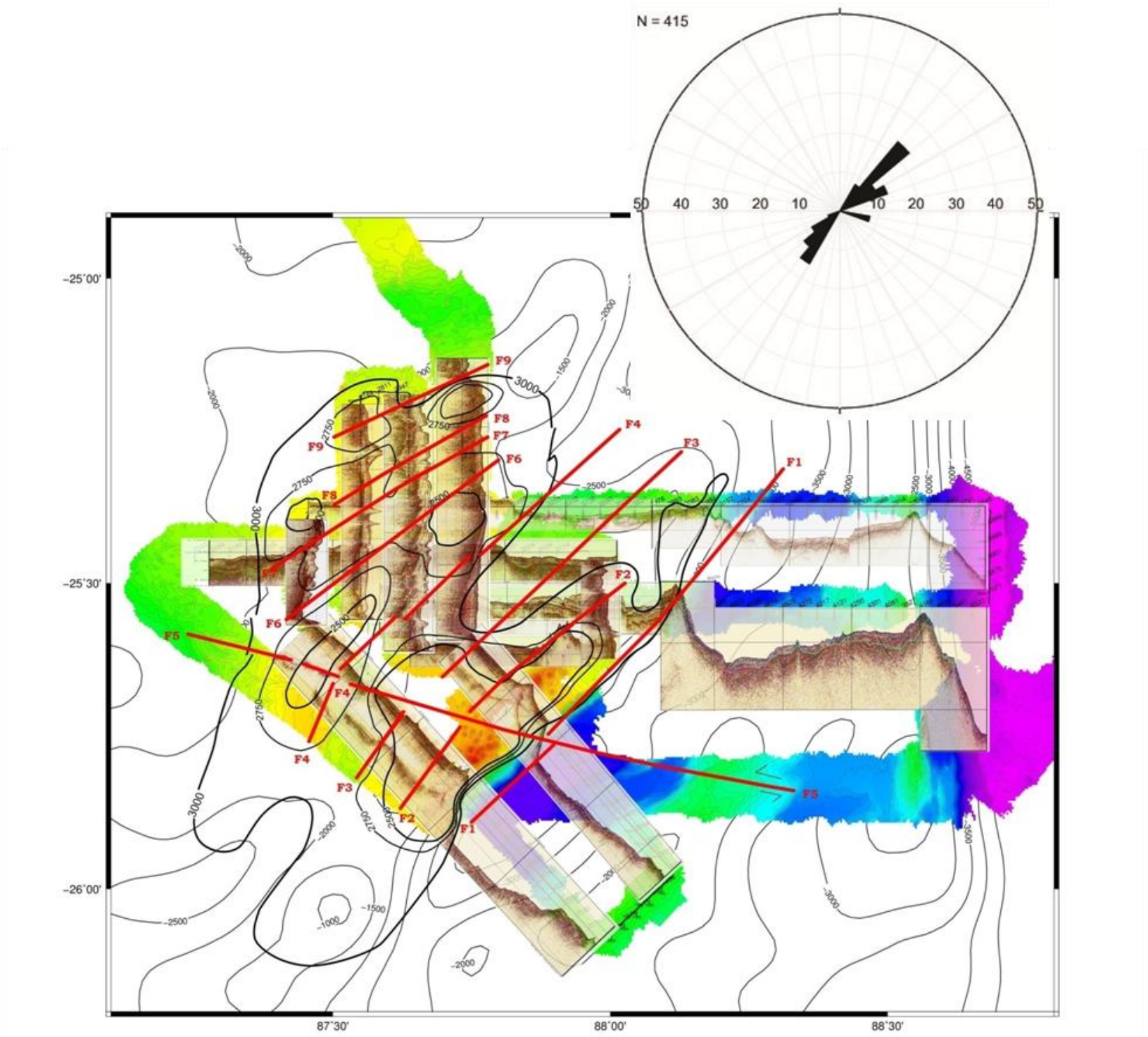

Figure 6.29: Site 253 - Fault strike analysis with interpreted seismic profiles overlaid on bathymetry. Rose diagram in stereonet of all the faults drawn is inserted.

indicates recent volcanism (Figure 6.27). Bathymetric lineations in this site are oriented in NE - SW direction (Figure 6.26). Most of the faults mapped different profiles depict extensional characteristics. But thrust faults are also active at the site as observed between F_4 and F_6 (Figures 6.27 and 6.29). According to fault analysis, most of the original normal faults are found to be reactivated with extension and recent compression also active at this part of the ridge.

Fault displacements are discussed with representative line-1 of the grid. Reflector sequences show high acoustic impedance contrast above R2 where sedimentation is observed in continuous strata, implying a quite period between R2 and R1 in terms of fault activity (Figure 6.28, Table 6.14 a, b). Active faults offsets R1 and above reflectors with similar throws at this site also implying similar continuing type of stress activity at this grid also as that of 214. Age correlation above ash layer (upper Eocene) is difficult at this site as the grid profiles as the DSDP Site 253 well analysis has not defined any acoustic boundary corresponding to biostratigraphy of top most layers. But the ooze chalk layer is subdivided in to five units according to biostratigraphy where the top 18 m is Quaternary to Pliocene and next 66 m belong to Miocene (DSDP 253, Shipboard Scientific Party). So that reflector R1 can be widely correlated to Miocene which is marked above half of the total thickness of ooze - chalk layer and the fault reactivation must have occurred younger to Miocene age.

A total of 9 faults are interpreted in this grid with major extensional activity. The mean direction for the extensional faults is approximately NE-SW as the net stress direction is NW-SE (Sager et al., 2013). This depicts the obvious change in stress direction from near NE-SW at north of the ridge to NW-SE at the southern part. The mean stress direction at DSDP Site 214, around 1500 km away from the present grid is WNW-ESE, which has changed to NW-SE at this location with similar type but resulting in more throw of faults. The observations are consistent with earth quake focal mechanisms derived from the stress directions.

6.4 Seismic structure and fault activity along the Ninetyeast Ridge according to interpretation of KNOX06RR grids

The evolution of the Ninetyeast Ridge has taken more than 42 M years in a near N-S strike with different emplacement rate of the plume and at different offsets from the spreading center. The difference in its structure from N-S is mainly due to the same

reason but also a component in macroscopic level to the regional stress prevalent at geologic times. The present day stress pattern is reign by combination of 3 diffuse plate boundaries on either of the ridge and the ridge acting as boundary of these plates in a diffuse manner. Indian and Capricorn plate diffuse plate motion began in about 8Ma (late Miocene) ago (Gordon, 2009). While the commencement of Indian Australian intraplate motion also been delineated to be in Late Miocene (Weins et al., 1985). Activation of Capricorn - Australian plates are also at the similar age (Gordon et al., 1998). These are obtained by method of Earth quake focal mechanism supported by borehole fracture data at available sites. Stress directions obtained from trend of presently reactivated faults are consistent with earth quake focal mechanism derived stress directions published by other researchers and the stress effect of diffused plate boundary poles.

6.5 Pattern of tectonic Activity on the Ninetyeast Ridge since its emplacement

The Ninetyeast Ridge was emplaced during the period approximately from 80 Ma to 40 Ma as a hotspot trail in the Indian Ocean during the fast northward migration of the Indian plate. The recent analysis focussed on evolution pattern of the ridge with geologic time reveals that most of its track was emplaced in close proximity to the Wharton Spreading center, except the northern part of the ridge till ~5°N, which formed away from the spreading ridge. This could have been the cause for compressive stress during the evolution of this segment of the ridge. The remaining part of the ridge south of this is different in emplacement setting as it could have formed in an extensional field of stress close to the diverging margin as indicated by the presence of abundant normal faults along this part of the ridge. The compression features still observed along the segment could be due to later on up thrust on the original faults as the older ridge moved away from the spreading centre.

Other than original faults formed at the time of ridge emplacement, the Neogene plate deformation has placed the whole Ninetyeast Ridge at its centre and affected the ridge with different tectonic regimes on either side varying from north to south. According to diffuse plate boundaries of the new plate deformations and their Euler poles, the northern portion of ridge is subjected to dominant compressive stress exerted by the Indian-Australian diffuse plate boundary at an azimuth of ~N45°W with respect to the

ridge also, while in the middle part of the ridge is subjected to N-S compression by India-Capricorn plate pairs. The southern part of the ridge is situated near the Capricorn -Australian plates and the main type of stress is extension (Royer and Gordon, 1997; Sager et al., 2013).

6.6 Fault activity along the Ninetyeast Ridge and their occurrence

The fault activity observed along the Ninetyeast Ridge is in accordance with various tectonic activities that were prevalent over the ridge during different geologic time. In the northern portion of the ridge located north of till 5°N latitude and formed during the period 80 Ma- 75 Ma, compressive movements along the faults are more dominant presently. Analysis of faults reveals the reactivation of original faults ~8-9 Ma time and provides a net direction of N-S to WNW-ESE, which gradually varies in southward direction. In the second grid at 1.5°N latitude, the faults activity continues to be of compression and to strike-slip types in WNW-ESE direction, with lesser density of thrust faults. The faults were again reactivated and the onset of reactivation is inferred to be around 9.5 to 10 Ma again in late Miocene (Table 6.16). The two grids close to each other (NER2 and NER3 at 6 - 8°S latitudes) on central part of the Ninetyeast Ridge are about 800 km away from the DSDP Site 216, hence a gradual variation in fault pattern is unable to reveal, but both grids NER2 and NER3 lie within the diffused triple junction zone (Figure 6.1). The complex of scissor faults typical to compression regime is marked at both the sites when active faults are correlated on the bathymetry map. A strike-slip fault is mapped in WNW-ESE direction in NER2, whereas at NER3 strike-slip motion along the faults is not obvious, but 3 sets of scissor fault complex trend in near E-W direction are delineated due to active compression in N-S direction. This implies the active stress completely changes to N-S compression by the location of NER3. The fault reactivation is weaker compared to other sites and the age of fault reactivation for these sites are slightly older than the northern sites by 1 to 2 Myr nearing the late to mid Miocene boundary according to present analysis.

The DSDP Site 214 is located on south border of the diffuse triple junction zone (Royer and Gordon, 1997) (Figure 6.1). The main faults observed are extensional nature trending in ENE-WSW direction and some amount of minor compression and strike-slip activities in near E-W direction are also noticed. The fault pattern reveals that the magnitude of Australia-Capricorn plate extension stresses are even influencing the

Table 6.16: Fault reactivation time and pattern along Ninetyeast Ridge as inferred in present analysis

Site	***Latitude***	***Age of Fault Reactivation (Ma)***	***Type of Reactivated fault***	***Azimuth***
758	5.2°N	8 - 9 Ma	compression	WNW-ESE
216	1.5°N	9.5 - 10	compression	NW-SE
NER2	6.5°S	10 - 11	weak compression	E-W
NER3	7.5°S	9.5 - 14?		
214	11°S	13	extension	ENE-WSW
253	25.5°S	13 or younger?	extension	NE-SW

region of the DSDP Site 214. All the faults are not active in this grid (Figure 6.20), reactivation is observed only at some major faults revealing the time of onset of the deformation during ~13 Ma or in middle Miocene time.

In the southernmost grid close to the location of DSDP Site 253, faults are active and almost purely extensional type with mean direction of NE-SW due to net stress of NW-SE direction. A strike-slip fault marked in WNW-ESE direction indicates a rare presence, but chance of strike-slip motion in near perpendicular direction to extension is possible due to horizontal orthogonal stresses. Most of the original normal faults in this grid have undergone reactivation when some compressional faults have originated revealing the time of onset of the deformation during middle Miocene time or younger. The observations of fault reactivations suggest that the diffused deformation has started at southern latitudes in middle Miocene or younger, which has gradually propagated to northern part of the eastern Indian Ocean by late Miocene developing its present geometry with time.

This chapter describes detailed analysis of seismic reflection data along the Ninetyeast Ridge for changes of internal structure in response to the deformation style from north to south. Further the chapter clearly presents observations and inferences of seismic stratigraphic work. Next chapter summarises the whole thesis with major findings and scope of the future work.

Chapter 7

7 Summary and Conclusions

7.1 Introduction

The present research work has given an opportunity to investigate magnetic anomaly data of the Ninetyeast Ridge and adjacent Central Indian and Wharton basins for mapping the unidentified seafloor spreading magnetic anomalies, fossil spreading centers and oceanic fracture zones. The fracture zones are further constrained by satellite free-air gravity anomaly data of the study region, which in turn helped in lateral extrapolation of E-W trending correlated magnetic anomalies and preparation of improved tectonic map of the northeastern Indian Ocean, particularly on either side of the Ninetyeast Ridge. The work was carried out with the compilation of magnetic data from different data sources such as NGDC, NIO, TIOG programme and new dataset acquired on-board Roger Revelle (KNOX06RR). The expedition of Roger Revelle was executed as an international scientific expedition in 2007 basically to acquire magnetic, multibeam, seismic reflection and basement rocks from the Ninetyeast Ridge to understand the tectonic evolution of the ridge, dynamics associated with the interactions between the spreading centers and Kerguelen hotspot, ridge morphology and its internal structure, effect of intraplate deformation over the ridge and geochemical signatures of the ridge. The implications of Neogene intraplate deformation on the ridge is studied in detail by analysis of faults from the seismic reflection data. 2D seismic and multibeam bathymetry data over the ridge at six selected grid locations are together analysed for identification of faults and mapping their spatial extent. Besides, major seismic boundaries are interpreted in correlation with lithostratigraphic boundaries of DSDP and ODP drilled wells available in each grid location, thereby ages are assigned to the reactivation of the faults. The study contributes to improve the understanding of structure, tectonics and variation of deformation along the ridge.

7.2 New understandings on structure and tectonics of the Ninetyeast Ridge

The new understanding on the evolution of the ridge and the implications on the evolution of the northeastern Indian Ocean spreading can be summarised as

- Magnetic anomaly studies of both the Central Indian and Wharton basins have provided precise locations of magnetic lineations from 19 through 34 and fossil ridge segments, which ceased spreading at 65 and 42 Ma. The lineation offsets are

further constrained by narrow gravity features of the satellite gravity data and interpreted them as oceanic fracture zones. From the trends of Ninetyeast Ridge bathymetry and fracture zones it is found that the Ninetyeast Ridge trends ~N10°E and obliquely crosses ~N5°E oriented fracture zones. Thus in the south, the 89°E FZ borders the Ninetyeast Ridge on east side, whereas in the north the same FZ borders the ridge on west side. In the central part between 11°S and 18°S, the fracture zone obliquely crosses the Ninetyeast Ridge.

- Interpretation of magnetic anomaly data revealed that the age of oceanic crust to the west of the 86°E FZ increases towards north from early Cenozoic to late Cretaceous, while the crust to the east of the 90°E FZ increases its age in both north and south directions about middle Eocene fossil ridge segments. Contrasting to these patterns, the crust between the FZs near Ninetyeast Ridge shows a complex age succession together with fossil ridge segments of different ages (65 and 42 Ma).
- Comparison of ages of oceanic crust, east and west of the Ninetyeast Ridge with newly determined radiometric ages at DSDP Sites 216, 214, 254 and ODP Sites 756-758 shows that the Ninetyeast Ridge formed at a rate twice that of adjacent oceanic crust.
- The resulting difference in lengths of the Ninetyeast Ridge (~3980 km) and adjacent oceanic crust (~2000 km) constructed from 77 to 43 Ma is remarkable and requires a geodynamical explanation. The Wharton spreading ridge segments, particularly in a strip between 86°E FZ and 90°E FZ, and the Kerguelen hotspot were often in close proximity due to ridge migration and ridge jumps. During the formation of the Ninetyeast Ridge, the distance between the Kerguelen hotspot and spreading ridge segments changed significantly due to the northward migration of the plate boundary represented by the Wharton spreading ridge relative to the Antarctic plate followed by southward ridge jumps toward the hotspot and possibly southward motion of the hotspot. Ridge migration caused the Kerguelen hotspot to drift beneath the Antarctic plate during the early Cenozoic and led to formation of volcanic edifices on the Antarctic plate by ridge-flank volcanism and by lateral transport of plume melt through ridge-axis. Thus the southward ridge jumps transferred part of the Ninetyeast Ridge originally formed on the Antarctic plate to the Indian plate and contributed to the extra length of the Ninetyeast Ridge.

The combined interpretations of multibeam bathymetry and 2D seismic reflection data at selected grid locations over the Ninetyeast Ridge are summarised below.

- In all grid locations over the Ninetyeast Ridge seismic reflection profile data are interpreted keeping in view of lithostratigraphy of DSDP and ODP drill sites. It is found that the sediment lithology is more or less similar at all the grids. An ash/ volcanic tuff layer of about 100 m overlies the basaltic basement followed by clay and nanno chalks and the top most layer is of nanno fossil/ foram rich ooze. The lithology of the sediment column and ash layer point to the similar environment for the volcanism, sedimentation and sinking history, implying the origin of all the sites of the ridge was at similar subtropic latitudes and later drifted towards north. This observation also substantiates the hotspot origin of the ridge.
- The northern most grid locations, ODP Site 758 and DSDP Site 216 on the ridge, are marked with major compression and strike-slip faults, the middle sites (NER2 and NER3) at 6-8°S latitudes had recorded weak compressions than other two types of faults (normal and strike-slip) and the southern grid locations (DSDP Site 214 and DSDP Site 253) have extensive normal faults with a small amount of strike-slip component. The strike directions also vary in similar pattern. NW-SE to N-S trending active faults are dominant at ODP Site 758 as well as DSDP Site 216, E-W trending at middle sites – NER 2 and NER3 and NE-SW strikes make majority trend at southern sites, DSDP 214 and DSDP 253. These observations are consistent with the stress orientations of the diffused plates with respect to the Ninetyeast Ridge.
- The offset patterns along the faults from basement to seafloor suggest at least one reactivation episode within the limitation of resolution of reflection data. The fault analysis together with broad assumptions of sedimentation rate and average interval velocities indicates that the faults were reactivated at about 8 -10 Ma at grid locations of ODP Site 758, DSDP Site 216, NER2 and NER3 with gradual increasing trend if error bar of at least 2 Myr is neglected. In southern grid locations, DSDP Sites 214 and 253 the fault analysis points to middle Miocene time for reactivation faults, which is continuing with more or less constant magnitude till present.

- The fault analysis further reveals that southern part of the Ninetyeast Ridge was reactivated initially during the middle Miocene, subsequently the northern part of the ridge was reactivated in late Miocene, i.e about 8-10 Ma. This suggest that the diffuse deformation zone in the central Indian Ocean was onset with an extensional activity in a smaller region during the middle Miocene, then in late Miocene time, the diffuse deformation zone has extended to the present geometry with additional compression and strike-slip components.

7.3 Suggestions for future Research

Magnetic anomaly identification can be continued using digital satellite magnetic anomaly (EMAG2) data or any up-coming ship-borne magnetic profile data acquisition for filling the data gaps in the study area especially south of 15°S immediately west to the Ninetyeast Ridge and north of 12°S between the Ninetyeast Ridge and 90°E FZ for comparison with ridge crest radiometric ages, thereby consolidating the hypothesis of ridge jumps and ridge migration.

There seems to be an opportunity with additional seismic reflection data over the Ninetyeast Ridge for further refining the models of the diffuse deformation zones from the commencement of the activity to the present. Seismic data of the region will be useful to correlate the stress effects of on-going seismicity in terms of faults and collectively to determine the dynamics of the diffuse plates of northeastern Indian Ocean.

Bibliography

Acton, G. D., 1999. Apparent polar wander of India since the Cretaceous with implications for regional tectonics and true polar wander, *Mem. Geol. Soc. India, 44, 129–175.*

Allmendinger, R. W., Cardozo, N. C., and Fisher, D., 2012.Structural Geology Algorithms: Vectors & Tensors: *Cambridge, England, Cambridge University Press,* 289 pp.

Anand, S. P., Rajaram, M., Majumdar, T. J., Bhattacharyya, R., 2009. Structure and tectonics of 85°E Ridge from analysis of Geopotential data, *Tectonophysics, 478 (1-2), 100-110.*

Angouluant-Coulon, M. P., Schlich, R., 1994. Mise en evidence d'une nouvelle direction tectonique sur le plateau de Kerguelen, *Comptes Rendus de l'Academie des Sciences Paris Serie. 2, 319, 929-935.*

Antretter, M., Steinberger, B., Heider, F., Soffel, H., 2002. Paleolatitudes of the Kerguelen hot spot: New plaeomagnetic results and dynamic modeling, *Earth Planet. Sci. Lett., 203, 635–650*.

Avraham, B. Z., Bunce, E. T., 1977. Geophysical study of the Chagos-Laccadive Ridge, Indian Ocean, *J. Geophys. Res, 82(8), 1295-1305.*

Bastia, R., Radhakrishna, M., Das, S., Kale, A. S., Catuneanu, O., 2010a. Delineation of the 85°E Ridge and its structure in the Mahanadi Offshore Basin, Eastern Continental Margin (ECMI), from seismic reflection imaging, *Mar. Petro. Geol, 27, 1841-1848.*

Berggren, W. A., Phillips, A., Bertels, Wall, D., 1967. Late Pliocene-Pleistocene stratigraphy in deep sea cores from the south central north Atlantic. *Nature, 216, 253-255.*

Berggren, W. A., Kent, D. V., Flynn, J. J, Van Couvering, J. A., 1985. Cenozoic geochronology, *Geol. Soc. Am., Bull., 96, 1407-1418.*

Besse, J., and V. Courtillot., 2002, Apparent and true polar wander and the geometry of the geomagnetic field over the last 200 Myr, *J. Geophys. Res., 107(B11), 2300.*

Bhattacharya, G. C., Chaubey, A. K., 2001. Western Indian Ocean - A Glimpse of the tectonic scenario. In: Gupta, R. S., Desa, E. (Eds), The Indian Ocean-A perspective. 2, 691-729.

Borissova, I., Coffin, M. F., Charvis, P., Operto, S., 2003. Structure and development of a microcontinent: Elan Bank in the southern Indian Ocean, *Geochemistry, Geophysics, Geosystems, 4(9), 107.*

Bowin, C. O., 1973. Origin of the Ninetyeast Ridge from studies near the Equator, *J. Geophys. Res , 78, 6029-6043.*

Brozena, J. M., White, R., 1990. Ridge jumps and propagations in the South Atlantic Ocean, *Nature, 348, 149–152, doi:10.1038/348149a0.*

Bull, J. M., Scrutton, R. A., 1990. Sediment velocities and deep structure from wide-angle reflection data around Leg 116 sites. In: Cochran, J.R. et al (Eds), *Proc. Ocean Drill Program, Sci. Results, 211-316.*

Bull, J. M., DeMets, C., Krishna, K. S., Sanderson, D. J, Merkouriev. S, 2010, Reconciling plate kinematic and seismic estimates of lithospheric convergence in the central Indian Ocean, *Geology, 38, 4, 307-310.*

Cande, S. C., Kristofferson, Y., 1977. Late Cretaceous magnetic anomalies in the North Atalantic. *Earth Planet. Sci. Lett., 35, 215-224*

Cande, S. C., Mutter, J. C., 1982. A Revised Interpretation of Seafloor Spreading Magnetic Anomalies between Australia and Antarctica, *Earth Planet. Sci. Lett, 58, 151-160.*

Cande, S. C., Kent, D. V., 1995. Revised calibration of the geomagnetic polarity time scale for the Late Cretaceous and Cenozoic, *J. Geophys. Res., 100, 6093–6095, doi:10.1029/94JB03098.*

Cardozo, N., Allmendinger, R. W., 2013. Spherical projections with OSX Stereonet, *Computers &Geosciences,v.51,no.0,p.193-205, doi: 10.1016/j.cageo.2012.07.021*

Chamot-Rooke, N., Jestin, F., de Voogd, B., Phedre working group, 1993. Intraplate shortening in the central Indian ocean determinde from a 2100-km-long north -south deep seismic reflection reflection profile, *Geology, 21, 1043-1046.*

Chaubey, A. K., Ramana, M. V., Sarma, K. V. L. N. S., Krishna, K. S., Murty, G. P. S., Subrahmanyam, V., Mittal, G. S., Drolia, R. K., 1991. Marine geophysical studies over the 85°E Ridge, in: *First International Seminar Exhibition on Exploration Geophysics in Nineteen Nineties, AEG publication, 2, 508-515.*

Chaubey, A. K., Gopala Rao, D., Srinivas, K., Ramprasad, T., Ramana, M. V., Subrahmanyam, V., 2002. Analysis of multichannel seismic reflection, gravity and magnetic data along a regional profile across the central-western continental margin of India. *Mar. Geol., 182, 303-323.*

Cochran, J. R., Stow, D. A. V., et al., 1989. Ocean Drilling Program. In: Proceedings of the Ocean Drilling Program, *Initial Reports Leg 116, College Station, TX, 197- 210.*

Cochran, J. R., 1990. Himalayan uplift, Sealevel, another record of Bengal Fan sedimentation at the ODP Leg 116, Sites. In: Cochran, J. R., D. A. V. Stow et al., (Editors), *Proc. Ocean Drilling Program, Scientific Results, Vol. 116, 397-414.*

Coffin, M. F., Davies, H. L., Haxby, W. F., 1986. Structure of the Kerguelen Plateau province from Seasat altimetry and seismic reflection data, *Nature, 324, 134- 136.*

Coffin, M. F., Munschy, M., Colwell, J. B., Schlich, R., Davies, H. L., Li, Z. G., 1990. Seismic stratigraphy of the Raggatt Basin, southern Kerguelen Plateau: tectonic and paleoceanographic implications, *Geological Society of American Bulletin, 102, 563-579.*

Coffin, M. F., Eldholm, O., 1994. Large igneous provinces: Crustal structure, dimensions, and external consequences, *Review Geophysics, 32, 1-36.*

Coffin, M. F., Frey, F.A. and Wallace, P.J., et al. (Eds)., 2000. Proceedings of the Ocean Drilling Program, Scientific Results, 183. *College Station, TX: Ocean Drilling Program, 101 pp.*

Coffin, M., Pringle, M. S., Duncan, R. A., Gladczenko, T. P., Storey, M., Müller, R. D., Gahagan, L. A., 2002. Kerguelen hotspot magma output since 130 Ma, *Journal of Petroleum, 43, 1121-1139.*

Cox, A., Doell, R. R., Darlymple, G. B., 1963a. Geomagnetic polarity epoches and Pleistocene Geochronology, *Nature, 198, 1049-1051*.

Cox, A., Doell, R. R., Darlymple, G.B., 1963b. Geomagnetic polarity epoches: Seerra Nevada II, *Science, 142, 382-385.*

Cox, A., Doell R. R., Darlymple, G. B., 1964. Reversals of Earth's magnetic field, *Science, 144, 1537-1543.*

Cox, A., Doell R. R., Darlymple, G. B., 1968. Radiometric time scale for geomagnetic reversals, *Geol. Soc. London, Quart. J, 124, 53-66.*

Curray, J. R., Moore, D. G., 1971. Growth of the Bengal deep sea fan and denudation in the Himalayas, *Geological Society of America Bulletin, 82, 563-573.*

Curray, J. R., Moore, G. D., 1974. Sedimentary and tectonic processes in the Bengal Deep Sea Fan and Geosyncline. In: Burke, C.A., Drake, C.L. (Eds.), *The Geology of Continental Margins, Springer-Verlag, New York, 617-627.*

Curray, J. R., Emmel, F. J., Moore, D. G., Russel, W. R., 1982. Structure, tectonics and geological history of the north-eastern Indian Ocean in *The Ocean Basins and Margins, Vol. 6, The Indian Ocean, edited by A.E. Nairn and F.G. Stehli, Plenum, New York, 399-450.*

Curray, J. R., Munasinghe, T., 1991. Origin of the Rajmahal Traps and the 85° E Ridge: preliminary reconstructions of the trace of the Crozet hotspot. *Geology 19, 1237-1240.*

Curray, J. R., 1994. Sediment volume and mass beneath the Bay of Bengal. *Earth Planet. Sci. Lett., 125, 371-383.*

Curray J. R., Emmel, F.J., Moore, D.G., 2003. The Bengal Fan: morphology, geometry, stratigraphy, history and processes. *Mar. Petrol. Geol., 19, 1191-1223.*

Delescluse, M., and N. Chamot-Rooke (2007), Instantaneous deformation and kinematics of the India-Australia plate, *Geophys.J.Int.,168, 818–842.*

Deplus, C., Diament, M., Hebert, H., Bertrand, G., Dominguez, S., Dubois, J., Malod, J., Patriat, P., Pontoise, B., Sibilla, J. J., 1998. Direct evidence of active deformation in the eastern Indian oceanic plate. *Geology 26, 131–134.*

Desa, M., Ramana, M. V., Ramprasad, T., 2009. Evolution of the Late Cretaceous crust in the equatorial region of the northern Indian Ocean and its implication in understanding the plate kinematics, *Geophys. J. Int., 177, 1265–1278.*

Dietz, R.S., 1961. Continent and ocean basin evolution by spreading of the sea floor. *Nature, 190, 854-857.*

Dietz, R. S., Holden, J. C., 1970. Reconstruction of Pangaea: Breakup and dispersion of continents, Permian to present, *J. Geophys. Res., 75, 4939-4956.*

Detrick, R. S. Watts, A. B., 1979. An Analysis of Isostasy in the World's Oceans 3, Aseismic Ridges. *J. Geophys. Res. 84, 3637-3653.*

Doell R. R., Darlymple, G.B., Cox, A., 1966. Geomagnetic polarity epoches: Seerra Nevada Data, *J. Geophys. Res, 71, 531-541.*

Duncan, R. A., 1978. Geochronology of basalts from the Ninetyeast Ridge and continental dispersion in the eastern Indian Ocean, *J. Volcanol. Geotherm. Res., 4, 283–305.*

Duncan, R. A., 1981. Hotspots in the southern oceans-an absolute frame of reference for motion of the Gondwana continents, *Tectonophysics, 74, 29-42.*

Duncan, R. A., 1990. The volcanic record of the Réunion Hotspot. In: Proceedings ODP, *Science Results, 115, 3-10.*

Duncan, R. A., 1991. The age distribution of volcanism along aseismic ridges in the Eastern Indian Ocean. *In: Weissel, J. K., et al. (Ed.), Proc. ODP, Sci. Res. Leg. : Ocean Drilling Program, 121. College Station, Texas, 507-517.*

Duncan, R. A., Storey, M., 1992. The life cycle of Indian Ocean hotspots. In:Duncan, R. A., Rea, D. K., Kidd, R. B., von Rad, U. & Weissel, J. K. (eds) Synthesis of Results from Scientific Drilling in the Indian Ocean. *Geophysical Monograph, American Geophysical Union 70, 91-103.*

Ewing, M., Worzel, J. L., Beall, A. O., Berggren, W. A. Jr., Bukry, D., Burk, C. A., Fischer, A. G., Pessagno, E. A, Jr., 1969. Initial Reports of the Deep Sea Drilling Project, Volume I. Washington (U. S. Government Printing Office).

Fisher, R. L., Sclater, J. G., McKenzie, D. P., 1971. Evolution of the central Indian Ridge, western Indian Ocean, *Geological Society American Bulletin, 82, 553- 562.*

Fisher, R. L., Sclater, J. G., 1974. Evolution of the East: Central Indian Ocean, with Emphasis on the Tectonic Setting of the Ninetyeast Ridge. *Geological Society of America Bulletin 01/1974; 85(5).*

Fisher, R.L., Jantsch, M.Z., Corner, R.L., 1982. General bathymetric chart of the Oceans GEBCO sheet 5.09, *Canadian Hydrographic Service, Ottawa.*

Francis, T. J. G., Shor, G. G., 1966. Seismic refraction measurements in the northwest Indian Ocean, *J. Geophys. Res., 71, 427-449.*

Francis, T. J. G., Raitt, R. W., 1967. Seismic refraction measurements in the southern Indian Ocean, *J. Geophys. Res., 72, 3015-3041*.

Frey, F. A., Dickey, J. S., Jr.,Thompson, G., Bryan, W. B., 1977. Eastern Indian Ocean DSDP sites: correlations between petrography, geochemistry and tectonic setting. *In Heirtzler, J. R., and Sclater, J. G. (Eds.), A Synthesis of Deep Sea Drilling in the Indian Ocean: Washington (U.S. Govt. Printing Office), 189-257.*

Frey, F. A., Sung, C.M., 1974. Geochemical results for basalts from sites 253 and 254. In: T. A. Davies and B. P. Luyendyk (Editors) *Initial Reports of the Deep Sea Drilling Project, 26. U.S. Gov. Print. Off., Washington, D. C., pp. 567--573.*

Frey, F. A., Coffin, M. F., Wallace, P. J., Weis, D., Zhao, X., Wise, S. W., Wähnert, V., Teagle, D. A. H., Saccocia, P. J., Reusch, D. N., Pringle, M. S., Nicolaysen, K. E., Neal, C. R., Müller, R. D., Moore, C. L., Mahoney, J. J., Keszthelyi, L., Inokuchi, H., Duncan, R. A., Delius, H., Damuth, J. E., Damasceno, D., Coxall, H. K., Borre, M. K., Boehm, F., Barling, J., Arndt, N. T., Antretter, M., 2000. Origin and evolution of a submarine large igneous province: The Kerguelen Plateau and Broken Ridge, southern Indian Ocean, *Earth Planet. Sci. Lett, 176, 73-89.*

Fritsch, B., Schlich, R., Munschy, M., Fezga, F., Coffin, M. F., 1992. Evolution of the southern Kerguelen Plateau deduced from seismic stratigraphic studies and drilling at sites 748 and 750, *in: S.W. Wise Jr., R. Schlich, et al., Proceedings Ocean Drilling Program, Scientific Results, 120, Ocean Drill. Prog., College Station, TX, 895-906.*

Fu, L. L., Chelton, D. B., Zlotnicki, V., 1988. Satellite altimetry: Observing ocean variability from space, Oceanography, 1(2), 4-11.Gaina, C., Müller, R. D., Brown, B., Ishihara, T., 2007. Breakup and early seafloor spreading between Indian and Antarctica, *Geophysics Journal International, 170, 151-169.*

Geller, C. A., Weissel, J. K., and Anderson, R. N., 1983. Heat transfer and intraplate deformation in the central Indian Ocean, *Geophys. Res., 88:1018-1032.*

Gladczenko, T. P., Coffin, M. F., Eldholm, O., 1997. Crustal structure of the Ontong Java Plateau: Modeling of new gravity and existing seismic data, *J. Geophys. Res, 102, 22,711-22,729.*

Gopala Rao, D., Krishna, K. S., Sar, D., 1997. Crustal evolution and sedimentation history of the Bay of Bengal since the Cretaceous, *J. Geophys. Res, 102, 17,747-17,768.*

Gopala Rao, D., Bhartacharya, G. C., Ramana, M. V., Subrahmanyam, V., Ramprasad, T., Krishna, K. S., Chaubey, A. K., Murty, G. P. S., Srinivas, K., Desa, M., Reddy, S. I., Ashalata, B., Subrahmanyam, C., Mittal, G. S., Drolia, R. K., Rai, S. K., Ghosh, S. K., Singh, R. N., Majumdar, R., 1994. Analysis of multichannel seismic reflection and magnetic data along 13°N latitude across the Bay of Bengal, *Marine Geophysical Research, 16, 225-236.*

Gordon, R. G., DeMets, C., Royer, J.Y., 1998. Evidence for long-term diffuse deformation of the lithosphere of the equatorial Indian Ocean, *Nature, 395, 370–374.*

Gradstein, F. M., Agterberg, F. P., Ogg, J. G., Hardenbol, J., van Veen, P., Thierry, J., Huang, Z., 1994. A Mesozoic timescale, *J. Geophys. Res, 99, 24 051-24 074.*

Grevemeyer, I., Flueh, E. R., 2000. Crustal—Underplating and its implications for subsidence and state of isostasy along the Ninetyeast Ridge hotspot trail, *Geophys. J. Int., 142, 643 – 649.*

Hardarson, B. S., Fitton, J. G., Ellam, R. M., Pringle M. S.,1997. Rift relocation—A geochemical and geochronological investigation of a paleorift in northwest Iceland, *Earth Planet. Sci. Lett., 153, 181–196, doi:10.1016/S0012-821X(97)00145-3.*

Haxby, W. F., Karner, D., LaBrecque, J. L., Weissel, J. K., 1983. Digital imagesof combined oceanic and continental datasets and their use in tectonic studies, *EosTrans.AGU, 64 (52), 995-1004.*

Hays, J. D., Opdyke, N.D., 1967. Antarctic radiolaria, magnetic reversal and climate change, *Science, 158, 1001-1010.*

He ´bert, H., Deplus, C., Diament, M., Origin of the 90 E ridge and Investigator ridge deduced from the analysis of bathymetric and gravimetric data, *C. R. Acad. Sci., Ser. II, 323, 105–112, 1996.*

Heezen, B. C., Ewing, M., Muller, E. T., 1953. Trans-Atlantic profile of total magnetic intensity and topography, Dakar to Barbados, *Deep-Sea Res. 1, 25-33.*

Heezen, B. C., Tharp, M., 1964. Physiographic diagram of the Indian Ocean, map, *Geol. Soc. America. Boulder, Colorado.*

Heirtzler, J. R., Dickson, G. O., Herron E. M., Pitman W. C., LePichon, III and X, 1968. Marine magnetic anamolies , geomagnetic field reversal, and motions of the ocean floor and continents, *J.Geophys. Res., 73, 2119-2136.*

Hekinian, R., 1974. Petrology of the Ninety East Ridge (Indian OCean) Compared to other Aseimsic Ridges, *Contr.Mineral. and Petrol.43, 125-147.*

Hess, H. H., 1962. History of the Ocean Basins. In: Engel, A. E. G, James, H. L., Leonard B. F. (Eds), *Petrologic studies. Geol. Soc. Am., 559-620.*

Houtz, R. E., Hayes, D. E., Mark, R. G., 1977. Kerguelen Plateau bathymetry sediment distribution and crustal structure, *Marine Geology, 25, 95-130.*

Johnson, B. D., Powell, C. McA., Veevers, J. J., 1976. Spreading history of the eastern Indian Ocean and greater India's northward flight from Antarctica and Australia. *Geol. Soc. Am. Bull., 87:1560-1566.*

Keen, M. J., 1963. Magnetic anamolies over the Mid-Atlantic Ridge, *Nature, 197, 888-890.*

Kent, R. W., Storey, M., Saunders, A. D., 1992. Large igneous provinces: sites of plume impact or plume incubation, *Geology, 20, 891–894.*

Klitgord, K. D., Huestis, S. P., Mudie, J. D., Parker, R. L., 1975. An analysis of near-bottom magnetic anamolies : Seafloor spreading and magnetised layer, *Geophys. J. Roy.Astron. Soc., 43, 387-424.*

Klootwijk, C. T., Jeff, S. G., Peirce, J. W., Smith, G. M., 1991. Constraints on the Indian-Asia convergence: Paleomagnetic results from Ninetyeast Ridge, *Proc. Ocean Drill. Program Sci. Results, 121, 777–882.*

Klootwijk, C. T., Gee, J. S., Peirce, J. W., Smith, G. M., McFadden, P. L., 1992. An early India–Asia contact: paleomagnetic constraints from Ninetyeast Ridge, ODP Leg 121, *Geology, 20, 395-398.*

Könnecke, L. K., Coffin, M. F., Charvis, P., Symonds, P. A., Ramsay, D., Bernadel, G., 1997. Crustal structure of Elan Bank, Kerguelen Plateau, EOS Transactions, *American Geophysical Union, 76, F712.*

Könnecke, L., Coffin, M. F., 1994. Tectonics of the Kerguelen Plateau, Southern Indian Ocean, EOS Transactions, *American Geophysical Union, 75:154.*

Krishna, K. S., Gopala Rao, D., Ramana, M. V., Subrahmanyam, V., Sarma, K. V. L. N. S., Pilipenko, A. I., Shcherbakov, V. S., Radhakrishna Murthy, I. V., 1995. Tectonic model for the evolution of oceanic crust in the northeastern Indian Ocean from the Late Cretaceous to the Early Tertiary, *J. Geophys. Res., 100, 20,011-20,024.*

Krishna, K. S., Ramana, M. V., Gopala Rao, D., Murthy, K. S. R., Malleswara Rao, M. M., Subrahmanyam, V., Sarma, K. V. L. N. S., 1998. Periodic deformation of oceanic crust in the central Indian Ocean. *J. Geophy. Res., 103, 17,859-17,875.*

Krishna, K. S., Gopala Rao, D., Subba Raju, L. V., Chaubey, A. K., Shcherbakov, V. S., Pilipenko, A. I., Radhakrishna Murthy, I. V., 1999. Paleocene on-axis hot spot volcanism along the Ninetyeast Ridge: An interaction between the Kerguelen hot spot and the Wharton spreading center, Proc. Indian Acad. Sci. *Earth Planet. Sci., 108, 255–267.*

Krishna, K. S., Gopala Rao, D., 2000. Abandoned Paleocene spreading center in the northeastern Indian Ocean: Evidence from magnetic and seismic reflection data, *Marine Geology, 162, 215-224*

Krishna, K. S., Bull, J. M., Scrutton, R. A., 2001a. Evidence for multiphase folding of the central Indian Ocean lithosphere, *Geology, 29, 715-788.*

Krishna, K. S., Neprochnov, Y. P., Gopala Rao, D., Grinko, B. N., 2001b. Crustal structure and tectonics of the Ninetyeast Ridge from seismic and gravity studies, *Tectonics 20, 416-433.*

Krishna, K. S., 2003. Structure and evolution of the Afanasy Nikitin seamount, buried hills and 85°E Ridge in the northeastern Indian Ocean. *Earth Planet. Sci. Lett., 209, 379-394.*

Krishna, K. S., Michael, L., Bhattacharyya, R., Majumdar, T. J., 2009a. Geoid and gravity anomaly data of conjugate regions of Bay of Bengal and Enderby

Basin: New constraints on breakup and early spreading, *J. Geophys. Res., vol.114(3); 21 pp.*

Krishna, K. S., Bull, J. M., Scrutton, R. A., 2009b. Early (pre-8 Ma) fault activity and temporal strain accumulation in the central Indian Ocean, *Geology, 37, 3, 227-230.*

Krishna, K. S., Abraham, H., Sager, W. W., Pringle, M., Frey, F. A., Gopala Rao, D., Levchenko, O. V., 2012. Tectonics of the Ninetyeast Ridge derived from the spreading records of the contiguous oceanic basins and age constraints of the ridge, *J. Geophys. Res. 117.*

Krishna, K. S, 2014. Two decades of Indian research on Ninetyeast Ridge reveal how seafloor spreading and mantle plume activities have shaped eastern Indian Ocean, *Curr. Sci.: 106(9); 2014; 1178-1179*

LaBrecque, J. L., Kent, D. V., Cande, S. C., 1977. Revised magentic polarity time scale for Late Cretaceoes and Cenozoic time, *Geology, 5, 330-335.*

Larson, R. L., Pitman, W. C., 1972. Worldwide correlation of Mesozoic magnetic anomalies and its implications. *Bulletin of Geological society of America, 83, 3645-3662.*

Laughton, A. S., Matthews, D. H., Fisher, R. L., 1970. The structure of the Indian Ocean. *In Maxwell, A. E. (Ed.), The Sea (vol. 4), New York (WileyInterscience), 543-586.*

Le Pichon, X., Heirtzler, J., 1968. Magnetic anomalies in the Indian Ocean and seafloor spreading, *J. Geophy. Res., 73, 2101-2117.*

Liu, C. S., Sandwell, D. T., Curray, J. F., 1982. The negative gravity field over the 85° E Ridge, *J. Geophy. Res., 87, 7673-7686.*

Liu, C. S., Curray, J. R., McDonald, J. M., 1983. New constraints on the tectonic evolution of the Eastern Indian Ocean, *Earth Planet. Sci. Lett.*, 65, 331-342. doi:10.1016/0012-821X(83)90171-1.

Lowrie, W., 2007. Fundamentals of Geophysics. 381p, Second Edtn., Cambridge University Press, Cambridge, United Kingdom.

Luyendyk, B. P., and Davies, T. A., 1974. Results of DSDP Leg 26 and the geologic history of the Southern Indian Ocean. *In Davies, T. A., Luyendyk, B. P., et al., Init. Repts. DSDP, 26: Washington (U.S. Govt. Printing Office), 909-943.*

Luyendyk, B. P., Rennick, W., 1977. Tectonic history of aseismic ridges in the eastern Indian Ocean. *Geol. Soc. Am. Bull., 88:1347- 1356.*

Mahoney, J. L., Macdougall, J. D., Lugmair, G. W., and Gopalan, K., 1983. Kerguelen hot-spot source for Rajmahal Traps and Ninetyeast Ridge, *Nature, 303:385-389.*

Maia, M., 2011. Building of the Amtersdam–St. Paul plateau: A 10 Myr history of a ridge-hot spot interaction and variations in the strength of the hot spot source, *J. Geophys. Res.*

McDougall, I., Chamlaun , F. H., 1966. Geomagnetic polarity scale of time, *Nature, 212, 1415-1418.*

McKenzie, D. P., Sclater, J. G., 1971. The evolution of the Indian Ocean since the Late Cretaceous, *Geophysical Journal of the Royal Astronomical Society, 25, 437- 528.*

Mendel, V., Munschy, V., Sauter, D., 2005. MODMAG, a MATLAB program to model marine magnetic anomalies, *Computers & Geosciences 31, 589–597*

Michael, L., Krishna, K. S., 2011. Dating of the 85°E Ridge (northeastern Indian Ocean) using marine magnetic anomalies. *Curr. Sci., 100, 1314-1322.*

Mishra, D. C., 1991. Magnetic crust in the Bay of Bengal, *Marine Geology, 99, 257- 261.*

Mittelstaedt, E., Ito, G., Behn, M. D., 2008. Mid-ocean ridge jumps associated with hot spot magmatism, *Earth Planet. Sci. Lett., 266, 256–270*

Mittelstaedt, E., Ito, G., Van Humen, J., 2011. Repeat ridge jumps associated with plume-ridge interaction, and ridge migration, *J. Geophys. Res., 116, B01102*

Moore, D. G., Curray, J. R., Raitt, R. W., Emmel, F. J., 1974. Stratigraphic-seismic section correlations and implications to Bengal Fan history, *Initial Reports Deep Sea Drilling Project, 22, 403-412.*

Morgan, W. J., 1971. Convection Plumes in the Lower Mantle. *Nature, 230, 42-43.*

Morgan W. J., 1972. Plate motions and deep convection. *Geol. Soc. Am. Mem., 132, 7-22.*

Morgan, W. J., 1981. Hotspot tracks and the opening of the Atlantic and Indian Oceans. In: C. Emiliani (Ed.), *The Sea (Vol. 7): The Oceanic Lithosphere, Wiley-Interscience, NewYork, 443-487.*

Mukhopadhyay, M., Krishna, M. R., 1991. Gravity field and deep structure of the Bengal fan and its surrounding continental margins, northeast Indian Ocean, *Tectonophysics, 186, 365-386.*

Müller, R. D., Royer, J. Y., Lawyer, L. A., 1993. Revised plate motions relative to the hotspots from combined Atlantic and Indian Ocean hotspot tracks. *Geology, 21, 275-278.*

Naini, B. R., Talwani, M., 1983. Structural framework and the evolutionary history of the continental margin of western India, In: Watkins, J. S., Drake, C. L. (Eds), *Studies in Continental Margin Geology, AAPG Mem., 34 167-191.*

Narain, H., Kaila, K. L., Verma, R. K., 1968. Continental margins of India, *Canadian Journal of Earth Sciences, 5, 4, 1051-1065.*

Nicolaysen, K., Bowring, S., Frey, F., Weis, D., Ingle, S., Pringle, M. S., Coffin, M. F., 2001. Provenance of Proterozoic garnet-biotite gneiss recovered from Elan Bank, Kerguelen Plateau, southern Indian Ocean, *Geology, 29, 235-238, doi:10.1130/0091-7613(2001)029<0235: POPGBG>2.0.CO;2.*

Nogi, Y., Seama, N., Isezaki, N., Fukuda, Y., 1996. Magnetic anomaly lineations and fracture zones deduced from vector magnetic anomalies in the West Enderby Basin, in Storey, B. C., King, E.C., and Livermore R. A. (Eds.), Weddell Sea Tectonics and Gondwana Break-up, *Geological Society Special Publication, 108, 265-273, doi: 10.1144/GSL.SP.1996.108.01.19.*

Norton, I. O., Sclater, J. G., 1979. A model for the evolution of the Indian Ocean and the breakup of Gondwanaland, *J. Geophys. Res.*, 84, 6803- 6830.

O'Neill, C., Müller, D., Steinberger, B., 2003. Geodynamic implications of moving Indian Ocean hot spots, *Earth Planet. Sci. Lett., 215, 151–168*

Patriat, P., 1987. Reconstitution de l'Evolution du Systeme de Dorsales de l'Ocean Indien par les Methods dela Cinematique des Plaques. *Territoires des Terres Australes et Antarctique.*

Patriat, P., Segoufin, J., 1988, Reconstruction of the central Indian Ocean, *Tectonophysics, 155, 211–234*

Peirce, J. W., 1978. The northward motion of India since the Late Cretaceous, *Geophys. J. R. Astron. Soc., 52, 277–311,*

Peirce, J. W., Weissel, J., et al., 1989. Site 758 Proceedings of the Ocean Drilling Program, *Initial Reports, vol. 121, 1000 pp., Ocean Drill. Program, College Station, Tex.359-453.*

Petroy, D. E., Wiens, D. A., 1989. Historical seismicity and implications for diffuse plate convergence in the northeast Indian Ocean, *J. Geophys. Res., 94, 12,301-12,319.*

Pilipenko, A. I., 1996. Fracture zones of the Ninetyeast Ridge area, Indian Ocean, *Geotectonics, Engl. Transl., 30, 441–451.*

Powell, C. M., Roots, S. R., Veevers, J. J., 1988. Pre-breakup continental extension in east Gondwanaland and the early opening of the eastern Indian Ocean, *Tectonophysics, 155, 261-283, doi:10.1016/ 0040-1951(88)90269-7.*

Pringle, M. S., Frey, F. A., Mervine, E. M., Sager, W. W., 2007. New Ar/Ar ages from the Ninetyeast Ridge, Indian Ocean: Beginning of a robust Indo-Atlantic hot spot reference frame, Eos Trans. *AGU, 88(52), Fall Meet. Suppl., Abstract U13A-0871.*

Pringle, M. S., Frey, F. A., Mervine, E. M., 2008. A simple linear age progression for the Ninetyeast Ridge, Indian Ocean: New constraints on Indian plate motion and hot spot dynamics, Eos Trans. *AGU, 89(53), Fall Meet. Suppl., Abstract T54B-03.*

Ramana, M. V., Nair, R. R., Sarma K. V. L. N. S., Ramprasad, T., Krishna, K. S., Subrahmanyam, V., D'Cruz, M., Subrahmanyam, C., Paul, J.,Subrahmany-am, A. S. Chandra Sekhar, D. V., 1994. Mesozoic anomalies in the Bay of Bengal, *Earth Planet. Sci. Lett., 121, 469-475.*

Ramana, M. V., Subrahmanyam, V., Chaubey, A. K., Ramprasad, T., Sarma, K. V. L. N. S., Krishna, K. S., Maria Desa., Murthy, G. P. S., 1997. Structure and origin of the 85°E Ridge, *J. Geophys. Res., 102, 1799-1801.*

Ramana, M. V., Ramprasad, T., Desa, M., 2001. Seafloor spreading magnetic anomalies in the Enderby Basin, East Antarctica, *Earth Planet. Sci. Lett., 191, 241-255.*

Richards, M. A., Duncan, R. A., Courtillot, V. E., 1989. Flood basalts and hot spot tracks: plume heads and tails, *Science, 246, 103-107.*

Rotstein, Y., Schlich, R., Munschy, M., Coffin, M. F., 1992. Structure and tectonic history of the southern Kerguelen Plateau (Indian Ocean) deduced from seismic reflection data, *Tectonics, 11, 1332-1347.*

Rotstein, Y., Munschy, M., Bernard, A., 2001. The Kerguelen province revisited: additional constraints on the development of the southeast Indian Ocean. *Mar. Geophys. Res., 22, 81-100.*

Royer, J. Y., Schlich, R., 1988. The Southeast Indian Ridge between the Rodriguez Triple Junction and the Amsterdam and Saint-Paul Islands: detailed kinematics for the past 20 m.y, *J. Geophys. Res., 93:13524-13550.*

Royer, J. Y., Sclater, J. G., Sandwell, D. T., 1989. A preliminary tectonic fabric chart of the Indian Ocean, Proceedings in Indian Academy Science, *Earth Planetary Science, 98, 7-24.*

Royer, J. Y., Sandwell, D. T., 1989. Evolution of the eastern Indian Ocean since the Late Cretaceous: constraints from Geosat Altimetry, *J. Geophys. Res., 94, 13755-13782.*

Royer, J. Y., Peirce, J. W., Weissel, J. K., 1991. Tectonic constraints on the hotspot formation of Ninetyeast Ridge: *In Proceedings of the Ocean Drilling Program Scientific Results, College Station, Texas, Ocean Drilling Program, 121, 763- 776.*

Royer, J. Y., Sclater, J. G., Sandwell, D. T., Cande, S.C., Schlich, R., Munschy, M., Dyment, J., Fisher, R. L., Muller, R. D., Coffin, M. F., Patriat, P. and Bergh, H., 1992. Indian Ocean plate reconstructions since the Late Jurassic. In:

Duncan, R. A., Rea, D. K., Kidd, R. B., Von Rad, U., Weissel, J. K. (Eds.), Synthesis of Results from Scientific Drilling in the Indian Ocean. *AGU Geophysical Monograph, 70, 471-475, Washington DC, USA*

Royer, J. Y., Coffin, M. F., 1992. Jurassic to Eocene plate tectonic reconstructions in the Kerguelen Plateau region, in: W. S. Wise, R. Schlich, et al., Proc. Ocean Drill. Prog., *Scientific Results 120, College Station, TX, 1992, pp. 917-928.*

Royer, J. Y., Gordon, R. G., 1997. The Motion and Boundary between the Capricorn and Australian Plates, *Science, 277, 1268-1274.*

Royer, J. Y., Chaubey, A. K., Dyment, J., Bhattacharya, G. C., Srinivas, K., Yatheesh, V., Ramprasad, T., 2002. Paleogene plate tectonic evolution of the Arabian and Eastern Somali basins. In: Clift, P.D., Kroon, D., Gaedicke, C., Craig, J. (Eds.), The Tectonic and Climatic Evolution of the Arabian Sea Region, 195. *Geological Society, London, 7-23.*

Ryan, W. B. F., Cita, M. B., Rawson, M., Burckle, L.H., Saito, T., 1974. A paleomagnetic assignment of Neogene stage boundaries and the development of isochronous datum planes between the Mediterranean, the pacific and Indian Oceans in order to investigate the response of the world oceans to the world oceans to the Mediterraen " Salinity crises". *Rivista Italiana Paleontogia, 80, 631-688.*

Sager, W.W. et al., 2007. Cruise Report KNOX06RR R/V Roger Revelle, pp. 1-82. (http://earthref.org/erda/1172).

Sager, W. W., Paul, C. F., Krishna, K. S., Pringle, M., Eisin, A. E., Frey, F. A., Gopala Rao, D., Levchenko, O., 2010. Large fault fabric of the Ninetyeast Ridge implies near-spreading ridge formation, *Geophys. Res. Lett., 37, L17304.*

Sager, W. W., Bull, J. M., Krishna, K. S., 2013. Active faulting on the Ninetyeast Ridge and its relation to deformation of the Indo-Australian Plate, *J. Geophys. Res. Solid Earth, 118, 4648–4668.*

Sandwell, D. T., Smith, W. H. F., 1997. Marine gravity from Geosat and ERS-1 satellite altimetry, *J. Geophys. Res., 102, 10,039–10,054.*

Sandwell, D. T., Smith, W. H. F., 2009. Global marine gravity from retracked Geosat and ERS-1 altimetry: Ridge segmentation versus spreading rate, *J. Geophys. Res. , VOL. 114, B01411*.

Schaming, M., Rotstein, Y., 1990. Basement reflectors in the Kerguelen Plateau, south Indian Ocean: Implications for the structure and early history of the plateau, *Geological Society of America Bulletin, 102, 580-592.*

Schlich, R., Patriat, P., 1971. Anomalies magnétiques de la branche Est de la dorsale médio-indienne entre les iles Amsterdam et Kerguelen. *C.R. Acad. Sci. Ser. 2, 272, 700-703.*

Schlich, R., 1975. Structure et âge de l'océan Indien occidental, *Mem. Hors-Ser. Soc. Geol. Fr, 6, 1-103.*

Schlich, R., 1982. The Indian Ocean: Aseismic ridges, spreading centers, and oceanic basins, In: Nairn, A.E.M. Stehli, F.G (Eds), *The Ocean Basins and Margins, vol. 6, The Indian Ocean, 51-148, Plenum, New York.*

Schlich, R., Munschy, M., Boulanger, D., Cantin, B., Coffin, M.F., Durand, J., Humler, E., Li, Z.G., Savary, J., Schaming, M., Tissot, J.D., 1988. Résultats préliminaires de la campagne océanographique de sismique reflexion multitraces MD47 dans le domaine sud du plateau de Kerguelen. *C. R. Acad. Sci. Ser. 2, 305,635-642.*

Sclater, J. G., Fisher, R. L., 1974. Evolution of the East Central Indian Ocean, with Emphasis on the Tectonic Setting of the Ninety East Ridge. *Geol. Soc. Am. Bull., 86, 683-702.*

Sclater, J. G., Luyendyk, B. P., Meinke, L., 1976. Magnetic lineations in the southern part of the Central Indian Basin. *Geol. Soc. Am. Bull., 87:371-378.*

Small, C., 1995.Observation of ridge–hot spot interactions in the Southern Ocean, *J. Geophys. Res., 100, 17,931–17,946.*

Smith, W. H. F., Sandwell, D. T., 1997. Global sea floor topography from satellite altimetry and ship depth soundings, *Science, 277(5334), 1956–1962.*

Sreejith, K. M., Radhkrishna, M., Krishna, K. S., Majumdar, T. J., 2011. Development of negative gravity anaomaly of 85 degrees E Ridge, northeastern Indian Ocean - A process oriented modelling approach, *J. Earth Syst. Sci.: 120(4); 605-615*

Sreejith, K.M., Krishna, K.S., 2013. Spatial variations in isostatic compensation mechanisms of the Ninetyeast Ridge and their tectonic significance, *J. Geophys. Res. B: Solid Earth, 118 (10), 5165-5184*

Sreejith, K. M., Krishna, K. S., 2015. Magma production rate along the Ninetyeast Ridge and its relationship to Indian plate motion and Kerguelen hot spot activity, *Geophysical Research Letters 42 (4), 1105-1112.*

Stagg, H. M. J., Colwell, J. B., Direen, N. G., O'Brien, P. E., Bernardel, G., Borissova, I., Brown, B. J., Ishihara, T., 2004. Geology of the continental margin of Enderby and MacRobertson Lands, East Antarctica: insights from a Regional data set, *Marine Geophysical Research, 25, 183-219.*

Stocks, C., 1960. Zur Bodengestlat des Indischen Ozeans Erdkunde, Arch, furwiss, *Geogr., 14, 161-170.*

Subrahmanyam, C., Thakur, N. K., Gangadhara Rao, T., Khanna, R., Ramana, M.V, Subrahmanyam, V., 1999. Tectonics of the Bay of Bengal: new insights from satellitegravity and ship-borne geophysical data. *Earth Planet. Sci. Lett., 171, 237-251.*

Subrahmanyam, C., Gireesh, R., Chand, S., Kamesh Raju, K. A., Gopala Rao, D., 2008. Geophysical characteristics of the Ninetyeast Ridge-Andaman island arc/trench convergent zone. *Earth Planet. Sci. Lett., 266, 29-45.*

Thompson, G., Bryan, W. B., Frey, F. A., Sung, C. M., 1974. Petrology and geochemistry of baslts and related rocks from Sites 214, 215, 216, DSDP Leg 22, Indian Ocean: In Initial Reports of the Deep Sea Drilling Project (eds) CC Von der Borch et al (Washington D C, U.S. Goverment printing office) 22 459-468.

Tinnon, M. J., Holt, W. E., Haines, A. J., 1995. Velocity gradients in the northern Indian Ocean inferred from earthquake moment tensors and relative plate velocities, *J. Geophys. Res., 100, 24,315–24,329.*

Tiwari, V. M., Diament, M., Singh, S. C., 2003. Analysis of satellite gravity and bathymetry data over Ninety-East Ridge: Variation in the compensation mechanism and implication for emplacement process, *J. Geophys. Res., 108(B2), 2109, doi:10.1029/2000JB000047.*

Turcotte, D. L., Schubert, G., 2002. Geodynamics. 456p, Cambridge University Press, Cambridge, United Kingdom.

Udintsev, G. B., 1975. Geological-Geophysical Atlas of the Indian Ocean, *151p, Pergamon, New York.*

Veevers, J. J., Jones, J. G., Talent, J. A., 1971. Indo-Australian stratigraphy and the configuration and dispersal of Gondwanaland. *Nature, 229:383-388.*

Veevers, J. J., 1986. Breakup of Australia and Antarctica estimated as mid-Cretaceous (95+5 Ma) from magnetic and seismic data at the continental margin, *Earth and Planetary Science Letters, 77, 91-99.*

Veevers, J. J., 2009. Palinspastic (pre-rift and -drift) fit of India and conjugate Antarctica and geological connections across the suture, *Gondwana Research 16, 90-108.*

Vine, F. J., Matthews, D. H., 1963. Magnetic anomalies over oceanic ridges. *Nature, 199, 947-949.*

Vine, F. J., 1966. Spreading of the ocean floor: new evidence, Science, 154, 1405-1415.

Vine, F. J., 1968. Magnetic anomalies associated with mid ocean Ridges. In: Phinnet , R. A., (Editor), The history of the earth's crust. *Pericenton University PRess, 73-89.*

Von der Borch, C. C., et al., 1972, Site 253, *Initial Rep. Deep Sea Drill. Proj., 26, 153–231*.

Von der Borch, C. C., et al., 1974a, Site 213, *Initial Rep. Deep Sea Drill. Proj., 22, 85–118*

Von der Borch, C. C., et al., 1974b, Site 214, *Initial Rep. Deep Sea Drill. Proj., 22, 119–192*

Von der Borch, C. C., et al. ,1974c, Site 215, *Initial Rep. Deep Sea Drill. Proj., 22, 193–211*.

Von der Borch, C. C., et al., 1974d, Site 216, *Initial Rep. Deep Sea Drill. Proj., 22, 213–265.*

Watts, A. B., Bodine, J. H., Ribe, N. M., 1980. Observations of flexure and geological evolution of the Pacific Ocean basin, *Nature, 283, 532–537.*

Weis, D., Frey, F. A., 1991. Isotope geochemistry of Ninetyeast Ridge basement basalts: SR, ND, and PB evidence for involvement of the Kerguelen hotspot: In *Proceedings of the Ocean Drilling Program, Scientific Results, College Station, Texas, Ocean Drilling Program, 121, 591-610.*

Weis, D., Ingle, S., Damasceno, D., Frey, F. A., Nicolaysen, K., Barling, J., 2001. Origin of continental components in Indian Ocean basalts: evidence from Elan Bank (Kerguelen Plateau, ODP Leg 183, Site 1137), *Geology, 29, 147-150.*

Weis, D., Mennessier, J.-P., Gautier, I., Cantagrel, J.-M., and Vidal, P., 1987b. Géochimie isotopique des Terres Australes (Archipel des iles Kerguelen). Actes Coll. Recherche Française dans les Terres Australes. *Strasbourg (CNFRA), 357-368.*

Weissel J., Karner, G., 1989. Flexural Uplift of Rift Flanks Due to Mechanical Unloading of the Lithosphere during extension. *J. Geophys., Res., 94, B10, doi: 10.1029/JB094iB10p13919.*

Weissel, J. K., Anderson, R. N., Geller, C. A., 1980. Deformation of the Indo-Australian plate. *Nature, 287:284-291.*

Wessel, P., Smith, W. H. F., 1995. New version of generic mapping tools, Eos Trans. AGU Electron. Suppl., Aug.15.

White, R., McKenzie, D., 1989. Magmatism at rift zones - The generation of volcanic continental margins and flood basalts. *J. Geophys. Res., 94, 7685-7729.*

Whitmarsh, R. B., 1974. Some aspects of plate tectonics in the Arabian Sea. In Whitmarsh, R. B., Weser, O. E., Ross, D. A., et al., *Initial Reports DSDP, 23, Washington (U.S. Govt. Printing Office), 527-536.*

Wiens, D. A., DeMets, C., Gordon, R. G., Stein, S., Argus, D., Engeln, J. F.,Lundggren, P., Quible, D., Stein, C., Weinstein, S., Woods, D. F., 1985, A diffuse plate boundary model for Indian Ocean tectonics, *Geophysical Research Lett., 12, 429-432.*

Wiens, D. A., Stein, S., DeMets, C., Gordon, R. G., Stein, C., 1986. Plate tectonics model for Indian Ocean intraplate deformation, *Tectonophysics, 132, 37-48*

Wilson, J. T., 1963. A possible origin of the Hawaiian Islands. *Can. J. Phys., 41, 863-870.*

List of publications from present research work

Krishna, K.S., Abraham, H., Sager, W.W., Pringle, M., Frey, F.A., Gopala Rao, D., Levchenko, O.V., 2012. Tectonics of the Ninetyeast Ridge derived from the spreading records of the contiguous oceanic basins and age constraints of the ridge, J. Geophys. Res. 117, B04101, doi:10.1029/2011JB008805.

Abraham, H., Krishna, K.S., Sager, W.W., Dobriyal, J.P., 2016. Structural style and timing of deformation along the Ninetyeast Ridge – new insights on plate break-up process in the Indian Ocean (in preparation).

Tectonics of the Ninetyeast Ridge derived from spreading records in adjacent oceanic basins and age constraints of the ridge

Kolluru S. Krishna,[1] Honey Abraham,[1] William W. Sager,[2] Malcolm S. Pringle,[3] Frederick Frey,[3] Dasari Gopala Rao,[4] and Oleg V. Levchenko[5]

Received 22 August 2011; revised 26 January 2012; accepted 13 February 2012; published 3 April 2012.

[1] Analysis of new and existing geophysical data for the Central Indian and Wharton Basins of the Indian Ocean were used to understand the formation and evolution of the Ninetyeast Ridge (NER), especially its relationship to the Kerguelen hot spot and the Wharton spreading ridge. Satellite gravity data and magnetic anomalies 34 through 19 define crustal isochrons and show fracture zones striking ~N5°E. One of these, at 89°E, crosses the ~N10°E trending NER, impacting the NER morphology. From 77 to 43 Ma the NER lengthened at a rate of ~118 km/Myr, twice that of the ~48–58 km/Myr accretion rate of adjacent oceanic crust. This difference can be explained by southward jumps of the Wharton spreading ridge toward the hot spot, which transferred portions of crust from the Antarctic plate to the Indian plate, lengthening the NER. Magnetic anomalies document a small number of large spreading ridge jumps in the ocean crust immediately to the west of the NER, especially two leaving observable 65 and 42 Ma fossil spreading ridges. In contrast, complex magnetic anomaly progressions and morphology imply that smaller spreading ridge jumps occurred at more frequent intervals beneath the NER. Comparison of the NER dates and magnetic anomaly ages implies that the hot spot first emplaced NER volcanoes on the Indian plate at a distance from the Wharton Ridge, but as the northward drifting spreading ridge approached the hot spot, the two interacted, keeping later NER volcanism near the spreading ridge crest by spreading center jumps.

Citation: Krishna, K. S., H. Abraham, W. W. Sager, M. S. Pringle, F. Frey, D. Gopala Rao, and O. V. Levchenko (2012), Tectonics of the Ninetyeast Ridge derived from spreading records in adjacent oceanic basins and age constraints of the ridge, *J. Geophys. Res.*, *117*, B04101, doi:10.1029/2011JB008805.

1. Introduction

[2] The Ninetyeast Ridge (NER), one of the longest linear volcanic features on the Earth, extends ~5600 km in the N-S direction from 34°S to 17°N (Figure 1). Its southern part intersects the E-W trending Broken Ridge and the northern part (north of 10°N) is entirely buried under thick Bengal Fan sediments [*Curray et al.*, 1982; *Gopala Rao et al.*, 1997; *Michael and Krishna*, 2011], beneath which it converges upon the Andaman arc at about 17°N [*Subrahmanyam et al.*, 2008]. The ridge has an average width of 200 km and elevation of more than 2 km along most of its length [*Sclater and Fisher*, 1974; *Fisher et al.*, 1982; *Krishna et al.*, 1995, 2001a]. The NER is often asymmetric in cross section and ranges from low-relief to high-relief seamounts and linear ridge segments with some portions having a flat-topped morphology (Figure 2). Although numerous explanations have been proposed for the formation of the NER, it is widely accepted that the ridge was formed by Kerguelen hot spot volcanism when the hot spot was located beneath the Indian plate during the Late Cretaceous and early Cenozoic [*Peirce*, 1978; *Peirce et al.*, 1989; *Royer et al.*, 1991]. This hypothesis is supported by new geochronology data generated for NER core samples from DSDP Leg 26 and ODP Leg 121 [*Pringle et al.*, 2008], which show that the southern ridge is 43 Ma in age at DSDP Site 254 near the Broken Ridge and 77 Ma in age at ODP Site 758 near the north end of the NER and with a remarkably linear age progression in between (Figures 3a and 3b).

[3] When compared to seafloor spreading in adjacent Central Indian and Wharton Basins as delineated by seafloor spreading magnetic anomalies [e.g., *Krishna et al.*, 1995, 1999], the new geochronology data [*Pringle et al.*, 2008] reveal that the volcanic propagation rate (~118 km/Myr) of the NER is double that of the half-spreading rates (48–58 km/Myr) of the adjacent oceanic basins and, as a result, the NER is ~11° longer than the length of Indian

[1]National Institute of Oceanography, Council of Scientific and Industrial Research, Dona Paula, India.
[2]Department of Oceanography, Texas A&M University, College Station, Texas, USA.
[3]Department of Earth and Planetary Sciences, Massachusetts Institute of Technology, Cambridge, Massachusetts, USA.
[4]Department of Geology, Osmania University, Hyderabad, India.
[5]Shirshov Institute of Oceanology, Russian Academy of Sciences, Moscow, Russia.

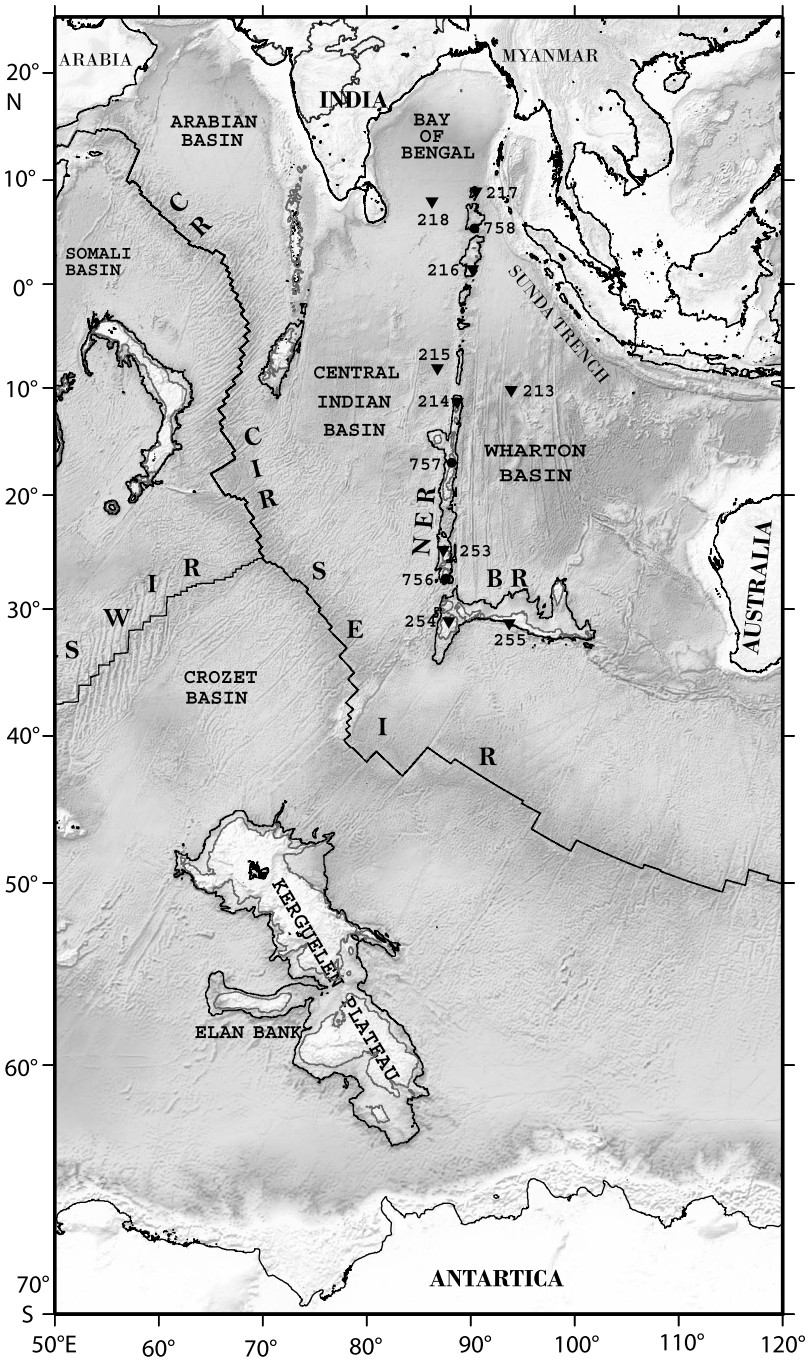

Figure 1. General bathymetry of the Indian Ocean showing mid-oceanic ridge systems, oceanic basins, aseismic ridges, and plateaus. Numbered solid triangles and circles show Deep Sea Drilling Program (DSDP) and Ocean Drilling Project (ODP) sites that are mentioned in the text, respectively. BR, Broken Ridge; CR, Carlsberg Ridge; CIR, Central Indian Ridge; SWIR, Southwest Indian Ridge; SEIR, Southeast Indian Ridge.

plate created contemporaneously [*Krishna et al.*, 1999]. Previously, *Royer et al.* [1991] and *Krishna et al.* [1995, 1999] have provided an explanation that the Wharton spreading ridge segments jumped southward several times, transferring lithosphere from Antarctic plate to the Indian plate. But the timing, location of the hot spot, and extent of these ridge jumps are uncertain because magnetic lineations near the NER are complex and magnetic data in the region are sparse.

[4] In this study we compiled and modeled magnetic anomaly profile data from the NER and adjacent basins (Figures 3a and 3b) and examined the implications of newly available geochronology data from DSDP Leg 22 and ODP Leg 121 cores [*Pringle et al.*, 2008]. The geophysical data

are mainly utilized for identification of magnetic patterns including fracture zones (FZs) and fossil ridge segments, of both the Wharton and Central Indian Basins adjacent to the NER. With the derived tectonic constraints and geochronology data, we propose a model for interactions between the Wharton spreading center and the Kerguelen hot spot during the emplacement of the NER. Finally we discuss the mechanisms of NER accretion and why its length is much longer compared to that of the adjacent normal oceanic lithosphere formed during the same time interval.

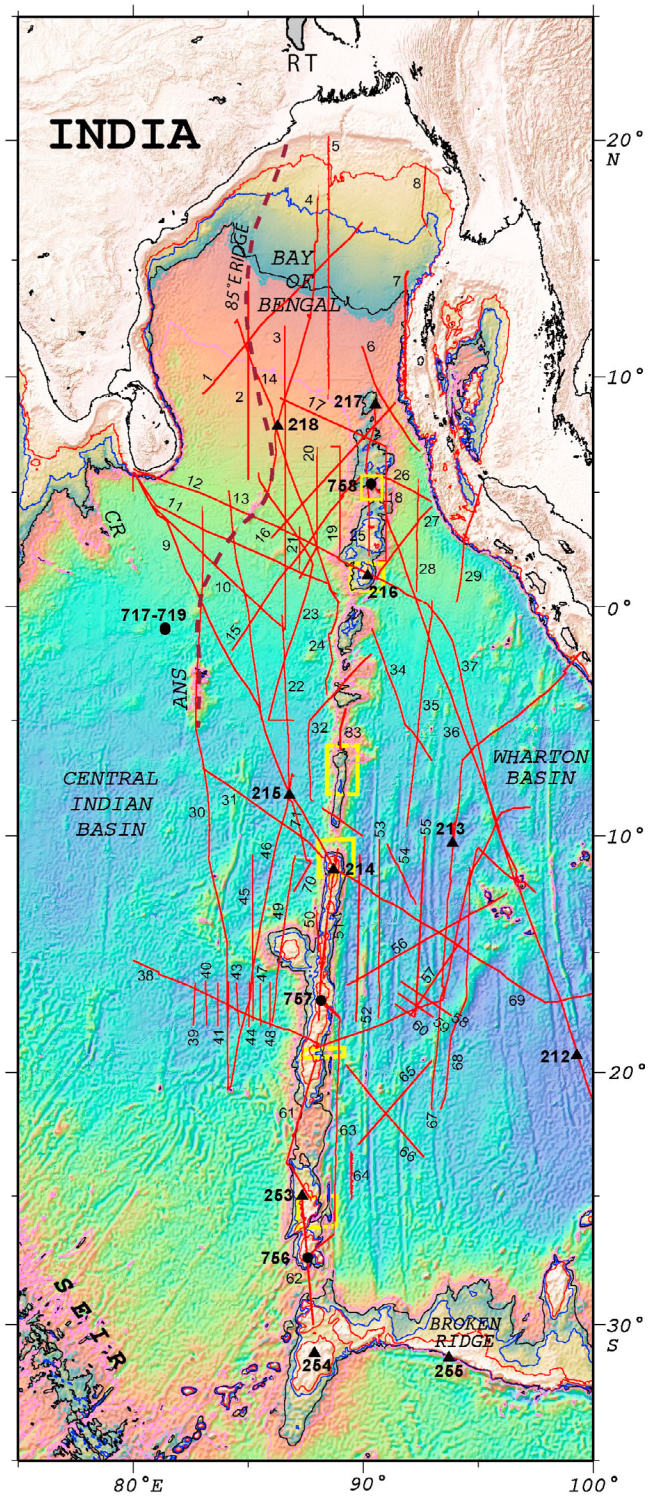

2. NER Tectonic Setting

[5] Major plate reorganizations of Indian Ocean seafloor spreading occurred at ~90 and ~42 Ma, moving the Kerguelen hot spot alternately beneath the Indian and Antarctic plates, respectively [*Liu et al.*, 1983]. Initially, at approximately 120 Ma, the hot spot was beneath the Antarctic plate, leading to the formation of the southern and central parts of the Kerguelen Plateau and the Broken Ridge [*Coffin et al.*, 2002]. The first major plate reorganization, at ~90 Ma, placed the hot spot beneath the Indian plate and resulted in the accretion of the world's largest linear aseismic ridge, termed the NER. The second major plate reorganization, at ~42 Ma, relocated the hot spot beneath the Antarctic plate and resulted in the accretion of the Northern Kerguelen Plateau, including the Kerguelen Archipelago, and Heard and McDonald Islands [*Coffin et al.*, 2002] since that time. It has been thought that during the formation of the NER, the Kerguelen hot spot was mostly located north of spreading ridge segments that were part of the western extremity of the Wharton Ridge, which separated the Indian and Australian plates and was connected to the India-Antarctica Ridge through the 86°E transform fault [*Krishna et al.*, 1995, 1999]. Concurrently with the NER emplacement, the adjacent Wharton and Central Indian Basins were also formed by the spreading of the Wharton and India-Antarctica ridges, respectively [*Liu et al.*, 1983; *Royer and Sandwell*, 1989; *Royer et al.*, 1991; *Krishna et al.*, 1995, 1999]. After the ~42 Ma plate reorganization, the Wharton spreading ridge effectively disappeared as the Southeast Indian Ridge formed, and the Indian and Australian plates merged together to form a single Indo-Australian plate [*Liu et al.*, 1983; *Krishna et al.*, 1995].

[6] During Neogene time, a large diffuse plate boundary formed in the central Indian Ocean, breaking the major Indo-Australian plate into three smaller component plates: Indian, Australian, and Capricorn plates [*Royer and Gordon*, 1997; *Gordon et al.*, 1998]. Almost the entire NER resides within this zone of complex deformation. Seismic results from Bengal Fan sediments reveal that the lithosphere within the boundary to the west of the NER displays reverse faulting (5–10 km spaced faults) and long-wavelength (100–300 km) folding [*Weissel et al.*, 1980; *Bull*, 1990; *Chamot-Rooke et al.*, 1993; *Krishna et al.*, 1998, 2001b]. Using seismic

Figure 2. Magnetic tracks in the vicinity of the NER. Red solid lines indicate magnetic profiles acquired from different data sources (KNOX06RR cruise, National Geophysical Data Center (NGDC), National Institute of Oceanography (NIO), and Trans Indian Ocean Geotraverse (TIOG) databases; the key of profile identifiers with specific cruises is given in Table 1), which are analyzed in the present study. Detailed geophysical data including multibeam bathymetry, tenfold multichannel seismic reflection, and magnetic profiles were acquired in locations represented by yellow rectangles on top of the Ninetyeast Ridge (NER). Solid triangles and circles indicate DSDP and ODP drill sites, respectively.

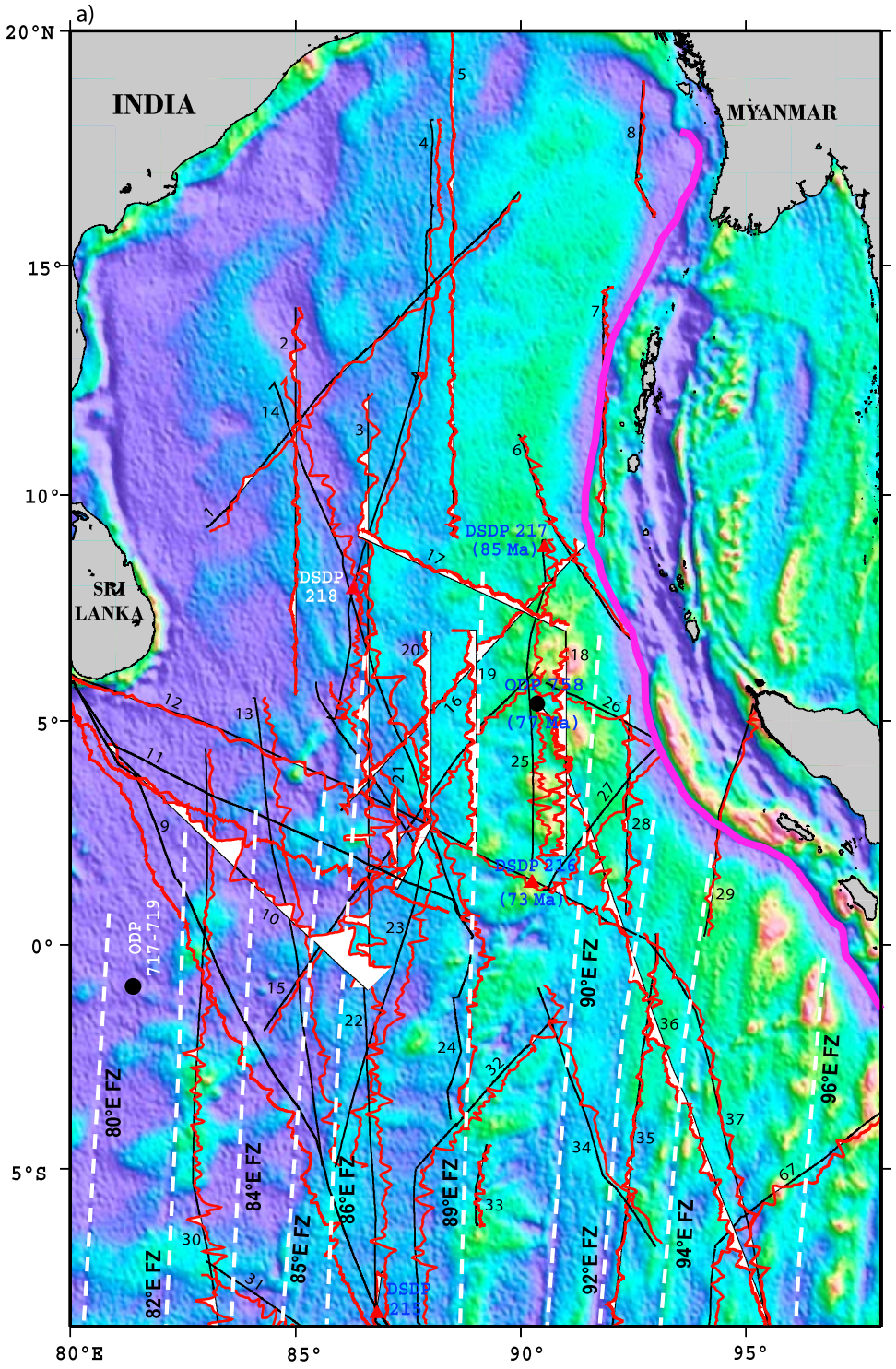

Figure 3. Magnetic anomaly profiles shown on top of the satellite free-air gravity image of the northeastern Indian Ocean (prepared from database of *Sandwell and Smith* [1997]). The map is divided into two parts for better visualization. (a) Magnetic anomaly data are plotted along the ship tracks. White dashed lines are drawn to follow narrow gravity features that define oceanic fracture zones. DSDP and ODP sites are shown by solid red triangles and solid black circles, respectively. Ages indicated at each drill site are from the geochronology data published by *Pringle et al.* [2008]. (b) Southern part of the satellite gravity and magnetic anomaly profile data of the northeastern Indian Ocean.

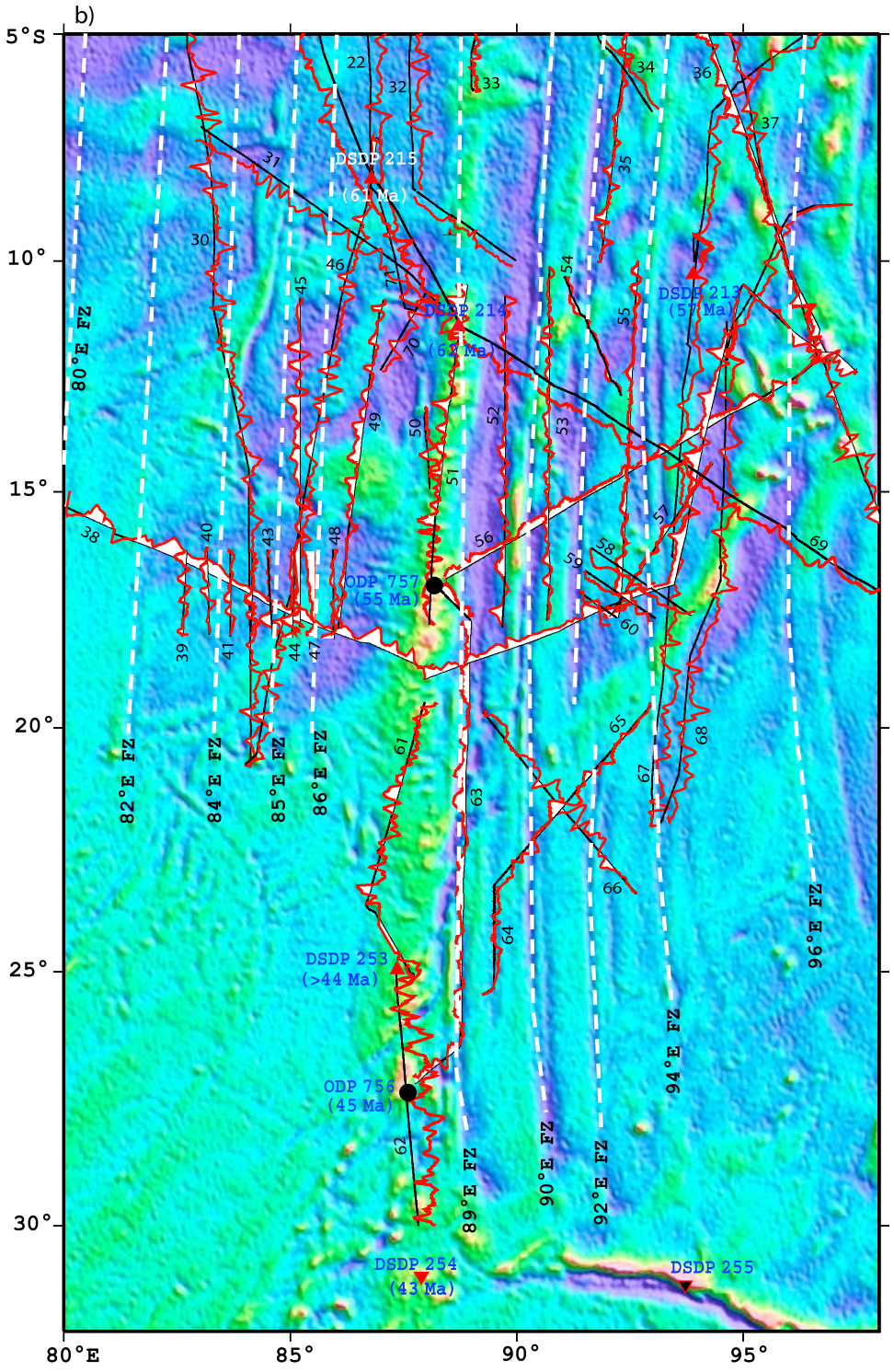

Figure 3. (continued)

stratigraphy and plate rotations, *Krishna et al.* [2009a] and *Bull et al.* [2010] subsequently determined that the lithospheric convergence began at 18–14 Ma within this plate boundary. Recent seismic results from the NER suggest that the ridge is dissected by numerous faults and experiencing ongoing deformation activity [*Sager et al.*, 2010]. Furthermore, the ridge is thought to be a structural partition that separates different styles of deformation in the Central Indian and Wharton Basins [*Deplus et al.*, 1998; *Delescluse and Chamot-Rooke*, 2007]. Despite this ongoing

Table 1. Details of Profiles IDs and Databases Used in the Present Study

Profile Number Used in the Present Study	Original Profile ID	Research Vessel Used for the Data Acquisition	Data Source[a]
1	CIRC03AR	R/V *Argo*	NGDC
2	SK82-14	ORV *Sagar Kanya*	NIO database
3	SK82-02	ORV *Sagar Kanya*	NIO database
4	ANTP11MV	R/V *Melville*	NGDC
5	SK100-10	ORV *Sagar Kanya*	NIO database
6	CIRC03AR	R/V *Argo*	NGDC
7	SK100-20	ORV *Sagar Kanya*	NIO database
8	CIRC03AR	R/V *Argo*	NGDC
9	WILKES815	USNS *Wilkes*	NGDC
10	SK82-01	ORV *Sagar Kanya*	NIO database
11	WILKES907	USNS *Wilkes*	NGDC
12	C0909	R/V *Conrad*	NGDC
13	C0909	R/V *Conrad*	NGDC
14	INMDO6MV	R/V *Melville*	NGDC
15	CIRC03AR	R/V *Argo*	NGDC
16	SK100-01c	ORV *Sagar Kanya*	NIO database
17	SK124-5	ORV *Sagar Kanya*	NIO database
18	SK124-6	ORV *Sagar Kanya*	NIO database
19	SK124-8	ORV *Sagar Kanya*	NIO database
20	SK124-10	ORV *Sagar Kanya*	NIO database
21	SK124-12	ORV *Sagar Kanya*	NIO database
22	DSDP22GC	R/V *Glomar Challenger*	NGDC
23	C1709	R/V *Conrad*	NGDC
24	WILKES907	USNS *Wilkes*	NGDC
25	CIRC03AR	R/V Argo	NGDC
26	RC1402	R/V Robert *Conrad*	NGDC
27	DSDP22GC	R/V *Glomar Challenger*	NGDC
28	8400121b	R/V *Jean Charcot*	NGDC
29	LUSI7BAR	R/V *Argo*	NGDC
30	CIRC05AR	R/V *Argo*	NGDC
31	RC1402	R/V *Robert Conrad*	NGDC
32	RC1402	R/V *Robert Conrad*	NGDC
33	KNOX06RR	R/V *Roger Revelle*	NGDC
34	INMDO6MV	R/V *Melville*	NGDC
35	8400121a	R/V *Jean Charcot*	NGDC
36	ODP121JR	*Joides Resolution*	NGDC
37	C0909	R/V *Conrad*	NGDC
38	MONS3AR	R/V *Argo*	NGDC
39	TIOG-7	R/V *Issledovatl*	ILTP database
40	TIOG-8	R/V *Issledovatl*	ILTP database
41	TIOG-9	R/V *Issledovatl*	ILTP database
42	TIOG-10	R/V *Issledovatl*	ILTP database
43	TIOG-11	R/V *Issledovatl*	ILTP database
44	TIOG-12	R/V *Issledovatl*	ILTP database
45	TIOG-13	R/V *Issledovatl*	ILTP database
46	CIRC05AR-B	R/V *Argo*	NGDC
47	TIOG-14	R/V *Issledovatl*	ILTP database
48	TIOG-15	R/V *Issledovatl*	ILTP database
49	TIOG-16	XVII *Syezo Profsoyuzov*	ILTP database
50	KNOX06RR	R/V *Roger Revelle*	NGDC
51	TIOG-17	XVII *Syezo Profsoyuzov*	ILTP database
52	TIOG-18	XVII *Syezo Profsoyuzov*	ILTP database
53	TIOG-19	XVII *Syezo Profsoyuzov*	ILTP database
54	TIOG-20	XVII *Syezo Profsoyuzov*	ILTP database
55	TIOG-21	XVII *Syezo Profsoyuzov*	ILTP database
56	ODP121JR	*Joides Resolution*	NGDC
57	TIOG-51	XVII *Syezo Profsoyuzov*	ILTP database
58	TIOG-60	XVII *Syezo Profsoyuzov*	ILTP database
59	TIOG-61	XVII *Syezo Profsoyuzov*	ILTP database
60	TIOG-62	XVII *Syezo Profsoyuzov*	ILTP database
61	KNOX06RR	R/V *Roger Revelle*	NGDC
62	DSDP26GC	R/V *Glomar Challenger*	NGDC
63	ODP121JR	*Joides Resolution*	NGDC
64	KNOX06RR	R/V *Roger Revelle*	NGDC
65	KNOX06RR	R/V *Roger Revelle*	NGDC
66	CIRC05AR	R/V *Argo*	NGDC
67	ANTP12MVa	R/V *Melville*	NGDC
68	ANTP12MVb	R/V *Melville*	NGDC
69	WILKES815	USNS *Wilkes*	NGDC
70	CIRC05AR-C	R/V *Argo*	NGDC
71	WILKES907	USNS *Wilkes*	NGDC

[a]NGDC, National Geophysical Data Center; NIO, National Institute of Oceanography.

tectonism, the overall deformation of the diffuse boundaries is small and thus can be ignored for our study of Late Cretaceous and early Cenozoic plate boundary motions.

[7] NER morphology is complex and varies along its length [*Fisher et al.*, 1982; *Krishna et al.*, 2001a; *Sager et al.*, 2010]. The southern ridge, south of 11°S, is tall, nearly continuous, and often highly asymmetric with a steep eastern slope and low western slope. In contrast, the ridge north of ~3°S consists of a series of mostly individual, large volcanoes with more symmetric cross sections. In between, the ridge is low with a combination of small linear segments and seamounts [*Krishna et al.*, 2001a]. The position of the Kerguelen hot spot with respect to the Wharton spreading centers, the strike of oceanic fracture zones, plate motions, hot spot drift, variable hot spot magma output, and deformation-related faults are all factors that have been implicated as controls on the morphology of the NER [e.g., *Royer et al.*, 1991].

3. Geophysical and Geological Data

[8] An international scientific expedition was carried out onboard R/V *Roger Revelle* (KNOX06RR) during the year 2007 over the NER (Figure 2). During the cruise multibeam bathymetry, magnetic and gravity data, and tenfold multichannel seismic reflection profiles, were acquired in the vicinity of ODP Site 758, DSDP Sites 216, 214 and 253 and at locations 6–8°S and 19°S. In addition to the geophysical data, basaltic rocks were also dredged at 22 sites along the NER (see *Sager et al.* [2007] for locations). Magnetic data utilized in this study were gathered from the KNOX06RR cruise, National Geophysical Data Center (NGDC) and National Institute of Oceanography (NIO) databases, and the Trans Indian Ocean Geotraverse (TIOG) program (Table 1) [*Krishna et al.*, 1995]. In addition we used newly determined $^{40}Ar/^{39}Ar$ radiometric ages [*Pringle et al.*, 2008] of basaltic core samples from DSDP Sites 214, 216, 254 and ODP Sites 756–758 along the NER (Figure 3).

4. Magnetic Anomaly Pattern of the Central Indian and Wharton Basins Adjacent to the Ninetyeast Ridge

[9] Magnetic anomaly profile data adjacent to the NER are plotted along ship tracks and are shown in Figures 3. The data are overlaid on satellite free-air gravity data [*Sandwell and Smith*, 1997] in order to constrain precise positions of fracture zones (FZ), thereby constraining extrapolation of the magnetic lineations. The satellite gravity image clearly shows the presence of a number of nearly N-S trending narrow gravity features, indicating the signatures of FZ

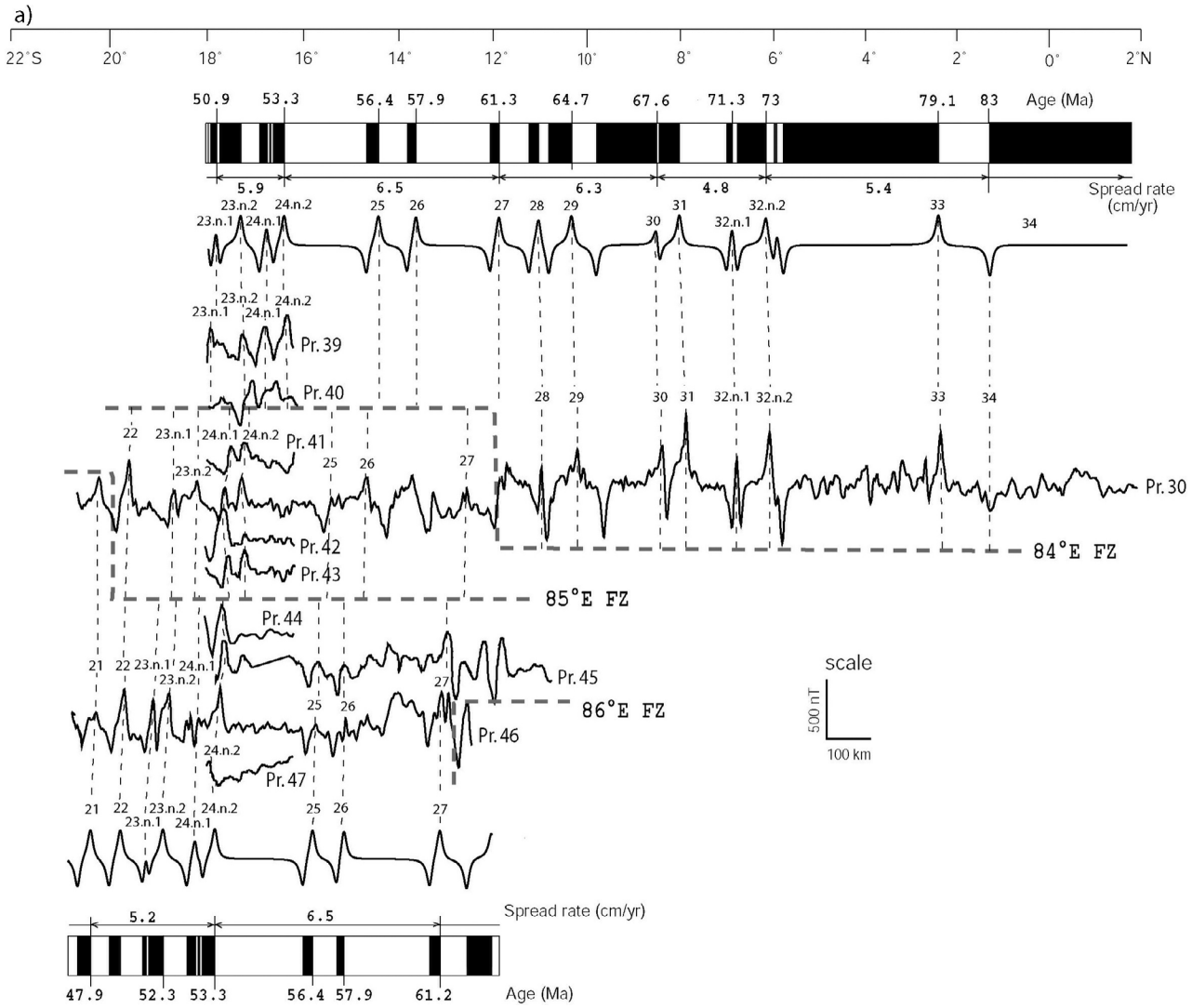

Figure 4. Observed magnetic anomaly profile data are correlated with synthetic magnetic profiles. (a) West of the 86°E Fracture Zone (FZ). Spreading-type magnetic anomalies 21–34 are identified and correlated from profile to profile. The geomagnetic polarity time scale of *Cande and Kent* [1995] was used for assigning the age to the magnetic lineations. (b) East of the NER. Magnetic anomalies 20–34 and fossil ridge segments (of middle Eocene age) are identified. The offsets in magnetic lineations are used to define several fracture zones. Hashed lines (FRS) denote abandoned ("fossil") spreading centers. (c) Between the 86°E FZ and the NER. Magnetic anomalies 21–34 are identified and fossil ridge segments (FRS) of latest Cretaceous and middle Eocene age are identified. The magnetic lineations identified between the FRS have lost systematic continuity in anomaly sequence because of ridge jumps.

created during the northward movement of the Indian plate. From these gravity features, we have traced ten FZ between 80° and 97°E longitudes (Figure 3). They trend in the N5°E direction, while the NER trends ~N10°E, consequently the 89°E FZ crosses the NER obliquely from east to west between 15°S and 10°S latitudes (Figure 3). Magnetic anomalies are, in general, well developed with moderate amplitudes except over the NER and on its immediate east side (Figures 3 and 4). In particular between the 89°E FZ and 94°E FZ, the anomalies are modestly developed with lower amplitudes (Figures 3a, 3b, and 4b). The anomalies within this corridor seem to be subdued because of excessive seafloor undulations created by oceanic fracture zones, strike-slip displacements and vertical faulting [*Pilipenko*, 1996; *Krishna et al.*, 2001a].

[10] Earlier magnetic anomaly identifications from both the Central Indian and Wharton Basins [*Peirce*, 1978; *Liu et al.*, 1983; *Peirce et al.*, 1989; *Royer et al.*, 1991; *Krishna et al.*, 1995, 2009b; *Krishna and Gopala Rao*, 2000] were considered to determine the spreading rates and magnetic polarity chronology for the calculation of synthetic magnetic anomaly profiles. Half-spreading rates ranging from 2.3 to 8.5 cm/yr and geomagnetic polarity timescale [*Cande and Kent*, 1995] for the period from Late Cretaceous to early Tertiary were used to create synthetic magnetic anomaly models (shown in Figure 4). Following

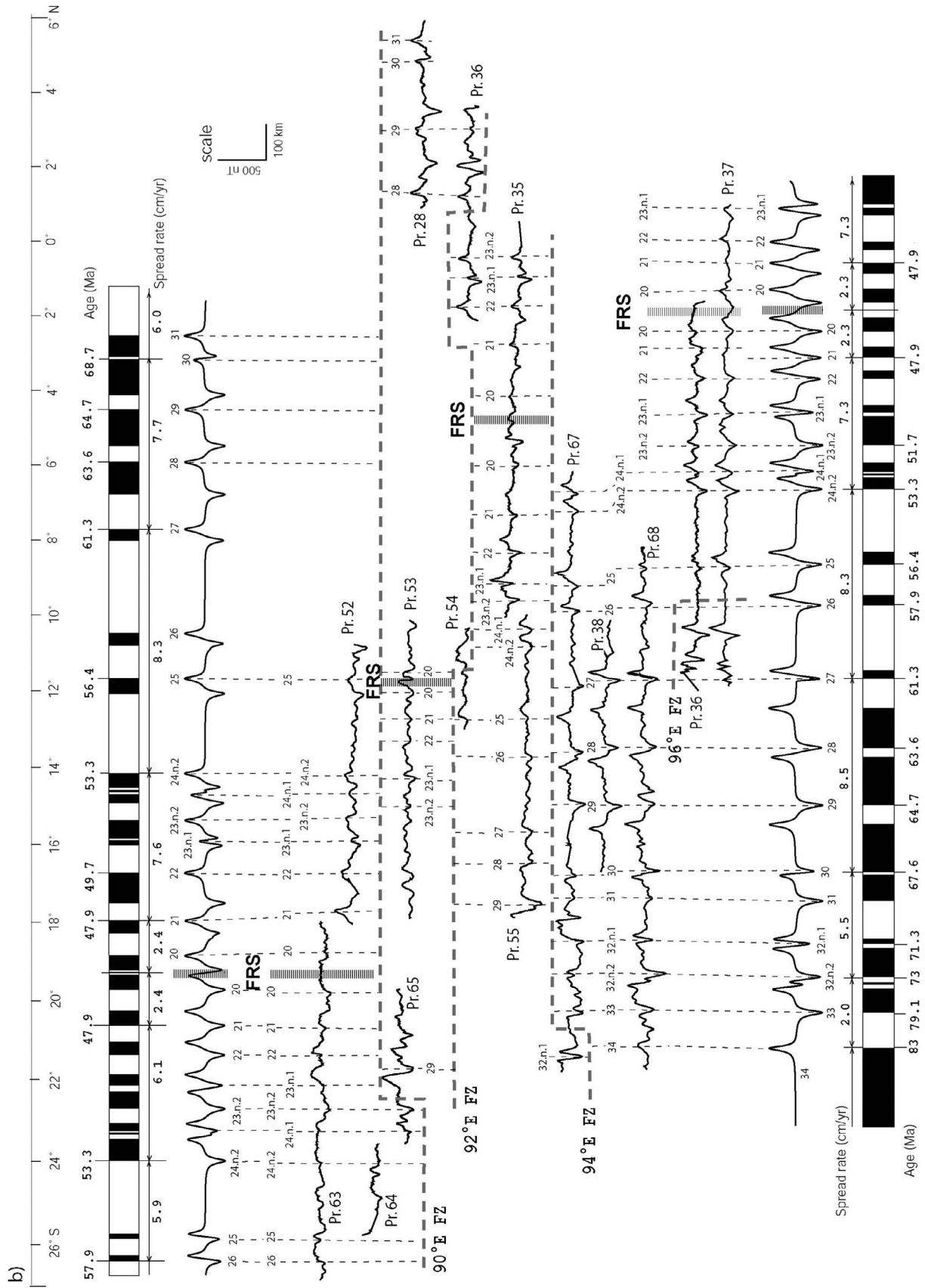

Figure 4. (continued)

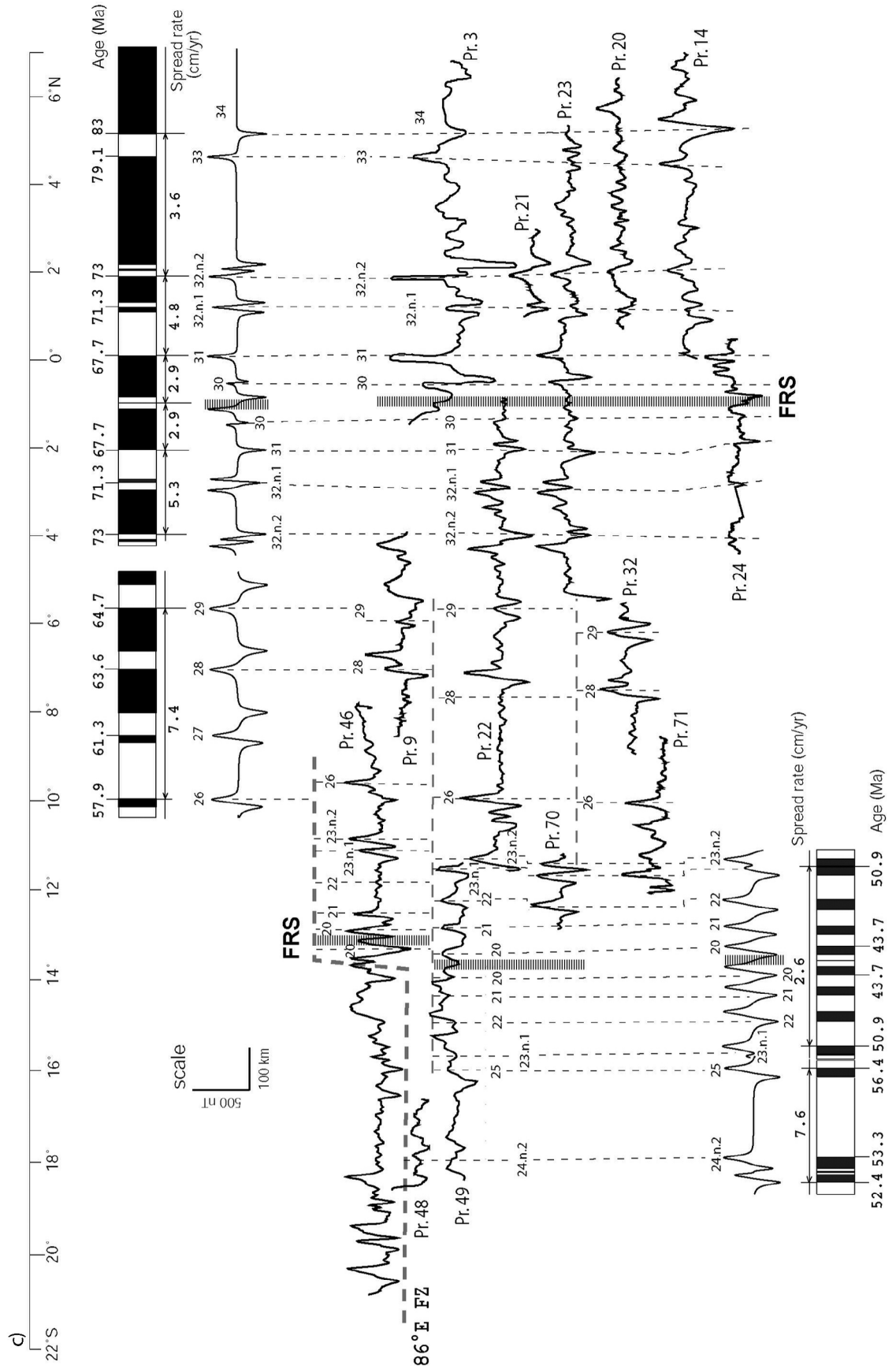

Figure 4. (continued)

the anomaly pattern within the study area (west of the 86°E FZ, east of the 90°E FZ, and the region in between) three magnetic models were generated using the Matlab-based MODMAG algorithm [*Mendel et al.*, 2005] and correlated to the magnetic anomaly profiles for identification of seafloor spreading magnetic anomalies, thereby assigning ages to the oceanic crust. The magnetic anomaly sequences in model profiles, particularly anomalies 30 through 32n.2 and 21 through 24n.2, have characteristic shapes (see Figure 4) generated by a unique arrangement of short-period geomagnetic polarity reversals. We used these distinctive anomaly shapes and patterns as reference picks for the correlation of observed anomalies to model profiles. With this approach most of our anomaly correlations have gained reasonably high confidence.

[11] A comparison of the observed magnetic anomaly data of both the Central Indian and Wharton Basins with synthetic model profiles (Figure 4) leads to the identification of seafloor spreading anomalies 19 through 34, several fossil ridge segments, and a number of nearly N-S oriented FZ along 84°E, 85°E, 86°E, 89°E, 90°E, 92°E, 94°E, and 96°E longitudes. It is observed that half-spreading rates are significantly reduced, as low as 2.9 and 2.3 cm/yr, close to the end phase of ridge segments at anomalies 30 and 19, respectively (Figures 4b and 4c). The ridge segments that ceased at anomaly 19 were part of the cessation of the entire Wharton spreading system, thereby contributing to the second major plate reorganization in the Indian Ocean and unification of Indian and Australian plates into a single major lithospheric plate. This event is thought to be a result of occurrence of continent-continent collision between India and Asia [*Liu et al.*, 1983; *Patriat and Segoufin*, 1988]. In regions to the west of the 86°E FZ and east of the NER, spreading anomalies 19 through 34 are identified with confidence and correlated with the anomaly picks from profile to profile (Figures 4a and 4b). To the west of the 86°E, FZ magnetic lineations from 26 to 23n.1 are offset approximately along the 84°E and 85°E longitudes in a right-lateral sense by about 90 and 45 km, respectively, revealing the presence of oceanic fracture zones, termed as the 84°E FZ and 85°E FZ (Figure 5). Likewise to the east of the NER the magnetic lineations from 32n.1 to 19 show large offsets approximately along 90°E, 92°E and 94°E longitudes in the opposite (left-lateral) sense by about 840, 820 and 150 km, respectively, revealing the presence of oceanic fracture zones, identified as the 90°E FZ, 92°E FZ and 94°E FZ (Figure 5).

[12] By comparison of the magnetic anomalies from profiles Wilkes815 (Pr. 9), sk82–02 (Pr. 3), dsdp22gc (Pr. 22), sk124–12 (Pr. 21), C1709 (Pr. 23), sk124–10 (Pr. 20), inmd06mv (Pr. 14), wilkes815 (Pr. 24), circ05AR-B (Pr. 46), tiog15 (Pr. 48), tiog16 (Pr. 49), circ05AR-C (Pr. 70), RC1402 (Pr. 32), and Wilkes907 (Pr. 71) with the synthetic magnetic model (Figure 4c), we identify symmetric pairs of anomaly sequences 30 through 32n.2 and 20 through 23n.1 on either side of anomaly signatures presumed to be associated with fossil ridge segments. These sequences evolved by the abandonment of ridge segments soon after anomaly 30 and at anomaly 19, respectively. In addition we identify anomalies 26 to 29 (increasing age toward the north) in between the aforesaid anomaly sequences, and anomalies 24n.2 and 25 on the south side of the younger anomaly sequence (Figures 4c, 5a, and 5b). Furthermore, minor dislocations, <50 km, are noted at two places, particularly in anomalies from 26 to 29 and 20 to 23n.2, and this led to recognition of smaller second-order fracture zones whose continuation is not observed in anomalies older than 30 (Figures 4c, 5a, and 5b). This suggests that these two fracture zones may have originated after magnetic anomaly 30 and continued up to anomaly 19. Thus the magnetic pattern in the corridor between the 86°E FZ and the NER has been disrupted by fracture zones and spreading ridge jumps, and as a result the magnetic pattern has become more complex in comparison to that of other regions west of the 86°E FZ and east of the NER. Previous studies have noted complex magnetic patterns west of the NER [*Royer et al.*, 1991; *Krishna et al.*, 1995; *Krishna and Gopala Rao*, 2000] and in the Wharton Basin [*Liu et al.*, 1983] in broader perspective. In this study we generated more accurate magnetic anomaly maps for the basinal regions on both sides of much of the NER using up-to-date available magnetic anomaly profile data and satellite gravity anomaly data (Figure 5), providing tighter constraints on the evolution of the NER and the interaction of the hot spot with spreading ridge segments.

[13] Ages of the oceanic crust obtained from the magnetic lineations agree with ages of rock samples recovered at DSDP Site 215 in the Central Indian Basin and basal sediments sampled from DSDP Site 213 in the Wharton Basin, giving confidence in the anomaly identifications. The rock samples at DSDP Site 215 show 61 Ma age oceanic crust [*Von der Borch et al.*, 1974a], which corresponds to magnetic anomaly 27 following the geomagnetic polarity timescale of *Cande and Kent* [1995]. This is in good agreement with anomalies 26 and 28–29 in the vicinity of the Site 215 (Figure 5b). Likewise the oldest sediments at DSDP Site 213 are 57 Ma in age [*Von der Borch et al.*, 1974b], which corresponds well with anomalies 25 and 26 on either side of the site.

[14] The magnetic pattern in the vicinity of the NER reveals that the age of the oceanic crust to the west of the 86°E FZ increases toward the north from early Cenozoic to Late Cretaceous, while the crust to the east of the 92°E FZ increases its age in both north and south directions symmetric about the middle Eocene fossil Wharton Ridge segments. Contrasting to these trends, the crust in between these FZ shows a complex age succession with different age (65 and 42 Ma) fossil ridge segments (Figure 5). The ridge segments abandoned at anomaly 30 and at anomaly 19 by ridge jumps are identified in the equatorial region and in the area between 12° and 14°S latitudes, respectively.

5. Tectonic Evolution of the Ninetyeast Ridge

[15] New $^{40}Ar/^{39}Ar$ ages of basaltic core samples from DSDP Sites 214, 216, 254 and ODP Sites 756–758 show that the NER is age progressive for a distance of 3980 km, north to south, spanning 77 to 43 Ma [*Pringle et al.*, 2007, 2008]. A plot of age versus latitude displays remarkable linearity (Figure 6), with age decreasing to the south and a volcanic propagation rate of 118 ± 5 km/Myr [*Pringle et al.*, 2008]. This contrasts with earlier dates that implied a significantly slower rate of 86 ± 12 km/Myr [*Duncan*, 1978, 1991]. Comparison of the NER age progression with nearby

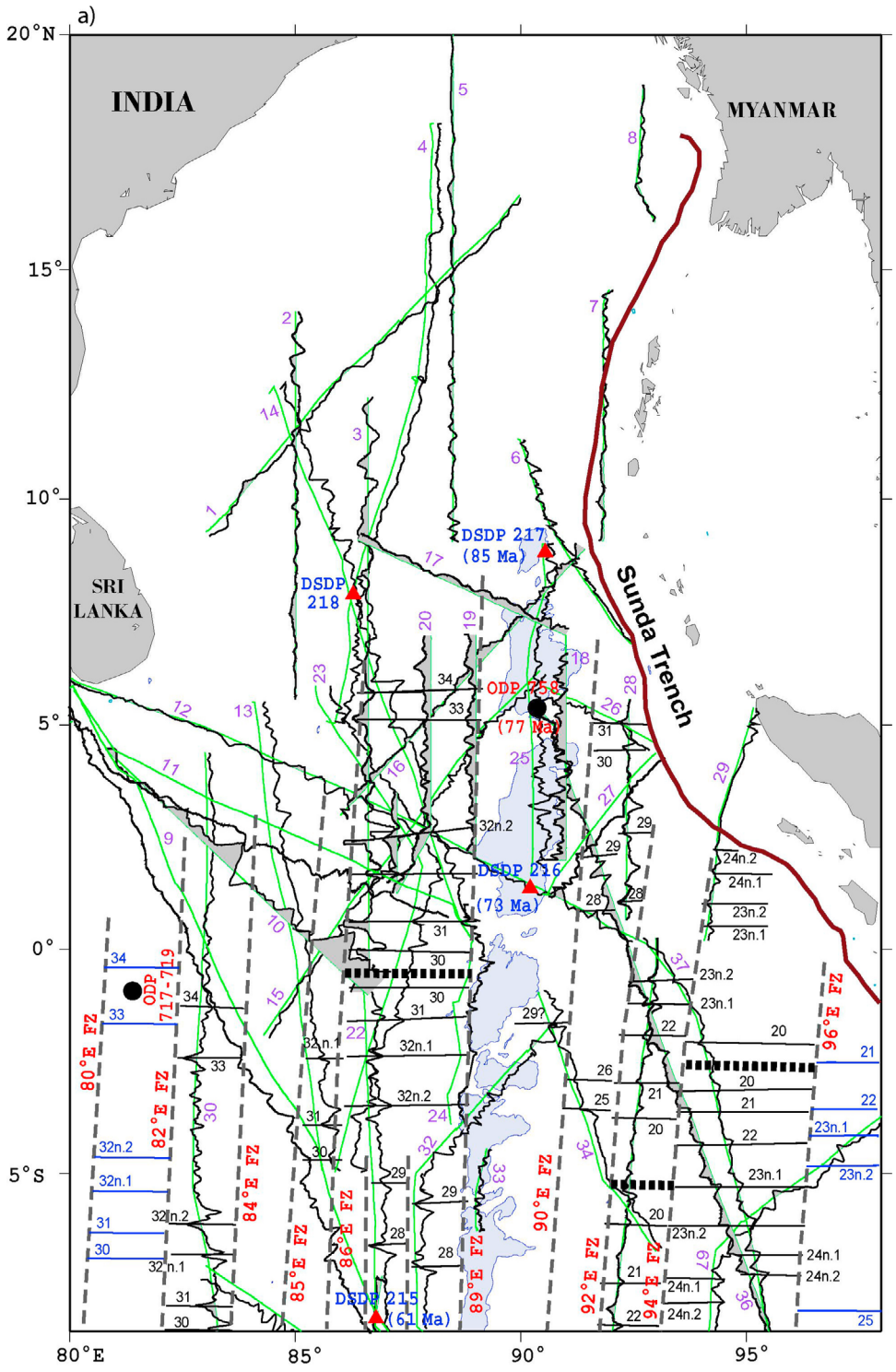

Figure 5. Interpreted magnetic lineations (black lines), fossil ridge segments (solid stippled line), and oceanic fracture zones (dashed lines) of the northeastern Indian Ocean. Magnetic lineations indicated with blue lines are adopted from earlier studies [*Royer et al.*, 1991; *Krishna and Gopala Rao*, 2000]. The tectonic map is divided into two parts for better visualization. Magnetic profiles are shown particularly to support the anomaly identifications, correlations, and offsets. Fracture zones are tightly constrained by satellite gravity data. Bathymetric contour at 3000 m and shallower water depths are shaded to outline the physiography of the NER and other features. (a) northern NER and (b) southern NER.

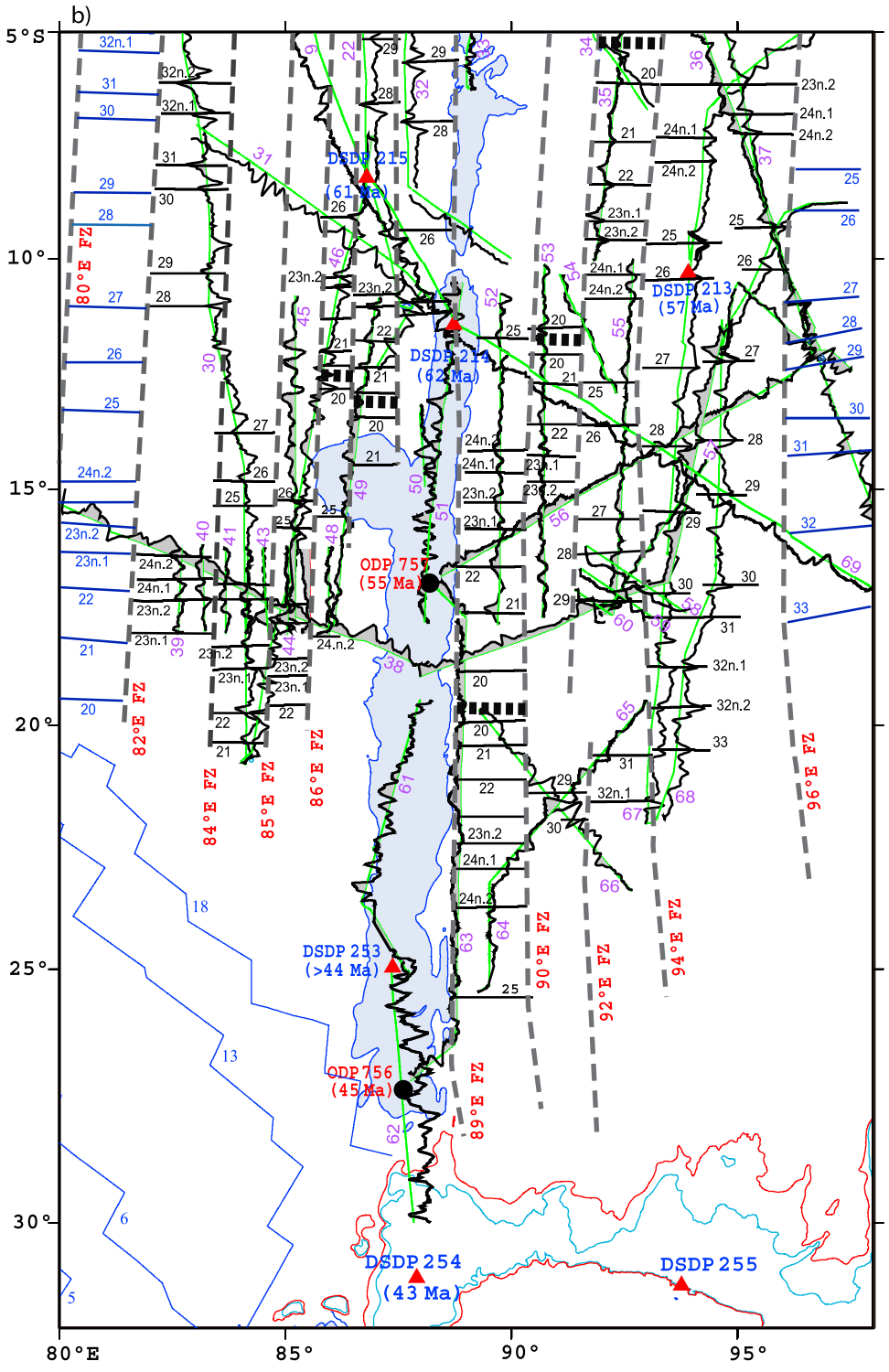

Figure 5. (continued)

magnetic anomalies indicates that the NER lengthened much more rapidly than adjacent lithosphere (Figure 6). In regions west of the 86°E FZ and east of the 90°E FZ, magnetic lineations 33 and 20, corresponding to approximately to 77 and 43 Ma, respectively, are separated by ~2000 km (Figure 6a), revealing that the crust was created at a rate of ~58 km/Myr. In other regions closer to NER (between 86°E FZ and NER; between 89°E FZ and 90°E FZ), the oceanic crust was formed at comparable rates ranging from 48 to 55 km/Myr (Figure 6b). This discrepancy is a result of the difference between relative plate velocity, recorded by seafloor magnetic lineations, and the volcanic propagation

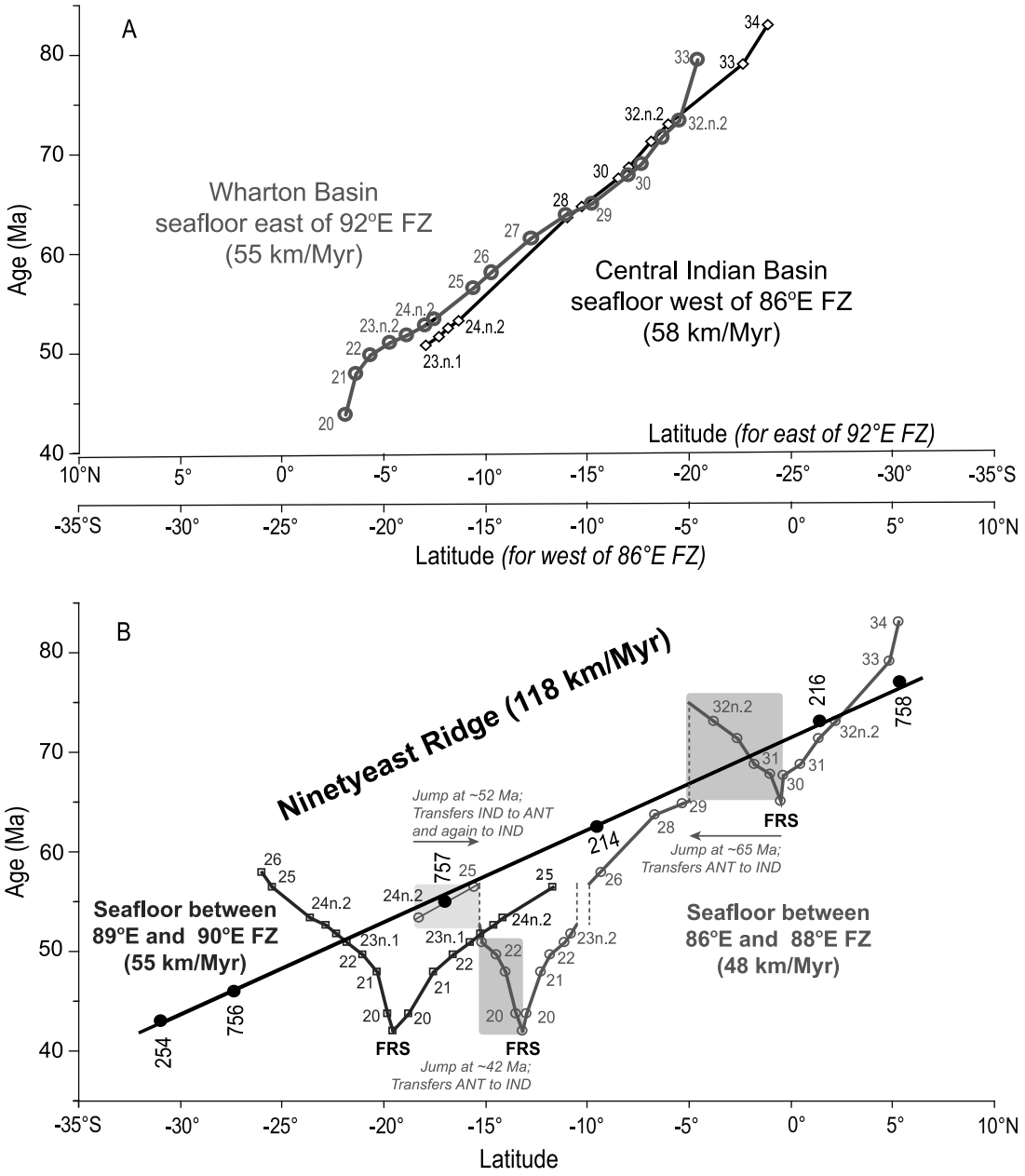

Figure 6. Comparison of rates of ocean crust creation in different spreading corridors and the volcanic propagation rate on the NER. (a) Seafloor created in the Central Indian and Wharton Basins, west of the 86°E and east of the 92°E fracture zones, respectively. (b) Radiometric ages from DSDP and ODP sites along the NER, seafloor created immediately to the west between the 88°E and 89°E fractures zones, and seafloor created immediately to the east between the 89°E and 90°E fracture zones. Black dots show ages of drill core samples [*Pringle et al.*, 2008]; open symbols denote seafloor spreading magnetic anomalies (Figures 4 and 5). FRS indicates fossil ridge segment. Note the northward spreading center jump in the seafloor between the 86°E and 88°E fracture zones after C24n.2 time into C25 age crust and subsequent spreading up to the FRS just after C20.

rate of the NER, which reflects the velocity of the Indian plate relative to the hot spot.

[16] The propagation rate of NER volcanism is about twice that of the half-spreading rates recorded on the Indian plate, or similar to the full-spreading rate between the Antarctic and Indian plates. The motion of the Antarctic plate relative to the hot spot reference frame at this time was slow [*Acton*, 1999; *Besse and Courtillot*, 2002]. Thus, relative to a nearly fixed Antarctic plate, the Indian plate was moving northward at about the full spreading rate, and the Wharton spreading center itself was migrating northward at about the half spreading rate. It would thus seem that the NER volcanic propagation simply records this full spreading rate as postulated previously [e.g., *Royer et al.*, 1991]. Because of

its rapid northward drift relative to the NER hot spot, the Wharton spreading ridge should have simply crossed over the hot spot, and subsequent volcanism would have occurred on the Antarctic plate. However, the eruption ages for the NER core samples are similar to the nearby magnetic anomalies indicating that the Wharton spreading ridge remained relatively close to the hot spot throughout much of the NER history (Figure 6). This circumstance required that some tectonic mechanism acted to keep the spreading ridge close to the hot spot; we argue that ridge jumps are that mechanism.

5.1. Wharton Ridge Segments and Kerguelen Hot Spot Interactions

[17] Using an updated magnetic data set, we present an improved interpretation of magnetic anomalies, particularly immediately to the east and west of the NER (Figure 5), which supersedes earlier anomaly identifications in this region [*Sclater and Fisher*, 1974; *Liu et al.*, 1983; *Royer et al.*, 1991; *Krishna et al.*, 1995]. From the trends of the FZ and the NER, it is found that the 89°E FZ crosses the NER obliquely between 15°S and 10°S latitudes (Figure 5). Consequently the NER was formed in two different spreading corridors of oceanic crust: the north part of the ridge active before ~62 Ma is situated between the 89°E FZ and the 90°E FZ, while the south part of the NER is located between the 86°E FZ and the 89°E FZ.

[18] As described in section 4, the oceanic crust between the 86°E and 90°E FZs shows nonmonotonic sequences of magnetic lineations caused by ridge jumps, with two major jumps occurring at 65 and 42 Ma (Figure 5). At ~90 Ma, the Indian plate was bounded on the southwest side by the Wharton and India-Antarctica ridges, which were connected through the 86°E transform fault [*Krishna et al.*, 1995] and the Kerguelen hot spot was located beneath the Indian plate at a moderate distance from the Wharton Ridge segments. During the first spreading reorganization during the Late Cretaceous, a ridge segment immediately west of the NER ceased its activity at ~65 Ma and jumped southward to a place between the locations of magnetic anomalies 33 and 32n.2. This spreading segment also broke into three smaller subsegments. The ridge jump created a fossil ridge segment, now located near the equator (Figure 5a), and transferred oceanic crust from the Antarctic plate formed between magnetic anomalies just younger than 30 to just older than 32n.2 to the Indian plate (Figures 5a and 7b). During the second spreading jump at ~52 Ma, two subsegments to the west of the NER jumped northward to crust formed between anomalies 25 and 26 (Figure 5b), and transferred oceanic crust from the Indian plate formed between magnetic anomalies just younger than 24n.2 to just older than 25 to the Antarctic plate (Figures 5b and 7d), while a third subsegment closer to the NER appears to have jumped southward into preanomaly 34 oceanic crust. Finally, in the third spreading reorganization the entire Wharton Ridge system, including all three subsegments, ceased spreading soon after middle Eocene anomaly 19. This process eventually led to unification of the Indian and Australian plates into a single Indo-Australian plate.

[19] Considering the complex magnetic anomaly derived age progression together with identified fossil ridge segments on both sides of the NER, the progression of ages determined from drill core samples (Figures 5 and 6), and proximity of the hot spot to spreading centers, we suggest two possible explanations for the ridge jumps with respect to the Kerguelen hot spot. With the observation of a few large ridge jumps to the west of the NER and the apparent continuity of the hot spot track, evolution of the NER may be explained by the positioning the Kerguelen hot spot beneath the Indian plate continuously from 77 to 43 Ma. This model requires a large amount of Antarctic plate lithosphere to be transferred to the Indian plate via spreading center jumps to the south away from the hot spot. Although this model appears to be simple because it allows the NER to form simply and with a monotonic age progression, the jumping of the ridge away from the hot spot appears counter to the widely held idea that the excess heat and dynamic uplift over the hot spot weakens the lithosphere, causing the spreading center to jump toward the hot spot position. Observations on ridge–hot spot interactions at other locations led several researchers [*Brozena and White*, 1990; *Small*, 1995; *Hardarson et al.*, 1997; *Mittelstaedt et al.*, 2011] to conclude that ridge segments jump repeatedly toward a hot spot, even when the overall motion of the ridge may be away from the hot spot. It is thought that warm upper mantle temperatures weaken the lithosphere and the hot spot–imposed stress field provides necessary conditions for rifting. A possible explanation for the unusual behavior of the ridge jumps near the NER is that regional stress changes caused these ridge jumps, overriding local stresses caused by the hot spot.

[20] An alternative model, which fits the notion of the spreading ridge jumping toward the hot spot, has the Wharton Ridge system drifting northward of the hot spot and the ridge segment beneath the NER repeatedly jumping back to the hot spot location, thereby accreting bits of the NER from the Antarctic plate to the Indian plate. NER components formed on the Antarctic plate should have reverse age progressions (i.e., become younger toward the north). The existing, reliable age data (Figure 6) are sparse, but remarkably consistent with a simple, linear age progression. Thus, if this explanation is true, reverse age segments must occur in the gaps between dated samples or the ridge jumps were frequent and small enough that the reversed age trends are not resolvable [*Sager et al.*, 2010]. Although it requires the added complexity of additional ridge jumps, we prefer this hypothesis because it allows the ridge segment to jump to the hot spot and it fits the observed hot spot–ridge offsets interpreted from magnetic lineations, which show the hot spot to the south of the Wharton Ridge during the Cenozoic (Figure 7).

[21] Various stages of possible interactions between the spreading center and the Kerguelen hot spot during the formation of the NER are presented in Figure 8. Initially the hot spot was beneath the Indian plate and possibly at some distance from the spreading center, resulting in intraplate volcanism on the Indian plate now in the Bay of Bengal region (Figure 8a). This postulation is supported by the presence of regional lithospheric flexure determined beneath the NER in the Bay of Bengal region [*Gopala Rao et al.*, 1997; *Tiwari et al.*, 2003; *Krishna et al.*, 2009b]. Subsequently, rapid northward migration of the Wharton spreading ridge allowed it to coincide with the hot spot for on-axis volcanism (Figure 8b), which may have emplaced sections of NER simultaneously on both plates (with much of that

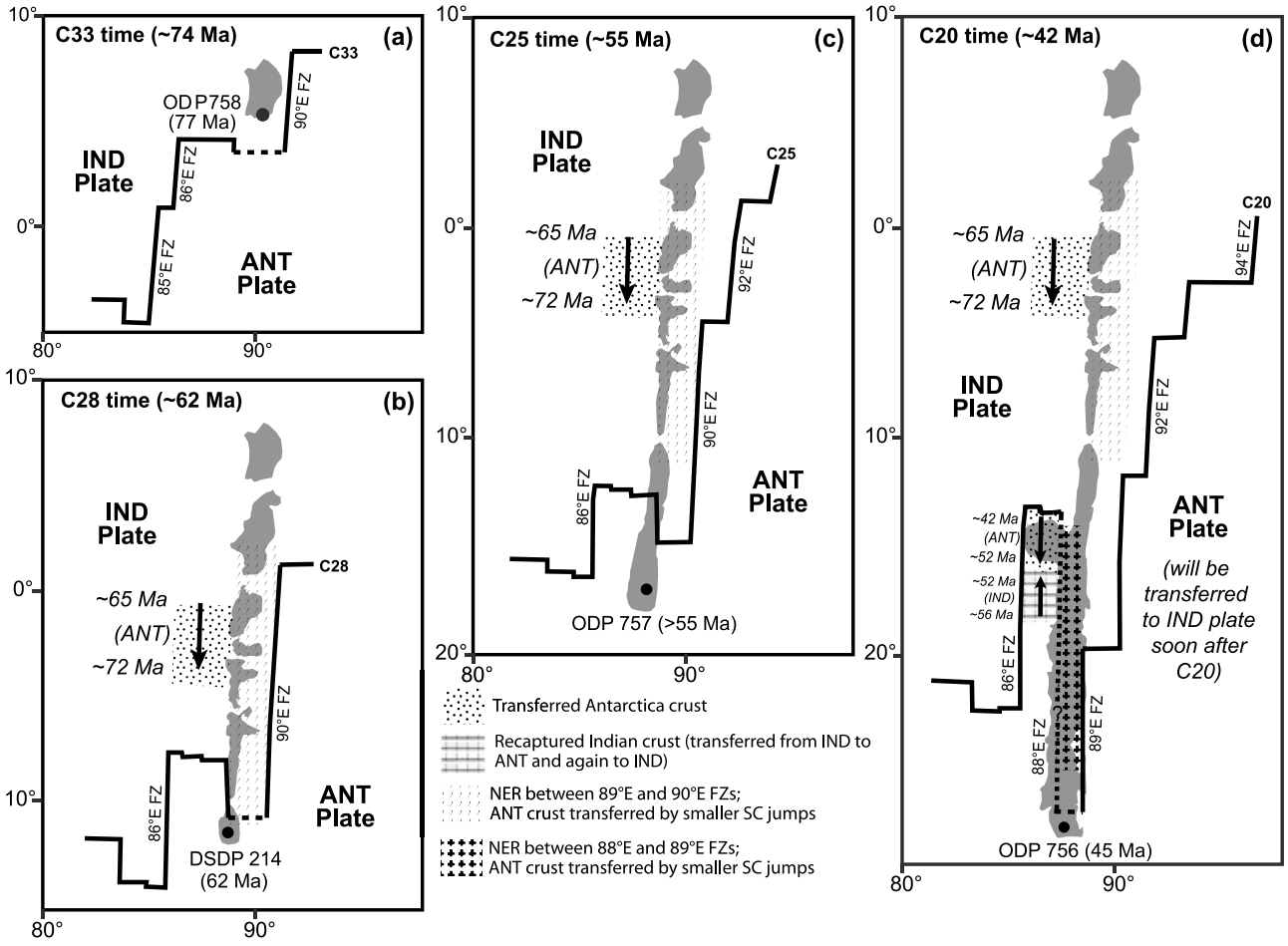

Figure 7. Tectonic evolution of the NER with respect to adjacent spreading ridge segments for four different ages from the Late Cretaceous to early Cenozoic. Solid lines show the relatively well constrained location of the Wharton spreading centers and transform faults on either side of the NER. Dashed lines represent the Wharton spreading segment active directly under the NER at that time; its location is only approximate because the complex volcanic history of the crust directly under the NER did not allow the formation of discernable magnetic anomaly patterns. Two episodes of spreading center jumps and transferred crust can be specifically identified directly to the west of the NER. The more frequent, smaller spreading center jumps proposed for the corridor directly under the NER cannot be specifically identified, but those corridors should include about 50% crust transferred from the Antarctic (ANT) to Indian (IND) plates.

formed on the Antarctic plate eventually captured via ridge jumps). Evidence of Kerguelen hot spot volcanism on the Antarctic plate during the formation of the NER is basalts from Skiff Bank (Kerguelen Plateau) dated at 68 Ma [*Coffin et al.*, 2002].

[22] Further spreading center migration would have placed the hot spot beneath the Antarctic plate for near-ridge or ridge-flank volcanism (Figure 8c). With continued ridge migration, the hot spot moved farther from the spreading ridge beneath the Antarctic plate. The stress field created by the hot spot may have caused uplift and weakening of the overlying oceanic lithosphere, resulting in the initiation of rifting and spreading within the Antarctic plate and leading to southward ridge jumps. It is possible that hot spot material flowed along the base of the lithosphere to reach the spreading center for on-axis volcanism (Figure 8d), even when the hot spot was not located in the vicinity of the spreading ridge crest. This mechanism has been called upon to explain some features of the Amsterdam–St. Paul plateau, which is nearby and had a similar history of construction [*Maia et al.*, 2011]. In addition, the magnetic anomalies suggest that the NER formed within a relatively narrow spreading center corridor with long-offset FZ segments (Figure 7), and some NER volcanism may have occurred along the FZ or the long offsets may have encouraged small bits to break off of the Antarctic plate (i.e., microplates or ridge jumps). The continuous process of hot spot–spreading ridge interaction may have provided necessary conditions to cause multiple ridge jumps. This behavior is also consistent with models of ridge–hot spot interaction in which ridge jumps are promoted by hot spot heating of the lithosphere and perturbations of the local stress field, and form preferentially in younger lithosphere in systems with relatively fast plate velocity [*Mittelstaedt et al.*, 2008, 2011].

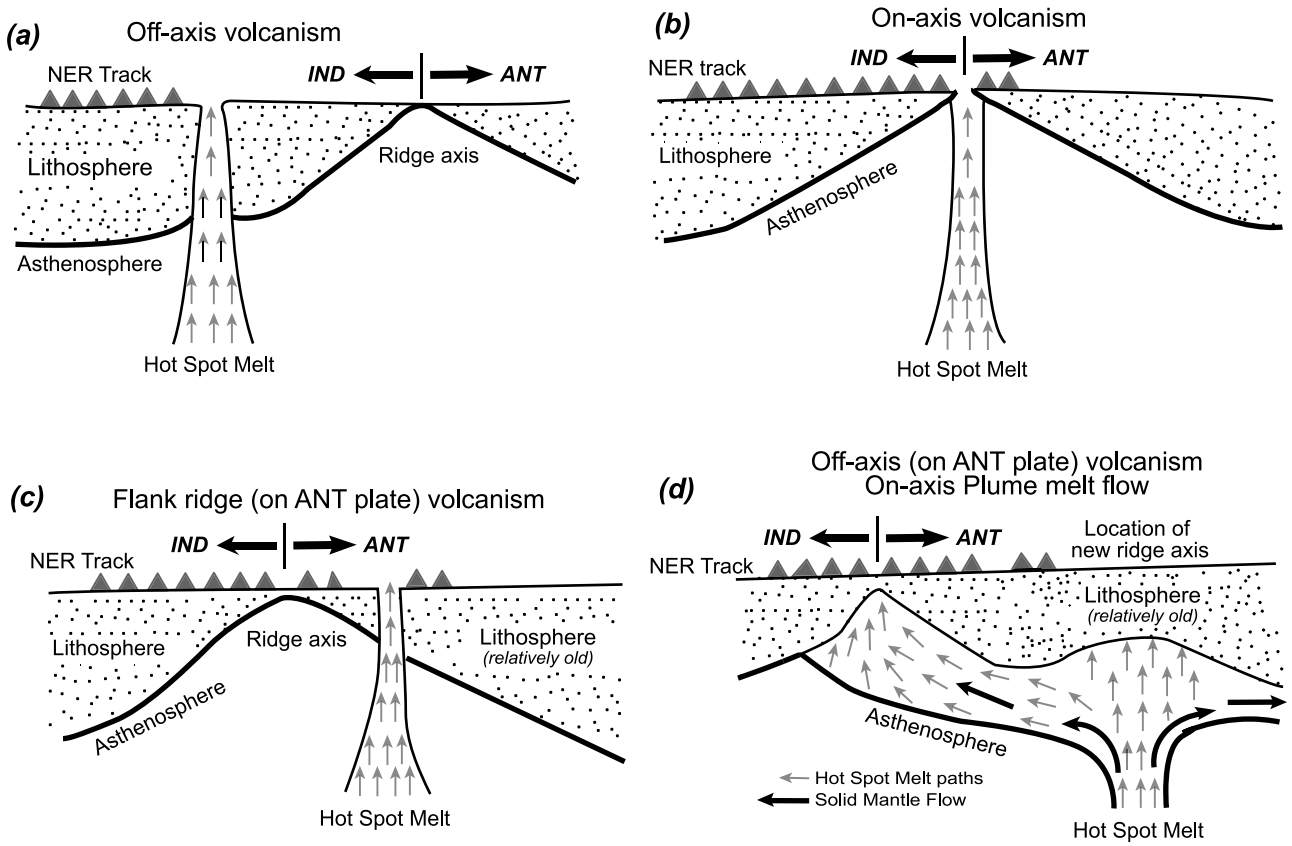

Figure 8. Sketch model showing possible interactions between the Kerguelen hot spot, proximal ridge segments, and oceanic lithosphere during the formation of the NER. The model is developed on the basis of the conceptual model of *Mittelstaedt et al.* [2011] and the results obtained from the present study. (a) Off-axis volcanism when the hot spot was located north of the spreading ridge segments. (b) On-axis volcanism when the hot spot was located at the spreading ridge after northward migration of the plate boundary (Wharton Ridge) with respect to a nearly fixed Antarctic plate. (c) Volcanism on the ridge flank when the hot spot was located beneath the weak lithosphere of the Antarctic plate. (d) On-axis melt flow when the hot spot was located off-axis beneath older lithosphere of the Antarctic plate.

5.2. Evolution of Extra Length of the NER With Respect to Simple Plate Drift

[23] It is obvious from age data of the NER and adjacent oceanic crust evolved within the same time frame (77 to 43 Ma) that the length of the NER is much greater than the stretch of the oceanic crust evolved on the Indian plate (Figure 6). The NER emplacement rate was almost a factor of 2 faster than the rate of accretion of oceanic crust. The extra length of the NER track is ~2000 km, and because the Wharton spreading ridge would have quickly passed the hot spot, it is necessary to postulate other explanations than simple plate drift. Furthermore, the linear trend of NER ages [*Pringle et al.*, 2008] implies that significant slowing of the Indian plate, considered as a response of the continental collision between India and Asia, did not start until completion of construction of the entire NER (~42 Ma). Slow spreading rates (2.4–2.9 cm/yr) observed in the present study (Figures 4b and 4c), particularly in two phases (anomalies 31 to 30 and again from 21 to 19) appear to indicate waning stages of ridge segments in the process of abandonment, but not a response to the slowing of the Indian plate motion.

[24] As discussed in section 5.1, the Kerguelen hot spot was initially in an off-ridge position during the formation of the NER in the Bay of Bengal region (Figure 8a), therefore the Wharton spreading ridge may have taken considerable time to reach the position of the hot spot and to move away to the north. In the process, the northern part of the NER, at least down to 5°N latitude, was created by two different plate motions, viz., by plate motion relative to the hot spot and by a plate boundary (Wharton spreading ridge) migration. The latter activity may have added some additional length of volcanic constructs to the NER track. During the emplacement of the central part of the NER, particularly from 5°N to 11°S latitudes, the hot spot and ridge segments were often in close proximity and this may have allowed the hot spot to form components of the NER on the Antarctic plate that were subsequently transferred to the Indian plate through southward ridge jumps (Figures 7b–7d).

[25] A critical question for NER evolution is how many such ridge jumps occurred. Our interpretation of the magnetic data set in basins adjacent to the NER is a small number of larger ridge jumps. However, both *Krishna et al.* [1999] and *Desa et al.* [2009] have mapped smaller

southward ridge jumps near the NER at ~76 and 54 Ma, respectively. *Sager et al.* [2010] concluded, on the basis of identification of extensive faulting within the NER structure, that numerous small-scale ridge jumps may have occurred and that the hot spot and Wharton spreading ridge may have remained in close proximity. Small ridge jumps are an attractive solution to the paradox that large ridge jumps would result in long segments of reversed age trend yet existing age data are remarkably linear (Figure 6). Such ridge jumps may also explain the apparent increased FZ offsets during the Cenozoic on the Wharton Ridge near NER (Figure 7).

[26] Although it is true that existing NER age data are sparse and might not detect a reversed age segment, the deviant segment would have to hiding in the gaps of the current data. Further, magnetic anomalies near the NER are very difficult to interpret (Figure 3) presumably because the extended history of hot spot and spreading center volcanism does not result in simple magnetization of the ocean crust and discernable patterns of magnetic anomalies. Another factor is that small ridge jumps can be difficult to detect because this requires the recognition of a repeated anomaly pattern that may not be clear unless there are several mirrored anomalies (i.e., a seafloor spreading for a significant time). Thus, despite the improvement with the current magnetic data set over prior compilations, it is not surprising that small ridge jumps are not recognized in the pattern of magnetic anomalies along the NER. More detailed magnetic surveys with closely spaced data would be needed to recognize of small jumps, as shown, for example, at Amsterdam–St. Paul Plateau [*Maia et al.*, 2011].

[27] Besides the processes discussed above, absolute hot spot movement also may have contributed to the lengthening of the NER. Paleomagnetic analyses and mantle flow models have been used to infer 7–10° (800–1100 km) of southward motion of the Kerguelen hot spot during the past 120 Myr [*Klootwijk et al.*, 1991; *Antretter et al.*, 2002; *O'Neill et al.*, 2003]. Such southward motion would also lengthen the NER, but we cannot quantify the north-south hot spot motion because our data set only shows the relative motions of the hot spot and spreading center.

6. Summary and Conclusions

[28] An investigation of magnetic anomaly profiles and other geophysical data around the NER and adjacent Central Indian and Wharton Basins together with newly determined radiometric ages from igneous rocks cored at DSDP and ODP Sites on the NER has provided new insights on the evolution of the NER and interactions between the Wharton spreading ridge segments and the Kerguelen hot spot. Important observations are as follows.

[29] 1. Magnetic anomaly studies of both the Central Indian and Wharton Basins have provided locations of magnetic lineations from 19 through 34 and fossil ridge segments which ceased spreading at 65 and 42 Ma. The lineation offsets are further constrained by narrow, linear gravity anomalies within satellite-derived gravity data that we interpret as fracture zone features. The NER trends ~N 10°E and obliquely crosses ~N 5°E oriented fracture zones. Thus in the south, the 89°E FZ borders the NER on the east side, whereas in the north the same fracture zone borders the ridge on the west side. In the central part between 11°S and 18°S, the fracture zone obliquely crosses the NER.

[30] 2. The age of oceanic crust to the west of the 86°E FZ (Central Indian Basin) increases toward the north from early Cenozoic to Late Cretaceous, while the crust to the east of the 90°E FZ (Wharton Basin) increases its age in both the north and south directions about 42 Ma fossil Wharton Ridge segments. Contrasting to these patterns, the crust between the FZs near the NER shows a complex age succession together with fossil ridge segments of different ages (65 and 42 Ma).

[31] 3. Comparison of ages of oceanic crust, directly to the east and west of the NER with newly determined radiometric ages at DSDP Sites 216, 214, 254 and ODP Sites 756–758 shows that the NER lengthened at a rate twice that of adjacent oceanic crust.

[32] 4. The resulting difference in lengths of the NER (~3980 km) and adjacent oceanic crust (~2000 km) constructed from 77 to 43 Ma is remarkable and requires a geodynamical explanation. During the formation of the NER, the distance between the Kerguelen hot spot and spreading ridge segments changed because of the northward migration of the Wharton spreading ridge, southward ridge jumps, and possibly southward motion of the hot spot. Spreading ridge migration probably resulted in the Kerguelen hot spot underlying the Antarctic plate during the early Cenozoic, and led to formation of volcanic edifices on the Antarctic plate by ridge-flank volcanism and by lateral transport of hot spot melt along the ridge axis. The southward ridge jumps transferred parts of the NER originally formed on the Antarctic plate to the Indian plate and were the major contribution to the extra lengthening of the NER.

[33] **Acknowledgments.** We are indebted to captain, crew, and technicians of the R/V *Roger Revelle* for their efforts during the international scientific expedition (KNOX06RR) of the Ninetyeast Ridge. The field program was supported by the National Science Foundation grants OCE-0550743 and OCE-05499852. H.A. is grateful to CSIR, New Delhi, for the support of student research fellowship (NET-JRF). D.G.R. is grateful to DST, New Delhi, for supporting his research activities through DST-RFBR project 1103. We thank Jon Bull, Chuck DeMets, and the anonymous associate editor for their critical comments and suggestions on the manuscript, which improved the paper greatly. This is NIO contribution 5133.

References

Acton, G. D. (1999), Apparent polar wander of India since the Cretaceous with implications for regional tectonics and true polar wander, *Mem. Geol. Soc. India*, *44*, 129–175.

Antretter, M., B. Steinberger, F. Heider, and H. Soffel (2002), Paleolatitudes of the Kerguelen hot spot: New plaeomagnetic results and dynamic modeling, *Earth Planet. Sci. Lett.*, *203*, 635–650, doi:10.1016/S0012-821X(02)00841-5.

Besse, J., and V. Courtillot (2002), Apparent and true polar wander and the geometry of the geomagnetic field over the last 200 Myr, *J. Geophys. Res.*, *107*(B11), 2300, doi:10.1029/2000JB000050.

Brozena, J. M., and R. White (1990), Ridge jumps and propagations in the South Atlantic Ocean, *Nature*, *348*, 149–152, doi:10.1038/348149a0.

Bull, J. M. (1990), Structural style of intraplate deformation, Central Indian Ocean Basin: Evidence for the role of fracture zones, *Tectonophysics*, *184*, 213–228, doi:10.1016/0040-1951(90)90054-C.

Bull, J. M., C. DeMets, K. S. Krishna, D. J. Sanderson, and S. Merkouriev (2010), Reconciling plate kinematic and seismic estimates of lithospheric convergence in the central Indian Ocean, *Geology*, *38*, 307–310, doi:10.1130/G30521.1.

Cande, S. C., and D. V. Kent (1995), Revised calibration of the geomagnetic polarity time scale for the Late Cretaceous and Cenozoic, *J. Geophys. Res.*, *100*, 6093–6095, doi:10.1029/94JB03098.

Chamot-Rooke, N., F. Jestin, and B. de Voogd, and the Phedre Working Group (1993), Intraplate shortening in the central Indian Ocean determined from a 2100-km-long north-south deep seismic reflection profile, *Geology*, *21*, 1043–1046, doi:10.1130/0091-7613(1993)021<1043:ISITCI>2.3.CO;2.

Coffin, M. F., M. S. Pringle, R. A. Duncan, T. P. Gladczenko, M. Storey, R. D. Müller, and L. A. Gahagan (2002), Kerguelen hot spot magma output since 130 Ma, *J. Petrol.*, *43*, 1121–1137, doi:10.1093/petrology/43.7.1121.

Curray, J. R., F. J. Emmel, D. G. Moore, and W. R. Russel (1982), Structure, tectonics, and geological history of the northeastern Indian Ocean, in *The Ocean Basins and Margins*, vol. 6, *The Indian Ocean*, edited by A. E. Nairn and F. G. Stheli, pp. 399–450, Plenum, New York.

Delescluse, M., and N. Chamot-Rooke (2007), Instantaneous deformation and kinematics of the India-Australia plate, *Geophys. J. Int.*, *168*, 818–842, doi:10.1111/j.1365-246X.2006.03181.x.

Deplus, C., M. Diament, H. Hebert, G. Bertrand, S. Dominguez, J. Dubois, J. Malod, P. Patriat, B. Pontoise, and J. J. Sibilla (1998), Direct evidence of active deformation in the eastern Indian oceanic plate, *Geology*, *26*, 131–134, doi:10.1130/0091-7613(1998)026<0131:DEOADI>2.3.CO;2.

Desa, M., M. V. Ramana, and T. Ramprasad (2009), Evolution of the Late Cretaceous crust in the equatorial region of the northern Indian Ocean and its implication in understanding the plate kinematics, *Geophys. J. Int.*, *177*, 1265–1278, doi:10.1111/j.1365-246X.2009.04096.x.

Duncan, R. A. (1978), Geochronology of basalts from the Ninetyeast Ridge and continental dispersion in the eastern Indian Ocean, *J. Volcanol. Geotherm. Res.*, *4*, 283–305, doi:10.1016/0377-0273(78)90018-5.

Duncan, R. A. (1991), Age distribution of volcanism along aseismic ridges in the eastern Indian Ocean, *Proc. Ocean Drill. Program Sci. Results*, *121*, 507–517.

Fisher, R. L., M. J. Jantsch, and R. L. Comer (1982), *General Bathymetric Chart of the Oceans (GEBCO)*, Can. Hydrogr. Serv., Ottawa.

Gopala Rao, D., K. S. Krishna, and D. Sar (1997), Crustal evolution and sedimentation history of the Bay of Bengal since the Cretaceous, *J. Geophys. Res.*, *102*, 17,747–17,768, doi:10.1029/96JB01339.

Gordon, R. G., C. DeMetes, and J.-Y. Royer (1998), Evidence for long-term diffuse deformation of the lithosphere of the equatorial Indian Ocean, *Nature*, *395*, 370–374, doi:10.1038/26463.

Hardarson, B. S., J. G. Fitton, R. M. Ellam, and M. S. Pringle (1997), Rift relocation—A geochemical and geochronological investigation of a paleorift in northwest Iceland, *Earth Planet. Sci. Lett.*, *153*, 181–196, doi:10.1016/S0012-821X(97)00145-3.

Klootwijk, C. T., S. G. Jeff, J. W. Peirce, and G. M. Smith (1991), Constraints on the Indian-Asia convergence: Paleomagnetic results from Ninetyeast Ridge, *Proc. Ocean Drill. Program Sci. Results*, *121*, 777–882.

Krishna, K. S., and D. Gopala Rao (2000), Abandoned Paleocene spreading center in the northeastern Indian Ocean: Evidence from magnetic and seismic reflection data, *Mar. Geol.*, *162*, 215–224, doi:10.1016/S0025-3227(99)00085-7.

Krishna, K. S., D. Gopala Rao, M. V. Ramana, V. Subrahmanyam, K. V. L. N. S. Sarma, A. I. Pilipenko, V. S. Shcherbakov, and I. V. Radhakrishna Murthy (1995), Tectonic model for the evolution of oceanic crust in the northeastern Indian Ocean from the Late Cretaceous to the early Tertiary, *J. Geophys. Res.*, *100*, 20,011–20,024, doi:10.1029/94JB02464.

Krishna, K. S., M. V. Ramana, D. Gopala Rao, K. S. R. Murthy, M. M. Malleswara Rao, V. Subrahmanyam, and K. V. L. N. S. Sarma (1998), Periodic deformation of oceanic crust in the central Indian Ocean, *J. Geophys. Res.*, *103*, 17,859–17,875, doi:10.1029/98JB00078.

Krishna, K. S., D. Gopala Rao, L. V. Subba Raju, A. K. Chaubey, V. S. Shcherbakov, A. I. Pilipenko, and I. V. Radhakrishna Murthy (1999), Paleocene on-axis hot spot volcanism along the Ninetyeast Ridge: An interaction between the Kerguelen hot spot and the Wharton spreading center, *Proc. Indian Acad. Sci. Earth Planet. Sci.*, *108*, 255–267.

Krishna, K. S., Y. P. Neprochnov, D. Gopala Rao, and B. N. Grinko (2001a), Crustal structure and tectonics of the Ninetyeast Ridge from seismic and gravity studies, *Tectonics*, *20*, 416–433, doi:10.1029/2001TC900004.

Krishna, K. S., J. M. Bull, and R. A. Scrutton (2001b), Evidence for multiphase folding of the central Indian Ocean lithosphere, *Geology*, *29*, 715–718, doi:10.1130/0091-7613(2001)029<0715:EFMFOT>2.0.CO;2.

Krishna, K. S., J. M. Bull, and R. A. Scrutton (2009a), Early (pre-8 Ma) fault activity and temporal strain distribution in the central Indian Ocean, *Geology*, *37*, 227–230, doi:10.1130/G25265A.1.

Krishna, K. S., L. Michael, R. Bhattacharyya, and T. J. Majumdar (2009b), Geoid and gravity anomaly data of conjugate regions of Bay of Bengal and Enderby Basin: New constraints on breakup and early spreading history between India and Antarctica, *J. Geophys. Res.*, *114*, B03102, doi:10.1029/2008JB005808.

Liu, C. S., J. R. Curray, and J. M. McDonald (1983), New constraints on the tectonic evolution of the eastern Indian Ocean, *Earth Planet. Sci. Lett.*, *65*, 331–342, doi:10.1016/0012-821X(83)90171-1.

Maia, M., et al. (2011), Building of the Amtersdam–St. Paul plateau: A 10 Myr history of a ridge-hot spot interaction and variations in the strength of the hot spot source, *J. Geophys. Res.*, *116*, B09104, doi:10.1029/2010JB007768.

Mendel, V., M. Munschy, and D. Sauter (2005), MODMAG, a MATLAB program to model marine magnetic anomalies, *Comput. Geosci.*, *31*, 589–597, doi:10.1016/j.cageo.2004.11.007.

Michael, L., and K. S. Krishna (2011), Dating of the 85°E Ridge (northeastern Indian Ocean) using marine magnetic anomalies, *Curr. Sci.*, *100*, 1314–1322.

Mittelstaedt, E., G. Ito, and M. D. Behn (2008), Mid-ocean ridge jumps associated with hot spot magmatism, *Earth Planet. Sci. Lett.*, *266*, 256–270, doi:10.1016/j.epsl.2007.10.055.

Mittelstaedt, E., G. Ito, and J. van Humen (2011), Repeat ridge jumps associated with plume-ridge interaction, and ridge migration, *J. Geophys. Res.*, *116*, B01102, doi:10.1029/2010JB007504.

O'Neill, C., D. Müller, and B. Steinberger (2003), Geodynamic implications of moving Indian Ocean hot spots, *Earth Planet. Sci. Lett.*, *215*, 151–168, doi:10.1016/S0012-821X(03)00368-6.

Patriat, P., and J. Segoufin (1988), Reconstruction of the central Indian Ocean, *Tectonophysics*, *155*, 211–234, doi:10.1016/0040-1951(88)90267-3.

Peirce, J. W. (1978), The northward motion of India since the Late Cretaceous, *Geophys. J. R. Astron. Soc.*, *52*, 277–311, doi:10.1111/j.1365-246X.1978.tb04234.x.

Peirce, J. W., et al. (1989), *Proceedings of the Ocean Drilling Program, Initial Reports*, vol. 121, 1000 pp., Ocean Drill. Program, College Station, Tex.

Pilipenko, A. I. (1996), Fracture zones of the Ninetyeast Ridge area, Indian Ocean, *Geotectonics, Engl. Transl.*, *30*, 441–451.

Pringle, M. S., F. A. Frey, E. M. Mervine, and W. W. Sager (2007), New Ar/Ar ages from the Ninetyeast Ridge, Indian Ocean: Beginning of a robust Indo-Atlantic hot spot reference frame, *Eos Trans. AGU*, *88*(52), Fall Meet. Suppl., Abstract U13A-0871.

Pringle, M. S., F. A. Frey, and E. M. Mervine (2008), A simple linear age progression for the Ninetyeast Ridge, Indian Ocean: New constraints on Indian plate motion and hot spot dynamics, *Eos Trans. AGU*, *89*(53), Fall Meet. Suppl., Abstract T54B-03.

Royer, J.-Y., and R. G. Gordon (1997), The motion and boundary between the Capricorn and Australian plates, *Science*, *277*, 1268–1274, doi:10.1126/science.277.5330.1268.

Royer, J.-Y., and D. T. Sandwell (1989), Evolution of the eastern Indian Ocean since the Late Cretaceous: Constraints from Geosat altimetry, *J. Geophys. Res.*, *94*, 13,755–13,782, doi:10.1029/JB094iB10p13755.

Royer, J.-Y., J. W. Peirce, and J. K. Weissel (1991), Tectonic constraints on the hot-spot formation of Ninetyeast Ridge, *Proc. Ocean Drill. Program Sci. Results*, *121*, 763–776.

Sager, W. W., et al. (2007), Cruise report KNOX06RR R/V *Roger Revelle*, 82 pp., Natl. Sci. Found., Washington, D. C. [Available at http://earthref.org/erda/1172.]

Sager, W. W., C. F. Paul, K. S. Krishna, M. Pringle, A. E. Eisin, F. A. Frey, D. Gopala Rao, and O. Levchenko (2010), Large fault fabric of the Ninetyeast Ridge implies near-spreading ridge formation, *Geophys. Res. Lett.*, *37*, L17304, doi:10.1029/2010GL044347.

Sandwell, D. T., and W. H. F. Smith (1997), Marine gravity from Geosat and ERS-1 satellite altimetry, *J. Geophys. Res.*, *102*, 10,039–10,054, doi:10.1029/96JB03223.

Sclater, J. G., and R. L. Fisher (1974), Evolution of the east central Indian Ocean, with emphasis on the tectonic setting of the Ninetyeast Ridge, *Geol. Soc. Am. Bull.*, *85*, 683–702, doi:10.1130/0016-7606(1974)85<683:EOTECI>2.0.CO;2.

Small, C. (1995), Observation of ridge–hot spot interactions in the Southern Ocean, *J. Geophys. Res.*, *100*, 17,931–17,946, doi:10.1029/95JB01377.

Subrahmanyam, C., R. Gireesh, S. Chand, K. A. Kamesh Raju, and D. Gopala Rao (2008), Geophysical characteristics of the Ninetyeast Ridge–Andaman island arc/trench convergent zone, *Earth Planet. Sci. Lett.*, *266*, 29–45, doi:10.1016/j.epsl.2007.10.016.

Tiwari, V. M., M. Diament, and S. C. Singh (2003), Analysis of satellite gravity and bathymetry data over Ninety-East Ridge: Variation in the compensation mechanism and implication for emplacement process, *J. Geophys. Res.*, *108*(B2), 2109, doi:10.1029/2000JB000047.

Von der Borch, C. C., et al. (1974a), Site 215, *Initial Rep. Deep Sea Drill. Proj.*, *22*, 193–211.

Von der Borch, C. C., et al. (1974b), Site 213, *Initial Rep. Deep Sea Drill. Proj.*, *22*, 85–118.

Weissel, J. K., R. N. Anderson, and C. A. Geller (1980), Deformation of the Indo-Australian plate, *Nature*, *287*, 284–291, doi:10.1038/287284a0.

H. Abraham and K. S. Krishna, National Institute of Oceanography, Council of Scientific and Industrial Research, Dona Paula, Goa 403004, India. (krishna@nio.org)

F. Frey and M. S. Pringle, Department of Earth and Planetary Sciences, Massachusetts Institute of Technology, Cambridge, MA 02139, USA.

D. Gopala Rao, Department of Geology, Osmania University, Hyderabad 500007, India.

O. V. Levchenko, Shirshov Institute of Oceanology, Russian Academy of Sciences, Moscow 117997, Russia.

W. W. Sager, Department of Oceanography, Texas A&M University, College Station, TX 77843-3146, USA.